Distribution Agreement

In presenting this dissertation as a partial fulfillment of the requirements for an advanced degree from Emory University, I hereby grant to Emory University and its agents the non-exclusive license to archive, make accessible, and display my dissertation in whole or in part in all forms of media, now or hereafter known, including display on the world wide web. I understand that I may select some access restrictions as part of the online submission of this dissertation. I also retain the right to use in future works (such as articles or books) all or part of this dissertation.

_____ _____

Sharon Soucek Date

Generation of Export-Competent mRNPs

By
Sharon Soucek
Doctor of Philosophy

Graduate Division of Biological and Biomedical Sciences
Graduate Program in Biochemistry, Cell and Developmental Biology

_____
Anita H. Corbett, Ph.D.
Advisor

_____
Graeme Conn, Ph.D.
Committee Member

_____
Yue Feng, Ph.D.
Committee Member

_____
Judy Fridovich-Keil, Ph.D.
Committee Member

_____
Daniel Reines, Ph.D.
Committee Member

Accepted:

_____
Lisa A. Tedesco, Ph.D.
Dean of the Graduate School

_____
Date

Generation of Export-Competent mRNPs

By

Sharon Soucek
B.S., Northeastern University, 2007

Advisor: Anita H. Corbett, Ph.D.

An abstract of
A dissertation submitted to the Faculty of the
James T. Laney of Graduate Studies of Emory University
in partial fulfillment of the requirements for the degree of
Doctor of Philosophy in the
Graduate Divisions of Biological and Biomedical Sciences
Biochemistry, Cell and Developmental Biology
2014

ABSTRACT

Generation of Export-Competent mRNPs

By Sharon Soucek

Gene expression is regulated to produce a protein expression profile that dictates the function of each cell. Messenger RNA (mRNA) serves as an intermediate between the genome and translation of proteins. Mature mRNA requires processing events including the addition of a 5'-cap, removal of introns, and 3'-end processing. These maturation steps are mediated by RNA binding proteins that associate with the mRNA throughout its post-transcriptional journey. Given that mRNA biogenesis is essential for proper gene expression, mutations within RNA binding proteins impair mRNA maturation and consequently lead to numerous human diseases. Of relevance to this work, mutations in the zinc finger RNA binding protein gene, *ZC3H14*, lead to a non-syndromic form of autosomal intellectual disability. The goal of this study is to understand how RNA binding proteins ensure proper processing of pre-mRNA to give rise to export-competent mRNA/protein complexes (mRNPs) within the nucleus. To address this goal, we focused our efforts on the Nuclear Poly(A) RNA Binding protein, Nab2, which is the putative budding yeast orthologue of ZC3H14. As a first step to define how RNA binding proteins regulate target mRNAs, we used a structure-function approach to reveal how Nab2 binds to polyadenosine RNA. We describe the structure of Nab2 zinc fingers 5-7, which are necessary and sufficient for high affinity polyadenosine RNA binding, and identify key residues involved. Structure-guided variants show that Nab2 modulates poly(A) tail length and functions in the generation of export-competent mRNPs. We extend this

analysis to understand how Nab coordinates splicing, 3'-end processing, and mRNA decay. We identified several genes that genetically interact with *NAB2* including other poly(A) RNA binding proteins, components of the splicing machinery, and the nuclear exosome. To add to our understanding of how RNA binding proteins modulate specific classes of RNA, we provide an initial characterization of the Mmi1 protein, which is essential for the regulation of meiotic transcripts. These findings contribute to an understanding of how multiple steps in nuclear mRNA processing are coordinated and lay the groundwork for probing key functions of ZC3H14 in the brain that lead to intellectual disability.

Generation of Export-competent mRNPs

By

Sharon Soucek
B.S., Northeastern University, 2007

Advisor: Anita H. Corbett, Ph.D.

A dissertation submitted to the Faculty of the
James T. Laney of Graduate Studies of Emory University
in partial fulfillment of the requirements for the degree of
Doctor of Philosophy in the
Graduate Divisions of Biological and Biomedical Sciences
Biochemistry, Cell and Developmental Biology
2014

ACKNOWLEDGEMENTS

I would like to thank my advisor, Dr. Anita Corbett, for guiding me through the scientific process. Anita's liberal use of the red pen and ability to give me the leeway to explore has made me a better scientist. When I entered graduate school, I knew I had to find the very best mentor for me and I wholeheartedly got what I wished for. I would like to thank the members of my committee, Danny Reines, Yue Feng, Graeme Conn, and Judy Fridovich-Keil, for challenging me and providing much needed support.

The past and present members of the Corbett lab deserve a special thanks as well. Thank you to the high school students and undergraduates that I mentored. Thanks Sang Go, Brittany Watchmaker, Michelle Vu, and Brahma for all your hard work and excitement while working in the lab. I would especially like to thank Sara Leung, Milo Fasken, Ayan Banerjee, Katherine Mills-Lujan, Callie Wigington, Jennifer Rha, Kevin Morris, Annie McPherson, Nick Bauer, Laura Mclane, Alexe Frere, Brianne Kallam, Shana Kerr, Seth Kelly, and Allison Lange. I was always free to ask for your help and received it promptly with enthusiasm. After spending so much time together, I not only consider you my colleagues, but also my dear friends.

I want to thank the Office of Technology Transfer, who showed me that science extends past the bench. Thank you Cory Acuff for being an amazing graduate school mentor by teaching me the business of science, giving me the chance to explore all the cool inventions at Emory, and advising me about future careers. I would also like

to thank Lisa Matragrano, Cliff Michaels, David Giannantonio, Phil Semprevio, and the fellow interns for their unique expertise and advise.

My interest in science started way before graduate school and I want to acknowledge everyone who planted that seed along the way. I would like to thank my AP Biology high school teacher, Dr. Frank Puma, who explained science in the most engaging way possible. Your replica model of a kinesin motor man still jogs my memory every time I hear about microtubules. I especially want to thank my college chemistry professor, Dr. Geoffrey Davies, who inspired me in so many ways. It's been a pleasure keeping up with your lab and I'm so thankful to have such an awesome mentor in college and beyond. I also apologize for breaking your expensive quartz cuvette one late Friday night. I would also like to thank Dr. Heike Laue, who mentored me in a small Swiss pharmaceutical company and taught me everything I need to know about sterilization. Finally, I would like to thank Phyllis Strauss for giving me the choice to study the exciting zebrafish model system.

To the most important people in my life, family, friends, and my husband, I give many thanks. I thank my parents, Otilia and Emanuel, for always being optimistic and believing that I could follow my dreams. To my brother Christopher, it has been exciting to see you grow up and weigh in on this journey. Thank you to my very best friends from grade school, Sally Bishay, Ceci Doddi, and Joy Chen. To my college pals that have dispersed across the US, thank you for keeping in touch as we started our new lives. To my Atlanta crew-Jennifer Colucci, Mariana Mandler, Brett Tuggle, Yoni Gabbay, Gina Lenzi, Shawn Alter, Tamara Schiff, Amy Cheng, and Chad Hume-you have made the nights after long days in the lab easy. I most want to thank

my partner in crime, my husband Rémi Fourreau. The minute you entered my life, I knew I couldn't be without your help, encouragement, and patience.

TABLE OF CONTENTS

FIGURES

TABLES

ABBREVIATIONS

3’-UTR	3’-untranslated region
5-FOA	5-fluoroorotic acid
AMP	Ampicillin
CCCH	Cysteine-Cysteine-Cysteine-
CTD	Carboxyl terminal domain
DAPI	4',6-diamidino-2-phenylindole
DIC	Differential interference microscopy
FISH	Fluorescence *in situ* hybridization
GFP	Green fluorescent protein
GST	Glutathione S-transferase
HYGRO	Hygromycin
IPTG	Isopropyl-thio-galactopyranoside
KAN	Kanamycin
LB	Luria broth
mRNP	Messenger RNA ribonucleoprotein complex
NAT	Natamycin
NMD	Nonsense mediated decay
NMR	Nuclear magnetic resonance
NLS	Nuclear localization signal
NPC	Nuclear pore complex
Pab	Poly(A) RNA binding protein
QQQP	Glutamine-Glutamine-Glutamine-Proline domain
PLAC	Pepstatin A, leupeptin, aprotinin, chymostatin
PMSF	Phenylmethylsulfonyl fluoride
PWI	Phenyl-Trytophan-Isoleucine domain
RNAP II	RNA polymerase II
RGG	Arginine-Glycine-Glycine
rRNA	Ribosomal RNA
SDS-PAGE	Sodium dodecyl sulfate polyacrylamide gel electrophoresis
snRNA	Small nuclear RNA
snoRNA	Small nucleolar RNA
TRAMP	Trf4/5-Air1/2-Mtr4 protein complex
TREX	Transcription and export complex
YEPD	Yeast extract peptone dextrose
ZnF	Zinc finger

Chapter 1: Introduction

A portion of this chapter is adapted from the following published work:

Soucek, S., Corbett, A.H., and Fasken, M. (2012) *Biochim Biophys Acta.* ***1819****, 546- 554.* "The Long and the Short of It: The Role of the Zinc Finger Polyadenosine RNA binding Protein, Nab2, in Control of Poly(A) Tail Length"

Regulation of gene expression

Two basic types of cells are found in the living world: prokaryotes and eukaryotes. In reference to the Latin name, eukaryotes possess a "true" nucleus whereas prokaryotes have no nuclei. The compartmentalization of the nucleus and the cytoplasm provides a way to precisely regulate the gene expression in eukaryotes. Inside the nucleus lies the DNA code that is used as a blueprint for all cell function. While all DNA content remains constant between cells within a given organism, the expression of specific genes varies greatly in multicellular organism or in response to environmental cues in unicellular organisms. The gene expression profile is dictated by both transcriptional and post-transcriptional processing events of the intermediate message, mRNA. In recent years, there has been a growing appreciation for the role of post-transcriptional events in the regulation of gene expression.

Proper gene expression in eukaryotic cells requires the production of mature processed mRNA transcripts in the nucleus and export of those transcripts to the cytoplasm for translation (Figure 1.1). Following transcription by RNA polymerase II, nascent mRNA transcripts undergo a series of co-transcriptional processing steps to reach maturity. Specifically, mRNA transcripts are bound by processing factors that perform 5'-end capping to add a 7-methylguanosine cap, splicing to remove introns, and 3'-end cleavage and polyadenylation to add a polyadenosine tail (1, 2). Transcripts that are improperly processed are recognized and destroyed by mRNA surveillance factors (3-5). Following nuclear processing, mRNA transcripts are exported through nuclear pore

complexes (NPCs) to the cytoplasm where they can be translated (6-8). Throughout their lifespan, mRNA transcripts interface with RNA binding proteins that regulate the post-transcriptional processing events.

At the heart of post-transcriptional gene control are the RNA binding proteins that associate with the mRNA transcripts to form messenger ribonucleoprotein (mRNP) complexes. By defining the RNA binding proteins that form the protein components of the mRNP during an mRNA life cycle, one can appreciate the enormous dynamic control and complexity that must be achieved to regulate gene expression. Given the extensive contacts between RNA binding proteins in the context of mRNPs, ascribing a precise function for any given RNA binding protein is a significant challenge. To address this challenge, the focus of this dissertation lies in characterizing RNA binding proteins in the context of multiple mRNA processing events. This approach can uncover previously unknown roles of RNA binding proteins in other mRNA processing events. By investigating mRNP assembly components, we begin to understand critical connections between each step of the mRNA life cycle and how perturbation of this pathway ultimately dictates mRNA fate.

To begin to understand the nuances of regulation between different RNA processing events, the myriad of RNA binding proteins that accompany transcripts must first be defined. Post-transcriptional processing events are highly conserved through evolution and many of the key studies that have defined components of the system were originally performed in the budding yeast, *Saccharomyces cerevisiae*. The steps of the

mRNA lifecycle are described in this Chapter with a rationale for and focus on the use of the budding yeast model system. This summary of pre-mRNA maturation events is followed by analysis of how these processes are coupled by RNA binding proteins. An introduction to the nuclear poly(A) RNA binding protein, Nab2, is presented. Finally, the implication of this dissertation work in the context of the RNA processing field will be described.

Post-transcriptional processing

Saccharomyces cerevisiae as a model system to study mechanisms of post-transcriptional processing

The mechanisms and factors required for mRNA processing and export are evolutionarily conserved from budding yeast to humans. Thus, experiments in *Saccharomyces cerevisiae* have contributed significantly to our understanding of mRNA biogenesis by elucidating the processes and factors required for proper gene expression. The simple unicellular yeast is a useful system to dissect the complexities of RNA metabolism, including RNA splicing, 3'-end processing, and export. *S. cerevisiae* is used for its ease of genetic and biochemical experiments with accessibility to genomic and proteomic information. However, studies in fission yeast, *Schizosaccharomyces pombe*, can complement studies in *S. cerevisiae* (Chapter 5).

5'-Capping

From the onset of transcription, a pre-mRNA transcript must be properly processed to become mature mRNA that is competent for export from the nucleus and primed for translation in the cytoplasm. RNA processing begins immediately after transcription is initiated, where a 7-methylguanosine cap is added to the 5' end of the transcript. Cap formation occurs co-transcriptionally when the pre-mRNA transcript is only 25-30 nucleotides long (9, 10). During transcription elongation, the capping enzymes remove the γ-phosphate from the first nucleotide, creating a diphosphate that is capped by a guanine monophosphate and later methylated at the N7 position of the guanine (9). The three component RNA capping apparatus is essential and conserved in all eukaryotes (9). The addition of a 5' 7-methylguanosine cap recruits the cap binding complex (CBC) to shield the transcript from exonucleases (11, 12), engage early splicing factors (13, 14), support cleavage (15), promote efficient mRNA export (14), and direct translation initiation (16).

Splicing

After addition of the 5' cap, non-coding sequences known as introns must be removed to produce mature mRNA. Splicing is the RNA processing event that removes introns and ligates exons together through two successive transesterification reactions (17). During the formation of mature mRNA, a dynamic ribonucleoprotein complex called the spliceosome is loaded onto pre-mRNA (Figure 1.2). The spliceosome is

composed of five small nuclear RNAs (U snRNAs) and a large number of proteins that assemble into a catalytic complex which excises introns (18). The spliceosomal components recognize consensus splice sites within the introns, including the 5' splice site, branch point, and 3' splice site (19). Over 170 proteins in the human spliceosome associate with the mRNA transcript during splicing (Figure 1.2) (20, 21). Many of these proteins have additional functions in other steps of mRNA processing (20, 21). However, a number of splicing factors have not been investigated for roles in other mRNA processing events.

Assembly of the spliceosome begins with the prespliceosome commitment complex (E complex) formation where U1 snRNA binds the 5' splice site (22). After 5' splice site recognition, the BBP/Msl5 (SF1 in mammals) and Mud2 (U2AF65 in mammals) auxiliary proteins bind the branchpoint splice site (23-25). In an ATP dependent step the DExD/H-box helicases, Sub2 and Prp5, remove Mud2 and BBP/Msl5, replacing them with the U2 snRNA (26). After establishment of the U1·U2 prespliceosome (A complex), the tri-snRNP U5·U4/6 is added (B complex) (27-30) and rearranged into a catalytically active spliceosome (C complex) (31, 32). Through two transesterification reactions, the intron lariat is excised out and the exons are ligated together to produce mature mRNA (17, 29, 33-36).

Some intron-containing transcripts are constitutively spliced, but others are alternatively spliced to generate multiple spliced isoforms from a single pre-mRNA species (37). Alternative splicing is prevalent in higher eukaryotes and increases their

genome complexity by producing unique proteins from a single gene (38, 39). Despite the differences between eukaryotic species in terms of the number of intron-containing genes, splicing is both conserved and essential for pre-mRNA processing. In fact, although *Saccharomyces cerevisiae* only have 250 intron-containing genes (~5%), over 50% of expressed mRNA transcripts undergo splicing (40).

3'-end processing

Following capping and splicing, the mRNA transcript undergoes additional processing at the 3'-end through a coupled cleavage and polyadenylation reaction (Figure 1.3) (1). The cleavage reaction begins with recognition of the poly(A) signal sequence, AAUAA, and downstream U or GU rich sequence elements by the polyadenylation machinery (41). After cleavage, the polyadenosine polymerase adds an untemplated stretch of monophosphate adenosines (poly(A)) (41). Addition of the poly(A) tail allows binding by polyadenosine RNA binding proteins that help to stabilize and guide mRNA processing (1). Synthesis of poly(A) tails by the 3'-end processing machinery is particularly critical for protecting the transcript from 3' end exonuclease degradation, promoting mRNA export, and facilitating translation initiation (42-44).

The polyadenylation signal (PAS), containing the AU-rich efficiency element (EE), A-rich positioning element (PE), and U-rich element (UE), is recognized by the 3′-end cleavage machinery (45). The 3'-end formation machinery includes the following complex components: cleavage factor IA (CFIA) containing Rna14, Rna15, Clp1 and

Pcf11; cleavage factor IB (CFIB) containing Hrp1/Nab4; and the cleavage and polyadenylation factor (CPF) including the riboendonuclease, Ysh1/Brr5 (CPSF73 in mammals), the poly(A) polymerase, Pap1, and the Pap1 regulation factor, Fip1 (45). The single RRM-containing protein, Rna15, associates with the scaffold protein, Rna14, which binds to the other CFIA subunits, Pcf11/Clp1, and recognizes the A-rich PE (e.g. AAUAAN) to position CPF to cleave the poly(A) site (45-47). The dual RRM-containing protein, Hrp1/Nab4, binds to the AU-rich EE (e.g. UAUAUAU) and contacts Rna14 and Rna15 to influence the efficiency of the cleavage reaction (45, 48, 49).

Following the cleavage reaction Pap1 synthesizes a poly(A) tail of adenosines in a template-independent manner (50). In budding yeast, this tail is ~ 60–80 adenosines long (50). As Pap1 is an inefficient distributive enzyme, Pap1 processivity requires stimulation/regulation by factors that bind Pap1 and tether it to the RNA (50). The mammalian RRM-containing Pab, PABPN1, enhances the processivity of poly(A) polymerase in this manner (51-53), and another mammalian component, nucleophosmin, also influences polyadenylation although the mechanisms have not yet been defined (54). In addition, the *S. cerevisiae* CPF component, Fip1, and its human CPSF counterpart, hFip, directly bind Pap and tether it to CPF/CPSF to stimulate/regulate Pap activity (55-57). A current challenge is to understand how poly(A) RNA binding proteins interface with these polyadenylation factors to regulate poly(A) tail length. More specifically, it is unclear whether *S. cerevisiae* poly(A) RNA binding proteins stimulate polyadenylation in a manner similar to higher eukaryotes.

As another added layer of gene control, mRNA transcripts can undergo alternative polyadenylation (58). RNA transcripts often contain more than one polyadenylation site at their 3'-ends (more than 50% of transcripts in mammals (58)), resulting in differential selection of polyadenylation signals by the core 3'-end processing machinery. Alternative polyadenylation generates a diverse set of transcripts with different coding regions or 3'-UTRS. When poly(A) sites are located within a coding region, the mRNA transcript has the potential to express distinct protein isoforms. Alternatively, poly(A) sites located within the 3'-UTR length can dictate whether regulatory sequences, such as miRNA binding sites or RNA binding protein target sequences, that have the potential to modulate transcript fate, are present (59, 60). Differential processing of multiple poly(A) sites can affect the stability, localization, transport, and translational properties of the mature mRNA (58). A few examples of alternative polyadenylation in yeast have been described (61-64); however, the mechanisms responsible for regulating alternative polyadenylation have not been explored (58).

RNA export

An essential step in the RNA lifecycle is the export of mRNA into the cytoplasm where mRNA transcripts contact the protein translational machinery. The first step of mRNA export is to process and package mRNPs, followed by targeting and translocation through the nuclear pore complex (NPC), and finally release of the mRNP complex in the cytoplasm. Throughout RNA processing, a myriad of RNA binding proteins associate and disassociate from the messenger ribonucleoprotein complex (mRNP) to mediate

RNA processing. The exact composition of RNA binding proteins critical for mRNA export are beginning to be defined, but it is unknown how many export adaptors must bind to a single mRNA transcript for efficient export.

Following proper mRNA processing and assembly of the mRNP, the mRNA transcript is transported out of the nucleus via NPCs (Figure 1.4). The NPC is a large protein complex embedded in the nuclear envelope. The NPC is comprised of nucleoporins and a class of nucleoporins termed phenylalanine-glycine (FG)-nucleoporins line the central channel of the NPC. These FG-nucleoporins form a barrier restricting the diffusion of macromolecules between the nucleus and cytoplasm. Therefore, the export of mRNPs is a regulated process requiring a variety of proteins that interact with the NPC.

In order to pass through the nuclear pore, an mRNP must be targeted to the nuclear pore and contain the relevant mRNP exporter receptors. Bulk mRNA is exported via the mRNA export receptor, Mex67-Mtr2. The Mex67-Mtr2 heterodimer is recruited early in mRNA processing through the transcription-export complex (TREX). The exchange of TREX components during mRNA processing facilitates the assembly of export-competent mRNPs. The current model of mRNA export suggests that the TREX component, Sub2, recruits Yra1 to the mRNP (65, 66). Upon recruitment of Yra1, Mex67-Mtr2 binds to the mRNP to stimulate export (65, 66). However, recent studies provide evidence that other nuclear adaptors may stimulate mRNP export. The nuclear adaptor protein, Nab2, aids in recruiting the mRNA export receptor, Mex67-Mtr2, to

promote nuclear export of the properly processed mRNA transcript (67). Nab2 also binds to the interface of the NPC through interactions with the export receptors, Mlp1/2 proteins, to facilitate targeting of transcripts to the NPC (68-70). Following Mex67-mediated export to the cytoplasm, Gfd1 helps tether Nab2 to the cytoplasmic face of the pore, while the DEAD-box RNA helicase, Dbp5, remodels the mRNP, leading to dissociation of Nab2, Mex67, and other nuclear-loaded RNA binding proteins from the transcript (71-74).

During mRNP remodeling at the cytoplasmic face of the pore, the transcript undergoes an exchange of RNA binding proteins in which cytoplasmic proteins replace nuclear proteins. The cytoplasmic RNA binding proteins target the transcript for translation or cytoplasmic processing steps, including mRNA decay (8).

RNA surveillance

Errors during mRNA processing must be recognized before faulty mRNA transcripts becomes translated into aberrant proteins. Aberrant RNAs can arise from misprocessing or suboptimal mRNP assembly and the cell has evolved numerous mechanisms to destroy faulty pre-mRNA that could be deleterious (75). Importantly, there are multiple quality control checkpoints throughout RNA processing that constantly detect such errors, providing a redundant system.

An erroneous transcript is targeted for decay via the RNA exosome (76). This macromolecular RNA processing machine is composed of a ten subunit complex that

forms a barrel-like structure with 3'-5' exoribonuclease activity that is responsible for both precise RNA processing and degradation of aberrant RNAs (76-79). The two catalytic subunits include Rrp44/Dis3 and a nuclear-specific 11th subunit, Rrp6 (76). A major outstanding question in the field is how the exosome distinguishes and targets aberrant RNAs for complete destruction. Given that the RNA exosome can process RNAs to produce mature RNA or degrade aberrant RNAs, there must be a mechanism by which the RNA exosome can distinguish between these two possible fates for a given RNA transcript.

One possibility is that the nuclear exosome relies on a variety of nuclear and cytoplasmic cofactors that modulate the function of the exosome *in vivo*. Two known nuclear exosome cofactors include Rrp6 and the TRAMP (Trf4/5, Air1/2, Mtr4) complex. The nuclear specific exosome component, Rrp6, is responsible for degrading transcripts with aberrant 3' polyadenosine tails (80-82), pre-mRNA transcripts containing introns (83-85), and with aberrant mRNP composition (86, 87). The nuclear exosome cofactor, TRAMP complex, is responsible for adding a short poly(A) tail to promote degradation by the exosome (88). The TRAMP complex contains one of two noncanonical poly(A) polymerases, Trf4/5, the RNA binding proteins, Air1 or Air2, and a putative RNA helicase, Mtr4 (88). Rrp6 and the TRAMP complex may serve to recruit or stimulate the exosome to degrade misprocessed transcripts. However, there may be other RNA exosome cofactors, including RNA binding proteins, that facilitate processing or degradation by the nuclear exosome.

Aberrant transcripts that escape nuclear quality control face cytoplasmic quality control mechanisms (75). The nonsense-mediated decay pathway (NMD) degrades transcripts with premature stop codons (89). Nonstop-mediated decay (NSD) targets transcripts that lack a stop codon (90). No-go decay (NGD) targets transcripts that become stalled on the ribosome during translation (91). The translation of RNA into proteins is a vital part of the Central Dogma, where errors can allow translation of aberrant protein that could be detrimental to the cell. RNA surveillance mechanisms in both the nucleus and cytoplasm help to ensure that only correctly processed transcripts are translated into protein.

mRNA biogenesis is coupled by RNA binding proteins

RNA binding proteins mediate the link between different RNA post-transcriptional processing events (Figure 1.5) (92). Genome-wide studies have revealed preferential association of certain RNA binding proteins with specific target mRNAs, suggesting that the full mRNP profile dictates the biogenesis, export, and translation of distinct mRNA transcripts or classes of RNA transcripts. In addition, many RNA binding proteins that contact the mRNA transcript throughout its post-transcriptional journey have more than one role in mRNA biogenesis. Due to the coupled nature of these events, mutations or defects in mRNA processing factors can give rise to defects in multiple mRNA maturation steps. Thus, the phenotype in cells that have defective RNA binding

proteins could be due to a block early in mRNA biogenesis that manifests itself as a defect detected later in RNA maturation. Alternatively, a defect late in RNA maturation could impair earlier processes. Cells have developed numerous overlapping quality control mechanisms to ensure that faulty mRNA transcripts are not translated into aberrant proteins that could disrupt cellular function (75). One important consequence of coupling RNA processing events is that it leads to a unique formation of mRNP complexes that dictate mRNA transcript fate. Given that RNA binding proteins play roles in multiple mRNA processing events and contact specific RNA targets, it is critical to explore all the molecular mechanisms responsible for integrating mRNA biogenesis. Prior to these studies described in this work, there were few *in vivo* studies investigating the connections between splicing, 3'-end processing, and decay.

Coupling transcription to splicing, 3'-end processing, and export

Many RNA processing reactions occur co-transcriptionally with the help of large proteinaceous complexes that associate with RNA polymerase II (RNAP II). As mRNA is synthesized, numerous RNA binding proteins are deposited onto the transcript to help guide its post-transcriptional journey. Co-transcriptional loading of proteins as well as specific RNA binding proteins allow for coupling between each step of mRNA processing to ensure that all the protein components and modifications necessary for the next step in mRNA biogenesis are present. The earliest form of coupling occurs co-transcriptionally on the C-terminal repeat domain (CTD) tail of RNAP II (2). The CTD consists of multiple repeats of an evolutionary conserved heptapeptide with the consensus

sequence Tyrosine-Serine-Proline-Threonine-Serine-Proline-Serine (YSPTSPS). The CTD is rich in potential phosphoacceptor amino acid residues, particularly at the serine 5 and serine 2 position, that can be subject to reversible phosphorylation. As RNAP II synthesizes pre-mRNA and proceeds from initiation to elongation, the CTD tail undergoes a shift in phosphorylation status from Serine 5 to Serine 2 (2). The CTD tail serves as a flexible scaffold for numerous proteins that are required for mRNA biogenesis. During RNAP II transcription, the RNA binding proteins that associate with the nascent transcript include the THO transcription complex, 5'-capping machinery, splicing factors, 3'-end processing proteins, and export receptors (6, 8, 93, 94). Recruitment of nuclear proteins through the CTD tail serves to couple transcription to other RNA processing events, including 5'-capping, splicing, 3'-end processing, and export.

The CTD plays a key role in linking the splicing machinery to RNA processing by recruiting splicing factors to splice sites. The phosphorylated form of the CTD promotes early spliceosome assembly whereby absence of CTD phosphorylation prevents the recruitment of splicing factors (95). Consistent with this model, truncated versions of the CTD do not support splicing *in vivo* (96). Furthermore, the spliceosomal U snRNPs enhance transcription elongation (97). Recent evidence shows that RNAP II pauses at the 3' end of an intron, accumulates late phosphorylation marks, and continues on to transcription elongation (98). This transcriptional checkpoint ensures that the correct splicing factors are loaded onto nascent pre-mRNA transcripts prior to 3'-end processing

and subsequent mRNA export. Given the link between transcription, splicing, and fidelity, it is interesting to speculate how defects in these processes affect downstream mRNA biogenesis events. Several previous studies have identified a link between splicing and polyadenylation. For example, splicing of the last intron depends on recognition of the poly(A) site (99-101) and conversely 3'-end processing depends on splicing of the last intron (100, 102, 103). This interdependence makes defining the role of specific players critical to understanding the mechanism of gene regulation at distinct steps of RNA processing.

The CTD also acts as a landing platform for 3'-end processing components, from the onset of transcription initiation to transcription termination. There is a progressive 5' to 3' recruitment of cleavage and polyadenylation factors, with the vast majority associating with mRNA towards the 3'end (104, 105). The cleavage factor IA components, Rna14 and Pcf11, interact with the serine 2 phosphorylated form of the CTD tail (2, 104, 106, 107). Co-transcriptional processing sets the stage for tethering multiple RNA processing complexes so that they are in close proximity to increase the rate and specificity of mRNA maturation. Coupling is illustrated by the fact that defects in 3'-end processing impact mRNA export as well as splicing as described in the previous section. The 3'-end processing proteins placed on the mRNA transcript during transcription not only perform their function in cleavage and polyadenylation, but also support efficient mRNA export. Mutations in Rna14, Rna15, and Pap1 block export of all poly(A) RNA (108) and mutations in export factors like Mex67 lead to defects in

poly(A) tails (109).

As the pre-mRNA is synthesized by RNA polymerase II, the transcript is immediately coated with RNA binding proteins required for maturation and packaging. The multiprotein TREX (transcription and export) complex is deposited on the transcript during transcription (110). The *S. cerevisiae* TREX complex consists of the evolutionarily conserved THO complex (Hpr1, Mft1, Thp2, and Tho2) and mRNA export adaptor proteins, Sub2 and Yra1 (66, 94, 111, 112). Both the recruitment and timing for loading of these components are highly regulated and conserved. Sub2 is an ATP-dependent helicase that plays a key role in coordinating splicing and export (113-115). Yra1 is implicated in 3'-end processing and export (116, 117). Interestingly, components of the THO complex copurify with both Yra1 and Sub2 (65, 66), an observation that led to the suggestion that the interaction between the THO complex and Yra1 is mediated by Sub2.

The importance of recruiting Yra1 via Sub2 and the THO complex is highlighted by the fact that Yra1 serves as an adaptor protein to the key mRNA export factor, Mex67 (117). As both Sub2 and Mex67 interact with the same domain of Yra1, there must be an exchange between these two factors (74, 118). An exchange between Sub2 and Mex67 is supported by the fact that the DEAD-box RNA helicase, Dbp2, facilitates loading of Yra1, Nab2, and Mex67 (119). Interestingly, overexpression of Dbp2 results in synthetic lethality with mutants in *mex67-5*, but not *sub2-85* (119). Therefore, Dbp2 is likely responsible for generating processed mRNPs downstream of Sub2 and upstream of

Mex67-mediated export. How other factors, including Nab2, facilitate generation of export-competent mRNPs remains unclear.

Coupling RNA processing to mRNA decay

Nearly every step of mRNA biogenesis requires quality control to detect defects in transcription, mRNA processing, and/or formation of an export-competent mRNP. Quality control mechanisms detect and destroy faulty transcripts, primarily through the help of the nuclear exosome (75). How faulty transcripts are detected and targeted to the RNA surveillance machinery is still poorly understood. However, insights into quality control checkpoints are beginning to uncover key factors that contribute to RNA surveillance. Importantly, many of these key factors are responsible for coupling RNA processing events to the nuclear exosome.

One nuclear quality control mechanism is to retain aberrant mRNAs near the site of transcription. The impaired mRNP assembly THO*/sub2* mutants retain the heat shock gene *HSP104* transcript near the site of transcription in an Rrp6-dependent manner (86, 120). In addition, the *HSP104* transcript is retained in *pap1* mutants that have shorter poly(A) tails (82) and synthetic transcripts lacking poly(A) tails are also retained near the transcription site (121). In budding yeast cells, mutations in the THO complex cause transcription elongation and mRNP assembly defects resulting in rapid transcript degradation by Rrp6 in a Trf4-dependent manner (122). These mRNP assembly defects

may be linked to polyadenylation defects where transcripts with shorter tails are retained and subsequently targeted to the exosome for degradation (120, 123). These data strongly suggest that poly(A) tails facilitate release of mRNA transcripts from the transcription site and that their retention relies on Rrp6-mediated surveillance.

Another facet of mRNA surveillance is nuclear retention of pre-mRNA transcripts. At least in budding yeast, the cells employ the splicing and retention complex (RES) to recognize intron-containing transcripts and retain them within the nucleus (124, 125). The RES complex relies on intact splice site sequences as well as the correct composition of RNA binding proteins (124, 125). Once the pre-mRNA is flagged as misprocessed, nuclear pore components such as the Mlp proteins are required for nuclear retention (126, 127). By retaining pre-mRNA transcripts at the nuclear pore, a choice can be made to continue with mRNA maturation or to proceed with mRNA decay. Both courses of action prevent unspliced RNA from exiting the nucleus and risking translation into protein.

Consequences of coupling RNA processing events: transcript specificity

All mRNAs interact with a series of RNA binding proteins during their mRNA lifecycle to form mRNPs. While many RNA binding proteins share similar RNA binding motifs, RNA binding proteins appear to influence many processes, including 5'-end capping, splicing, 3'-end processing, export, and RNA decay. To understand how numerous RNA binding proteins cooperate to regulate specific transcripts, the RNA

binding protein-protein interactions and RNA binding protein-RNA interactions must be defined. Comprehensive studies comparing multiple RNA binding proteins and their mRNA targets have provided evidence that the same RNA can be bound by multiple factors (128). Cataloguing these RNA binding proteins and their targets has revealed novel functions for RNA binding proteins (128-130). In addition, complementary structural studies have provided important mechanistic information about how RNA binding proteins contact their mRNA targets (128). By understanding the mRNA targets and the function of RNA binding that contact them, we can begin to speculate on how specific transcripts are precisely regulated by their host of RNA binding proteins.

To gain insight into protein-protein and protein-RNA interactions that underlie RNA processing, it is beneficial to investigate cellular programs that require precise gene control. For example, differentiation, proliferation, morphogenesis, pathogenesis, environmental cues, and cell stress all cause large coordinated changes in gene expression. Many of these changes are controlled at the transcriptional level; however, post-transcriptional regulation is a key point of regulation (131). Importantly, many of the RNA processing factors involved in post-transcriptional gene regulation are conserved between these cell processes and function in similar ways to regulate transcript fate (132). Therefore, the question arises about how specific classes of transcripts required for a particular cell process are regulated.

One process that requires extensive post-transcriptional RNA processing is meiosis, whereby a large gene expression profile change is observed in the cell cycle

switch from mitosis to meiosis (133, 134). Recent studies have revealed that meiotic transcripts are expressed during mitosis and subsequently degraded to prevent entry into meiosis (135). Importantly, the meiotic transcripts expressed during mitosis are regulated through post-transcriptional processing events (135). For example, meiotic transcripts remain unspliced and hyperadenylated when bound to the fission yeast RNA binding protein, Mmi1 (136). The Tyrosine-Threonine-Histidine (YTH)-containing Mmi1 protein specifically binds the determinant of selective removal (DSR) element in meiotic transcripts (137). Mmi1 then interfaces with the canonical splicing, 3'-end processing, and nuclear exosome machinery to eliminate meiotic transcripts in vegetative cells (136, 138, 139). This finding is groundbreaking as it is the first evidence that a long poly(A) tail can stimulate RNA degradation. The Mmi1 protein provides an excellent example of achieving transcript specificity through the combination with other RNA binding proteins. One interesting question from these studies is whether Mmi1 interacts with poly(A) RNA binding proteins to mediate hyperadenylation. As Mmi1 has only been characterized in *S. pombe,* another point to investigate is if Mmi1 is conserved in budding yeast or other eukaryotes. If there is a *S. cerevisiae* orthologue, what RNA processing machinery does it contact? Investigating the Mmi1 protein will elucidate some of the post-transcriptional mechanisms the cell uses to control gene expression. Tailored mRNP composition enables transcripts to be regulated in a manner that is appropriate for their function.

Proteins implicated in multiple steps of post-transcriptional regulation couple RNA processing events

A large number of RNA binding proteins bind to and affect the fate of mRNA transcript post-transcriptionally, but one class of proteins that influences gene expression is comprised of poly(A) RNA binding proteins (Pabs) (140). Studies implicate Pabs in a variety of functions including the regulation of mRNA polyadenylation (140), stability (141), nuclear export (142, 143), and translation (144). Conventional Pab proteins bind specifically to the poly(A) tail of RNA through an RNA Recognition Motif (RRM) which consists of a globular domain of four-stranded beta sheets and two alpha helices (145). However, recent studies from our laboratory have defined a new family of zinc finger Pabs (146). The *S. cerevisiae* Nuclear poly(A) RNA Binding protein, Nab2, is the founding member of the zinc finger Pab family (147).

Nuclear poly(A) RNA binding protein, Nab2, is a zinc finger RNA binding protein that is implicated in multiple steps of mRNA biogenesis

Nab2 was first identified as a protein that co-purifies with poly(A) RNA (148) and is essential for the viability of *S. cerevisiae* (149). Although Nab2 is localized to the nucleus at steady state (149), the protein shuttles between the nucleus and the cytoplasm (150). Budding yeast cells mutant for *nab2* contain RNA with extended poly(A) tails and show poly(A) mRNA accumulation in the nucleus (150-152), implicating Nab2 in the control of 3'-end processing and export in budding yeast.

The Nab2 protein contains four key domains (Figure 1.6): an N-terminal domain (residues 1-97), a glutamine (Q)-rich domain (residues 104-169), an Arginine-Glycine-Glycine (RGG) domain (residues 201-261), and a C-terminal tandem zinc finger domain (residues 262-473) (149, 150). The N-terminal domain of Nab2, which facilitates poly(A) RNA export, forms a five alpha-helix bundle with a Proline-Tryptophan-Isoleucine (PWI)-like fold (68, 150). The RGG domain, which is important for nuclear import, mediates interaction with the import receptor, Kap104 (150, 153-155). The Q-rich domain, which is not essential, has not yet been ascribed a function (150). The C-terminal zinc finger domain, which contains seven tandem CCCH-type zinc fingers (ZnF), mediates high affinity binding to polyadenosine RNA (146, 149, 150). The functionally important N- and C-terminal domains of Nab2 are the best characterized domains and play roles in mRNA export and poly(A) tail length control, respectively.

The N-terminal domain of Nab2 (Nab2-N) is functionally important and critical for poly(A) RNA export in budding yeast cells (150, 152). Specifically, *nab2*-Δ*N* cells exhibit severely impaired growth, significant accumulation of bulk poly(A) RNA in the nucleus, and extended poly(A) tails on bulk poly(A) RNA (150, 152, 156). The N-terminal domain of Nab2 (Nab2-N) physically interacts with two key nuclear pore-associated proteins, Mlp1 and Gfd1 (68-72). One face of Nab2-N directly interacts with the large myosin-like platform protein, Mlp1, which localizes to the nuclear side of the nuclear pore complex (NPC) and functions in pre-mRNA retention (68, 126, 157, 158). A second face of Nab2-N directly interacts with the small coiled-coil protein, Gfd1, which

localizes to the cytoplasmic face of the nuclear pore and helps to facilitate mRNP disassembly (71, 72, 159). Nab2 may therefore bind to Mlp1 to concentrate properly processed mRNAs at the nuclear side of the pore for nuclear export and bind to Gfd1 to tether the mRNP at the cytoplasmic face of the pore for disassembly.

The essential C-terminal CCCH-type zinc finger (ZnF) domain of Nab2 is a novel polyadenosine RNA binding domain that specifically recognizes polyadenosine RNA and plays an important role in the regulation of poly(A) tail length (146, 149, 152, 156, 159). Biochemical and genetic analyses of the seven zinc fingers of the Nab2 ZnF domain have revealed that ZnF5-7 are necessary and sufficient for high affinity binding to polyadenosine RNA (152, 156). Critically, cells expressing *nab2* ZnF domain mutants exhibit cold-sensitive growth and poly(A) RNA with extended poly(A) tails (151, 156). Notably, *nab2* mutant cells do not show nuclear accumulation of poly(A) RNA at 16 °C (151, 156). The combined data on Nab2 structure and function thus indicate that Nab2 binds to the poly(A) tails of transcripts during their polyadenylation via the C-terminal ZnF domain and then facilitates targeting of these transcripts to the nuclear pore for nuclear export via the N-terminal PWI-like domain .

A putative human orthologue of Nab2, ZC3H14, shares homology with the N-terminal and C-terminal domains (147). ZC3H14 also exhibits some of the same functions as Nab2 including high affinity binding to polyadenosine RNA and poly(A) tail length control (146, 156). Interestingly, ZC3H14 colocalizes with the splicing factor, SC35, in nuclear speckles, which are nuclear domains enriched in splicing and 3'-end

processing factors (160). These data suggest possible roles for Nab2 in splicing that have not yet been investigated. Notably, mutations in *ZC3H14* result in a form of non-syndromic intellectual disability, revealing a key role for ZC3H14 in neuronal function (147, 161). In order to understand how ZC3H14 modulates brain function, the complete role of ZC3H14 in mRNA biogenesis must be characterized. Given the ease of manipulation of the budding yeast system, studies of Nab2 can inform that function of ZC3H14 and lay groundwork for subsequent studies in analysis of human ZC3H14.

Nab2 and the regulation of poly(A) tail length

Nab2-mediated regulation of poly(A) tail length suggest that Nab2 could genetically and physically interact with 3′-end processing and polyadenylation components. Indeed, *NAB2* genetically interacts with genes encoding the CFIA cleavage factor, *RNA15*, the poly(A) polymerase, *PAP1*, the CPF subunit, *SYC1*, the cytoplasmic Pab, *PAB1*, the nuclear exosome subunit, *RRP6*, and components of the Ccr4-Not deadenylation/transcription complex (93, 151, 156, 162). Nab2 also physically interacts with the Ccr4-Not complex deadenylases, Ccr4 and Caf1/Pop2, and the cleavage factor, Hrp1 (163-165). These data suggest that Nab2 could regulate poly(A) tail length by indirectly modulating cleavage efficiency or by recruiting the exosome to trim polyadenosine tails.

The growing array of proteins implicated in control of poly(A) tail length suggests that the regulation of poly(A) tail length plays a critical role in fine-tuning gene expression. Proper poly(A) tail length depends upon the right balance of polyadenosine synthesis by poly(A) polymerase and polyadenosine trimming by ribonucleases. RNA binding proteins, in particular the poly(A) RNA binding proteins, facilitate control of poly(A) tail length by modulating Pap or ribonuclease activity. However, the RNA binding proteins involved in mediating poly(A) tail length are not well understood in budding yeast. As Nab2 makes numerous contacts with cleavage and polyadenylation factors, deadenylases, and ribonucleases, and causes transcript hyperadenylation upon depletion, Nab2 may sit at the epicenter of poly(A) tail regulation. Understanding the precise molecular mechanism by which Nab2 controls poly(A) tail length will be crucial for understanding to role of Nab2 in mRNA biogenesis.

To gain a more comprehensive view of the regulation of 3′-end processing of an mRNA transcript, the consequences of altered poly(A) tail length must be addressed. Steps in mRNA processing upstream of cleavage and polyadenylation, such as transcription or splicing, and events downstream, such as nuclear export, could have a dramatic impact on the quality of the 3′-end of an mRNA transcript. Changes in the poly(A) tail length of the transcript could act as a signal to the RNA quality control machinery, in which Pabs assist in the recognition of a faulty transcript and communicate this information to nuclear pore components to block the export of the transcript or

trigger ribonucleases to degrade the transcript. Prior to my work, these predictions have not been tested.

A major challenge will be integrating the function of the human Nab2 counterpart, ZC3H14, into the already complicated mammalian RNA processing machinery. To elucidate the mechanisms underlying human disease caused by mutations in genes encoding RNA binding proteins, a major goal is to define the precise mechanistic role or roles of RNA binding proteins in key mRNA processing events.

RNA binding proteins and disease

The coupling of RNA processing events serves as a quality control mechanism to ensure that only correctly processed mature transcripts are produced; and when these processing events go awry, various diseases can develop. Many of these diseases arise from mutation in genes encoding RNA binding proteins (166). Given that RNA binding proteins coordinate an elaborate network of RNA-protein and protein-protein interactions, disrupting RNA binding protein function leads to complex and multifaceted phenotypes. To understand how impaired RNA binding protein function results in human disease, the molecular mechanisms controlling RNA biogenesis must be investigated. In addition, deciphering how ubiquitously expressed RNA binding proteins leads to tissue specific disease must be approached from a mechanistic view.

In fact, several tissue-specific diseases have now been linked to mutations in poly(A) RNA binding proteins. Mammalian nuclear poly(A) RNA binding proteins (Pabs), such as the Nab2 counterpart, ZC3H14, and the nuclear Pab, PABPN1, are ubiquitously expressed in mammalian tissues (160, 167) and likely regulate the expression of numerous mRNA transcripts. Intriguingly, mutations in genes encoding such ubiquitous RNA binding proteins that recognize a broad range of target mRNAs lead to a variety of tissue-specific diseases, including muscular dystrophy and neurological disorders (147, 166, 168, 169). At present, there are two diseases caused by mutations in genes that encode the ubiquitously expressed nuclear Pab proteins. Oculopharyngeal muscular dystrophy (OPMD), an adult onset disease characterized by eyelid drooping, difficulty in swallowing, and weakness in proximal limb muscles, is caused by mutations in the *PABPN1* gene (169, 170). In contrast to the muscle disease caused by mutations in the *PABPN1* gene, mutations in the *ZC3H14* gene causes a form of non-syndromic autosomal recessive intellectual disability (161). Taken together, the ties between RNA binding proteins and disease demonstrate the importance of understanding how RNA processing is modulated to ultimately effect gene control.

Scope and significance of dissertation

The cell has developed numerous co- and post-transcriptional mechanisms to regulate gene expression. Many of these gene control mechanisms are dictated by the function of RNA binding proteins. To understand the complex network underlying

mRNA regulation, I examined how mRNA targets are recognized by RNA binding proteins, how RNA processing events are coupled by RNA binding proteins, and what the functional consequences of altered pre-mRNA processing is. Using Nab2 as a model to understand RNA biogenesis, I was able to define specific residues that Nab2 uses to recognize poly(A) RNA and examine functional consequences that ensue when this poly(A) RNA binding is altered. I identified an interaction between Nab2 and other proteins that function in splicing, degradation, and poly(A) RNA binding. I also began an initial characterization of the meiotic RNA binding protein, Mmi1, to understand how RNA binding proteins cooperate to regulate gene expression. Ultimately, the goal of my dissertation work was to identify how Nab2 and other RNA binding proteins function together to generate export-competent mRNP complexes and ensure proper gene expression.

To gain an understanding of the molecular mechanisms used by zinc fingers to recognize polyadenosine RNA, we used a structure-function based approach in Chapter 2. The solution structure of the Nab2 zinc fingers was solved in collaboration with the Stewart laboratory and critical analysis of the structure revealed several conserved basic and aromatic residues. Given that the Nab2 ZnF conserved residues were solvent exposed, we hypothesized that these amino acids were critical for polyadenosine RNA binding. These predictions were tested by generating amino acid substitutions and performing binding studies *in vitro*. From these studies, we found that several specific basic and aromatic residues mediate the interaction between Nab2 and polyadenosine

RNA. These results were further confirmed by testing amino acid substitutions *in vivo*. A genetic interaction between *NAB2* and genes encoding factors crucial for mRNP assembly was observed. Furthermore, these genetic interactions resulted in poly(A) tail length defects that are not dependent on the affinity for polyadenosine RNA, but are dependent on the interplay between Nab2 and the export machinery. Taken together, our results suggest that Nab2 specifically binds polyadenosine and functions in mRNP assembly.

Given the extensive coupling between RNA processing steps as well as studies of human ZC3H14, I hypothesized that Nab2 may play a role in coupling splicing to 3'-end processing and export. In Chapter 3, I demonstrated that *nab2* mutants result in an accumulation of pre-mRNA both *in vivo* and *in vitro*. I also identified genetic interactions between mutant alleles of *nab2* and genes encoding the splicing factor, *MUD2,* and the RNA exosome, *RRP6*, with *in vivo* consequences of altered pre-mRNA splicing and poly(A) tail length control. I suggest a model where splicing and 3'-end processing are coupled to ensure properly processed mRNA is exported and faulty mRNA is degraded. Thus, a novel link between Nab2, the splicing machinery, and mRNA decay was found in the course of this study.

Multiple Pabs coexist in the nuclei of most eukaryotes. The functional interplay and coordination between these nuclear Pabs is unclear. Importantly, *Schizosaccharomyces pombe* is a genetic model system that contains two nuclear Pabs, Pab2 and Nab2, unlike *Saccharomyces cerevisiae*. The *S. pombe* Nab2 was not

characterized prior to this dissertation. Using sequence analysis in Chapter 4, I confirmed that the budding and fission yeast systems share homology in the N-terminal domain important for export and the C-terminal domain critical for polyadenosine RNA binding. By characterizing the *S. pombe* orthologue of Nab2, we show that the two major fission yeast nuclear Pabs, Pab2 and Nab2, have opposing roles in post-transcriptional gene regulation, at least for specific target RNAs.

During the course of study in Chapter 4, we identified a protein-protein interaction between Nab2 and the fission yeast meiotic RNA binding protein, Mmi1. I, Chapter 5, I carried out an initial characterization of the Mmi1 protein in the budding yeast to understand how meiotic transcripts are regulated in budding yeast. Importantly, these studies lay the groundwork to understand the full collection of RNA binding proteins in the nucleus that influence gene expression. This work provides a model for understanding how specific classes of RNA, including meiotic transcripts, are regulated at the post-transcriptional level.

In summary, this dissertation characterizes the role of Nab2 in generation of export-competent mRNPs. I demonstrate that perturbation to the zinc finger domain of Nab2 results in suboptimal assembly of mRNP export complexes. I propose that the role of Nab2 in splicing contributes to generation of aberrant mRNP complexes as evidenced by an increase in intron-containing transcripts and extended poly(A) tails. I show that these misprocessed mRNAs are targeted to the nuclear exosome. In light of these studies, I also identified the *S. pombe* Nab2 and showed that the fission yeast Nab2 functions in

splicing and RNA decay in tandem with Pab2. Finally, I extend these studies by characterizing the Mmi1 protein to understand how gene expression is regulated by RNA binding proteins in different cellular contexts. Taken together, these studies contributed to the current models of mRNA maturation and quality control by introducing new factors in these processes and by providing data on their mechanism.

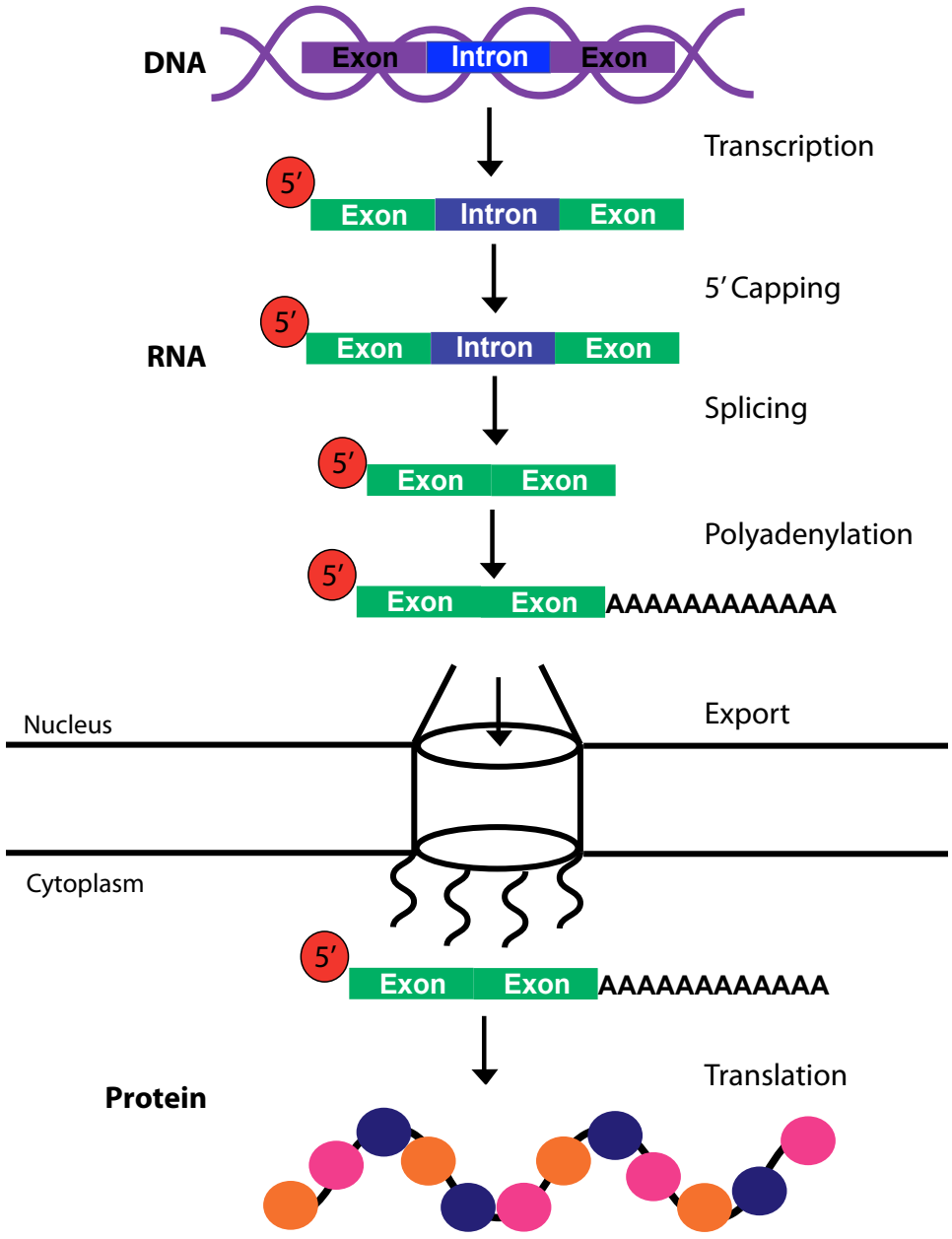

Figure 1.1:Post-transcriptional processing of RNA plays a central role in dictating eukaryotic gene expression. DNA is transcribed into pre-mRNA which undergoes RNA processing to generate mRNA. RNA processing includes capping of the 5' end, pre-mRNA splicing 3'- end processing. Following RNA processing and export into the cytoplasm, the mRNA may be translated into protein.

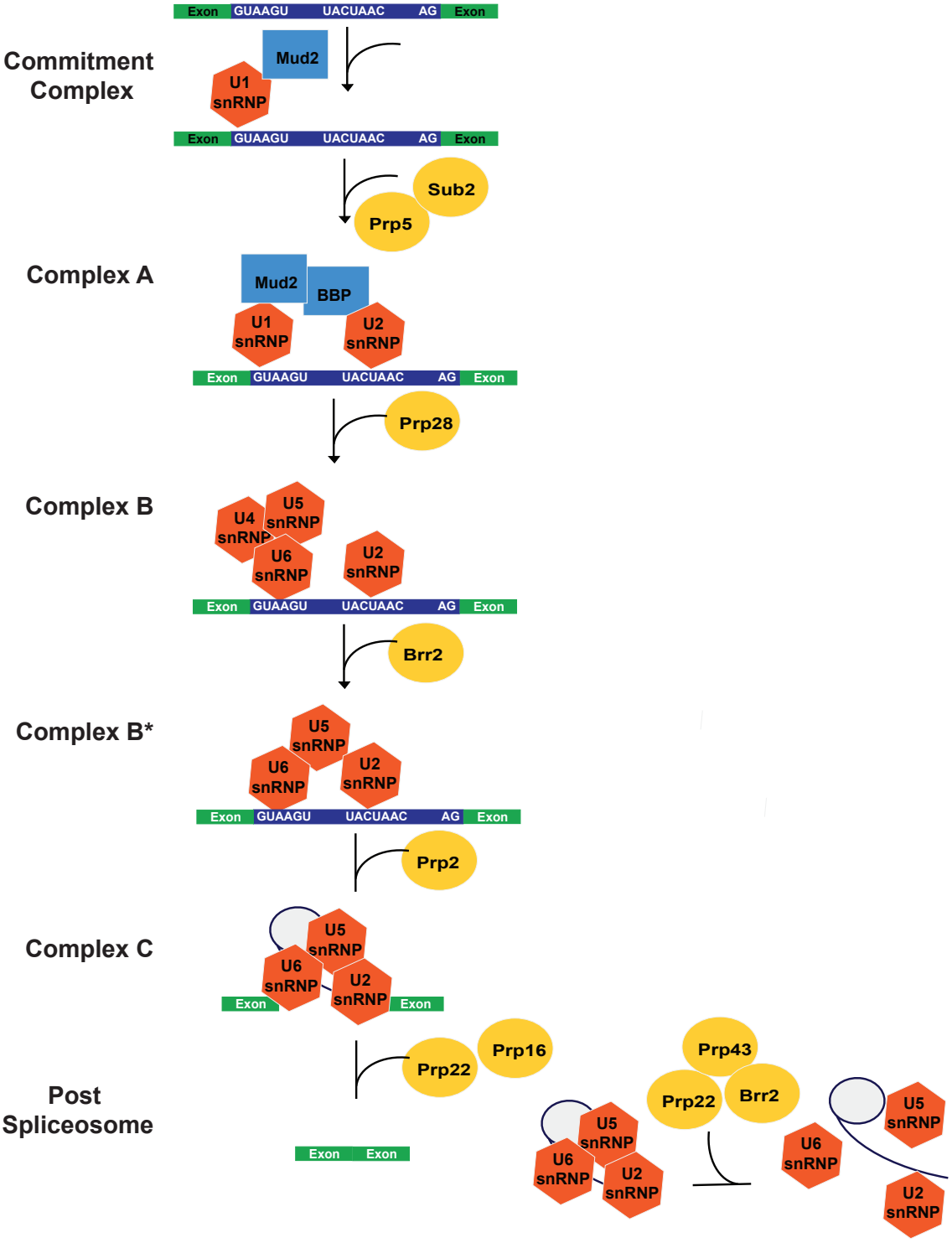
Commitment Complex
Exon GUAAGU UACUAAC AG Exon
Mud2
U1 snRNP
Exon GUAAGU UACUAAC AG Exon
Sub2
Prp5
Complex A
Mud2
BBP
U1 snRNP
U2 snRNP
Exon GUAAGU UACUAAC AG Exon
Prp28
Complex B
U4 snRNP
U5 snRNP
U6 snRNP
U2 snRNP
Exon GUAAGU UACUAAC AG Exon
Brr2
Complex B*
U5 snRNP
U6 snRNP
U2 snRNP
Exon GUAAGU UACUAAC AG Exon
Prp2
Complex C
U5 snRNP
U6 snRNP
U2 snRNP
Exon
Exon
Prp16
Prp22
Post Spliceosome
Exon Exon
Prp43
Prp22
Brr2
U5 snRNP
U6 snRNP
U2 snRNP
U5 snRNP
U6 snRNP
U2 snRNP

Figure 1.2: Pre-mRNA splicing is mediated by snRNAs and proteins. Stable association of U1 snRNP at the 5' splice site initiates commitment of the pre-mRNA to the splicing pathway (Commitment complex). Binding of U2 snRNP to the branchpoint forms Complex A. Addition of the tri-snRNP to the pre-spliceosome forms the complete spliceosomal complex (Complex B), but the subsequent removal of U1 snRNP and U4 snRNP is required to make catalytically active spliceosomes (Complex B* and C). The spliceosome is disassembled to release the lariat and join exons (Post spliceosome). Eight DExD/H-box ATPases (Prp5, Sub2, Prp28, Brr2, Prp2, Prp16, Prp22, and Prp43) contribute to sequential assembly of the spliceosome at the noted steps.

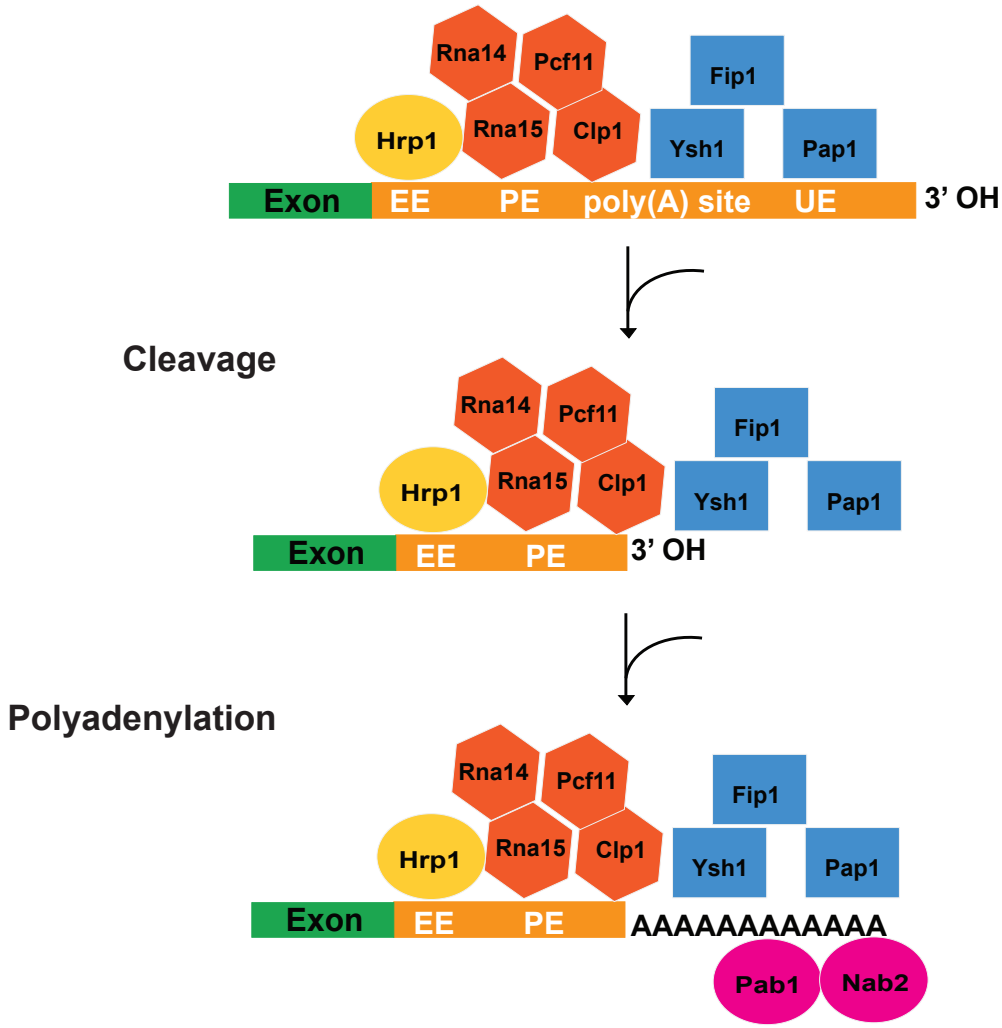

Figure 1.3: 3'-end processing is a coupled cleavage and polyadenylation reaction. The polyadenylation signal (PAS) in the 3′-UTR of the transcript is recognized by the cleavage machinery, cleavage factor IA ((CFIA); Rna14, Rna15, Clp1 and Pcf11), cleavage factor IB ((CFIB); Hrp1), and the cleavage and polyadenylation factor ((CPF); a complex including riboendonuclease, Ysh1/Brr5 (CPSF73 in mammals), the poly(A) polymerase, Pap1, and the Pap1 regulation factor, Fip1). For cleavage at the poly(A) site (pA) in the 3′-UTR of the transcript, Rna15 together with other CFIA subunits recognizes the A-rich positioning element in the PAS to position CPF to cleave the poly(A) site. Hrp1 binds to the AU-rich efficiency element in the PAS and influences the efficiency of the cleavage reaction. Following cleavage, CPF-stimulated Pap1 processively synthesizes the poly(A) tail. During polyadenylation, the poly(A) RNA binding proteins, Nab2 and Pab1, bind to the nascent poly(A) tail.

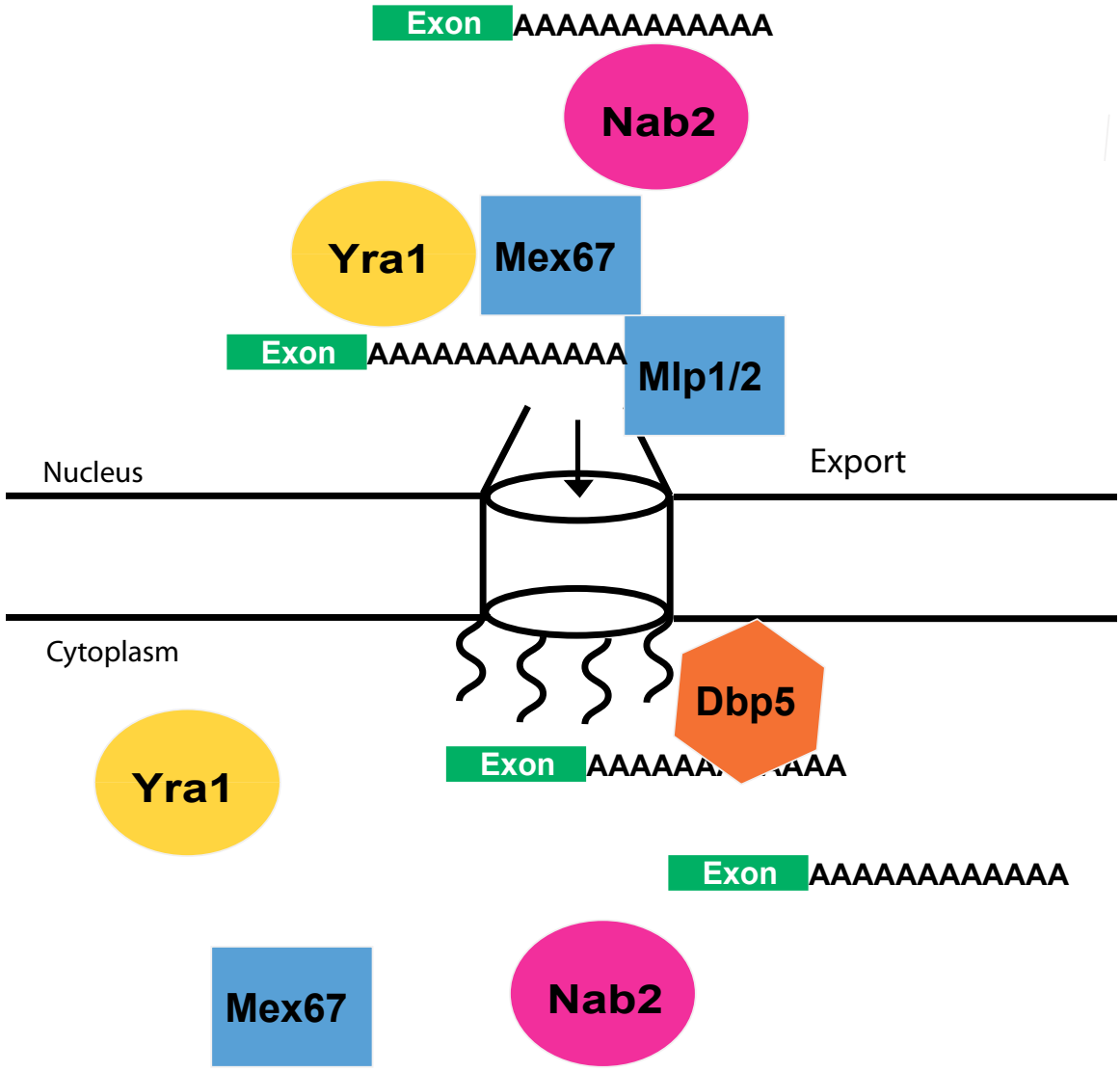

Figure 1.4: Translocation of mRNP complexes through the nuclear pore. After RNA processing, mRNA export adaptor proteins, including Nab2 and Yra1, associate with the mRNA transcript. Nab2 contacts the nuclear pore associated protein, Mlp1/2. After the transcript acquires the correct RNP composition, the mRNP associates with the mRNA export receptor, Mex67. The mRNP then passes through the nuclear pore and the RNP factors are disassociated via the DEAD-box RNA helicase, Dbp5.

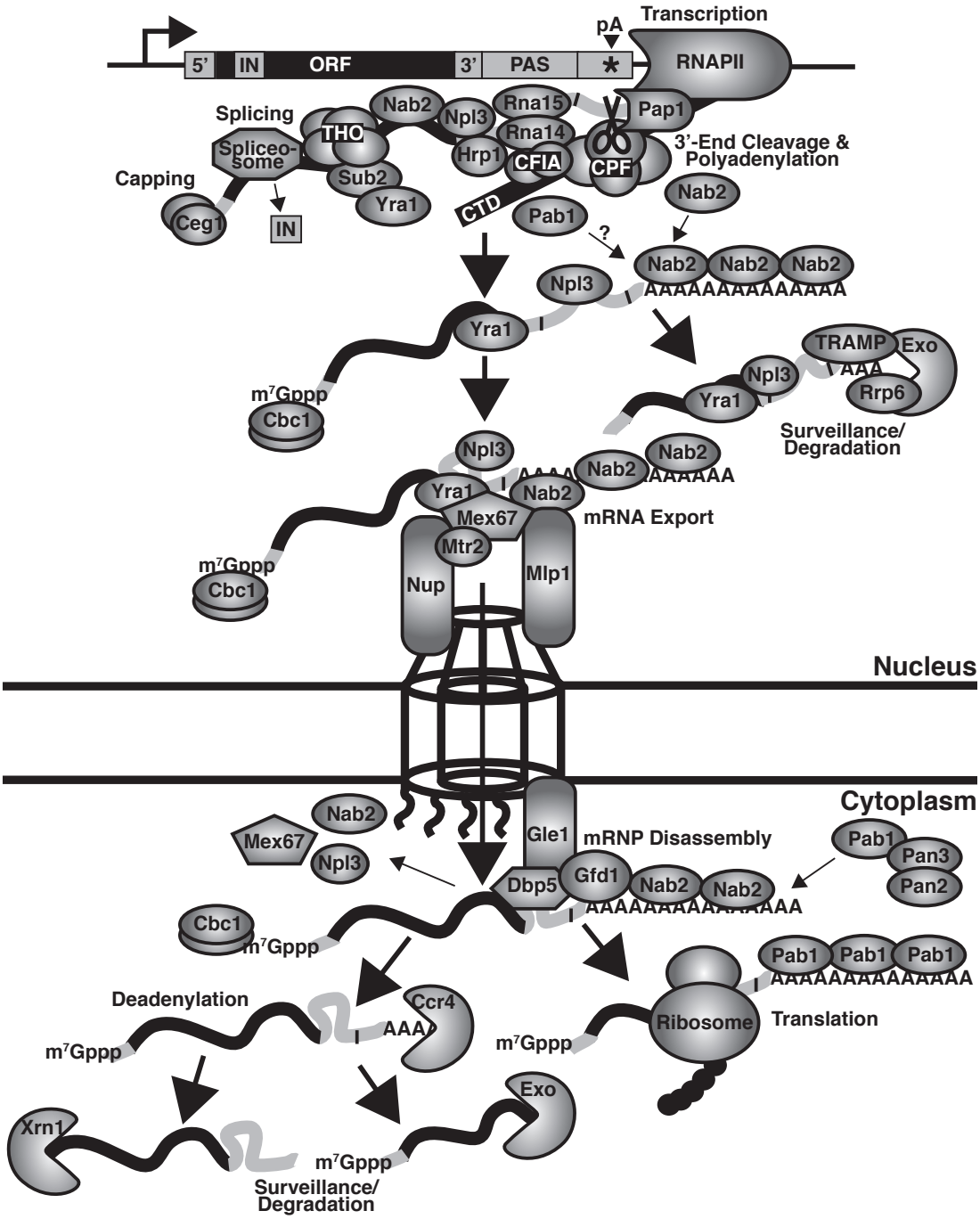
Transcription
pA
5'
IN
ORF
3'
PAS
*
RNAPII
Splicing
Spliceo-some
Nab2
Npl3
Rna15
Pap1
THO
Rna14
Hrp1
CFIA
CPF
3'-End Cleavage & Polyadenylation
Capping
Ceg1
IN
Sub2
Yra1
CTD
Pab1
?
Nab2
Nab2
Nab2
Nab2
AAAAAAAAAAAAAA
Npl3
Yra1
m7Gppp
Cbc1
TRAMP
Exo
AAA
Npl3
Yra1
Rrp6
Surveillance/ Degradation
Npl3
Nab2
Nab2
AAAAAA
Yra1
Nab2
Mex67
mRNA Export
Mtr2
m7Gppp
Cbc1
Nup
Mlp1
Nucleus
Cytoplasm
Nab2
Mex67
Npl3
Gle1
mRNP Disassembly
Pab1
Pan3
Pan2
Dbp5
Gfd1
Nab2
Nab2
AAAAAAAAAAAAAAA
Cbc1
m7Gppp
Pab1
Pab1
Pab1
AAAAAAAAAAAAAA
Deadenylation
Ccr4
AAA
m7Gppp
Ribosome
Translation
m7Gppp
Exo
Xrn1
m7Gppp
Surveillance/ Degradation

Figure 1.5: RNA processing is coupled by RNA binding proteins. During RNA polymerase II (RNAPII) transcription, the THO transcription elongation complex (Tho2, Hpr1, Mft1, and Thp2), the ATPase, Sub2, the mRNA export cofactor, Yra1, the mRNA binding SR protein, Npl3, the poly(A) binding protein, Nab2, and other mRNA processing factors are all recruited to the nascent transcript. Following capping and splicing, the polyadenylation signal (PAS) in the 3′-UTR of the transcript is recognized by the cleavage machinery, cleavage factor IA ((CFIA); Rna14, Rna15, Clp1 and Pcf11), cleavage factor IB ((CFIB); Hrp1/Nab4), and the cleavage and polyadenylation factor ((CPF); a complex including riboendonuclease, Ysh1/Brr5 (CPSF73 in mammals), the poly(A) polymerase, Pap1, and the Pap1 regulation factor, Fip1). For cleavage at the poly(A) site (pA) in the 3′-UTR of the transcript, CFIA protein, Rna15, which contains a single RNA recognition motif (RRM), together with other CFIA subunits recognizes the A-rich positioning element (e.g. AAUAAN) in the PAS to position CPF to cleave the poly(A) site. Hrp1, which contains two RRMs, binds to the AU-rich efficiency element (e.g. UAUAUAU) in the PAS and influences the efficiency of the cleavage reaction . Following cleavage, CPF-stimulated Pap1 processively synthesizes the poly(A) tail. During polyadenylation, Nab2 likely binds to the nascent poly(A) tail. Transcripts that are improperly processed (e.g. contain short poly(A) tails) due to defective 3′-end processing and polyadenylation are recognized, retained in the nucleus and degraded by the nuclear exosome riboexonuclease complex (Exo), containing the 3′-5′ riboexonuclease subunit, Rrp6. Recognition of RNA targets by the exosome is facilitated by exosome cofactors, such as TRAMP. Together with the mRNA export cofactor, Yra1, Nab2 helps to recruit the heterodimeric mRNA export receptor, Mex67-Mtr2, to facilitate the nuclear export of the transcript . Nab2 also interacts with the nuclear pore complex-associated protein, Mlp1, to facilitate targeting of the transcript to the pore. Following Mex67-mediated export to the cytoplasm, Gfd1 helps tether Nab2 to the cytoplasmic face of the pore, while the RNA helicase, Dbp5, facilitates mRNP dissociation of Nab2, Npl3, Mex67, and other RNA-binding proteins from the transcript. During mRNP remodeling, the cytoplasmic Pab, Pab1, may bind to the poly(A) tail of the transcript to replace Nab2 in an exchange step. As Pab1 shuttles between the nucleus and cytoplasm and can bind the Rna15 CFIA cleavage factor, Pab1 likely initially loads onto the transcript in the nucleus. The cytoplasmic Pab1-bound transcript can then be translated or turned over. For cytoplasmic mRNA decay, the transcript is first deadenylated by the Ccr4-Not complex deadenylases, Ccr4 and Caf1. The transcript body is then decapped by Dcp2 and degraded from the 5′-end by the 5′-3′ riboexonuclease, Xrn1, or degraded from the 3′-end by the cytoplasmic exosome. Pab1 can also recruit the Pan2-Pan3 deadenylase complex (Pan2 is the deadenylase) to trim the poly(A) tails of specific transcripts. (171)

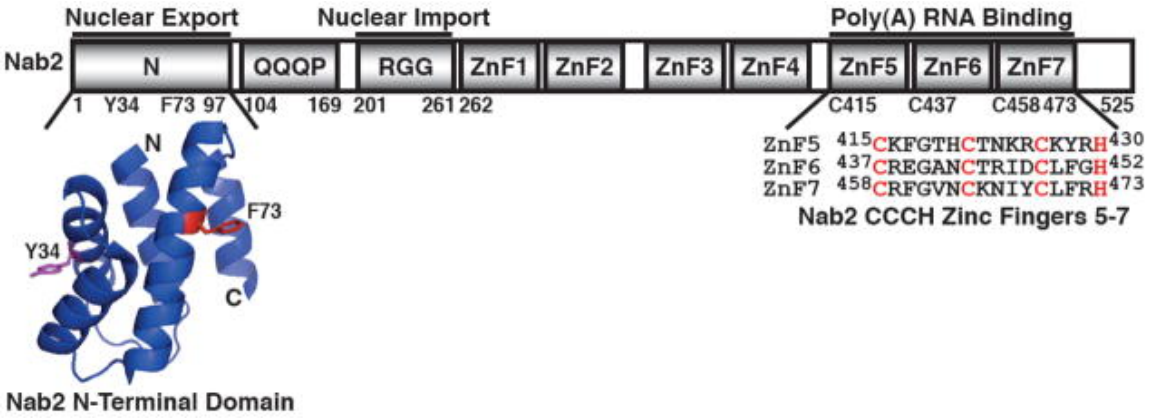

Figure 1.6: Functional domains of Nab2. Nab2 is a 525 residue protein that possesses four key domains: an N-terminal domain (residues 1–97), a Q-rich domain (residues 104–169), an RGG domain (residues 201–261), and C-terminal tandem zinc finger domain (residues 262–473). The N-terminal domain of Nab2 (Nab2-N) facilitates nuclear export of poly(A) RNA and interacts with nuclear pore-associated Mlp1 protein in the nucleus and the nuclear rim-associated Gfd1 protein in the cytoplasm. The crystal structure of the N-terminal domain of Nab2 reveals that Nab2-N forms a five alpha-helix bundle with a proline–tryptophan–isoleucine (PWI)-like fold. The key residue Phe73 (red) that is important for interaction with Mlp1 and Tyr34 (magenta) that is critical for interaction with Gfd1 are highlighted. The RGG domain mediates interaction with the Nab2 import receptor, Kap104. The Q-rich domain is not essential and currently has no characterized function. The C-terminal zinc finger domain contains seven tandem CCCH-type zinc fingers (ZnF) and mediates specific high affinity binding to polyadenosine RNA. (171)

Chapter 2: Structural and Functional Basis for Polyadenosine Binding by Nab2

A portion of this chapter is adapted from the following published work:

Brockman, C., **Soucek, S**., Kuhlmann, S., Lujan K. M., Kelly, S.M., Yang, J., Iglesias N., Stutz, F., Corbett, A.H., Neuhaus, D., and Stewart, M. (2011) *Structure* **20,** 1007- 1018. "Structural Basis for Poly(A) RNA Binding by a Nab2 Zn Finger Repeat and its Function in Nuclear Export."

Structural studies were performed by Christoph Brockmann, Ph.D. and Murray Stewart, Ph.D. at the MRC Laboratory of Molecular Biology in Cambridge, UK.

INTRODUCTION

Nuclear export of mRNA is the culmination of the nuclear phase of the gene expression pathway and appears to be mediated by a Brownian ratchet mechanism that involves three principal steps: formation of an export-competent mRNP (messenger ribonucleoprotein); translocation of this mRNP though nuclear pore complexes (NPCs); and disassembly of the export complex in the cytoplasm (7, 172, 173). Before export, nascent transcripts progress through a coordinated series of modifications, including 5'-capping, splicing, and 3'-cleavage/polyadenylation, that are mediated by a host of mRNA-binding proteins (8, 94, 172-175). In budding yeast, nuclear export of bulk mRNA is mediated primarily by Mex67:Mtr2 that binds both mRNPs and NPC proteins (8, 94, 172-175). Generation of export-competent mRNPs (reviewed by (8, 94, 172-175)) is accomplished following termination of 3' end processing and polyadenylation, in which the 3'-end processing factor Pcf11 recruits the Yra1 adaptor that then recruits Mex67:Mtr2 (116). This recruitment may be assisted by Nab2 (176), a conserved polyadenosine-RNA-binding Zn-finger protein required for both mRNA export and polyadenylation regulation (146, 149-152, 160, 161) that appears to become attached to the mRNP after splicing and during or immediately after polyadenylation (176). After Mex67:Mtr2 binds, the mRNP is remodeled, during which Yra1 is removed (74), although Nab2 remains attached. Transport directionality is imposed by the RNA helicase, Dbp5, removing Mex67:Mtr2 in the cytoplasm, thereby preventing return of the mRNP to the nucleus (7, 177-179). The *dbp5(rat8-2)* conditional allele (180) has been

used extensively to study mRNA nuclear export and is thought to encode Dbp5 with impaired helicase activity(71-73, 156, 181).

How Nab2 contributes to mRNP assembly and disassembly is currently unclear. Nab2 appears to associate with the bulk of mRNAs before they are exported and although localized to the nucleus at steady-state, it shuttles between the nucleus and cytoplasm (150, 152). The Nab2 protein contains four domains: an N-terminal PWI-like domain that interacts with NPCs (71) (68, 72) followed by a Gln-rich linker; then an Arg-Gly (RGG) domain required for nuclear import (153); and finally a domain containing seven tandem CCCH Zn-fingers (ZnF) that binds polyadenosine-RNA *in vitro* and also contributes to polyA tail length control and the checkpoint for proper 3' processing (146, 156). Zinc-fingers 5-7 (ZnF5-7) are necessary and sufficient for high affinity polyadenosine-RNA binding (156). Nab2 remains attached to mRNPs during passage through NPCs and is removed at their cytoplasmic face by Dbp5 (73). Interestingly, mutation of the gene encoding the human Nab2 counterpart, *ZC3H14*, leads to an inherited form of intellectual disability (146, 160), highlighting the importance of this protein in the brain of higher organisms.

Here we describe the solution structure of Nab2 ZnF5-7 and explore their interaction with polyadenosine-RNA. These three Zn-fingers have almost identical folds and, most unusually, associate with one another to form a single coherent structural unit. ZnF5-7 bind to eight consecutive adenines and chemical shift perturbations identify residues on each finger that interact with RNA. These data, combined with the changes in

affinity associated with mutation of key residues within each finger, indicate that the binding of ZnF6 to polyadenosine-RNA is different to that of fingers 5 and 7 and also indicate that Nab2 Zn-fingers function in the generation of export-competent mRNPs.

RESULTS

Nab2 Zn-fingers 5-7 form a single domain

The solution structure of a Nab2 fragment (residues 409-483) containing Zn-fingers 5-7 (ZnF5-7) was determined using NMR spectroscopy (Figure 2.1 Table 2.1). A striking and unexpected feature of the structure was that the three Zn-fingers (residues 410-480) formed a single ordered domain (Figure 2.1A,B). The relative orientations of the Zn-fingers were defined by unambiguous inter-finger NOE contacts. There were 69 contacts assigned between ZnFs 5 and 6 (mainly linking Lys410 to Ile446; Leu412 to Thr444 and Ile446; Gln414 and Lys416 to Ile454; and Ala431-Ser433 to Leu449-Gly451), 27 contacts between ZnFs 6 and 7 (mainly linking Met436 to Tyr468 and Leu470; and Ile454 to Leu470 and Phe471) and 14 contacts between Zn-fingers 5 and 7 (mainly linking Gln414, Gly418 and Ala431 to Leu470, and His434 to Tyr468). The spatial organization of ZnF5-7 resulted in the overall precision of the fragment when considered as a single entity (average pairwise backbone rmsd of residues 410-480 was 0.41Å) being comparable to those of the individual Zn-fingers. Average pairwise backbone rmsds for ZnF5, (residues 414-431), ZnF6 (residues 436-453) and ZnF7

(residues 457-474) were 0.26Å, 0.14Å, and 0.12Å, respectively. (Figure 2.1A,B). Moreover, superpositions of the ensembles of individual Zn-fingers (Figure 2.1D,E,F) were only marginally superior to the ensemble for the entire structure (Figure 2.1A,B).

Analysis of heteronuclear NOEs confirmed the relatively fixed relationship between the three Zn-fingers. Apart from a small number of residues at each end of the construct (N-terminal GPLGS cloning artifact and residues 481-483), the backbone rigidity as evidenced by the heteronuclear NOE data was essentially uniform along the entire fragment, with no additional flexibility evident in the inter-finger linker regions. Zn-fingers 5, 6 and 7 form an approximate right-handed helix, although the relative orientation between fingers 6 and 7 is not a precise recapitulation of that between fingers 5 and 6.

Structure of individual Zn fingers

Each finger has an identical CCCH pattern of Zn-ligating residues (Figure 2.2). For convenience, we refer to residues in corresponding locations across the seven Nab2 Zn-fingers using a numbering scheme in which the first metal-binding Cys in each finger is assigned position 1 (Figure 2.2). Thus, the Zn-binding residues correspond to positions 1, 7, 12 and 16 (residues Cys415, Cys421, Cys426 and His430 in ZnF5; Cys437, Cys443, Cys448 and His452 in ZnF6; and Cys458, Cys464, Cys469 and His473 in ZnF7). In each finger, the coordination by His is through N^{e2} and the absolute chirality of Zn-binding is

R (see (182)). Compared to other Zn-fingers, those in Nab2 are very small, with each containing only 17 residues, and are devoid of secondary structure, consisting only of short loops running between the Zn-binding residues. All three fingers have similar structures (Figures 2.1 and 2.3), consistent with their sequence conservation (Figure 2.2). Their fold has some similarity to the ssRNA-binding tandem Zn-finger motifs found in TIS11d (183) and MBNL1(184) (Figure 2.3A), although the short helix found between Zn ligands 1 and 2 in other tandem Zn finger motifs is absent in Nab2 and there are generally two or three fewer residues between Zn-ligands 1 and 2 in each of the Nab2 fingers. There are also structural differences in the region between Zn-ligands 2 and 3, where the Nab2 Zn-fingers each contain four residues. The way in which Nab2 ZnF5-7 interact with one another to form a pseudo-helical arrangement (Figure 2.1A,B) is quite novel. In contrast, the two fingers of TIS11d are structurally independent (183) and in MBNL1 the head-to-tail arrangement of the two fingers is determined by a small anti-parallel b-sheet that forms between them (184).

RNA binding surface of Zn-fingers 5-7

Determination of the affinity of progressively longer polyadenosine-RNAs using ITC indicated that Nab2 Zn-fingers 5-7 bound eight adenines (Figure 2.4). Thus, the affinity of A_6 and A_7 was 14 μM but increased to the order of 100 nM for A_8, A_9 and A_{10}. Although chemical shift titration experiments with RNA containing more than three

adenines were difficult to interpret because of line-broadening, for AMP and A_3 the extent of line-broadening caused by complex formation with Nab2 ZnF5-7 was sufficiently low to enable high-resolution measurements to be made, possibly because the lower affinities of these ligands moved the exchange rates into a faster regime that was more favourable for detection of NMR signals. Figure 2.5A,B shows amide chemical shift perturbation experiments in which either AMP or A_3 was added to ZnF5-7. With AMP, all three fingers showed the strongest perturbation at a highly conserved basic residue adjacent to the first Zn-binding Cys (position 2; Lys416, Arg438, Arg459) and its immediate neighbours (Figures 2.1C, 2.2, 2.5A). The response to A_3 binding was somewhat less clear-cut and involved additional residues (Figure 2.5B), consistent with the larger ligand forming a larger and more complex set of interactions. The largest and most extensive perturbations were seen for finger 5 and, as seen with AMP, there were large perturbations at or near the basic residue at position 2 for all three fingers, albeit now affecting a larger group of residues in this region. There were additional large perturbations at sites at or near position 9 (Asn423, Ile446, Lys465) and the conserved aromatic residue at position 14 (Tyr428, Phe450, Phe471). Generally these residues are conserved between the seven Nab2 Zn-fingers, especially the basic residue at position 2 and the aromatic at position 14 (Figure 2.2). For some other positions conservation is more limited and is restricted to Zn-fingers 3, 5 and 7. This trend is particularly clear for the aromatic residue at position 3, which becomes a charged residue in Zn-fingers 2, 4 and 6, and to a lesser extent for the Asp at position 9.

Approximate binding constants for the individual fingers of ZnF5-7 derived from the A_3 chemical shift perturbation data (Figure 2.5C) indicated that ZnF6 has a markedly lower binding affinity for A_3 than do ZnF5 or ZnF7. Sequence comparisons indicated that the lower affinity exhibited by ZnF6 might be due to the absence of an aromatic residue at position 3 (which is instead Glu at position 439). Consistent with this hypothesis, the Nab2-E439F variant restored the affinity of ZnF6 to levels comparable to those of fingers 5 and 7 (Figure 2.5D). Overall these results indicate that, although fingers 5 and 7 interact with polyadenosine-RNA in similar ways, finger 6 appears to contribute to binding in a different way. The seven Nab2 Zn-fingers probably bind 20-25 adenosines *in vitro* (185). Although the three high affinity binding Zn-fingers of Nab2, ZnF5-7, bind to a stretch of eight adenosines, fingers 1-4 exist as two closely spaced pairs separated by a 39-residue linker and so are unlikely to form a compact structure similar to that observed for fingers 5-7. Thus, an estimate of an additional 12-17 nucleotides bound by fingers 1-4 in addition to the 8 nucleotides bound by fingers 5-7 seems quite consistent with the measurements obtained for all seven fingers.

Nab2-C437S destabilizes ZnF6 and structural coherence between ZnF5 and ZnF7 is lost

The importance of the structural coherence between Zn-fingers 5-7 is underlined by Nab2 variants in which Cys437, one of the Zn-binding residues of ZnF6, is mutated

(to Ala, Ser or Arg). These variants bind polyadenosine -RNA more weakly than wild-type Nab2 and suppress the *dbp5(rat8-2)* phenotype(73, 146, 156). Mutation of Cys437 would be expected to destabilize ZnF6, because a Zn-binding residue is altered. Direct comparison of the ^{15}N-HSQC spectra of wild-type and C437S-Nab2 ZnF5-7 (Figure 2.6A,B) showed that peaks close to the original positions of the finger 5 and 7 amides are retained, consistent with these fingers still being folded, whereas most of the peaks from ZnF6 are significantly broadened, indicating exchange between different conformations. The comparison of ^{1}H-^{15}N RDC data from the wild-type construct and from the mutant indicates Nab2-C437S has a higher degree of relative mobility, since RDCs of fingers 5 and 7 are significantly reduced in magnitude for the mutant (Figure 2.6C). In addition, a strong correlation was seen between RDCs measured for ZnF7 in the wild-type and those measured in the C437S mutant, whereas a similar correlation was not seen for RDCs measured for ZnF5 (Figure 2.6D). This finding suggests that the alignment to the medium may be dominated by ZnF7 in both cases, but because the orientation of ZnF5 is no longer rigidly related to that of ZnF7 in the C437S mutant, the RDCs observed at ZnF5 in the mutant become markedly different to those in the wild type protein. Taken together, these results indicate that in C437S-Nab2, fingers 5 and 7 retain their structure, whereas ZnF6 is destabilized, leading to an enhanced flexibility of ZnF5 relative to ZnF7. Significantly, the affinity of the C437S variant for A_8 was reduced ~40-fold to 19 μM (Table 2.2), consistent with the structural coherence of ZnFs 5-7 being important for the binding to polyadenosine -RNA.

Engineered Nab2 variants confirm the chemical shift perturbation results

The role of the interactions detected using chemical shift perturbations was explored using a range of engineered Nab2 variants. ZnF6 differs from fingers 5 and 7 in having Glu rather than Phe in position 3 (Figure 2.2) and NMR titrations indicated that ZnF6 had substantially reduced affinity for A_3 relative to fingers 5 or 7 (Figure 2.5C). The importance of position 3 was confirmed by interchanging these residues. Mutating Phe in position 3 to Glu in either finger 5 or 7 (F417E and F460E, respectively) reduced the affinity of ZnF5-7 for A_8 by roughly 40-fold, and simultaneous mutation of both Phe417 and Phe460 reduced affinity further (Table 2.2). Mutation of the Glu of ZnF6 to Phe (E439F) increased affinity for A_8 marginally (Table 2.2) (although for binding of A_3 the corresponding increase was greater; Figure 2.5B). Decreases in affinity for A_8 to ~10-50 μM were observed following mutation of the basic residues in position 1 of each finger (K416A, R438A or R459A), albeit the decrease in affinity seemed to be about 2-fold greater for ZnF6, consistent with its making a different contribution to polyadenosine-RNA binding than fingers 5 and 7. The affinity of C437S was similar to that observed for F417E or F460E and was consistent with each finger in this variant now binding polyadenosine-RNA independently rather than in concert as in the wild-type.

Functional impact of mutations in Nab2 fingers 5-7

The role of specific residues within Nab2 ZnF5-7 was examined by engineering amino acid substitutions in Nab2 and assessing their function in yeast lacking the endogenous essential *NAB2* gene using a plasmid shuffle assay (Table 2.2). None of the individual residues examined was absolutely required for the essential function of Nab2 because in each case cell growth was identical to wild-type cells at 30˚C (Table 2.2 and Figure 2.7A). Previous work showed that the C437S mutation, which decreases the affinity of Nab2 for polyadenosine-RNA, suppresses the temperature-sensitive phenotype of the *rat8-2* allele of *DBP5,* which remodels the mRNP at the NPC cytoplasmic face (73, 156). Significantly, several engineered Nab2 Zn-finger variants showed at least some suppression (Table 2.2 and Figure 2.7B) of the temperature sensitive growth of *dbp5(rat8-2).* Although C437S-Nab2 was the strongest suppressor, variants in ZnF6 (C437S, R438A, F450A) that had reduced affinity for A_8 also showed some suppression. However, several Zn-finger 5 and 7 variants that had similarly reduced affinity (K416A, R459A, F460E) did not show suppression of *dbp5(rat8-2)*. The only variant not located in ZnF6 to show substantial suppression combined changes in both fingers 5 and 7 (F417E+F460E double mutant) and had very low affinity for polyadenosine-RNA. Overall, these findings are not consistent with the hypothesis (73) that simply decreasing the affinity of Nab2 for polyadenosine-RNA leads to suppression of the temperature-sensitive growth of *dbp5(rat8-2)* cells. Although a minimum threshold affinity for

polyadenosine-RNA (stronger than ~20 μM) might be necessary for suppression of *dbp5(rat8-2)*, the most consistent correlation was with mutations located in ZnF6.

Several Nab2 Zn-finger variants generated mRNAs with longer polyA tails (Figure 2.7C and Table 2.2). However, although some variants (K416A, R459A, F460E) in which the affinity for polyadenosine-RNA *in vitro* was reduced to ~20 μM retained wild-type polyA tail length control, there was a stronger correlation between suppression of *dbp5(rat8-2)* and hyperpolyadenylation, both of which were observed for the C437S, R438A, F450A, and F417E+F460E variants (Table 2.2). As observed previously for Nab2-C437S and -F450A(156), none of the Nab2 Zn-finger variants tested showed aberrant nuclear accumulation of polyA-RNA, indicating that they are not rate-limiting for polyA-RNA export (Figure 2.8).

In addition to suppressing *dbp5*(*rat8-2)*, many of the engineered Nab2 Zn-finger variants also suppressed the *GFP-yra1-8* mutant (186) (Vinciguerra et al. 2005) (Table 2.2 and Figure 2.7D). Yra1p functions as an adapter for recruiting Mex67:Mtr2 but it is removed from mRNP complexes prior to exit from the nucleus(74). Again, *nab2-C437S* showed the strongest suppression and generally variants that showed some suppression of *dbp5(rat8-2)* also suppressed *GFP-yra1-8* and showed altered polyA tail length. Strikingly these defects do not correlate simply with a decreased affinity for polyadenosine-RNA, indicating that Nab2 has an additional function early in the mRNA export pathway associated with the generation of export-competent mRNPs.

DISCUSSION

Implications for mRNA nuclear export

The *in vivo* results obtained using structure-based variants indicate that, in addition to controlling polyA tail length, Nab2 functions in the generation of export-competent mRNPs. Nuclear mRNA export is terminated by the removal of Mex67:Mtr2 by Dbp5 at the NPC cytoplasmic face (7, 74, 177-179). Because *nab2-C437S* suppresses the temperature-sensitive growth of *dbp5(rat8-2)* cells, it has been suggested that Dbp5 could remove Nab2 as well as Mex67:Mtr2 from the mRNP (73).This hypothesis was supported by the finding that Nab2-C437S binds more weakly to polyadenosine-RNA than wild-type and is more readily removed from RNA by Dbp5 (73, 146). However, this weaker binding of Nab2-C437S to polyadenosine-RNA does not appear to explain its suppression of *dbp5(rat8-2)*, because, as shown in Table 2.2, we generated several other Nab2 variants that bind polyadenosine-RNA with affinity comparable to that of Nab2-C437S, but which do not suppress the *dbp5(rat8-2)* allele. Therefore, suppression of *dbp5(rat8-2)* by *nab2* alleles does not seem to stem directly from removal of Nab2 at the NPC cytoplasmic face. Instead, the suppression of *dbp5(rat8-2)* by *nab2* alleles may derive from suboptimal mRNP assembly within the nucleus generating a configuration that can be more easily disassembled by Dbp5 to remove Mex67:Mtr2. In principle, Nab2-C437S could influence mRNP export complex disassembly either by increasing the efficiency of disassembly, or by weakening the binding of Mex67:Mtr2 to the mRNP, either through an impaired adaptor function or by generating an aberrant export complex

that is less stable than wild-type. Although the activity of Dbp5 can be augmented by Gfd1(180), which appears to function as a scaffold to increase the local concentration of the components of the mRNP disassembly machinery (71, 72), it is not easy to see how mutating the Nab2 Zn-fingers could enable Gfd1 to function in this way. Similarly, although Nab2 may also act as an adaptor to recruit Mex67:Mtr2 to the mRNP (67), the interaction between these proteins involves the Nab2 RGG domain and not the Zn-fingers. Taken together, these results indicate that it is unlikely that the suppression of *dbp5(rat8-2)* by the ZnF6 C437S mutation results from a direct effect in the cytoplasm.

Although the affinity of the Nab2 variants for RNA did not correlate with genetic suppression of *dbp5(rat8-2)*, this suppression correlated more closely with impaired control of polyA tail length and also with suppression of the GFP-*yra1-8* allele (Table 2.2 and Figure 2.7C,D). As Nab2 is thought to modulate polyA tail length within the nucleus, this correlation suggests that the suppression of *dbp5(rat8-2)* may be closely linked to events that occur in the nucleus and render the resulting mRNP easier to disassemble in the cytoplasm, rather than directly facilitating the removal of Nab2 by Dbp5. Consistent with Nab2 influencing the generation of export-competent mRNPs in the nucleus as well as polyadenylation, the addition of Nab2 and Yra1 to the mRNP occurs at the termination of polyadenylation and is influenced by components of the cleavage and polyadenylation factor (CPF) such as Pcf11(116, 187). In this context, it is significant that *nab2* mutants exacerbate the growth defect of the GFP-*yra1-8* allele, whereas over-expression of *NAB2* suppresses this phenotype (67, 186) and, moreover,

Yra1 stimulates the interaction between Nab2 and Mex67(67). Because Yra1 is removed from mRNPs before export (74), these observations strongly suggest that Nab2 participates together with Yra1 in the generation of export-competent mRNPs. Although the specific steps leading to generation of export-competent mRNPs have not all been defined, there appears to be a remodelling of the mRNP that is coupled to the termination of polyadenyation (116, 187-189) by which stage Nab2 has been added (176). This remodelling results in the removal of Yra1 from the mRNP coupled with attachment of Mex67:Mtr2. Although some of our *nab2* variants also generate longer polyA tails, it is unlikely that this is related to the suppression of *dbp5(rat8-2)* because mutations in *SAC3* and *APQ12* that generate longer tails (190) are synthetically lethal with *dbp5(rat8-2)* (191). Because Yra1 functions in the generation of export-competent mRNPs and is removed from them prior to export, our finding that a range of *nab2* variants, including *nab2-C437S,* suppress the conditional growth of *GFP-yra1-8* cells (Table 2.2 and Figure 2.7D) strongly supports the hypothesis that Nab2 plays a key role in the nucleus in ensuring proper assembly of an export-competent complex. Therefore, this result would be more consistent with the *nab2-C437S*-mediated suppression of the *dbp5(rat8-2)* allele deriving from production of sub-optimally assembled mRNPs in which Mex67:Mtr2 can be more easily removed by Dbp5-mediated remodelling at the NPC cytoplasmic face rather than weakening the direct interaction between Nab2 and Mex67 or RNA.

In summary, Nab2 ZnF5-7 have a novel conformation in which they form a single coherent structural unit that binds eight consecutive adenosines. Both chemical

shift measurements and engineered mutations indicate that all three fingers bind to polyadenosine-RNA, albeit the way in which ZnF6 binds appears to be different to that seen for fingers 5 and 7. Engineered mutations guided by the structure of fingers 5-7 indicated that basic residues in position 1 were important for the interaction, as were aromatic residues in position 2 of fingers 5 and 7, together with Phe450 in ZnF6. The way in which these mutations influenced polyA tail length and cell growth in *dbp5(rat8-2)* or *GFP-yra1-8* backgrounds, indicate that Nab2 functions in the generation of export-competent mRNPs and that specific changes within fingers 5-7 generate mRNPs that, once they reach the cytoplasm, are disassembled more readily by Dbp5 than wild-type mRNPs.

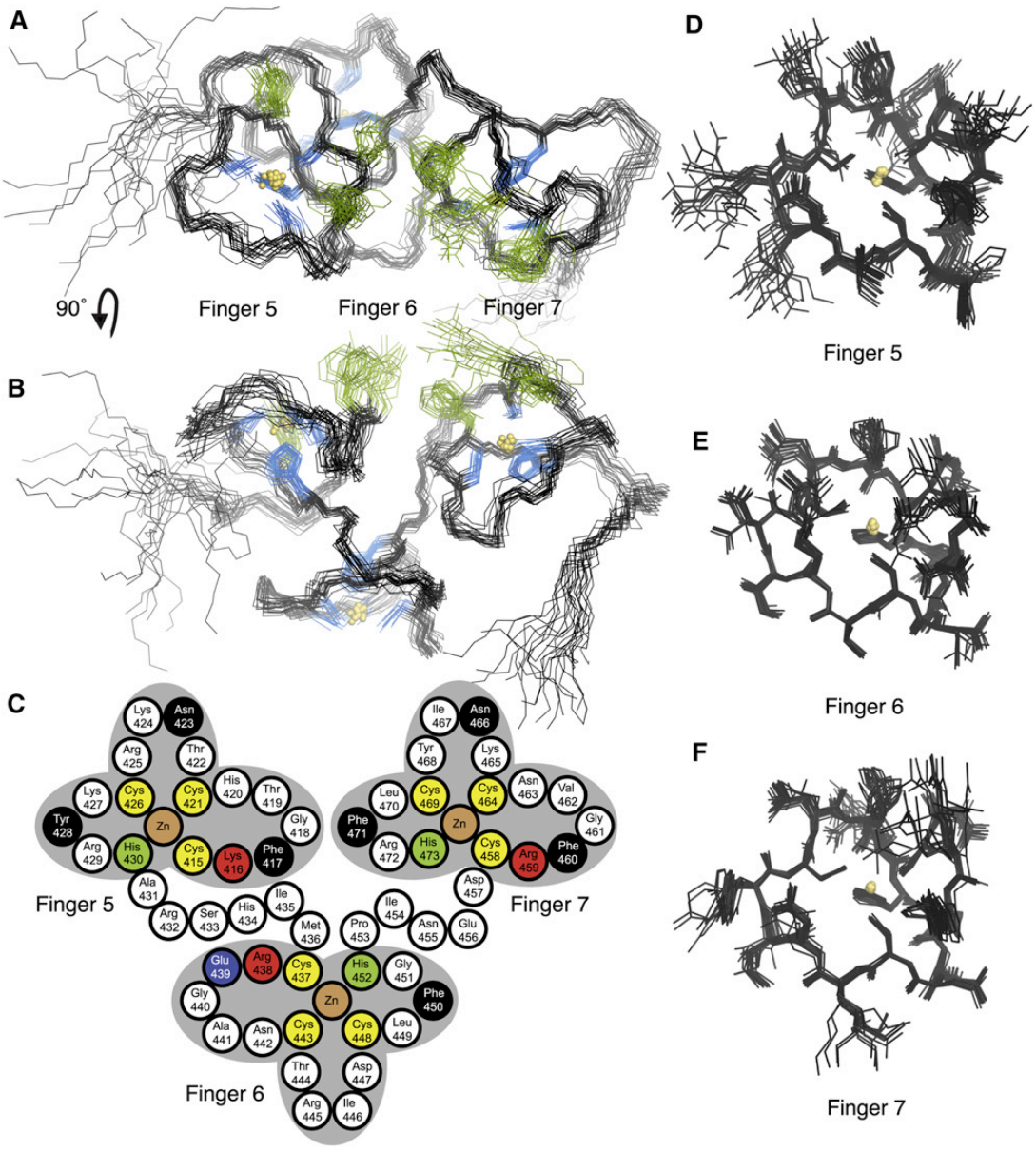
A
90˚
Finger 5
Finger 6
Finger 7
B
C
Finger 5
Finger 7
Finger 6
D
Finger 5
E
Finger 6
F
Finger 7

Figure 2.1: NMR structure of Nab2 Zn-fingers 5-7. A,B: Ensembles of the NMR structure of Nab2 residues 409-483. Of 200 calculated structures, 20 were selected by lowest total energy. The structures are superimposed based on the backbone of residues 410-480. Side chains of the Zn-coordinating residues are shown in blue. The RNA-binding residues on Zn-fingers 5 and 7 (see text) are shown in green. The three fingers associate to form a novel single structural domain in which individual fingers pack together to produce a pseudo-helical arrangement. **C:** Schematic illustration of the structure of fingers 5-7. Three Cysteines (yellow) and a Histidine (green) bind the Zn ion (brown) in each finger. Isoleucines 435 and 454, located in the linkers between fingers are buried in the interfaces between the fingers. Residues located in finger 5 (red: Lys 416; black: Phe417, Asn423, Tyr428) and finger 7 (red: Arg459; black: Phe460, Asn466, Phe471) show large chemical shift changes on addition of A_3. Finger 6 has Glu439 (blue) instead of an aromatic residue in position 2. Mutation of Lys416 or Phe417 in finger 5; Cys437, Arg438 or Phe450 (black) in finger 6; or Arg459 or Phe460 in finger 7, decreases the affinity for polyadenosine (see Table 2.2). **D,E,F:** The same ensemble of structures is shown as in A and B, but is now shown superimposed on the Cα positions from the individual fingers (**D:** Zn-finger 5: residues 414-431, **E:** Zn-finger 6: residues 436-453, and **F:** Zn-finger 7: residues 457-474).

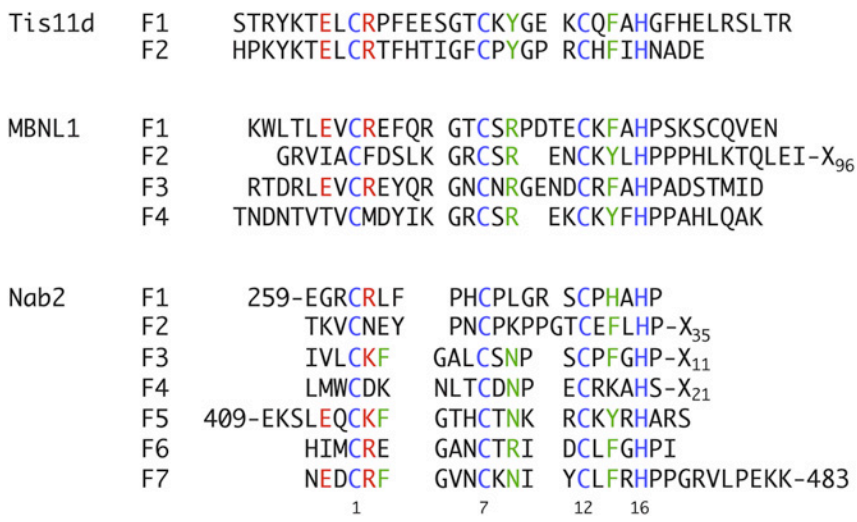

Figure 2.2: Alignment of the sequences of related Zn-fingers. Shown are the seven zinc fingers of Nab2 itself, as well as the closely related fingers from the proteins Tis11d and MBNL1. Residue positions within each finger are numbered taking the first cysteine residue as position 1.

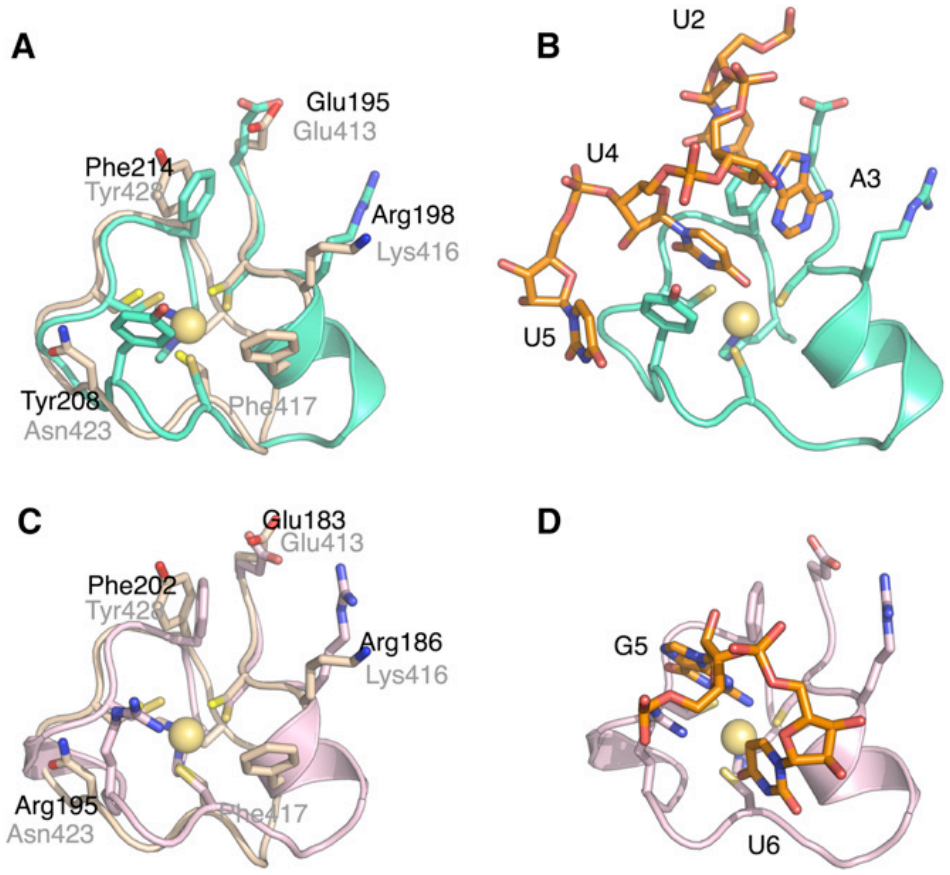

Figure 2.3: Comparison of Nab2 with other tandem Zn-finger domains A: Structural alignment of Nab2 Zn-finger 5 (wheat) with Zn-finger 2 of the Tis11d tandem Zinc-finger domain (shown in cyan) (pdb: 1RGO). Side chain residues involved in RNA binding in the Tis11d structure are shown. **B**: RNA (orange) bound structure of Tis11d. **C**: Structural alignment of Nab2 Zn-finger 5 (shown as wheat) with Zn-finger 3 of the MBNL1 tandem Zn-finger domain (shown in pink) (pdb: 3D2S), side chain residues involved in RNA binding in chain A in the MBNL1 are shown. **D**: RNA (orange) bound structure of MBNL1.

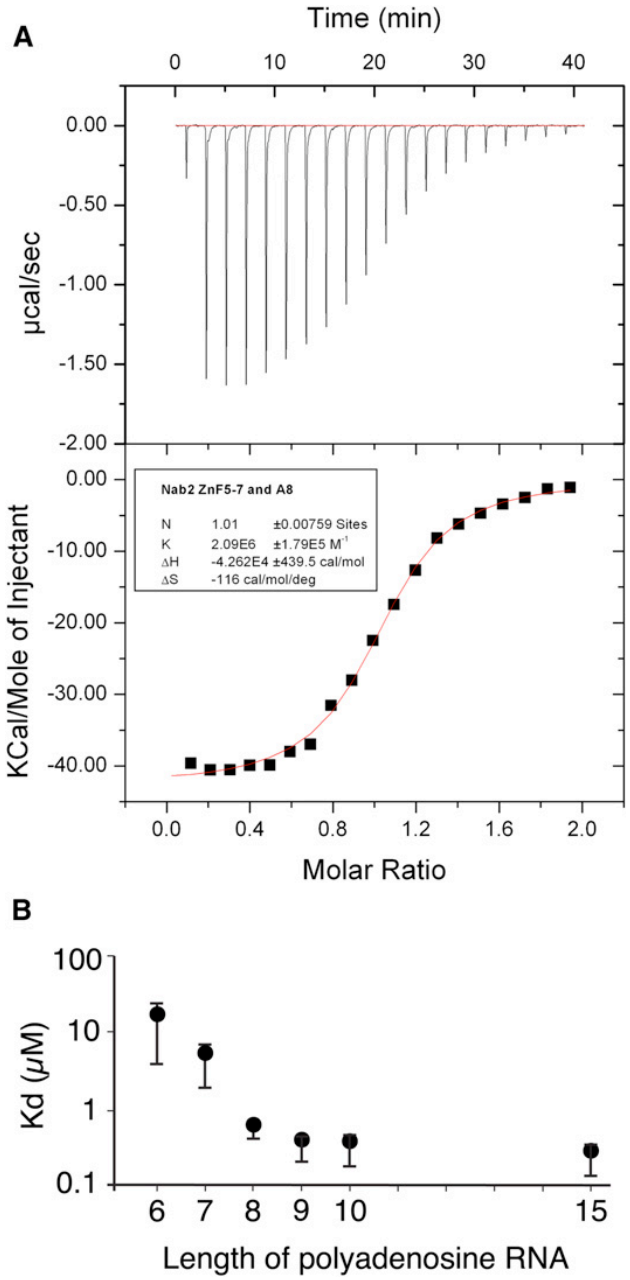

Figure 2.4: Affinity of polyadenosine-RNA for Nab2 Zn-fingers 5-7 A: ITC raw data (upper panel) for binding of A_8 to Nab2 Zn-fingers 5-7 with integrated peaks and fitting curve (lower panel). **B**: Influence of the length (A_6 to A_{10}) of polyadenosine-RNA on the affinity for Nab2 Zn-fingers 5-7. Error bars represent standard deviation from three independent measurements.

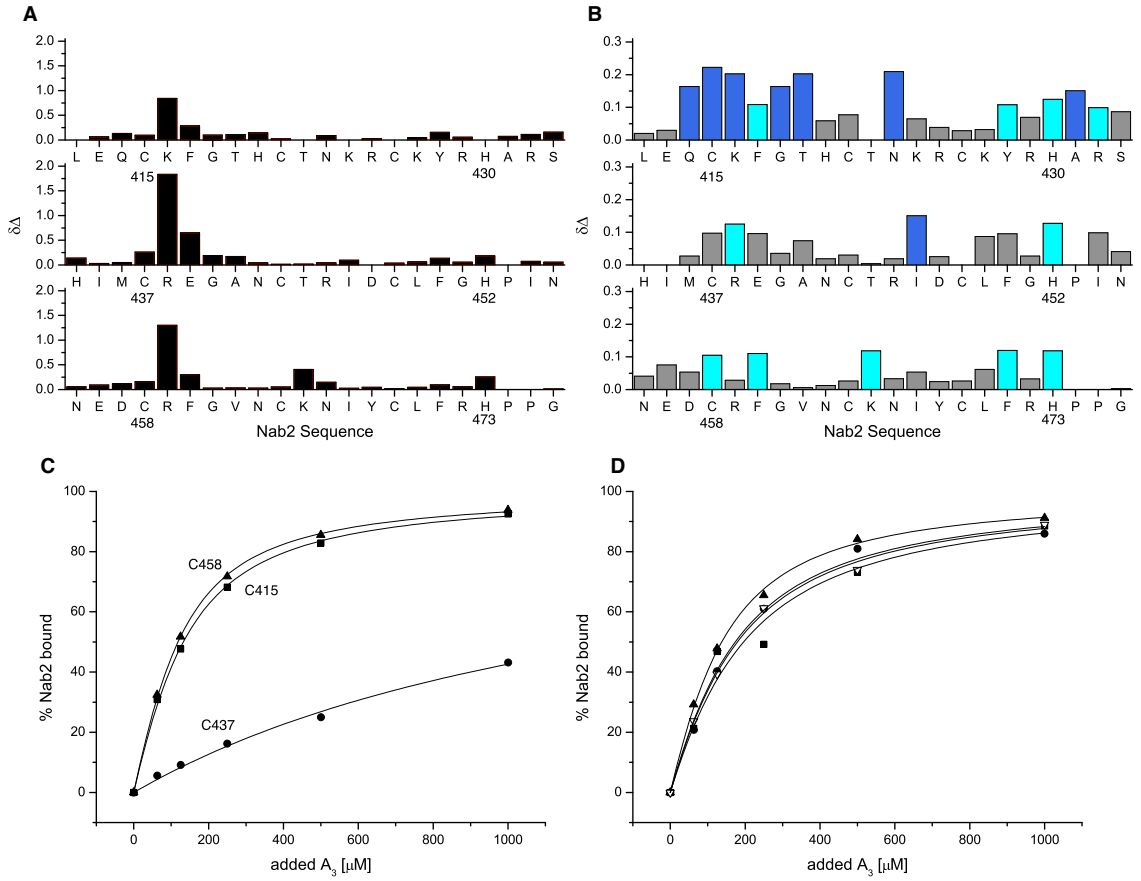

Figure 2.5: Binding of Nab2 Zn-fingers 5-7 to polyadenosine RNA. A: Chemical shift perturbation of backbone amide groups of wild-type Zn-fingers 5-7 in the presence of 5 mM AMP. **B**: Chemical shift perturbation of backbone amide groups of wild-type Nab2 fingers 5-7 in the presence of 250 μM A_3. **C**: Normalized binding isotherms extracted from the titration data summarized in B, following residues C415 (n), C437 (l) and C458 (p). **D**: Binding isotherms extracted from the titration of the E439F mutant with A_3, following residues C415 (n), H420 (s), C437 (l) and C458 (p).

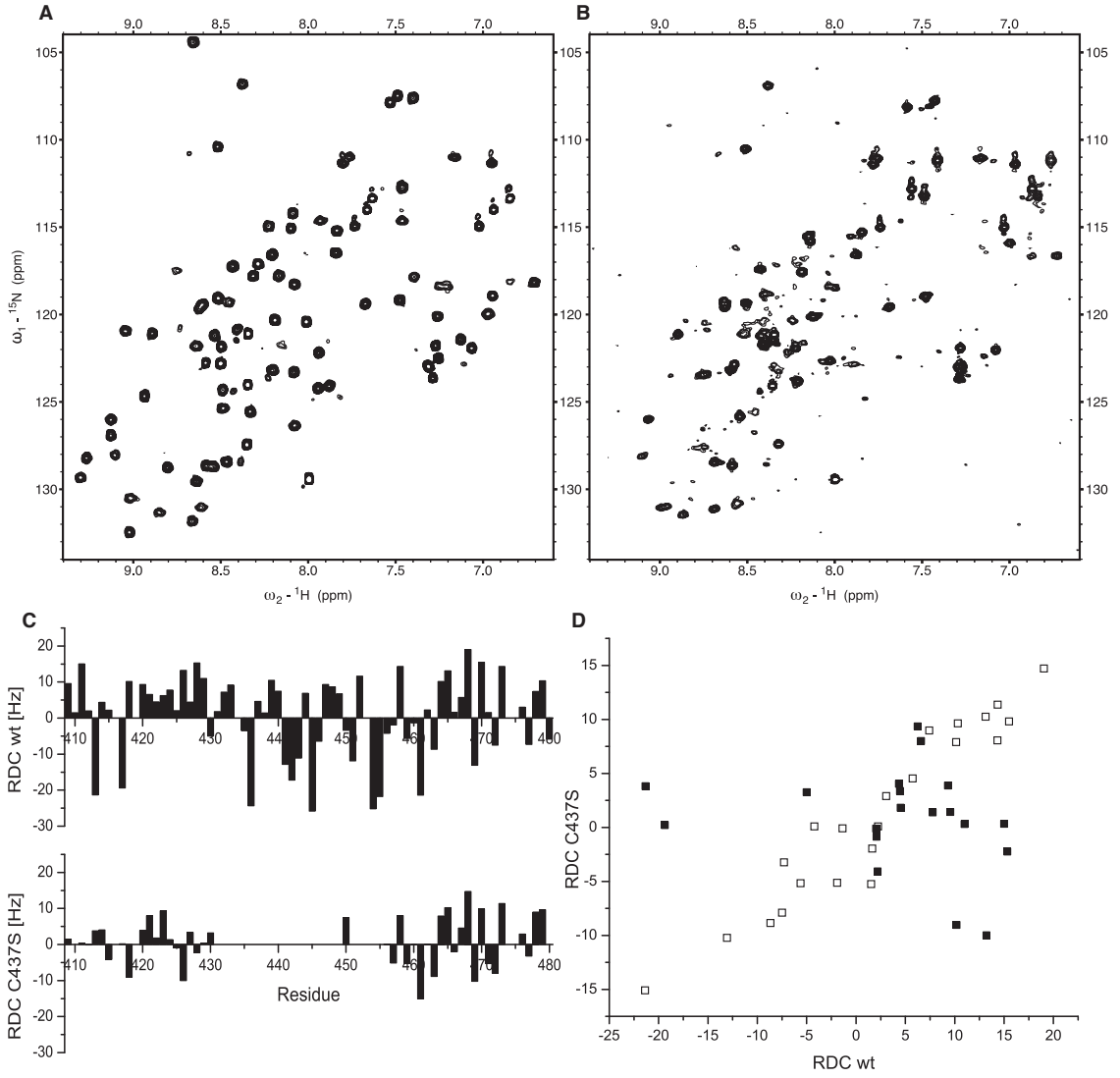
A
B
C
D
ω_1 - ^{15}N (ppm)
ω_2 - ^{1}H (ppm)
RDC wt [Hz]
RDC C437S [Hz]
Residue
RDC C437S
RDC wt

Figure 2.6. Effects of the C437S mutant on the structure of Nab2 Zn fingers 5-7. A: ^{15}N-HSQC spectrum of wild-type Nab2$^{409-483}$. **B**: The same spectrum as shown in A but for the C437S Nab2 mutant. Comparison of (A) and (B) showed that peaks close to the original positions of the finger 5 and 7 amides are retained, consistent with these fingers still being folded, whereas most of the peaks from ZnF6 are significantly broadened, probably indicating exchange between different conformations. **C**: comparison of backbone ^{1}H-^{15}N RDC values obtained for the wild-type and C437S Nab2 proteins. The absence of measurable values for ZnF6 reflects the broad or unresolved nature of the corresponding peaks in these cases, while the reduced magnitudes of the RDCs in ZnF7 and (especially) ZnF5 indicates a higher degree of relative mobility for these fingers in the mutant. **D**: Correlation plot of N-H RDC values obtained for the wild-type and C437S Nab2 proteins. RDC data obtained for Zn finger 5 (residues 410-430) are shown using filled squares whereas RDC data obtained for Zn finger 7 (residues 458-479) are shown using open squares. A strong correlation is visible between the RDCs measured for the wild-type and the C437S mutant for ZnF7, but such a correlation is absent for the corresponding RDC data for ZnF5**.** This suggests that the alignment is dominated by effects involving ZnF7 in both the wild-type and mutant proteins, but that in the mutant ZnF5 is mobile relative to ZnF7, thereby rendering the alignment for ZnF5 in the mutant independent of that for ZnF7.

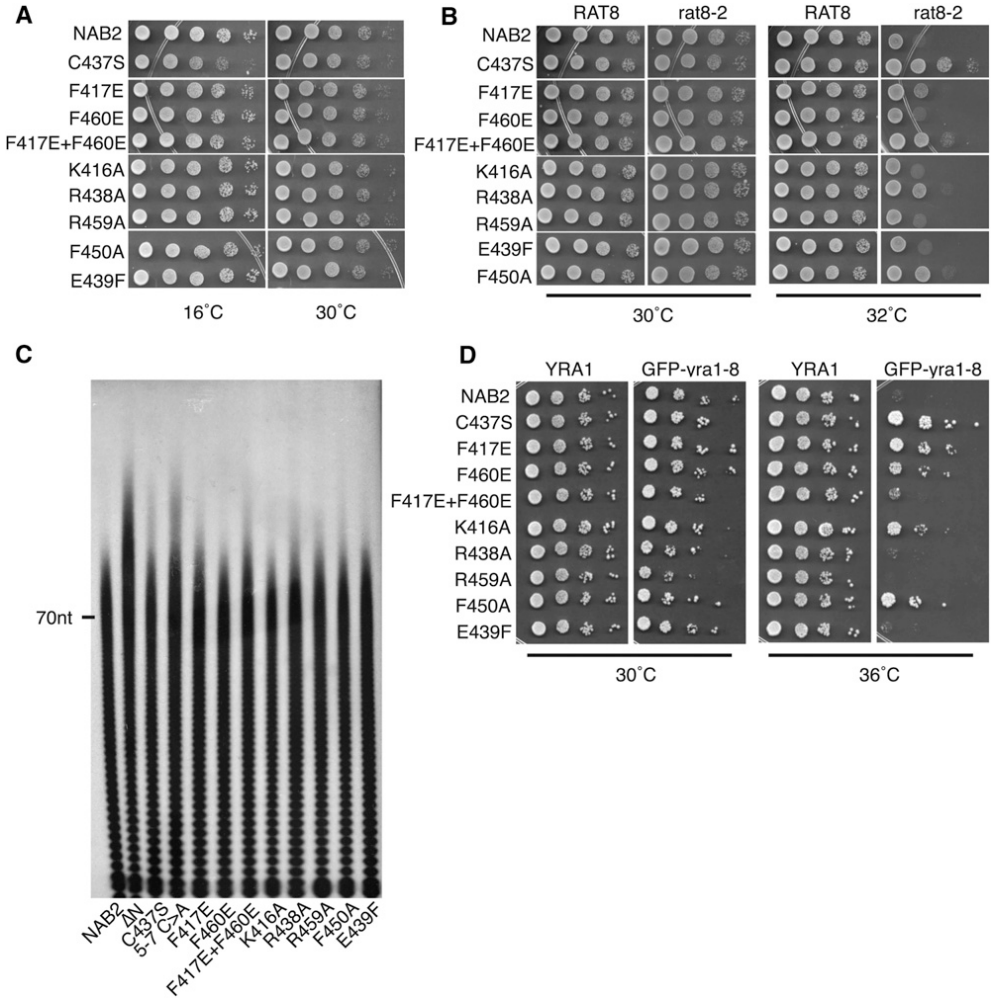
A
NAB2
C437S
F417E
F460E
F417E+F460E
K416A
R438A
R459A
F450A
E439F
16˚C
30˚C
B
RAT8
rat8-2
RAT8
rat8-2
NAB2
C437S
F417E
F460E
F417E+F460E
K416A
R438A
R459A
E439F
F450A
30˚C
32˚C
C
70nt
NAB2
ΔN
C437S
5-7 C>A
F417E
F460E
F417E+F460E
K416A
R438A
R459A
F450A
E439F
D
YRA1
GFP-yra1-8
YRA1
GFP-yra1-8
NAB2
C437S
F417E
F460E
F417E+F460E
K416A
R438A
R459A
F450A
E439F
30˚C
36˚C

Figure 2.7: Functional analysis of Nab2 variants *in vivo*. The function of Nab2 variants was assessed using a plasmid shuffle assays such that each variant was examined as the only functional copy of the essential Nab2 protein. Results of these experiments are summarized in Table 2. For growth assays, yeast cells expressing each Nab2 variant were serially diluted and spotted on plates. **A**: Nab2 Zn finger variants can function in place of Nab2. Each variant supports normal cell growth at 30°C, but *nab2-C437S* shows slow growth at 16°C indicating a cold-sensitive growth phenotype. **B**: Suppression of the temperature-sensitive growth phenotype of *dbp5(rat8-2)* mutant cells by Nab2 variants. A plasmid shuffle assay in Δ*NAB2 rat8-2* mutant cells was employed to examine suppression of the temperature-sensitive growth of *dbp5(rat8-2)* mutant cells at 32°C. As controls, no suppression is observed with wild-type *NAB2* whereas *nab2-C437S* suppresses robustly. **C**: Bulk poly(A) tail length was examined by an RNAseA/T1 assay. Cells expressing each Nab2 variant as the sole copy of Nab2 were grown to log phase and poly(A) tails were labelled and resolved by gel electrophoresis. The position of a 70-nucleotide (70nt) marker is indicated. **D**: Suppression of the temperature-sensitive growth phenotype of GFP-*yra1-8* mutant cells. A plasmid shuffle assay in Δ*NAB2* GFP-*yra1-8* mutant cells was employed to examine suppression. As a control, no suppression is observed with wild-type *NAB2*. In contrast, *nab2-C437S* robustly suppresses, and some but not all of the variants suppress the temperature sensitive growth of GFP-*yra1-8* cells at 36°C.

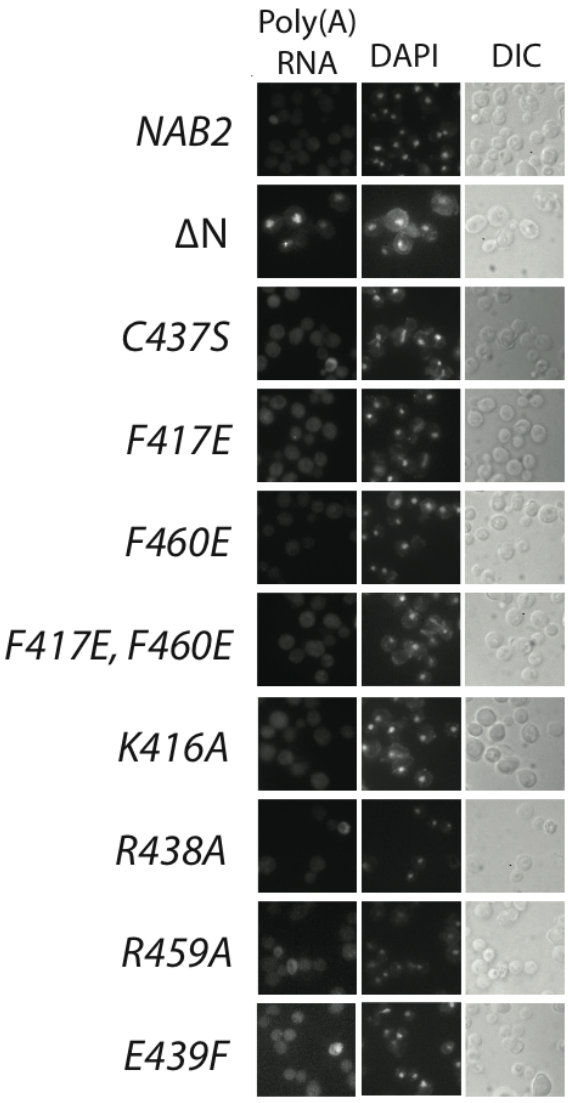

Figure 2.8: Poly(A) RNA localization is not altered in cells expressing any of the Nab2 zinc finger variants. Bulk poly(A) RNA localization was analyzed by fluorescence in situ hybridization as described in the methods. In addition to visualization of poly(A) RNA, samples were also stained with DAPI to visualize the position of the nucleus and imaged by DIC imaging to show the position of the cells. Cells expressing the indicated variants of Nab2 as the sole copy of Nab2 were analyzed. Nuclear accumulation of poly(A) RNA was not observed in wild-type control (*NAB2*) or any zinc finger mutant analyzed (K416A, F417E, C437S, R438A, E439F, F450A, R459A, F460E, F417E+F460E) although, as control, nuclear accumulation of poly(A) RNA was clearly observed in the Nab2-ΔN variant.

Table 2.1: Statistical data relating to the final ensemble of structures of Nab2 F5-F7

Table 1. Statistical Data Relating to the Final Ensemble of Structures of NAB2 F5-F7	
Structural Restraints	
NOE-derived distance restraints	
Intraresidue	2
Sequential	371
Medium (2 % ji jj % 4)	132
Long (ji jj > 4)	277
Ambiguous	76
Total	858
RDC restraints	
NH N	61
Statistics for Accepted Structures	
Number of accepted structures	20
Mean AMBER energy terms (kcal mol ^{1} ± SD)	
E(total)	3,805.9 ± 10.5
E(van der Waals)	541.3 ± 9.1
E(distance restraints)	25.8 ± 3.0
Distance violations >0.2 Å (average per structure)	7.4 ± 1.7
Maximum distance violation	0.52 Å
Mean absolute RDC violation	1.85 ± 1.64 Hz
Rmsd from the ideal geometry used within AMBER	
Bond lengths	0.011 Å
Bond angles	2.46
Ramachandran Statistics for Residues 410–480	
Most favored	89.0%
Additionally allowed	11.0%
Generously allowed	0.0%
Disallowed	0.0%
Average Atomic Rmsd to Mean Structure (±SD) for Residues 410–480	
N, C^{a}, C^{0} atoms	0.69 ± 0.15 Å
All heavy atoms	1.18 ± 0.14 Å

Table 2.2: Characterization of the *S. cerevisiae* Nab2 ZnF variants

Nab2 variant	Zinc Finger	Growth			Affinity for A_8 (μM)	Poly(A) tail length
		ΔNAB2	*dbp5 (rat8-2)*	*GFP-yra1-8*		
Wild-type		wt	-	-	0.5	wt
K416A	5	wt	-	+	15	wt
F417E	5	wt	+	++	18	+
C437S	6	cs	+++	+++	19	++
R438A	6	wt	++	-	58	+
E439F	6	wt	-	-	0.4	wt
F450A	6	wt	++	++	31	++
R459A	7	wt	-	-	7	wt
F460E	7	wt	-	+	28	wt
F417E+ F460E	5+7	wt	++	+/-	71	++

Growth Scale: - (no growth); +/- (some modest growth in most concentrated spot); + (growth in most concentrated spot); ++ (growth in most concentrated and 1:10 dilution); +++ (growth in most concentrated,1:10 dilution, and 1:100 dilution).

EXPERIMENTAL PROCEDURES

NMR spectroscopy and structure calculations

Data were acquired at 17˚C on Bruker DMX600 and DRX500 spectrometers, each equipped with a triple resonance ($^{1}H/^{15}N/^{13}C$) cryoprobe. ^{1}H, ^{15}N and ^{13}C chemical shifts were calibrated using sodium 3,3,3-trimethylsilylpropionate (TSP) as an external ^{1}H reference. Unless stated otherwise, all NMR experiments for the free protein were performed using ^{15}N- or ^{15}N, ^{13}C-labelled protein samples in the buffer used for gel-filtration, supplemented with 5% D_2O.

An essentially complete set of resonance assignments was made using a standard suite of triple resonance NMR experiments, and structural constraints were derived from NOESY and RDC data. For experiments used to derive structural constraints, samples contained 1.2 mM ^{15}N, ^{13}C-labelled solutions of Nab2 409-483. The following spectra were acquired: 2D: [^{15}N-^{1}H] HSQC, long-range-optimised [^{15}N-^{1}H] HMQC to correlate His ring ^{1}H and ^{15}N signals,(192) [^{13}C-^{1}H] HSQC covering the full ^{13}C spectral width, constant-time [^{13}C-^{1}H] HSQC covering only the aliphatic ^{13}C region, constant-time [^{13}C-^{1}H] HSQC covering only the aromatic ^{13}C region; 3D data sets: CBCANH, CBCACONH, HBHACONH, [^{1}H-^{13}C-^{1}H] HCCH-TOCSY, [^{13}C-^{13}C-^{1}H] HCCH-TOCSY, ^{15}N NOESY-HSQC (t_m = 120 ms and t_m = 50 ms), ^{13}C NOESY-HSQC (t_m = 150 ms; separate datasets acquired for ^{13}C aliphatic and aromatic spectral regions). Residual dipolar couplings were measured using a 0.6 mM ^{15}N, ^{13}C-labelled solution of

Nab2 409-483, to which Tobacco Mosaic Virus was added to a final concentration of 25 mg/ml; splittings were measured in F_1 cross-sections of [^{15}N-^{1}H] HSQC IPAP and HNCO IPAP spectra.

Initial structures for the free proteins were calculated using the semi-automatic program CYANA, for which the input comprised the protein sequence, the full resonance assignment and the following 3D NOESY datasets: ^{15}N NOESY-HSQC (t_m = 120 ms), ^{13}C aliphatic region NOESY-HSQC (t_m = 150 ms) and ^{13}C aromatic region NOESY-HSQC (t_m = 150 ms). During the CYANA calculations no metal was represented explicitly, but the effect of metal binding was approximated by including inter-ligand distance constraints as follows: Sϒ to Sϒ, 3.7-4.0Å; Sϒ to His-N, 3.4-3.8Å; His-N to His-N, 3.1-3.5Å.

To enable ^{15}N-HMQC data explicit Zn bonding and geometry terms in the force-field to be employed together with constraints based on RDC measurements, we next calculated structures using XPLOR-NIH . As input, these calculations used the set of NOE restraints generated by the final (seventh) cycle of CYANA, re-imported into CCPNMR Analysis and curated manually. Since the XPLOR-NIH calculations employed r^{-6} summation for equivalent and non-stereospecifically assigned groups, and since no stereoassignments were made (and the stereoassignment-swapping protocol within XPLOR-NIH was not applied), the constraints for all such groups were converted to group constraints (i.e. such groups were specified using wildcards such as HB*). All lower bounds were set to zero. The pattern of zinc connectivities to the His residues was

established using long-range ^{15}N-HMQC experiments, which showed unambiguously that the N^{e2} atom binds the zinc in all three cases. Structures were calculated from polypeptide chains with randomized f and y torsion angles using a two-stage simulated annealing protocol within XPLOR-NIH, but employing larger numbers of cycles as follows: first-stage calculations comprised Powell energy minimization (500 steps), dynamics at 1000K (25000 steps), increase of the van der Waals force constant and tilting of the NOE potential function asymptote (4000 steps), switching to a square-well NOE function then cooling to 300K in 2000 step cycles, and final Powell minimization (1000 steps). Second-stage calculations used Powell minimization (500 steps), increasing dihedral force constant during 4000 step cycles of dynamics at 1000K (with a strong van der Waals force constant and square-well NOE potential function), cooling to 300K in 1000 step cycles, and 2000 steps of final Powell minimization. A final refinement against measured values of amide group ^{15}N-^{1}H and Ca-CO residual dipolar couplings was employed using the ISAC protocol.

NMR Chemical Shift Titrations

[^{1}H, ^{15}N]-HSQC spectra were acquired at 24°C or 17°C using Bruker DMX600 and DRX500 spectrometers during stepwise addition of either AMP or A_3 to ^{15}N-labelled wild-type Nab2 fingers 5-7 or the E439F variant in 50mM Tris-HCl pH 6.75, 50mM NaCl, 50mM Glu/Arg, 10μM $ZnCl_2$ and 5mM b-mercaptoethanol at a concentration of 100μM for A_3 and 200μM for AMP. Spectra were processed using XWINNMR (Bruker Biospin GmbH, Karlsruhe, Germany) and visualized in Sparky. ^{15}N-HSQC spectra were

recorded with the Nab2 sample alone and then after stepwise addition of AMP to 6.25, 12.5, 25, 50 mM or A_3 to 62.5, 125, 250, 500, 1000 μM. The chemical shift perturbation (CSP) data shown in Figure 5 for the Nab2 fragments binding to A_3 and AMP were obtained for each residue by comparing the amide chemical shift values of ^{15}N-Nab2 fingers 5-7 alone with those of ^{15}N- Nab2 fingers 5-7 in the presence of a 2.5 fold molar excess A_3 and a 250 fold excess of AMP. Values were calculated using the equation

$$CSP = \sqrt{((0.2\Delta dN)^2 + (\Delta dH^2))}$$

and apparent binding constants for the individual fingers were extracted from the A_3 data by following residues Cys415, Cys437, Cys458 and His420 using a model for one site binding, neglecting ligand depletion from other binding sites.

Isothermal Calorimetry

ITC measurements were performed using a Microcal ITC200 with ZnF5-7 and polyadenosine RNA of different defined lengths, dialyzed against 50mM Tris-HCl pH 8.5, 50mM NaCl, 10μM $ZnCl_2$, and 5mM b-mercaptoethanol. In a typical experiment, 30μM polyadenosine-RNA was pipetted into the sample cell containing a 200μM protein solution. Pipetting 30μM RNA into buffer showed a negligible change and so corrections were unnecessary. Protein and RNA concentrations were determined by extinction at 280nm and 260nm, respectively.

Cloning and Protein Purification

S. cerevisiae Nab2 residues 409–483 were cloned into the *BamHI* and *XhoI* sites of pGEX6P-1 (GE Healthcare), which resulted in an additional N-terminal sequence GPLGS being retained on the final protein. The plasmid was transformed into E. coli strain BL21 DE3, and cells were grown in M9 minimal medium at 37°C to an optical density (OD) of 0.6. Protein expression was induced by addition of 200 μM IPTG and 250 μM ZnCl2. Expression was carried out at 20°C overnight. The protein was then purified using standard GST-purification methods in 50 mM Tris (pH 8.0), 200 mM NaCl, 10 μM ZnCl2, and 5 mM β-mercaptoethanol. The GST-fusion protein was eluted using reduced glutathione and cleaved overnight at 4°C using "PreScission" 3C-protease (GE Healthcare). The cleaved protein was concentrated and subjected to gel filtration chromatography on a S75 column (GE Healthcare) in 50 mM Tris-HCl (pH 6.75), 50 mM NaCl, 50 mM Glu/Arg, 10 μM ZnCl2, and 5 mM β-mercaptoethanol. Fractions containing the desired Nab2 fragment were pooled and concentrated up to 1.2 mM. Nab2 variants were generated using site-directed mutagenesis and cloned into the same vector. The mutants were purified using the same protocols as for the native protein.

Chemicals, Plasmids, and *S. cerevisiae* Manipulations

Chemicals were obtained from Fisher Scientific (Pittsburgh), Sigma-Aldrich (St. Louis), or US Biological (Swampscott, MA, USA) unless otherwise noted. DNA manipulations were performed according to standard methods and all media were prepared by standard procedures. *S. cerevisiae* strains and plasmids are described in

Table S1. Plasmids encoding Nab2 variants were generated by site-directed mutagenesis of a wild-type NAB2 plasmid (pAC717) using the QuikChange Site-Directed Mutagenesis Kit (Stratagene). All plasmids were fully sequenced.

***In Vivo* Functional Analysis**

The *in vivo* function of each Nab2 mutant was tested using a plasmid-shuffle assay (193). *S. cerevisiae* cells deleted for NAB2 (ACY427) and containing a wild-type NAB2 URA3 plasmid (pAC636) were transformed with LEU2 plasmids expressing various Nab2 mutants. Transformants were grown to saturation and then cells were plated on 5-Fluoroorotic acid (5-FOA) to select for loss of the wild-type maintenance plasmid. These cells were then grown to saturation, normalized for cell number, and serially diluted and spotted onto ura− leu− glucose plates. Plates were then incubated at 18°C, 25°C, 30°C, or 37°C for 3–5 days. For analysis of either *dbp5 (rat8-2)* or *GFP-yra1-8* suppression, a plasmid-shuffle assay was performed as described by (73). Briefly, *ΔNAB2 rat8-2* or *ΔNAB2 GFP-yra1-8* cells transformed with plasmids expressing wild-type or mutant Nab2 were first grown on selective media containing 5-FOA, then grown on rich media (YPD), and finally grown to saturation, serially diluted, and spotted onto YPD. Plates were then incubated at 16°C, 25°C, 30°C, 32°C, or 36°C for 3–5 days.

PolyA Tail Length

Cells expressing wild-type or mutant Nab2 proteins were inoculated into YPD media and grown to saturation at 30°C. Cells were then diluted into 50 ml of YPD and grown at either 30°C or 16°C until they reached OD600 of 0.4–0.6. Twenty OD units of

cells was harvested from each culture, and polyA tail length was determined as described (194, 195). Briefly, total RNA was end labeled with 32P-pCp and T4 RNA ligase, after which it was digested with RNases A/T1 to remove non-polyA-RNA, and the 32P-labeled RNA was then ethanol precipitated. Resuspended RNA was then resolved by denaturing urea-acrylamide gel electrophoresis and imaged using a phosphoimager.

Fluorescence *In Situ* Hybridization

Cells expressing wild-type Nab2 or Nab2 mutant proteins were initially grown in 2 ml cultures to saturation at 30°C. These starter cultures were then used to inoculate 10 ml cultures that were grown overnight (approximately 12–16 hr) at 30°C. Cultures were then split into two 5 ml cultures and grown at either 30°C or 16°C. Cells were then fixed by the addition of 700 µl of 37% formaldehyde and incubated at 30°C or 16°C for 90 min, and fluorescence in situ hybridization (FISH) using an oligo d(T) probe to detect poly(A) RNA was performed as described(196). Cells were also stained with DAPI to visualize DNA within the nucleus.

Accession Codes

Atomic co-ordinates and constraints for the NMR ensemble have been deposited in the PDB with accession code 2LHN, and the corresponding chemical shift assignments have been deposited in the BMRB with accession code 17858.

Chapter 3: Nab2 Plays a Role in mRNA Splicing and Surveillance

A portion of this chapter is adapted from the following paper:

Soucek, S., Zheng, Yi., Bellur, M., Bergkessel, M., Guthrie, C., Staley, J.P., and Corbett, A.H. (2014) In revisions. "A Role for the Polyadenosine RNA Binding Protein, Nab2, in Splicing and RNA Surveillance."

Microarray studies were performed by Meagan Bergkessel Ph.D. and Christine Guthrie, Ph.D. at the University of San Francisco. The *in vitro* splicing assays were performed by Yi Zheng, Deepti Bellur, and Jon Staley at the University of Chicago.

INTRODUCTION

Gene expression is temporally and spatially regulated to produce a precise protein expression profile that dictates the function of each cell. Although much of this control occurs at the level of transcription, post-transcriptional events also play key regulatory roles. Newly synthesized mRNAs undergo post-transcriptional processing events including 5' capping, splicing, 3'-end processing, and export to the cytoplasm (131). Ensuring perfect synchrony of mRNA biogenesis requires RNA binding proteins that not only perform the processing tasks but also couple the events to ensure that only properly processed mRNAs are available for translation (92).

Splicing is an RNA processing event that removes introns and ligates exons together through two successive transesterification reactions. Splicing is carried out by the spliceosome which is composed of splicing factor proteins and small nuclear RNAs that recognize consensus sequences present within each intron (17, 18, 197). Splicing begins with commitment complex (E) formation where U1 snRNP binds the 5' splice site and U2 snRNP is recruited to the branchpoint (124). After establishment of the U1·U2 prespliceosome (A complex), the tri-snRNP U5·U4/6 is added (B complex) and rearranged into a catalytically active spliceosome (C complex) (198-202). Through two transesterification reactions, the intron lariat is excised out and the exons are ligated together to produce mature mRNA (17, 18).

In addition to splicing, most pre-mRNAs are cleaved and polyadenylated at their

3’-ends. Cleavage is performed by the cleavage and polyadenylation specificity factor (CPSF) which recognizes the hexameric AAUAAA sequence in the 3’UTR of transcripts (203, 204). Following cleavage, poly(A) polymerase (PAP) adds a stretch of polyadenosines to form a 70 non-templated long poly(A) tail (205). The poly(A) tail acts as a binding platform for poly(A) RNA binding proteins which modulate downstream mRNA biogenesis events (50, 171).

Each step of RNA processing is often depicted as a separate event, but these processing events are intimately coupled. A number of studies reveal coupling between splicing and 3’-end processing in human cells (102). Mutations in splice site and polyadenylation consensus sequences mutually disrupt both splicing and polyadenylation in a process that is linked to transcription termination (103). In addition, purification of the 3’-end processing complex pulled down a number of splicing factors (206). One splicing factor identified was U2AF65, which is known to act as a bridge between the U2 snRNP and the 3’-end processing machinery (101, 207, 208). Understanding the mechanism of coupling splicing to polyadenylation will reveal how defects in one step of mRNA biogenesis influence RNA processing to ensure production of properly processed RNAs. Cells have developed numerous overlapping mechanisms to ensure that faulty mRNA transcripts are not translated into proteins, suggesting that there must be constant mRNA surveillance during mRNA biogenesis.

One facet of mRNA surveillance is nuclear retention of pre-mRNA transcripts. The splicing and retention complex (RES) is composed of splicing factors that are critical for

both recognizing intron-containing transcripts and retaining them within the nucleus (124, 125). The RES complex relies on intact splice site sequences as well as the correct composition of RNA binding proteins to form an mRNP (124, 125). For example, mutations in genes encoding the *S. cerevisiae* early splicing factors, Mud2 and Msl5, result in a stalled commitment complex (23, 26, 124, 125, 209). Once the stalled pre-mRNA is recognized as misprocessed, nuclear pore components such as the Mlp proteins are required for nuclear retention (126, 127). By retaining pre-mRNA transcripts, a choice can be made to continue with mRNA maturation or to proceed with mRNA decay (75). In addition, some pre-mRNAs may be exported to the cytoplasm where they contact cytoplasmic exonucleases or undergo translation-dependent nonsense mediated decay (210, 211). Both courses of action prevent translation of unspliced RNAs into faulty proteins.

An essential complex that mediates both RNA processing and degradation is the evolutionarily conserved RNA exosome complex (76, 212). The core exosome consists of ten subunits that form a barrel-like structure with 3'-5' exoribonuclease activity with an additional subunit, Rrp6, present in the nucleus (75, 213, 214). The exosome processes key RNAs including ribosomal RNA (rRNA), small nuclear RNA (snRNA), and small nucleolar RNA (snoRNA) (77, 78), but also degrades RNA in both the nucleus and cytoplasm (76). A variety of nuclear and cytoplasmic cofactors modulate the function of the exosome *in vivo* (79). For example, the nuclear-specific exosome component, Rrp6, is responsible for degrading transcripts with aberrant 3' polyadenosine tails (80), pre-

mRNA transcripts containing introns (83), and transcripts lacking proper messenger ribonucleoproteins (mRNP) composition (86, 87). One exosome cofactor, the Trf4/5, Air1/2, Mtr2 (TRAMP) complex, adds a short poly(A) tail to promote exosome-mediated degradation (88). Understanding how the cell integrates the function of RNA binding proteins that process RNA targets with the exosome and exosome cofactors will provide insight into the surveillance decision to process or perish.

RNA binding proteins that play roles in multiple mRNA processing events are candidates for performing surveillance functions to ensure that only properly processed mRNAs are exported to the cytoplasm. Examples include the *S. pombe* Pab2 polyadenosine RNA binding protein that functions with Rrp6 to degrade polyadenylated pre-mRNA transcripts (84). Interestingly, the interplay between Pab2 and the evolutionarily conserved zinc finger nuclear polyadenosine RNA binding protein, Nab2/ZC3H14, serve as an important model for understanding how splicing, 3'-end processing, and mRNA decay are coupled (215). Recent work suggests that the *S. pombe* Nab2 antagonizes the nucleus poly(A) RNA binding protein, Pab2, to impede degradation of unspliced *rpl30-2* mRNA (216). However, *S. pombe* Nab2 does not play a role in poly(A) tail length control despite its ability to bind polyadenosine RNA. These data raise the question of whether *S. cerevisiae* Nab2 can influence splicing in addition to its role in the control of poly(A) tail length. In addition, analysis of human ZC3H14 suggests possible contributions to other processing events including splicing (150, 156). ZC3H14 co-localizes in nuclear speckles with the splicing factor, SC-35 (215).

Importantly, recent work reveals that mutations in ZC3H14 lead to autosomal recessive intellectual disability (147, 161), highlighting the importance of defining the full spectrum of functions for this protein.

Here, we employ molecular, genetic, and biochemical approaches to demonstrate that the polyadenosine RNA binding protein, Nab2, provides links between splicing and 3'-end processing. We show that Nab2 associates with the early branchpoint binding factors, Mud2 and Msl5, to guide proper pre-mRNA splicing and 3'-end processing. Our results also reveal a role for the splicing factor, Mud2, in modulating poly(A) tail length. The requirement for the association between Nab2 and early splicing factors is mitigated when nuclear exosome activity is decreased by removing Rrp6. Our data supports a model where Nab2 and Mud2 serve as a RNA surveillance factors to coordinate splicing, 3'-end processing, and mRNA decay.

RESULTS

Unspliced pre-mRNA accumulates in *nab2* mutants

To investigate a possible role for Nab2 in splicing, we employed two conditional alleles of *NAB2*, *nab2*-Δ*N* (*nab2-1)* and *nab2*-$C_{5\text{-}7}A$ (Figure 3.1A). The *nab2*-Δ*N* (*nab2-1)* allele is an N-terminal deletion within the Proline-Tryptophan-Isoleucine (PWI)-like domain of Nab2, which is critical for proper poly(A) RNA export (152). The *nab2*-$C_{5\text{-}7}A$ mutant alters conserved cysteine residues within the 5th, 6th, and 7th zinc fingers and

severely compromises RNA binding (156). These *nab2* alleles both confer cold-sensitive growth although growth of *nab2-ΔN* is more severely impaired at all temperatures (Figure 3.1B).

To test for the presence of intron-containing RNAs in wildtype and *nab2* mutant cells, cells were grown to mid-log phase at 30˚C and qRT-PCR was performed. To detect the intron-containing transcripts, qRT-PCR was performed with primers flanking the intron-exon boundary of several well-characterized and abundant intron-containing *S. cerevisiae* transcripts (Figure 3.2A). To detect total levels of transcripts, qRT-PCR was also performed with primers within an exon (Figure 3.2A). To obtain a representative sample across different classes of mRNA, the analysis was performed with the nonribosomal protein transcripts, *ACT1* and *TUB1*, and the ribosomal protein transcript, *RPL28*. Relative to wildtype cells, the *nab2* mutant cells exhibited a 2-3 fold increase in unspliced pre-mRNA (Figure 3.2B). In contrast, *nab2* mutants did not show a significant change in total mRNA levels compared to wildtype. As a control, a splicing factor mutant, *prp2-1*, was grown to mid-log phase at 30˚C, shifted to the nonpermissive temperature at 37˚C for one hour, and qRT-PCR was performed. RNA isolated from *prp2-1* showed a significant increase in intron accumulation and significant corresponding decrease in total RNA levels (31, 217). These data provide the first evidence that *nab2* mutant cells could have defects in ensuring efficient splicing.

Nab2 is required for splicing a subset of pre-mRNAs

To assess the requirement for Nab2 in splicing within the transcriptome of *S. cerevisiae*, we employed a splicing microarray (218, 219). This microarray platform contains three probes targeted to each intron-containing transcript. The probes are located: 1) within the intron to detect unspliced pre-mRNA; 2) across the exon-exon boundary to detect mature, spliced mRNA; and 3) within the exon to detect total RNA. As shown in Figure 3, both *nab2* mutants analyzed display a mild, but constitutive increase in unspliced pre-mRNA relative to wildtype. Over half of transcripts analyzed in both *nab2* alleles show intron accumulation; however, only a small number of transcripts exceed a $\log_2$ ratio of >1.

More than 60% of transcripts analyzed in both *nab2* alleles show decreased exon expression; however, the transcripts with decreased total RNA do not correlate with an increase in intron accumulation (r^2=0.032). A Venn diagram shows a shared population of unspliced pre-mRNA transcripts that are affected in each of the *nab2* mutants (Figure 3.3B). However, the shared RNA expression levels varied between the two *nab2* mutants as indicated by an average Pearson correlation value of 0.42. These data suggest that each *nab2* mutant differentially affects the same population of intron-containing transcripts and could reflect the fate of RNA during the different mRNA processing events.

To confirm the results obtained from the microarray analysis, qRT-PCR was utilized to validate the results. Eight different intron-containing and intronless transcripts were chosen for validation. For the intron-containing transcripts, the unspliced pre-mRNA, mature spliced mRNA, and total RNA levels were measured for each specific transcript. Specific mRNA transcripts were assessed by qRT-PCR and the fold changes observed were compared to the $\log_2$ ratio obtained from the splicing microarray. A positive correlation was observed between the microarray and qRT-PCR (Figure 3.11). These observations indicate that *nab2* mutant cells have a mild, but constitutive accumulation of intron-containing RNAs.

Interestingly, those pre-mRNA transcripts most affected in *nab2* mutant cells are among the few transcripts that contain more than one intron in budding yeast. These transcripts included the ribosomal protein transcripts, *RPL7B* and *RPS22B*, and the microtubule dynein transcript, *DYN2*. In *nab2* mutant cells, *RPL7B* and *RPS22B* total RNA levels were severely reduced (Figure 3.3C). In addition, *DYN2* total mRNA levels were slightly reduced *nab2* mutant cells. It is interesting to note that in all three transcripts, the production of mature, spliced mRNA is altered. While *RPL7B*, *RPS22B,* and *DYN2* all share the same canonical intron consensus sequences in both introns, these results may suggest a unique pathway for processing transcripts with more than one intron in *nab2* mutant cells. One possibility is that these transcripts are alternatively spliced, however exon 2 skipping was not observed in *nab2* mutant cells (data not shown). Another possibility is that transcripts with more than one intron are improperly

processed are targeted for decay. These results suggest that transcripts with more than one intron are more sensitive to defects in RNA processing and are therefore more prone to RNA decay.

Evidence for Nab2 function in splicing *in vitro*

Results of the splicing array show accumulation of intron-containing RNAs in *nab2* mutant cells but do not directly assess whether Nab2 is directly required for splicing or is required for ensuring efficiency of splicing. To determine if Nab2 is required for splicing *in vitro*, we utilized a well-characterized *in vitro* splicing assay using total yeast extract and the *ACT1* pre-mRNA (220). We analyzed the *in vitro* splicing activity of cell lysates prepared from mutant cells with a very mild allele of *NAB2*, *nab2-C437S* (see Figure 3.1). The C437S amino acid substitution is a conservative cysteine to serine change in the 6th zinc finger of Nab2 that confers a slight cold sensitive growth defect (Figure 3.1A and 3.1B). As a control, we included lysates prepared from cells lacking a known splicing factor, Δ*mud2* (214). Consistent with previous studies, Figure 4 shows that deletion of *MUD2* results in accumulation of pre-mRNA (126, 221). Extracts from *nab2* mutant cells accumulate uncleaved *ACT1* pre-mRNA, with a concomitant decrease in lariat and mature mRNA. The *in vitro* splicing assay was quantified to determine which step of splicing is most affected in the absence of Nab2. As shown in Figure 3.4B, there was a significant increase in *ACT1* pre-mRNA compared to lariat, indicating that

the branching efficiency is most affected in *nab2* mutant cells. These data suggest that Nab2 function is required at an early splicing step in this *in vitro* splicing assay. However, we cannot rule out that these results are indirect.

Genetic interactions between *NAB2* and genes encoding splicing factors

To further probe what splicing step is most affected by loss of functional Nab2, we employed a genetic approach testing for genetic interactions between *NAB2* and genes encoding splicing factors. We analyzed double mutants of *nab2* alleles in combination with deletion of nonessential splicing factors (Table 3.1) involved in each of the following steps of splicing: early spliceosome assembly; transesterification of introns; and spliceosome disassembly. The early spliceosome assembly factors involved in complex E and A formation include components of the U1 snRNP (Mud1 and Nam8) (199, 200) and U2 snRNP (Mud2, Cus2, Msl1, and Lea1) (199, 200, 202). The catalytic transesterification reaction factors involved in complex B and C formation include the tri-snRNP U5·U4/6 snRNP (Snu66, Snu309, Prp18, Isy1, and Bud13) (199, 200, 202). The post-spliceosomal disassembly factors include Isy1 and Bud13 (199, 200, 202).

For these studies, we used a very mild allele of *NAB2*, *nab2-C347S,* and a more severe allele of *NAB2*, *nab2-*$C_{5\text{-}7}A$ along with *nab2-*Δ*N*, *nab2-*Δ*RGG*, and *nab2-*Δ*QQQP* (152). Genetic interactions were assessed based on the cell growth of the double mutants as analyzed by serial dilution and spotting growth assays. Complete results of this

analysis are summarized in Table 3.1. Mutants of *NAB2* genetically interact with a subset of mutants in genes encoding splicing factors involved in all steps of splicing. A synthetic growth phenotype was observed in C-terminal mutants of *nab2* combined with Δ*bud13,* Δ*mud2*, Δ*msl1*, Δ*prp18*, Δ*snt309*, and Δ*snu66*. Four out of the six splicing factors identified in this genetic analysis play additional roles in retention of pre-mRNA by interacting with the nuclear pore to prevent pre-mRNA export (222). As *nab2* mutants genetically interact with mutants in genes encoding splicing factors including *BUD13, MUD2, MSL1,* and *PRP18* (126, 221, 222) that are also implicated in the splicing and retention complex, we hypothesized that Nab2 may be involved in ensuring that improperly spliced transcripts are not exported to the cytoplasm. To test this hypothesis, we assessed genetic interactions between *NAB2* and alleles of genes encoding retention factors (Table 3.2). Consistent with previous studies that identified a genetic interaction between *nab2*-Δ*N* and genes encoding the retention machinery (127), our results reveal genetic interactions with alleles of genes encoding retention factors (Table 3.2). A synthetic growth phenotype was observed in *nab2-C437S* combined with Δ*bud13,* Δ*mud2*, Δ*msl1*, Δ*prp18,* and Δ*pml1*. A less severe synthetic growth phenotype was observed in mutants of *nab2* combined with Δ*mlp1/2*. Taken together, these genetic experiments demonstrate that *NAB2* is linked to the splicing and retention machinery in the nucleus.

To illustrate results summarized in Table 3.1 and 3.2, a growth assay is shown for two splicing factors, Mud2 and Cus2 (214, 223). Mud2 is an RRM-containing RNA

binding protein that associates with branchpoint binding protein (BBP/Msl5/SF1) to assemble spliceosomes and commit to splicing (23, 124, 214). Cus2 is an assembly factor important for U2 snRNP folding involved later in the splicing process than Mud2 (223). A profound negative genetic interaction was identified between *NAB2* and *MUD2*, where the double mutant Δ*mud2 nab2-C437S* cells show severely impaired growth compared to either single mutant (Figure 3.5A, B). In contrast, no genetic interaction was detected between *NAB2* and *CUS2* (Figure 5A). Thus, the genetic interaction between *NAB2* and genes encoding splicing factors are specific for a subset of splicing factors.

To confirm the genetic interaction between *NAB2* and *MUD2*, an integrated mutant in the sixth zinc finger of Nab2, *nab2-C437S*, was combined with a deletion in *MUD2*. We utilized the mild allele of Nab2, *nab2-C437S*, because it does not have a strong growth phenotype on its own. In addition, deletion of *MUD2* alone does not have any detectable growth phenotype. Therefore, utilizing these two mutants provides a useful system for probing genetic interactions. As observed in the plasmid shuffle assay (Figure 3.5A), the loss of *MUD2* in combination with *nab2-C437S* exacerbates the growth phenotype, resulting in severe growth defects (Figure 3.5C). The doubling times at 30°C for wildtype cells is 1.6 hours, Δ*mud2* cells is 1.6 hours, *nab2-C437S* cells is 2.4 hours, and Δ*mud2 nab2-C437S* cells is 3.9 hours. These data confirm that *NAB2* genetically interacts with the early splicing and retention factor, *MUD2*. The negative genetic interaction between *NAB2* and *MUD2* implies an important functional link for

these two RNA processing factors. To begin the understand the functional interaction between Nab2 and Mud2, we further characterized this interaction biochemically.

MUD2 RRM3 is functionally important for *NAB2*

To refine the molecular basis for the genetic interaction between *NAB2* and *MUD2*, we altered specific residues in Mud2 implicated in distinct functions and performed a rescue experiment in the Δ*mud2 nab2-C437S* double mutant. As shown in Figure 6A, Mud2 contains a serine arginine (SR)-rich domain proposed to interact with the pre-mRNA (224) as well as several RNA recognition motif (RRM) domains. The first two RRMs mediate RNA binding (225) and the last RRM mediates binding to the branchpoint binding protein, Msl5 (226), as determined for the human protein. The yeast and human proteins are distantly related with the first two RRMs lacking significant sequence identity (~11%) whereas the 3rd RRM is 31% identical and 49% similar. Despite differences in sequence identity, residues in the RNP, which mediate RNA recognition, are conserved. Amino acid changes were guided by alignment of the Mud2 amino acid sequence with conserved orthologues in fission yeast (Prp2) and human (U2AF65) (Figure 3.12) (225, 226). We created: an SR domain mutant with amino acid substitutions, (R130A, R131A, R133A, R139A, R140A, and R142A); an RRM1 mutant containing amino acid substitutions: (V210A, I211A, and F266A); an RRM2 mutant containing amino acid substitutions: (N310A, F373A, and V375A); and an RRM3

mutant: (L425A, L427A, N480A, Y482A, and Y484A) (227). Of these Mud2 mutants, only the RRM3 could not rescue the growth of Δ*mud2 nab2-C437S* double mutant cells (Figure 3.6B). These data suggest that interaction of Mud2 RRM3 with Msl5 is critical when Nab2 function is impaired.

Nab2 physically associates with the commitment complex

Given that *NAB2* genetically interacts with the early splicing factor *MUD2*, we hypothesized that these factors might physically interact either directly or via binding to shared mRNA targets. Mud2 physically interacts with the essential branchpoint binding protein, Msl5, which is crucial for commitment complex formation (125, 228). As shown in Figure 3.6B, our genetic data suggests that the Mud2 association with Msl5 is critical when Nab2 is impaired. We therefore examined whether Nab2 physically associates with Mud2 and/or Msl5. To examine these interactions, we analyzed co-purification of Myc-tagged Nab2 with TAP-tagged Mud2 or Msl5 expressed in *S. cerevisiae* cells. As a control, we included TAP-tagged Pub1, a factor that interacts with Nab2, and Srp1, a nuclear import receptor that does not interact with Nab2 (141). As shown in Figure 3.7B, Nab2 associates with Pub1, Mud2, and Msl5 whereas no binding was observed with the negative control protein, Srp1. The addition of RNase reduced the association between Nab2 and members of the commitment complex, Mud2 and Msl5, largely indicative of RNA-dependent binding. To determine which domain of Nab2 is responsible for the

physical association with the commitment complex proteins, we examined the binding of Myc-tagged Nab2 deletion mutants, Nab2-ΔN-myc or Nab2-ΔZnF6-7-myc, in TAP-tagged strains. The zinc finger deletion mutant, ΔZnF6-7, removes the last two zinc fingers critical for RNA binding (146, 229). While Nab2-ΔN-myc still bound to Mud2 or Msl5, all association was eliminated with Nab2-ΔZnF6-7-myc (Figure 3.7C). These data suggest that Nab2 and Mud2/Msl5 are present on the same pool of RNAs. These results also suggest that Nab2 and Mud2/Msl5 do not directly interact, but rather are associated with the same RNA.

Δ*mud2 nab2-C437S* mutant cells show accumulation of pre-mRNA and extended poly(A) tails

The genetic interaction between *NAB2* and *MUD2* suggests a function connection. To begin to understand the functional relationship between Nab2 and Mud2, we utilized the Δ*mud2 nab2-C437S* double mutant to probe for post-transcriptional RNA processing defects. Nab2 has been implicated in limiting poly(A) tail length as well as promoting export of properly processed mRNAs (151). Mud2 is implicated in splicing (214) and nuclear retention of pre-mRNA (221). As Mud2 and Nab2 are important for splicing, one possibility is that splicing defects are exacerbated in a double mutant. To determine the amount of unspliced pre-mRNA in Δ*mud2 nab2-C437S* cells, qRT-PCR was performed for *ACT1*, *RPL21B*, and *RPL36A* transcripts. For all transcripts examined, there was a

significant increase in pre-mRNA in the double mutant compared to the single mutants (Figure 3.8A-C). Interestingly, the amount of mature mRNA for *RPL21B* and *RPL36A* decreased in Δ*mud2 nab2-C437S* cells, consistent with the inability to efficiently complete nuclear processing steps. These data show that pre-mRNA splicing is strongly affected in the double mutant and also that a subset of mature mRNA transcripts are decreased.

Nab2 is implicated in the control of poly(A) tail length and we reasoned that the growth defect in Δ*mud2 nab2-C437S* cells could be attributed to a defect in poly(A) tail length. We assessed poly(A) RNA tail length by utilizing a bulk poly(A) RNA tail length assay. As previously described, *nab2-C437S* mutant cells accumulate extended poly(A) tails as compared to wildtype cells (Figure 3.8D and 3.8E). In contrast, deletion of *MUD2* results in short poly(A) tails and this is the first evidence showing that Δ*mud2* leads to shorter poly(A) tails *in vivo*. Interestingly, Δ*mud2 nab2-C437S* double mutant cells show a long, heterogeneous poly(A) tails as compared to *nab2-C437S* alone. This observation suggests that the increased level of hyperadenylated RNAs in the double mutant may specifically affect transcripts in a Nab2-dependent manner.

Both Nab2 and Mud2 interact with quality control factors present at the nuclear pore, leading to the hypothesis that Nab2 and Mud2 can cooperate to retain improperly processed RNAs. Therefore, Δ*mud2 nab2-C437S* mutant cells would result in export defects due to accumulation of 3'-end extended, intron containing mRNA transcripts. To examine poly(A) RNA export, we performed fluorescence *in situ* hybridization. As

previously described, poly(A) RNA accumulates in the nucleus in *nab2*-Δ*N* cells, but no nuclear accumulation is observed in the *nab2-C437S* mutant (156). We detect no changes in bulk poly(A) RNA localization when *nab2* mutants were combined with Δ*mud2* (Figure 3.8F). While we can not rule out the possibility that a specific subset of RNAs are retained in this bulk poly(A) RNA export assay, this result suggests that Δ*mud2 nab2-C437S* mutant cells do not significantly impact export. One possibility is that misprocessed RNAs are leaked into the cytoplasm, escaping the nuclear pore RNA surveillance checkpoint. However, mutants of *nab2* do not result in pre-mRNA leakage to the cytoplasm (data not shown). Another possibility is that improperly processed transcripts are targeted for decay by the nuclear exosome.

Loss of Rrp6 rescues the growth, pre-mRNA accumulation, and poly(A) tail length defect in Δ*mud2 nab2-C437S* mutants

One prediction from our data is that Nab2 and Mud2 could interact with the exosome to serve as a surveillance cofactor, alerting the cell to misprocessed pre-mRNA. We hypothesized that the misprocessed mRNA transcripts in these mutants may be targeted for decay by the RNA exosome. The exosome is a multisubunit complex with 3'-5' exoribonuclease activity that relies on cofactors to assist in mRNA processing and degradation (213), including the nuclear specific component, Rrp6, and the TRAMP complex consisting of the RNA binding factors Air 1/2, the poly(A) polymerase Trf 4/5,

and the helicase Mtr4 (76, 88).

To determine if Δ*mud2 nab2-C437S* is linked to the decay machinery, we probed for a genetic interaction between *NAB2* or *MUD2* and *RRP6* or *TRF4*. No changes in growth were detected in mutants of *NAB2* combined with Δ*trf4* and only a slight growth defect was observed in Δ*mud2*Δ*trf4* (Figure 3.9A). However, deletion of *RRP6* in combination with *nab2-C437S* or Δ*mud2 nab2-C437S* rescued the cold sensitive growth of *nab2-C437S* cells at 16°C. Remarkably, growth was nearly restored to wildtype levels in the Δ*rrp6*Δ*mud2 nab2-C437S* triple mutant. These data suggests that the absence of *RRP6* and presumably a decrease in the catalytic activity of the nuclear exosome can rescue the growth defect of *nab2-C437S* and Δ*mud2 nab2-C437S* cells.

To test if the catalytic activity of the exosome is required for the poor growth in Δ*mud2 nab2-C437S* double mutant, we utilized a mutant that inactivates the exonuclease activity of Rrp6. This catalytically impaired mutant, *rrp6-1,* contains an aspartate to asparagine amino acid substitution at residue 268 *(rrp6-D238N)*(230). We transformed Δ*rrp6*Δ*mud2 nab2-C437S* cells with vector plasmid, wildtype Rrp6, or the catalytically inactive mutant, *rrp6-D238N*. As shown in Figure 3.9B, the growth of the Δ*rrp6*Δ*mud2 nab2-C437S* triple mutant was reduced with expression of wildtype Rrp6 and is comparable to the growth in Δ*mud2 nab2-C437S* double mutant. In contrast, there was no change in the growth of the Δ*rrp6*Δ*mud2 nab2-C437S* triple mutant with expression of *rrp6-D238N*. These results indicate that the loss Rrp6 catalytic activity in Δ*mud2 nab2-C437S* mutant cells restores cell growth.

To determine if the poly(A) tail length is impacted upon loss of Rrp6, we examined bulk poly(A) tail length. As shown previously (Figure 3.8E), extended heterogeneous tails are observed in Δ*mud2 nab2-C437S* cells when compared to Δ*mud2* or *nab2-C437S* alone. Consistent with the growth assay, no additional changes in poly(A) tail length were detected in mutants of *nab2* or *mud2* in combination with the TRAMP poly(A) polymerase, Δ*trf4* (Figure 3.9C and D). In contrast, poly(A) tails in Δ*rrp6* cells are extremely long, but are shortened when combined with mutants in *nab2* or *mud2*. Interestingly, Δ*rrp6* Δ*mud2 nab2-C437S* poly(A) tails are as long as poly(A) tails in wildtype cells, consistent with the rescue of cell growth observed in this triple mutant. This result suggests that the hyperadenylated tails in Δ*mud2 nab2-C437S* are restored to an average poly(A) tail length in the absence of Rrp6.

We investigated the levels of both pre-mRNA and mature mRNA to follow mRNA processing. To determine the effect of Δ*rrp6* on pre-mRNA transcript levels, qRT-PCR was performed on *ACT1*, *RPL21B*, and *RPL36A* transcripts. As shown in Figure 3.10 (A-C), Δ*rrp6* cells did not result in accumulation of intron-containing transcripts compared to wildtype cells (81). In addition, pre-mRNA levels did not change in Δ*rrp6 nab2-C437S* double mutant cells compared to *nab2-C437S* cells. In contrast, a slight decrease in pre-mRNA was observed in Δ*rrp6* Δ*mud2* mutant cells compared to Δ*mud2* cells. Consistent with growth data, the level of pre-mRNA decreased to near wildtype levels in Δ*rrp6* Δ*mud2 nab2-C437S* cells when compared to Δ*mud2 nab2-C437S* cells.

To determine the effect of Δ*rrp6* on total mRNA transcript levels, qRT-PCR was performed on *ACT1*, *RPL21B*, and *RPL36A* transcripts. As shown in Figure 3.10 (D-F), deletion of *RRP6* resulted in a striking increase of total mRNA levels in *nab2-C437S* cells. In addition, an increase of total mRNA levels for *RPL21B* and *RPL36A* was observed in Δ*rrp6* Δ*mud2 nab2-C437S* cells. These results suggest that in the absence of Rrp6, the levels of intron-containing transcripts is reduced and total RNA is increased in *nab2-C437S* and Δ*mud2 nab2-C437S* mutant cells.

DISCUSSION

This study provides the first evidence in support of a role for Nab2 in cooperating with splicing factors to ensure proper nuclear mRNA processing. A combination of genetic and biochemical approaches reveal that mutations in *nab2* impair splicing both *in vitro* and *in vivo*, resulting in pre-mRNA accumulation at the first step of splicing. Further results identify a family of splicing factors, including the commitment complex protein, Mud2, that show interactions with Nab2. Consistent with functional overlap, cells mutant for both *mud2* and *nab2* (Δ*mud2 nab2-C437S*) show severe growth defects, significant pre-mRNA accumulation, and extended poly(A) tails. Interestingly, the accumulation aberrant RNAs in the *nab2 mud2* double mutant cells was eliminated upon deletion of the nuclear exosome factor, *RRP6*. These findings provide evidence that

Nab2 associates with pre-mRNA to promote proper RNA processing and prevent accumulation of aberrant RNAs via interaction with the nuclear exosome.

Coupling RNA Splicing and 3'-end Processing

While cells mutant for *nab2* clearly result in accumulation of pre-mRNA, we hypothesize that Nab2 likely influences RNA splicing indirectly. One possibility for the accumulation of intron containing pre-mRNAs in mutants of *nab2* is that the role of Nab2 in 3'-end processing influences splicing. There is extensive evidence linking the core 3'-end processing machinery with splicing machinery, whereby each process is functionally coupled to transcription (103). However, 3'-end processing mutants do not accumulate pre-mRNA *in vivo* (219). Therefore, Nab2 serves as a unique factor involved in 3'-end processing and splicing. The crosstalk between splicing and 3'-end processing is also exemplified by the interaction between Nab2 and Mud2. Here, we identified a novel role for the splicing factor, Mud2, in 3'-end processing *in vivo*. The data presented here are consistent with studies in human cells that revealed a role for the putative Mud2 orthologue, U2AF65, in stimulating poly(A) polymerase *in vitro*. These results indicate that Nab2 and Mud2 functionally overlap to influence splicing and 3'-end processing. This functional overlap ensures a fail-safe mechanism for proper RNA processing and prevention of pre-mRNA accumulation. One implication of this model is that Nab2 and Mud2 serve as adaptor proteins for the nuclear exosome.

RNA Surveillance Monitors pre-mRNA Processing

Misprocessed RNAs are targeted for the nuclear exosome with the help of adaptor proteins that recognize the faulty pre-mRNA. In fact, the vast amount of pre-mRNA intermediates are targeted for decay in wildtype cells, indicating a fine balance between RNA processing and decay (231). Interestingly, we find that deletion of genes encoding the nuclear exosome component, Rrp6, but not the poly(A) polymerase TRAMP component, Trf4, (76, 88) can suppress the cold sensitive growth of the *nab2-C437S* mutant at 16°C and that suppression is even more profound for the Δ*mud2 nab2-C437S* double mutant.

These results suggest that the time required to produce a mature mRNP is critical to produce mature mRNA in Δ*mud2 nab2-C437S* mutant cells. In this case where RNA processing is likely impaired, removing an exonuclease provides the cell with more time to perform mRNA processing whereas in the single mutants, Rrp6 may contribute to efficient degradation of RNAs perceived as aberrant. As suppression of the Δ*mud2 nab2-C437S* mutant by deletion of *rrp6* occurs at 16°C, an attractive possibility is that mRNA processing kinetics are slowed at a low temperature and extra time is required to achieve proper mRNA processing and mRNP assembly. Therefore in wildtype cells, Nab2 interacts with the splicing and 3'-end processing machinery and signals to the exosome to promptly degrade aberrant mRNAs (Figure 3.11A).

In Δ*mud2 nab2-C437S* mutant cells, the unspliced pre-mRNA and extended poly(A) tails may delay export, subsequently targeting these RNAs for the exosome. As there is still an increase in the accumulation of aberrant RNAs, some RNAs may either escape nuclear degradation because of alternative decay pathways or these RNAs are not targeted as efficiently to the exosome (Figure 3.11B).

In Δ*rrp6* Δ*mud2 nab2-C437S* mutant cells, the aberrant RNAs are no longer targeted for the nuclear exosome, allowing more time to complete splicing and 3'-end processing (Figure 3.11C). In addition, these results suggest that aberrant transcripts reenter the RNA processing pathway and this RNA recycling pathway relies on the function of Nab2. In support of this, Δ*rrp6 nab2-C437S* mutant cells accumulate both pre-mRNA and mRNA, indicating that pre-mRNA intermediates are not degraded and slowly undergo proper processing. Interestingly, the absence of Mud2 in Δ*rrp6 nab2-C437S* improves cell growth even further, perhaps because overcoming the commitment to splicing enhances processing. However, the production of mature mRNA is reduced in Δ*rrp6* Δ*mud2 nab2-C437S* mutant cells compared to Δ*rrp6 nab2-C437S* mutant cells. In contrast, poly(A) tail length is restored in Δ*rrp6* Δ*mud2 nab2-C437S* mutant cells compared to Δ*rrp6 nab2-C437S* mutant cells. These data suggest that the primary reason for improved growth in Δ*rrp6* Δ*mud2 nab2-C437S* mutant cells is restoration of poly(A) tail length.

One implication of this model is that there is extensive competition between pre-mRNA splicing, 3'-end processing, and mRNA decay. In support of this model,

Nab2 is found in complexes with poly(A) transcripts in an *in vitro* reconstituted system in the absence of Rrp6 (81). It is interesting to speculate that the interplay between Nab2 and Rrp6 is primarily due to the 3'-end processing defects found in *nab2* mutants. Previous studies have shown that most intron-containing transcripts are targeted by Dis3, not Rrp6, (231) and Dis3-dependent transcripts are able to reenter the splicing pathway when the catalytic activity of Dis3 is altered. Our studies show that Nab2-dependent pre-mRNA decay requires Rrp6 catalytic activity. These results are surprising in light of Dis3, but they may point to highly divergent pre-mRNA decay pathways that depend on unique RNA processing events and their associated RNA binding proteins.

Interplay between Poly(A) RNA Binding Proteins to Regulate pre-mRNA Decay

One outstanding question is how other poly(A) RNA binding proteins coordinate with Nab2 in the nuclear surveillance pathway. Recent work suggests that the *S. pombe* Nab2 antagonizes the nucleus poly(A) RNA binding protein, Pab2, to impede degradation of unspliced *rpl30-2* mRNA (216). Interestingly in *S. pombe*, deletion of *nab2* in combination with Δ*pab2* results in slow growth, hyperadenylated transcripts, and accumulation of pre-mRNA. These data is consistent with the phenotypes observed here in budding yeast cells mutant for *nab2* alone. However, the *S. cerevisiae* genome does not encode an obvious Pab2 orthologue, raising the possibility that Nab2 function could differ in the two organisms.

One possibility is that the *S. cerevisiae* cytoplasmic poly(A) RNA binding protein, Pab1, may collaborate with Nab2 (232). Upon Nab2 depletion, hyperadenylated species accumulate with a concommitment block in mRNA export. Overexpression of Pab1 suppresses the growth and export defect in Δ*nab2* cells, but does not rescue the hyperadenylation phenotype (151). It has been proposed that Pab1 protects polyadenylated transcripts from Rrp6-mediated decay whereas the presence of Nab2 on polyadenylated transcripts stimulates Rrp6-mediated decay (81). This study reinforces the model where Nab2 is present before Rrp6 senses the aberrant transcript. However, while the presence of Nab2 may stimulate RNA decay, our model predicts that Nab2 may also facilitate proper RNA processing. The choice between each pathway likely relies on extensive contacts with other RNA processing factors, which in turn influence RNA processing events like splicing and 3'-end processing. These results suggest that Nab2 serves as an important RNA surveillance factor with functional links to the nuclear exosome.

Identifying the molecular mechanisms underlying mRNA biogenesis reveals a new role of Nab2 in splicing and nuclear RNA surveillance. The findings reported here raise the question of whether these multiple roles in post-transcriptional regulation identified for Nab2 apply to Nab2 orthologues in higher eukaryotes. Little is known about the molecular functions of the human counterpart of Nab2, ZC3H14 (215), which is lost in a form of inherited intellectual disability (161). However, post-transcriptional regulation is particularly critical in neurons which rely on sophisticated spatial and

temporal control of gene expression. Thus, the role of Nab2/ZC3H14 is coordinating multiple processing events to ensure the generation of proper, mature mRNAs could provide insight into why mutations in human *ZC3H14* lead to brain dysfunction (161). The studies described here lay the framework for future analysis of ZC3H14 function as well as understanding the complex interplay between polyadenosine RNA binding proteins.

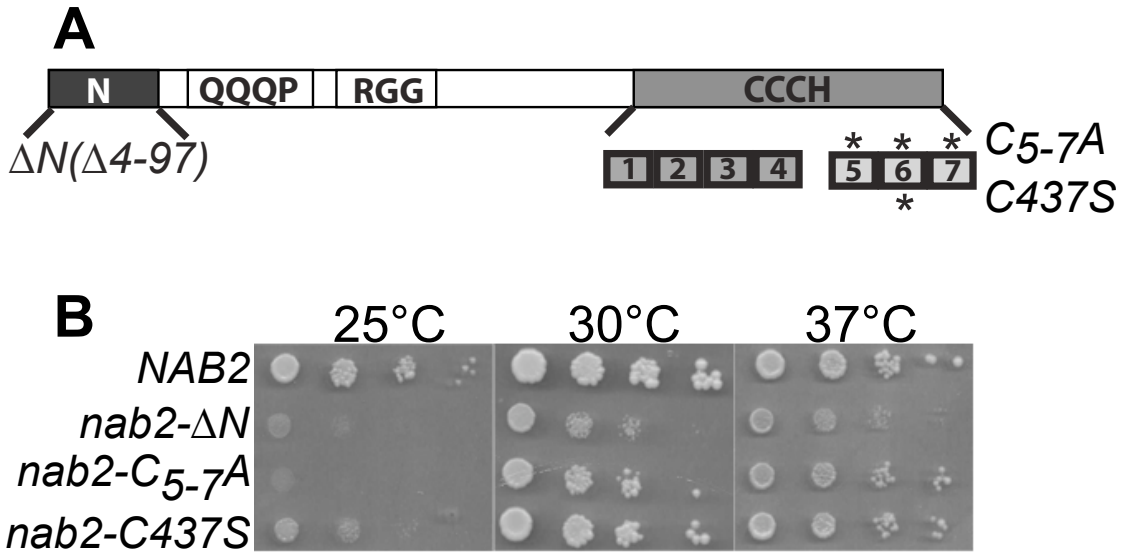

Figure 3.1: Cells mutant for *NAB2* show growth defects. (A) The full-length Nab2 protein consists of the following domains: A Proline-Tryptophan-Isoleucine (PWI)-like N terminal domain; a glutamine rich region (QQQP); an Arginine-Glycine-Glycine (RGG) domain required for nuclear localization; and a tandem Cysteine-Cysteine-Cysteine-Histidine (CCCH) zinc finger domain comprised of seven zinc fingers (152). Shown below the zinc finger domains are the last three zinc fingers which are critical for high affinity binding to polyadenosine RNA (146). The asterisks above the first cysteine residues in ZnF 5, 6, 7 indicate the cysteine residues altered to alanine to generate *nab2-$C_{5\text{-}7}A$*. The asterisks in the 6th zinc finger shows the cysteine residue altered to serine to generate *nab2-C437S.* The residues removed (4-97) to generate the N terminal mutant, *nab2-ΔN,* are also indicated. (B) Wildtype *NAB2* cells and the integrated *nab2* mutants: *nab2-ΔN, nab2-$C_{5\text{-}7}A$,* and *nab2-C437S* were grown at 25°C, 30°C, and 37°C serially diluted, and spotted onto YEPD plates at the indicated temperatures.

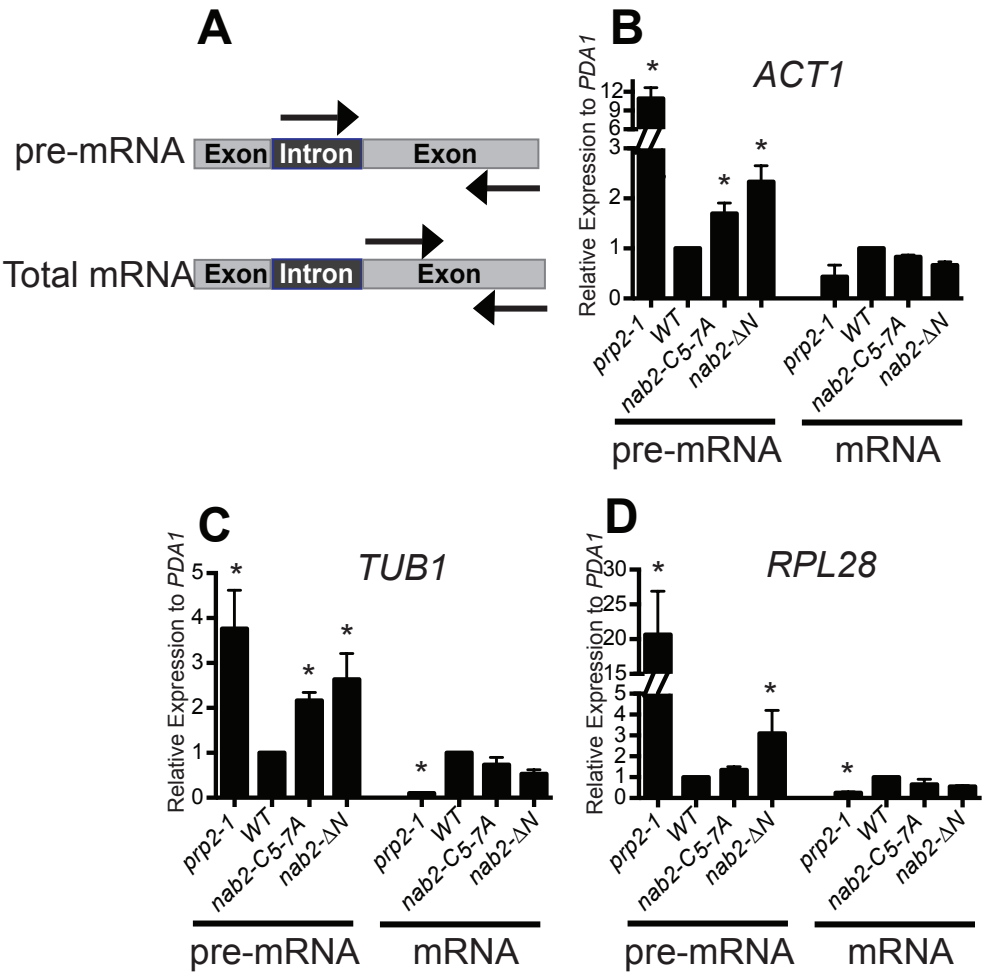

Figure 3.2: Unspliced transcripts accumulate in *nab2* mutant cells. (A) Schematic of primer locations used to amplify unspliced pre-mRNA and total mRNA. For each transcript, unspliced pre-mRNA was detected with primers that span intron-exon boundaries and total mRNA was detected with primers within the exon. (B-D) Total RNA was prepared from wildtype *NAB2*, *nab2-C$_{5-7}$A,* and *nab2-ΔN* cells as well as a control splicing mutant, *prp2-1* (31, 217). Quantitative real-time PCR analysis was performed to amplify (B) *ACT1* (C) *TUB1* (D) *RPL28A* transcripts. Results were normalized to the *PDA1* transcript and values were plotted relative to wildtype cells which was set to 1.0. Experiments were performed in triplicate, error bars=SEM, and statistical significance (indicated by the asterisks) was calculated for both pre-mRNA and mRNA using one-way ANOVA.

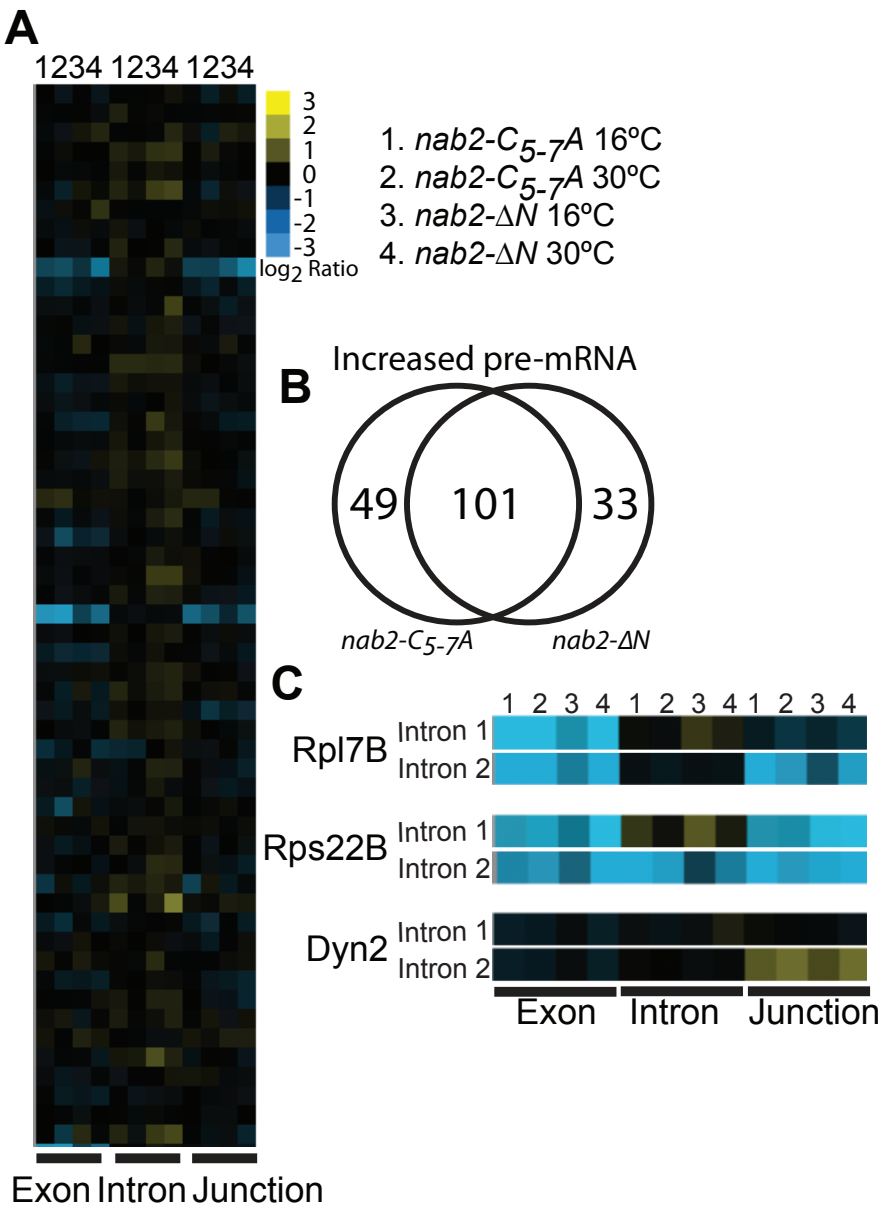

Figure 3.3: A splicing microarray reveals a mild, but constitutive accumulation of unspliced transcripts in *nab2* mutants. (A) Wildtype *NAB2*, *nab2-C*$_{5\text{-}7}$*A,* and *nab2-ΔN* cells were grown at 30°C and shifted to 16°C for one hour, RNA was collected, cDNA was generated, and hybridized to a splicing microarray as described in Materials and Methods. The microarray contains probes that identify pre-mRNA (Intron), mature mRNA (Junction), and total mRNA (Exon). (B) A Venn diagram illustrates the number of shared pre-mRNA transcripts that accumulate in *nab2-C*$_{5\text{-}7}$*A* and *nab2-ΔN* cells (C) Microarray data for transcripts that contain two introns, including *RPL7B*, *RPS22B*, and *DYN2*.

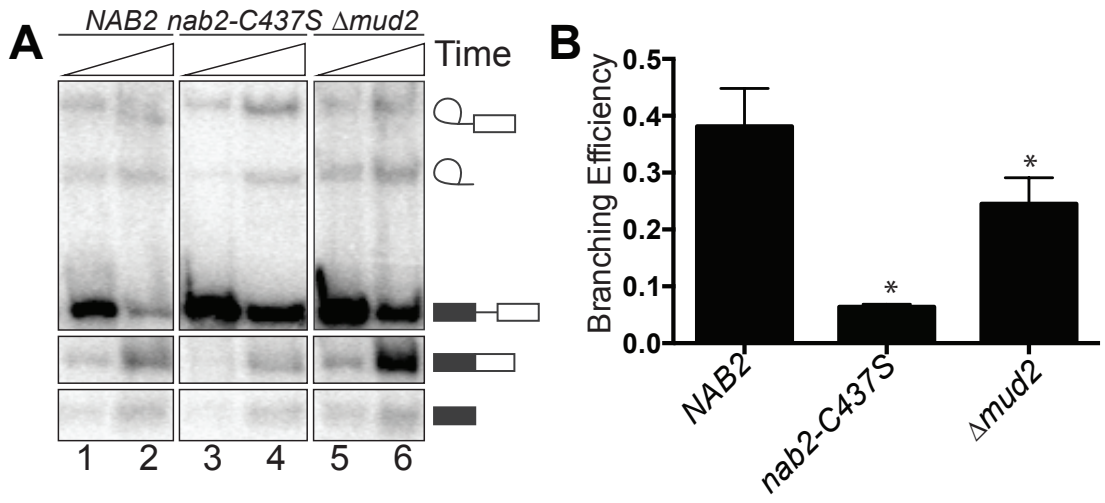

Figure 3.4: *In vitro* splicing assay shows a reduction in the efficiency of the 1st step of splicing in lysates prepared from *nab2* mutant cells. (A) Radiolabelled *ACT1* pre-mRNA was incubated with lysates isolated from wildtype *NAB2*, *nab2-C437S* cells as well as control lysates isolated from a splicing mutant, Δ*mud2* (214). Radiolabelled splicing products were separated on an acrylamide gel. The positions of the precursor, splicing intermediates, and spliced product are indicated by the schematic. (B) The branching efficiency in *nab2-C437S* lysates is compromised by at least 6-fold compared to wildtype. The splicing species were quantified from (A) and replicates using totalLab Quant. The branching efficiency is calculated as (5' + M)/(5' + M + P). 5', 5' exon; M, mRNA; P: pre-mRNA. Error bars=SD ($n \geq 2$). Statistical significance (indicated by the asterisks) was calculated using one-way ANOVA.

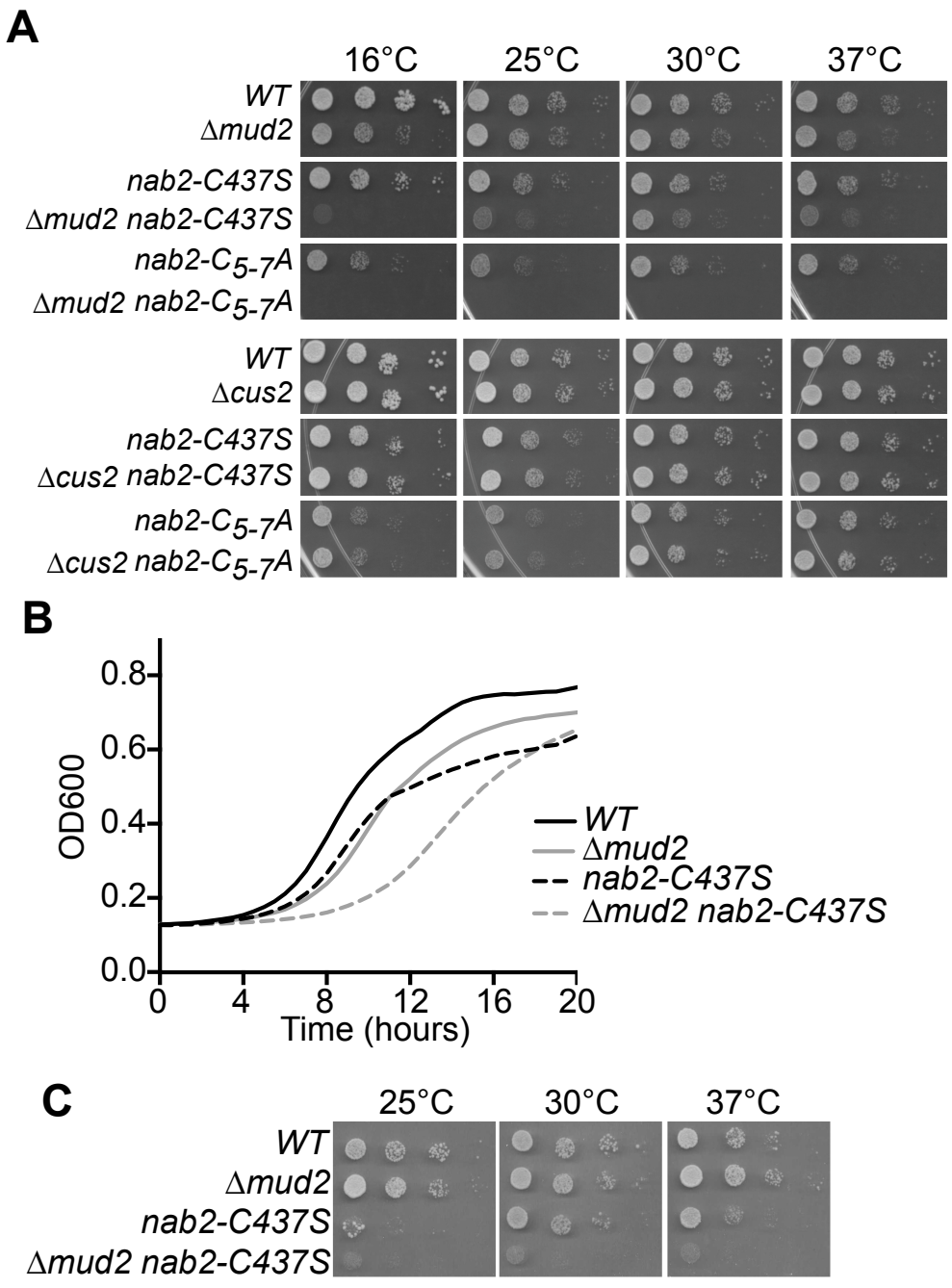
A
16°C
25°C
30°C
37°C
WT
Δmud2
nab2-C437S
Δmud2 nab2-C437S
nab2-C5-7A
Δmud2 nab2-C5-7A
WT
Δcus2
nab2-C437S
Δcus2 nab2-C437S
nab2-C5-7A
Δcus2 nab2-C5-7A
B
OD600
0.0
0.2
0.4
0.6
0.8
0
4
8
12
16
20
Time (hours)
WT
Δmud2
nab2-C437S
Δmud2 nab2-C437S
C
25°C
30°C
37°C
WT
Δmud2
nab2-C437S
Δmud2 nab2-C437S

Figure 3.5: Growth assays to examine genetic interactions between *nab2* mutants and alleles of splicing factors. (A) As described in Materials and Methods, a plasmid shuffle assay was used to analyze the growth of the splicing factor mutants in combination with *nab2* mutants. Δ*nab2* (ACY427), Δ*nab2*Δ*mud2* (ACY2138), and Δ*nab2*Δ*cus2* (ACY2136) cells maintained by a *URA3* plasmid encoding wildtype *NAB2* were transformed with *LEU2* plasmids encoding wildtype *NAB2*, *nab2-$C_{5\text{-}7}A$,* or *nab2-C437S.* Cells were selected on 5-FOA to eliminate the *NAB2* maintenance plasmid and grown, serially diluted, and spotted onto plates lacking leucine to assess growth at 16°C, 25°C, 30°C, and 37°C. (B) Growth curves were generated for Δ*nab2* or Δ*nab2*Δ*mud2* cells carrying wildtype *NAB2*, *nab2-$C_{5\text{-}7}A$,* or *nab2-C437S* mutant plasmids in liquid media. The cells were grown to saturation and diluted, and their optical density was measured at A_{600} for 20 hr at 25°C. (C) Isogenic integrated strains were generated by deleting *MUD2* in wildtype (ACY402) and *nab2-C437S* (ACY2202) cells to produce Δ*mud2* (ACY2270) and Δ*mud2 nab2-C437S* (ACY2273) cells. Wildtype, Δ*mud2, nab2-C437S* and Δ*mud2 nab2-C437S* cells were grown, serially diluted, and spotted onto YEPD plates at 25°C, 30°C, and 37°C.

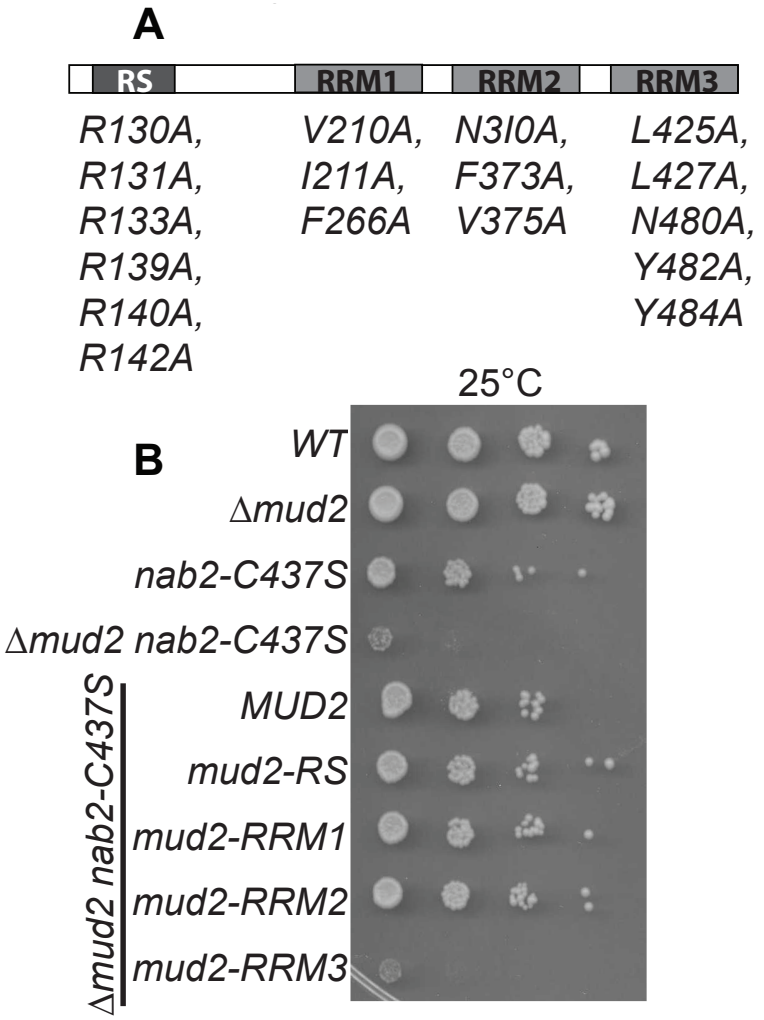

Figure 3.6: Interaction between Mud2 and Msl5 is required when Nab2 function is impaired. (A) Schematic of Mud2 showing the Serine-Arginine (SR) domain and three RNA Recognition Motifs (RRM): RRM1, RRM2, and RRM3. Amino acid substitutions designed to impair the function of each domain are illustrated. The amino acid substitutions are in the: SR domain (R130A, R131A, R133A, R139A, R140A, and R142A); RRM1: (R208A, V210A, I211A, and F266A); RRM2: (N310A, I311A, and F373A); and RRM3: (L425A, L427A, N480A, Y482A, and Y484A). (B) Wildtype (WT) cells and integrated mutant Δ*mud2, nab2-C437S,* and Δ*mud2 nab2-C437S* cells were transformed with a vector plasmid and are shown as controls. Δ*mud2 nab2-C437S* cells were transformed with Mud2 plasmids expressing wildtype *MUD2* or *mud2* mutants in the SR, RRM1, RRM2, and RRM3 domains. Cells were grown, serially diluted, and spotted onto plates lacking uracil to assess growth at 25°C

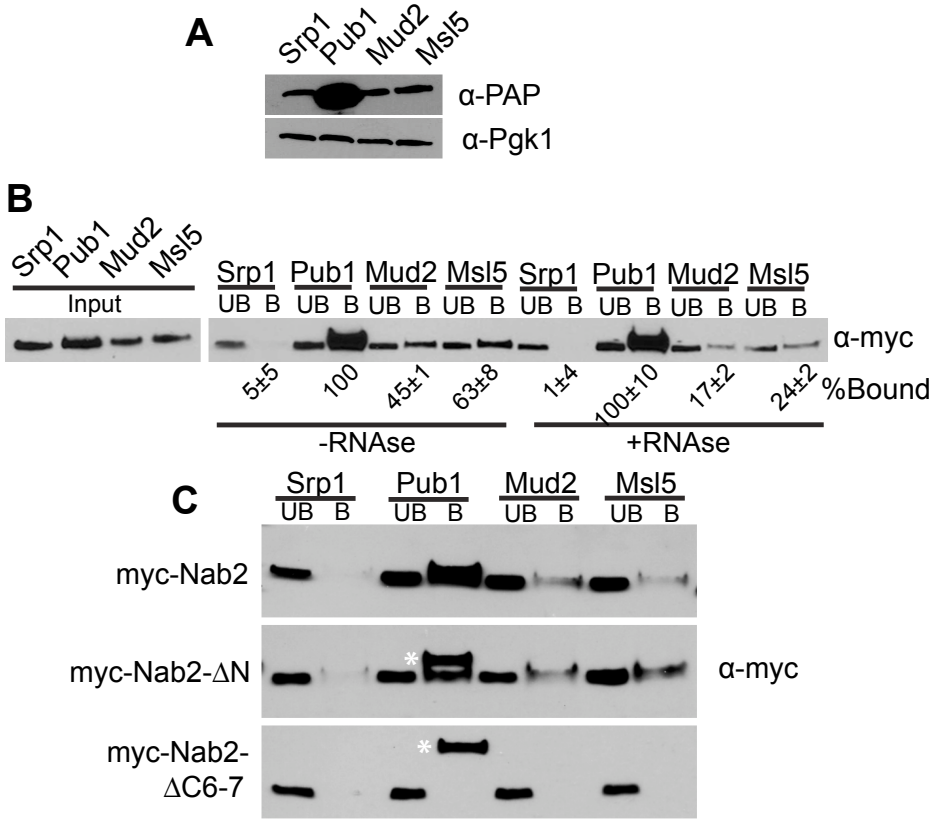

Figure 3.7: Nab2 physically interacts with the commitment complex in an RNA-dependent manner. Immunoblot showing expression of TAP-tagged proteins: Srp1, Pub1, Mud2, or Msl5. Immunoblotting was performed with α-PAP antibody to detect TAP-tagged protein expression and with α-PGK1 to use as a loading control. (B) Cells expressing C-terminal TAP-tagged proteins: Srp1, Pub1, Mud2, or Msl5 were transformed with a Nab2-myc plasmid. The TAP-tagged proteins were purified and Nab2-myc was detected by immunoblotting in the Input, unbound (UB), and bound (B) fractions. Samples were treated with (+RNAse) or without RNAse (-RNAse) to assess the RNA dependence of the interaction. The percentage of bound Nab2 protein relative to the amount of input protein and Nab2 bound to Pub1 (% Bound) is indicated below the bound fractions. Experiments were performed in triplicate and standard deviation was calculated. (C) To map the domain of Nab2 required for interaction with Mud2/Msl5, cells expressing TAP-tagged Srp1, Pub1, Mud2, or Msl5 were transformed with full length Nab2-myc, Nab2-ΔN-myc, or Nab2-ΔC6-7-myc plasmids. The TAP-tagged proteins were precipitated from yeast lysates and immunoblotting was performed with α-myc antibody to detect Nab2 in the unbound (UB) and bound (B) lane. The extra band in the Pub1 observed in the Nab2-ΔN-myc or Nab2-ΔC6-7-myc bound fraction is a cross reacting band of similar size to the Nab2 protein. The cross reacting band is indicated by the asterisks.

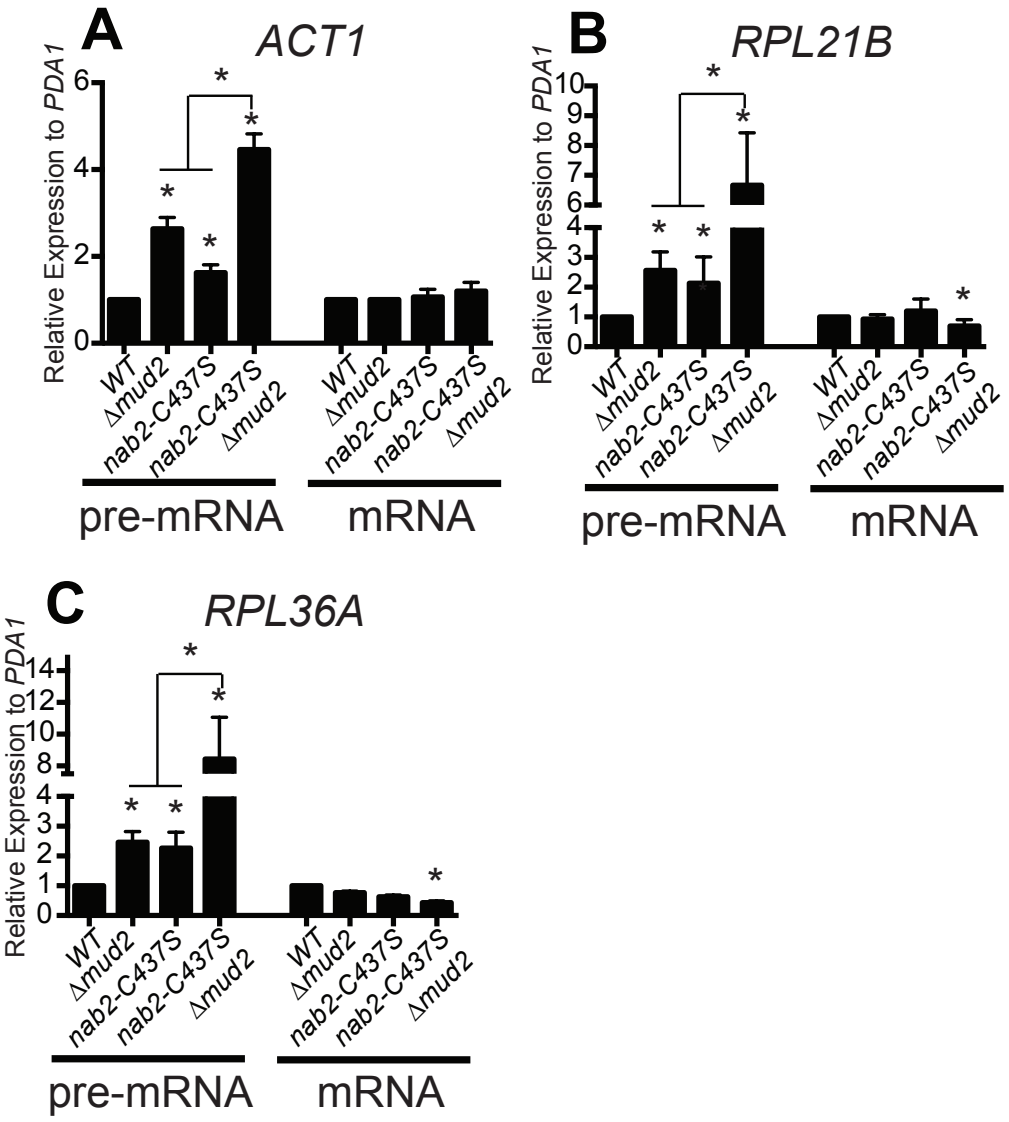
A
ACT1
Relative Expression to PDA1
WT
Δmud2
nab2-C437S
nab2-C437S Δmud2
pre-mRNA
mRNA
B
RPL21B
C
RPL36A

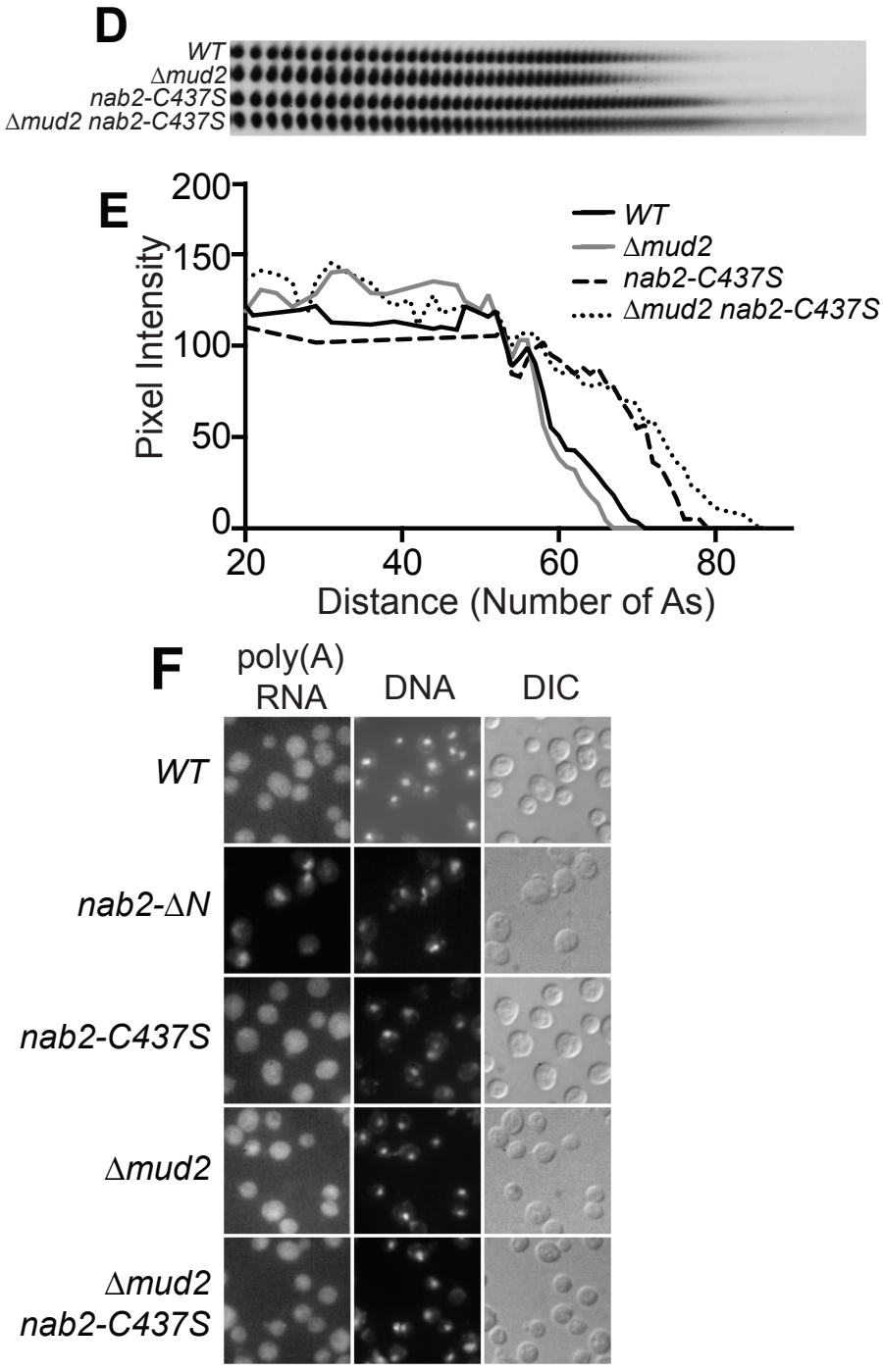
D
WT
Δmud2
nab2-C437S
Δmud2 nab2-C437S
E
Pixel Intensity
200
150
100
50
0
20
40
60
80
Distance (Number of As)
WT
Δmud2
nab2-C437S
Δmud2 nab2-C437S
F
poly(A) RNA
DNA
DIC
WT
nab2-ΔN
nab2-C437S
Δmud2
Δmud2 nab2-C437S

Figure 3.8: Mutants in *nab2* and *mud2* show defects in poly(A) tail length control and mRNA splicing. (A-C) Total yeast RNA was isolated from wildtype and integrated mutant Δ*mud2, nab2-C437S,* and Δ*mud2 nab2-C437S* cells grown at 30°C. Quantitative real-time PCR analysis was performed to amplify (A) *ACT1,* (B) *RPL21B,* and (C) *RPL36A* intron-containing transcripts. For each transcript, unspliced pre-mRNA was detected with primers that span intron-exon boundaries and total mRNA was detected with primers within the exon. Results were normalized to the *PDA1* transcript and values were plotted relative to wildtype cells which was set to 1.0. Experiments were performed in triplicate, error bars=SEM, and statistical significance (indicated by the asterisks) was calculated for both pre-mRNA and mRNA using one-way ANOVA. (D) Total yeast RNA isolated from wildtype, Δ*mud2, nab2-C437S,* and Δ*mud2 nab2-C437S* cells grown at 30°C was analyzed for bulk poly(A) tail length as described in Materials and Methods. (E) Poly(A) tails were quantified using ImageJ by calculating pixel intensity along the length of the poly(A) tail and plotted relative to the number of As as described in Materials and Methods. (F) To examine poly(A) RNA export, wildtype, *nab2*-Δ*N, nab2-C437S,* Δ*mud2,* and Δ*mud2 nab2-C437S* cells grown at 30°C were probed with oligo-dT to detect poly(A) RNA and DAPI to detect DNA. Differential interference contrast (DIC) images are also shown.

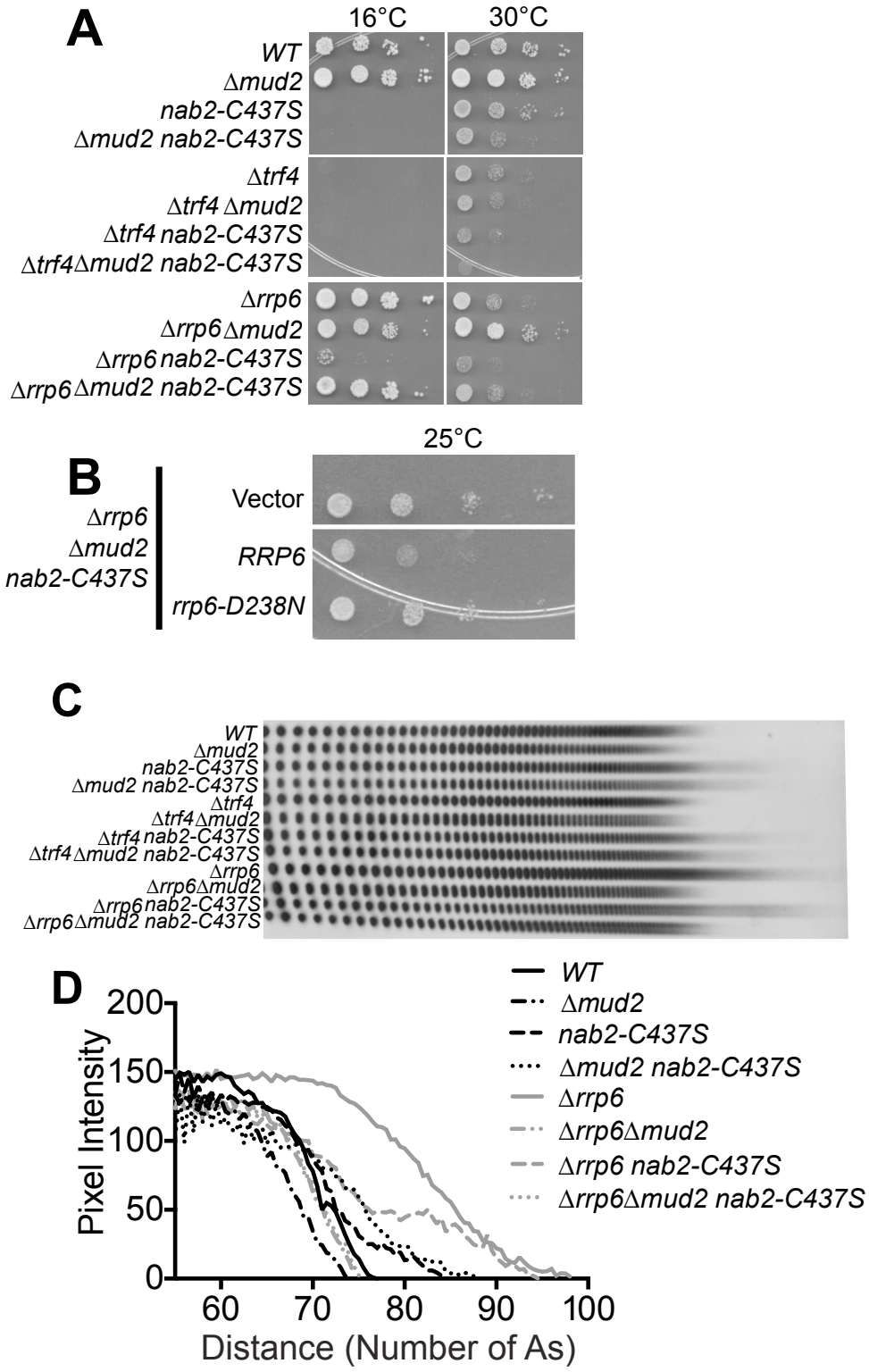
A
16°C
30°C
WT
Δmud2
nab2-C437S
Δmud2 nab2-C437S
Δtrf4
Δtrf4 Δmud2
Δtrf4 nab2-C437S
Δtrf4Δmud2 nab2-C437S
Δrrp6
Δrrp6Δmud2
Δrrp6 nab2-C437S
Δrrp6Δmud2 nab2-C437S
B
25°C
Δrrp6
Δmud2
nab2-C437S
Vector
RRP6
rrp6-D238N
C
WT
Δmud2
nab2-C437S
Δmud2 nab2-C437S
Δtrf4
Δtrf4Δmud2
Δtrf4 nab2-C437S
Δtrf4Δmud2 nab2-C437S
Δrrp6
Δrrp6Δmud2
Δrrp6 nab2-C437S
Δrrp6Δmud2 nab2-C437S
D
Pixel Intensity
200
150
100
50
0
60
70
80
90
100
Distance (Number of As)
WT
Δmud2
nab2-C437S
Δmud2 nab2-C437S
Δrrp6
Δrrp6Δmud2
Δrrp6 nab2-C437S
Δrrp6Δmud2 nab2-C437S

Figure 3.9: Genetic interactions between the nuclear exosome subunit, *RRP6*, and *NAB2*. (A) Wildtype cells and integrated mutant Δ*mud2* (ACY2270)*, nab2-C437S* (ACY2202)*,* and Δ*mud2 nab2-C437S* (ACY2273) cells were combined with deletion of the TRAMP poly(A) polymerase, *TRF4*, or nuclear exosome component, *RRP6*, gene. Cells were grown, serially diluted, and spotted onto YEPD plates at 25°C, 30°C, and 37°C. (B) Δ*rrp6* Δ*mud2 nab2-C437S* (ACY2313) cells were transformed with vector plasmid and are shown as control. Δ*rrp6* Δ*mud2 nab2-C437S* cells were transformed with Rrp6 plasmids expressing wildtype *RRP6* or *rrp6-D238N* catalytic mutant. Cells were grown, serially diluted, and spotted onto plates lacking uracil to assess growth at 16°C. (C) Total yeast RNA was isolated from wildtype, Δ*mud2, nab2-C437S,* and Δ*mud2 nab2-C437S* cells combined with Δ*trf4* or Δ*rrp6* and analyzed for bulk poly(A) tail length as described in Materials and Methods. (D) Poly(A) tails were quantified using ImageJ by calculating pixel intensity along the length of the poly(A) tail and plotted relative to the number of As as described in Materials and Methods.

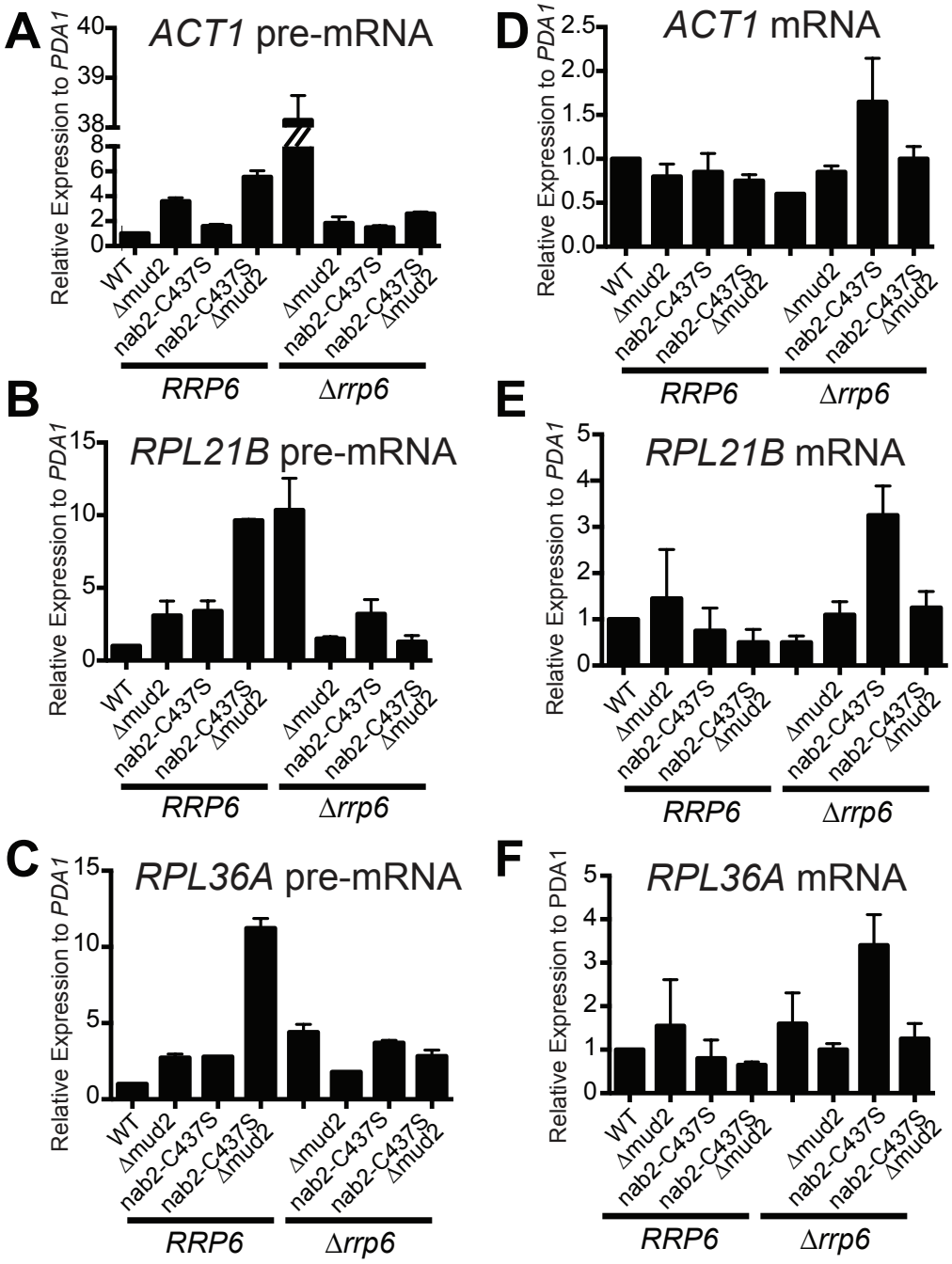
A
ACT1 pre-mRNA
Relative Expression to PDA1
40
39
38
8
6
4
2
0
WT
Δmud2
nab2-C437S
nab2-C437S Δmud2
Δmud2
nab2-C437S
nab2-C437S Δmud2
RRP6
Δrrp6
D
ACT1 mRNA
Relative Expression to PDA1
2.5
2.0
1.5
1.0
0.5
0.0
WT
Δmud2
nab2-C437S
nab2-C437S Δmud2
Δmud2
nab2-C437S
nab2-C437S Δmud2
RRP6
Δrrp6
B
RPL21B pre-mRNA
Relative Expression to PDA1
15
10
5
0
WT
Δmud2
nab2-C437S
nab2-C437S Δmud2
Δmud2
nab2-C437S
nab2-C437S Δmud2
RRP6
Δrrp6
E
RPL21B mRNA
Relative Expression to PDA1
5
4
3
2
1
0
WT
Δmud2
nab2-C437S
nab2-C437S Δmud2
Δmud2
nab2-C437S
nab2-C437S Δmud2
RRP6
Δrrp6
C
RPL36A pre-mRNA
Relative Expression to PDA1
15
10
5
0
WT
Δmud2
nab2-C437S
nab2-C437S Δmud2
Δmud2
nab2-C437S
nab2-C437S Δmud2
RRP6
Δrrp6
F
RPL36A mRNA
Relative Expression to PDA1
5
4
3
2
1
0
WT
Δmud2
nab2-C437S
nab2-C437S Δmud2
Δmud2
nab2-C437S
nab2-C437S Δmud2
RRP6
Δrrp6

Figure 3.10: Deletion of *RRP6* restores pre-mRNA processing in mutants of *nab2* and *mud2*. (A-C) To assess splicing efficiency, total yeast RNA was isolated from wildtype, Δ*mud2, nab2-C437S,* and Δ*mud2 nab2-C437S* cells combined with Δ*rrp6*. Quantitative real-time PCR analysis was performed to amplify (A) *ACT1*, (B) *RPL21B*, and (C) *RPL36A* intron-containing transcripts with primers that span the intron-exon boundary. Results were normalized to the *PDA1* transcript and values were plotted relative to wildtype cells which was set to 1.0. (D-F) To assess levels of total mRNA, quantitative real-time PCR analysis was performed to amplify (D) *ACT1*, (E) *RPL21B*, and (F) *RPL36A* intron-containing transcripts with primers within the exon. Results were normalized to the *PDA1* transcript and values were plotted relative to wildtype cells which was set to 1.0

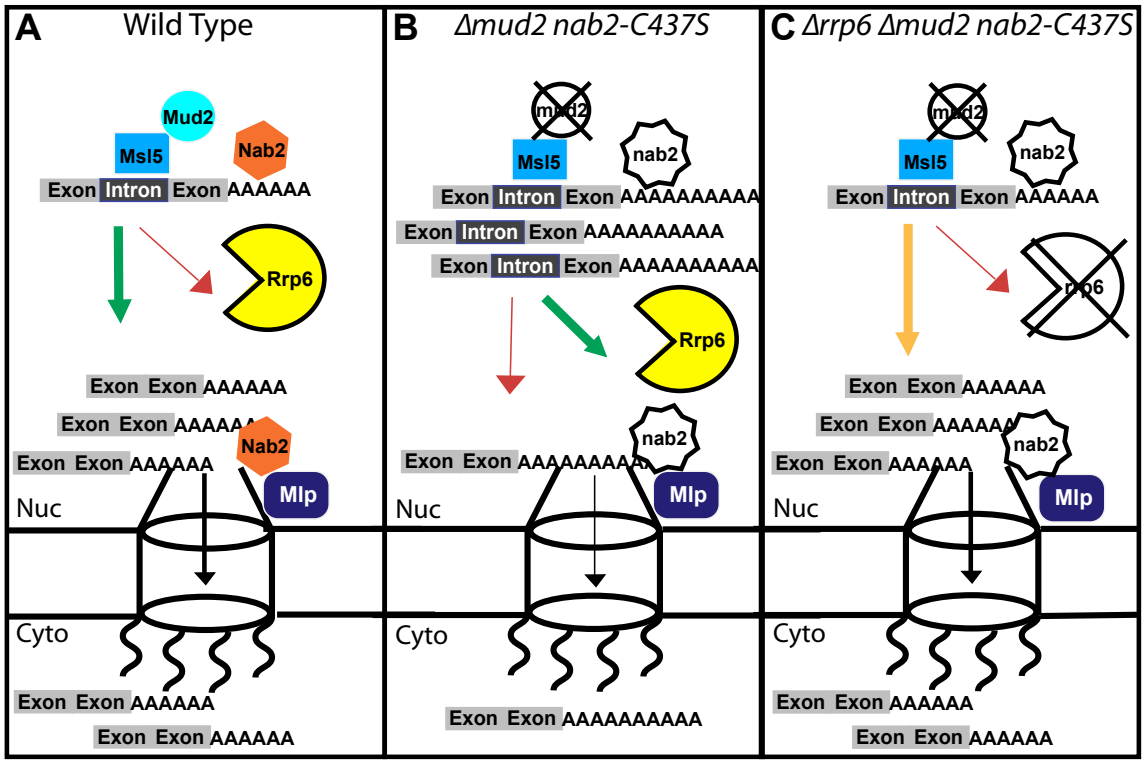

Figure 3.11: Model for Nab2 and Mud2 in splicing and mRNA surveillance. (A) In wildtype cells, Mud2 and Nab2 work together to promote efficient splicing and polyadenylation of mRNA as indicated by the thick green line. Nab2 interacts with Mlp proteins at the face of the nuclear pore to facilitate efficient export of processed transcripts. (B) In cells lacking functional *mud2* or *nab2*, transcript processing is impaired, triggering degradation by the nuclear exosome Rrp6 as indicated by the thick green line. Although some transcripts may escape nuclear surveillance and exit the nucleus, they may be improperly processed, resulting in extended poly(A) tails and/or missplicing. (C) In cells mutant for *mud2*, *nab2*, and *rrp6*, RNA processing is inefficient, more time is allotted to produce mature transcripts without degradation by Rrp6 as indicated by the yellow line. As a result, the transcript is eventually processed properly and exported to the cytoplasm.

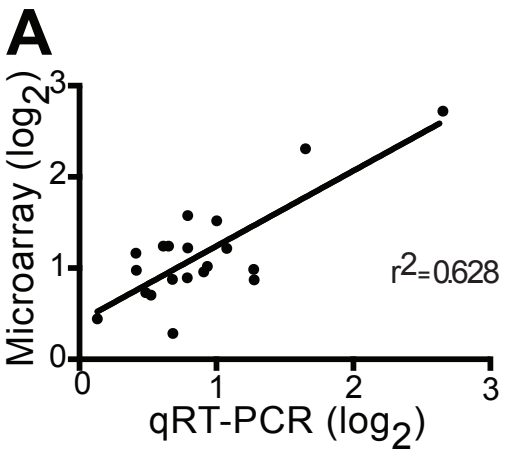

Figure 3.12: A splicing microarray is validated by qRT-PCR (A) The microarray data was validated by qRT-PCR to determine relative expression in selected transcripts. The relative expression for 20 transcripts assayed in qRT-PCR or microarray were paired and plotted for linear regression analysis. A positive correlation (r^2=0.628) is observed between the microarray and qRT-PCR data.

A

RS

```
                          *.*.. *.*..  .**.*. . .
S. cerevisiae 125--------RQRDERRGRNERFDRRGRNGNGN14
H. sapiens    17ERDKENRHRKRSHSRSRSRDRKRRSRSRDRR47
```

RRM1

```
              ..   ** .  .    . ...  ..  .       .   .          . .
S. cerevisiae 203SKANSRLVISGLS-QSSDPSIVARLKDLLENFISGLQKTESNAEDFKISNFYIGE
S. pombe      195SRQARRLVVTGIPNEFVEDAFVSFIEDLFI--STTYHKPETK----HFSSVNVCK
H. sapiens    145TRQARRLYVGNIPFGITEEAMMDFFNAQMR--LGGLTQAPGN----PVLAVQINQ

                .  ..*  .   .*                  ** .* ..*
S. cerevisiae GRPDHIIVEFSSQICSTMVLACRSFFNAKLGTFDLKWRRPNDY---------299
S. pombe      EE-NFAILEVATPEDATFLWGLQSES--YSNDVFLKFQRIQNYI-VPQITPE291
H. sapiens    DK-NFAFLEFRSVDETTQAMAFDGII--FQGQS-LKIRRPHDYQPLPGMS--240
```

RRM2

```
               *       *         .    *    *     *      .    *   * .
S. cerevisiae 314VIALENLENIGEGEDYRMKELFSSLNVTNGTAKPLFYKCSSNTNNTGKESEFTK
S. pombe      306VLDSKDKIYISNLPLNLGEDQVVELLKPFGDLL-SFQLIKNIADGSSKGFCFCE
H. sapiens    255VPDSAHKLFIGGLPNYLNDDQVKELLTSFGPLK-AFNLVKDSATGLSKGYAFCE

                    .   *.      .  .  .    .  .  .                .    .  .
S. cerevisiae CILLLSFEVVTQDILDKLKPY-KWFKPNDGKISQVTSWITFQ----------SLPNLVTQSVR---418
S. pombe      FKNPSDAEVAISGLDGKDTYGNKLHAQFACVGLNQAMIDKS----NGMAILTELAKASSQSI----415
H. sapiens YVDINVTDQAIAGLNGMQLGDKKLLVQRASVGAKNATLVSPPSTINQTPVTLQVPGLMSSQVQMGG372
```

RRM3

```
                 . ** * * .   .. *     .* * ..   .    .   .  .   .       *
S. cerevisiae 419VESRVLLLLNCLDPLDLKDETFITEIKETLKYSIAGADTIKICQPGVDYRLNFENLASG
S. pombe      416-PTRVLQLHNLITGDEIMDVQEYEDIYESVKTQFSNYGPLIDIK--IPRSIGTRNSGLG
H. sapiens    373HPTEVLCLMNMVLPEELLDDEEYEEIVEDVRDECSKYGLVKSIE--IPRPVDG-VEVPG
               *... .  .    . **. . * .* .* ..  .   * .
S. cerevisiae AGNIYIKFKTLEAAKHAMEELPGTQFNDRTVLCTYIDEDDFDMMEATQLS527
S. pombe      TGKVFVRYSDIRSAEVAMEEMKGCKFNDRTIVIAFYGEDCYKANAW----517
H. sapiens    CGKIFVEFTSVFDCQKAMQGLTGRKFANRVVVTKYCDPDSYHRRDFW---475
```

B

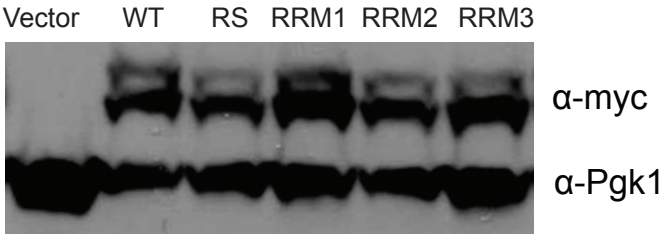

Figure 3.13: Alignment of Mud2 and U2AF65. (A) The sequence of the *S. cerevisiae* Mud2 RS domain is shown. The residues that were changed to alanine are indicated in bold. (B) Domain alignment of *S. cerevisiae* Mud2, *S. pombe* Mud2, and *H. sapiens* U2AF65. The identical amino acids above the alignment are indicated by the *. The RNP2 and RNP1 motifs are highlighted in the gray boxes. The residues that were changed to alanine are indicated in bold. (C) Wildtype cells were transformed with a vector plasmid and are shown as control. Wildtype cells were transformed with Mud2 plasmids expressing wildtype Mud2 or mud2 mutants in the SR, RRM1, RRM2, and RRM3 domains. Immunoblotting was performed with α-myc antibody to detect myc-tagged Mud2 protein and with α-PGK1 to use as a loading control.

TABLE 3.1.
Genetic interaction between *nab2* mutant alleles and alleles of splicing factors.

	Spliceosomal Complex	*NAB2*	*nab2-C437S*	*nab2-$C_{5-7}A$*	*nab2-ΔN*	*nab2-ΔQQQP*	*nab2-ΔRGG*
WT		+++	+++	++	++	+++	+++
Δmud2	E	+++	++	-	+	+++	+++
Δnam8	E and A	+++	+++	++	++	+++	+++
Δcus2	A	+++	+++	++	++	+++	+++
Δmud1	A and B	+++	+++	+	++	+++	+++
Δmsl1	A and B	+++	+	-	-	+++	+++
Δlea1	A and B	+++	+++	ND	-	ND	ND
Δsnu66[b]	B and C	+++	+	+	++	+++	+++
Δsnt309	B and C	+++	+	+	+	+++	+++
Δprp18[a]	C	+++	+	+	++	+++	+++
Δisy1	B, C, and Post	+++	+++	++	++	+++	+++
Δbud13	B, C, and Post	+++	++	++	++	+++	+++

Approximate colony diameters at 30°C: -, no growth; ±, visible but <0.25 mm; +, 0.5 mm; ++, 1.0 mm; +++, 2.0 mm. ND is not determined.
[a]+++ growth for *nab2-ΔN* at 16°C
[b]Growth at 16°C and 37°C

TABLE 3.2.
Genetic interaction between *nab2* mutant alleles and alleles of retention factors.

	Spliceosomal Complex	*NAB2*	*nab2-C437S*	*nab2-ΔN*
WT		+++	+++	++
Δmud2	E	+++	++	+
Δmsl1	A and B	+++	+	-
Δprp18[a]	C	+++	+	++
Δbud13[a]	B, C, and Post	+++	++	++
Δpml1	B, C, and Post	+++	++	++
Δpml39		+++	+++	+++
Δmlp1		+++	++	+++
Δmlp2		+++	++	+++

Approximate colony diameters at 30°C: -, no growth; ±, visible but <0.25 mm; +, 0.5 mm; ++, 1.0 mm; +++, 2.0 mm.
[a]+++ growth for *nab2-ΔN* at 16°C

EXPERIMENTAL PROCEDURES

Plasmids, Strains, and Chemicals

All media were prepared by standard procedures and all DNA manipulations were performed according to standard methods (233). Chemicals were obtained from Sigma-Aldrich, U.S. Biological (Swampscott, MA), or Fisher unless otherwise noted. The *S. cerevisiae* strains and plasmids used are described in Table 1. All deletion mutants were generated by using PCR-based gene disruption as described previously (234). The Mud2 plasmid (generous gift from S. Shuman (235)) was subcloned into pRS316 (236) to create *URA3 CEN MUD2* plasmid. Mud2 amino acid substitutions were generated by site-directed mutagenesis using the Quikchange site-directed mutagenesis kit (Stratagene). All plasmids were sequenced to ensure the presence of desired changes and absence of additional changes.

Total RNA Isolation

To prepare total RNA, 10 ml cultures were grown in appropriate media to an A_{600}=0.4-0.6 at 30°C. Total RNA was isolated using the Trizol method (237). Two scoops of glass beads were added to cell pellets, and bead beating was performed for two minutes. For each sample, 100 μl of 1-bromo-3-chloropropane was added, the sample was vortexed for 15 seconds, and incubated at room temperature for 2 minutes. Samples were centrifuged for 8 minutes at 16,300 X *g* at 4°C and the upper layer was transferred to a fresh tube. RNA was precipitated with 500 μl of isopropanol, vortexed, and

centrifuged for 8 minutes at 16,300 X *g* at 4°C. The supernatant was decanted and the RNA pellet was washed with 75% ethanol. Samples were centrifuged for 5 minutes at 16,300 X *g* at 4°C, the supernatant was decanted, and the pellet was air dried. The RNA pellet was resuspended in 30 μl of 10 mM Tris-HCl pH7.5.

Quantitative RT-PCR

For quantitative RT-PCR, 1 μg of total RNA was transcribed to cDNA using QuantiTect Reverse Transcription Kit (Qiagen) according to the manufacturer protocol. Quantitative RT-PCR analysis was performed in triplicate using an iCycler iQ real time machine (Bio-Rad). The real time PCR mixture contained 10 ng cDNA, 0.1 uM of primers, and QuantiTect SYBR Green Master Mix. Pre-mRNA levels were detected by using primers spanning the intron-exon junction and total RNA levels were detected using primers in the exon. The mRNA level was normalized to the *PDA1* housekeeping gene. Relative quantification of RNA levels was analyzed using the ΔΔCT method (238). Statistical significance was determined using One-Way ANOVA.

Splicing Microarray

All microarray analyses were carried out as previously described (219) with the following modification: Yeast cultures were grown to log phase in 50 ml YEPD at 30˚C and then shifted to the nonpermissive temperature at 16˚C for 1 hour. Each microarray profile shown is an average of two biological replicates. Gene axis was ordered by

hierarchical clustering using the C Clustering Library version 1.32 (239). Data were clustered using average linkage and Pearson correlation as the distance measure.

In vitro Splicing Assay

Splicing extracts were prepared using the liquid nitrogen method as described by (220), except that frozen cells were disrupted in a ball mill (MM301, Retsch) for 3 min at 10 Hz for 5 cycles. Splicing reactions containing splicing buffer (3% (w/v) PEG 8000, 2.5 mM MgCl2, 60 mM potassium phosphate (pH 7.0)), 40% (v/v) budding yeast extract, 2 mM ATP and 0.4 nM radiolabelled *ACT1* pre-mRNA substrate were incubated for 7.5 – 30 min at 20°C (220). Splicing gels were exposed to a phosphor screen and imaged with a Storm PhosphroImager (GE Healthcare). Extracts were prepared at least three independent times and the most active *nab2-C437S* lysate is shown and quantified in Figure 4.

Cell Growth Assays

Cultures were grown to saturation, serially diluted, and spotted onto selective media plates at 16°C, 25°C, 30°C, and 37°C for 3-5 days. For growth curve analysis, cells were grown overnight to saturation, diluted 100-fold in selective media, and added to wells of a MicroWell F96 microtiter plate (Nunc) in triplicate. Samples were grown at 25°C for 20 hours while measuring A_{600} every 30 minutes.

To assay for synthetic growth defects, various *nab2* mutants were combined with deletion of candidate genes using a plasmid shuffle assay. The shuffle strain Δ*nab2*

(ACY427) was targeted for deletion of *MUD2* and *CUS2*. Cells deleted for *nab2* (ACY427) were maintained by a wildtype *NAB2 URA3* plasmid (pAC636) and were transformed with mutant *LEU2 nab2* plasmids. Transformants were grown on 5-FOA to select against the wildtype *NAB2 URA3* plasmid (240). Cells were grown to saturation, serially diluted, and spotted onto plates lacking leucine at 16°C, 25°C, 30°C, and 37°C for 3-5 days. Mud2 rescue experiments were performed by transforming *nab2*Δ*mud2* (ACY2273) with *mud2* variant plasmids, grown to saturation, serially diluted, and spotted onto ura-leu-glucose plates at 25°C for 3 days.

Protein Binding Assays

To assess binding between Nab2 and either Mud2 or Msl5, (TA)-tagged strains (Srp1-TAP, Pub1-TAP, Mud2-TAP, and Msl5-TAP) were transformed with plasmids expressing C-terminally myc-tagged variants of Nab2. Cells were grown in 50 ml of minimal media to A_{600}=0.4-0.6. Cell pellets were resuspended in Lysis buffer (10 mM Tris-HCL pH8.0, 100 mM NaCl, 0.1% NP40, 1 mM Phenylmethanesulfonyl fluoride (PMSF), and 10 mM Pepstatin Leupeptin Aprotinin Cocktail (PLAC)) and lysed by bead beating 4 X 2 minutes. A total of 3 mg of protein lysate was incubated with IgG sepharose beads for 3 hours. Beads were then washed 3x times for 1 minute to purify the TAP-tagged protein and any associated proteins. Bound and Unbound samples were analyzed by SDS-PAGE/ immunoblotting using a 1:2500 dilution of anti-Myc mouse monoclonal antibody (Cell signaling) to detect myc-tagged Nab2 copurified with TAP-tagged proteins.

Poly(A) Tail Length Assay

Bulk poly(A) tail was performed as described previously (194, 195). Briefly, total RNA was end labeled with P^{32}-pCp and T4 RNA Ligase. RNA was digested using RNAse A/T1 to remove nonpoly(A) RNA, purified with phenol chloroform, and ethanol precipitated. Poly(A) tails were resolved on an 8M Urea/TBE/10% polyacrylamide gel. Poly(A) tails were quantified using ImageJ to measure pixel densitometry along the length of the tail.

Fluorescence in situ Hybridization

Poly(A) RNA localization was assayed by a fluorescence *in situ* hybridization (FISH) as described previously (196). Ye*ast cells* were grown in YEPD to log phase at 30°C. Cells were fixed with formaldehyde, digested with zymolyase, and permeabilized. A digoxigenin-labeled oligo$(dT)_{50}$ probe coupled with a fluorescein isothiocyanate-conjugated anti-digoxigenin antibody (Roche Molecular Biochemicals) was used to detect poly(A) RNA. DAPI (4′,6′-diamidino-2-phenylindole) was used to stain chromatin and indicate the position of the nucleus. DIC images were taken to visualize whole cells.

Chapter 4: The Interplay between RNA Binding Proteins and mRNA Processing

A portion of this chapter is adapted from the following paper:

Grenier-St-Sauveur,V., **Soucek, S.,** Corbett, A.H., Bachand, F. (2013) *Mol. Cell. Biol*. In press. Poly(A) Tail-mediated Gene Regulation by Opposing Roles of Nab2 and Pab2 Nuclear Poly(A)-binding Proteins in Pre-mRNA Decay.

Biochemical studies were performed by Valerie Grenier-St-Sauveur and Francois Bachand, Ph.D. at the Université de Sherbrookein in Québec, Canada.

INTRODUCTION

Messenger RNA (mRNA) production in eukaryotic cells is a multi-step procedure that involves extensive RNA processing events, such as 5' end capping, removal of introns by RNA splicing, 3' end cleavage, and polyadenylation. Contrary to the general view that poly(A) tails only contribute positively to gene expression, polyadenylation has recently received considerable interest in the field of gene regulation and nuclear RNA surveillance, as recent evidence reveals that polyadenylation can promote RNA turnover in eukaryotic cells (88, 139, 241-243). However, the extent to which polyadenylation contributes to degradation during eukaryotic gene expression and the mechanisms that specify this specialized RNA decay pathway remain poorly understood.

The fundamental role of RNA polyadenylation in gene expression is conferred by the poly(A)-binding proteins (PABPs) that bind to the 3' poly(A) tail of eukaryotic mRNAs. Two evolutionarily conserved RNA recognition motif (RRM)-containing PABPs bind the poly(A) tract of mRNAs in most eukaryotic cells: PABPC1 in the cytoplasm and PABPN1 in the nucleus (241). Biochemical studies on PABPN1 led to a model in which this protein promotes efficient polyadenylation during mRNA synthesis (244). Although a role for PABPN1 in modulating poly(A) tail length is supported by studies in primary mouse myoblasts (245), studies in human cell lines have recently revealed novel functions for PABPN1. One study demonstrated that PABPN1 modulates the use of alternative polyadenylation sites by occluding access to weak polyadenylation signals for a select group of human genes (246, 247). In addition, a recent genome-wide

study that addressed the global impact of depletion of PABPN1 for human gene expression uncovered a role for PABPN1 in the negative regulation of long noncoding (lnc) RNAs (248). Interestingly, a 3' poly(A) tail is a prerequisite for PABPN1 to promote lncRNA turnover (248), consistent with a mechanism of polyadenylation-triggered degradation. Importantly, the identification of a role for PABPN1 in polyadenylation-dependent RNA decay echoes findings that originate from studies of the fission yeast PABPN1 homolog, Pab2. Accordingly, Pab2 promotes efficient nuclear turnover of specific meiotic transcripts during the mitotic cell cycle (139). This function of Pab2 is mediated through physical association with the exosome (249), a ring-like complex that contains ten core subunits, including the 3'→5' exonuclease Dis3/Rrp44, and an additional 3'→5' exonuclease, Rrp6, in the nucleus (250, 251). Pab2 also functions in a nuclear pre-mRNA decay pathway that controls the expression of specific intron-containing genes (84). In the case of the intron-containing ribosomal protein gene, *rpl30-2*, its paralog, Rpl30-1, acts as a negative regulator by interfering with *rpl30-2* splicing. Importantly, splicing inhibition of *rpl30-2* by Rpl30-1 sensitizes the unspliced *rpl30-2* pre-mRNA to nuclear decay via Pab2 and the exosome subunit, Rrp6 (84). The equilibrium between Pab2/Rrp6-mediated pre-mRNA decay and RNA splicing thus provides an important mechanism to maintain balanced levels of paralogous ribosomal proteins in yeast.

In contrast to PABPN1 and Pab2, which bind to poly(A) RNA using a single and conserved RRM (140, 144), a different class of evolutionarily conserved nuclear PABPs

that recognize poly(A) RNA via Cys-Cys-Cys-His (CCCH) zinc finger motifs has also been described (146, 229). *S. cerevisiae* Nab2 is the CCCH zinc finger PABP that has been most extensively characterized to date. *NAB2* encodes an essential nuclear protein that harbors seven CCCH zinc fingers (ZnF) motifs, of which ZnF 5-7 are necessary and sufficient for high affinity binding to poly(A) RNA (146, 229). Functionally, Nab2 has been implicated in two distinct steps of budding yeast gene expression: mRNA export and poly(A) tail length control (171). Nab2 contributes to the RNA export process by recruiting mRNA export factors (67) and by interacting with nuclear pore-associated proteins (252), interactions that involve a Pro-Trp-Ile (PWI)-like fold located in the amino-terminal region of Nab2 (68). RNA from *nab2* mutant cells also display longer poly(A) tails (151). The findings that Nab2 mutants with substitutions in ZnF5-7 are impaired in poly(A) binding *in vitro* and that cells expressing such Nab2 mutants show hyperadenylated RNA *in vivo*, suggested that the function of Nab2 in polyadenylation control requires poly(A)-bound Nab2 (156). As of yet, however, the identity of the hyperadenylated transcripts in Nab2-deficient cells remains unknown. Interestingly, although Nab2 appears to associate with the bulk of the *S. cerevisiae* mRNA transcriptome (176), cells deficient for Nab2 mainly affect the expression of intron-containing genes (81). Specifically, *nab2*-deficient cells accumulate unspliced pre-mRNAs, but not spliced mRNAs (81). Although the exact mechanism by which Nab2 controls unspliced pre-mRNA levels remains to be determined, a physical interaction detected between Nab2 and the exosome subunit Rrp6 have led to a model in which Nab2

functions in the quality control of gene expression by promoting Rrp6-mediated decay in the nucleus (81).

Nab2 orthologs have also been identified in *Drosophila, C. elegans,* and humans, referred to as dNab2 and ZC3H14, respectively (147). In *Drosophila*, *dnab2* mutants flies exhibit defects in poly(A) tail length control, but do not appear to be affected in poly(A) RNA export (161). In *C. elegans*, Sut2 was identified as a suppressor of Tau pathology, but molecular functions have not been reported(253). In humans, nuclear and cytoplasmic isoforms are expressed from the *ZC3H14* gene (215), but the functions of these ZC3H14 isoforms remain to be determined although loss of the nuclear isoforms lead to intellectual disability suggesting a key role for this protein in neurons in humans and highlighting the importance of defining the function of this class of proteins.

How different PABPs coexist in the eukaryotic nucleus and whether there is functional interplay between nuclear PABPs, such as between Nab2/ZC3H14 and Pab2/PABPN1, remains elusive. In this study, we characterize the fission yeast ortholog of ZC3H14/Nab2 and provide evidence that *S. pombe* Nab2 and Pab2 have opposing roles in fission yeast gene regulation. By studying the Pab2-regulated gene, *rpl30-2*, we show that Nab2 functions as a positive regulator of *rpl30-2* expression, in contrast to Pab2. We also find that Nab2 preferentially binds to the *rpl30-2* unspliced pre-mRNA relative to the spliced transcript. Consistent with this finding, the ability of Nab2 to promote *rpl30-2* expression requires the *rpl30-2* intron. Our data support a model in

which Nab2 impedes Pab2/Rrp6-mediated degradation of unspliced *rpl30-2* pre-mRNA in the nucleus by competing with Pab2 for access to the poly(A) tail.

RESULTS

The *S. cerevisiae* and human poly(A)-binding protein (PABP), Nab2 and ZC3H14, respectively, are part of a novel class of evolutionarily conserved PABPs that recognize poly(A) RNA via tandem CCCH zinc finger motifs (146). To search for Nab2/ZC3H14 orthologs in the fission yeast *Schizosaccharomyces pombe*, we performed BLAST analyses to identify an ortholog containing CCCH zinc fingers with similar spacing ($CX_5CX_{4-6}CX_3H$) to those found in *S. cerevisiae* Nab2 and human ZC3H14 (146). Our sequence analyses identified a *S. pombe* protein, SPAC14C4.06c, with tandem CCCH zinc finger motifs that share a similar domain structure with Nab2 proteins from *S. cerevisiae*, *C. elegans*, *Drosophila*, and humans (Figure 4.1A). Comparison of the overall sequence similarity of SPAC14C4.06c with Nab2 orthologs reveals a high level of similarity between the functionally important N-terminal and C-terminal domains, with less sequence conservation in the central region (Figure 4.S1). Importantly, *in silico* structure simulations of the N-terminal region of *S. pombe* SPAC14C4.06c (Figure 4.1B) nicely match to the resolved structure of the PWI-like domain of *S. cerevisiae* Nab2 (68). As illustrated in Figure 1C, *S. pombe* SPAC14C4.06c contains three zinc finger domains, whereas *S. cerevisiae* Nab2 and human ZC3H14 contain seven and five zinc fingers,

respectively. Importantly, only three zinc fingers (closely spaced ZnF5-7) within *S. cerevisiae* Nab2 are required for high affinity binding to polyadenosine RNA (156)and also to fold into a stable polyadenosine RNA binding module (229). Thus, *S. pombe* SPAC14C4.06c, which contains only three CCCH zinc fingers may represent a minimal version of this protein family. Indeed comparison of the amino acid sequences within the CCCH zinc fingers of *S. pombe* SPAC14C4.06c to sequences in the zinc finger motifs documented to mediate RNA binding in *S. cerevisiae* Nab2 show conservation of key intervening residues required to mediate RNA binding in addition to the structural Cys and His residues (Figure 4.1C). On the basis of the sequence and structural similarities described here, we named *S. pombe SPAC14C4.06c*, Nab2.

Fission yeast Nab2 is a nonessential nuclear poly(A)-binding protein.

We constructed a diploid strain in which one of the two alleles of *nab2* was disrupted to address whether *nab2* is essential for viability in fission yeast. Germination of the spores after meiosis followed by tetrad microdissection resulted in a 2:2 segregation ratio of geneticin resistance, indicating that *nab2*-null cells are viable in *S. pombe*. Examination of cell growth revealed that *nab2*-null cells grow comparably to wildtype cells at different temperatures (Figure 4.2A). We next monitored Nab2 localization in live *S. pombe* cells using a GFP fusion. As shown in Figure 4.2B, GFP-Nab2 localized to cell nuclei and was excluded from the cytoplasm at steady state (Figure

4.2B, panels d-f). Thus, in contrast to *S. cerevisiae* and *Drosophila*, nuclear Nab2 is not essential for mitotic growth in fission yeast.

S. cerevisiae Nab2 specifically binds synthetic adenylate chains *in vitro* (146). To test whether *S. pombe* Nab2 shares the same function, we expressed the full-length *S. pombe* Nab2 protein in *E. coli* as a GST fusion and examined the binding to polyadenosine RNA in gel shift assays using a Cy3-labeled poly$(A)_{25}$ RNA (Cy3-r$(A)_{25}$) oligonucleotide. As can be seen in Figure 4.2C, GST-Nab2 robustly bound the poly(A) RNA oligonucleotide (lanes 6-9), whereas the control, GST alone, did not (lanes 2-5). As a positive control, the other fission yeast nuclear poly(A)-binding protein, Pab2 (254), also bound to the Cy3-r$(A)_{25}$ oligonucleotide (Figure 4.2C, lanes 10-13). Binding of Nab2 was specific for poly(A) RNA, as neither poly(C) RNA nor single-stranded poly-$_{deoxy}$(A) could compete binding between GST-Nab2 and Cy3-r$(A)_{25}$ (Figure 4.2D, lanes 7-12), whereas unlabeled poly(A) RNA efficiently competed for binding (lanes 4-6). We next addressed the importance of the zinc finger domains of *S. pombe* Nab2 in binding to poly(A) RNA by generating variants of Nab2 in which the first cysteine of each CCCH zinc finger domain (C184, C217, and C254) was individually substituted to an alanine residue. Expression and purification of GST-Nab2 C184A, GST-Nab2 C217A, and GST-Nab2 C254A yielded levels of recombinant protein similar to wildtype GST-Nab2, suggesting that the stability of Nab2 zinc finger variants was not substantially affected. Notably, no detectable Nab2-r$(A)_{25}$ complex was observed for the Nab2 C184 and Nab2 C217A variants (Figure 4.2E, lanes 4-6 and 7-9, respectively), whereas wildtype GST-

Nab2 bound strongly to the Cy3-labeled poly(A) RNA oligonucleotide (lane 3). Nab2 C254A showed smearing of the labeled poly(A) RNA probe in the gel shift assay (Figure 4.10-12), which likely reflects transient and/or unstable binding. Altogether, these *in vitro* binding results indicate that *S. pombe* Nab2 can specifically bind to poly(A) RNA and that the zinc finger motifs within Nab2 are important to mediate stable binding to poly(A) RNA.

Nab2 is not required for general control of mRNA polyadenylation and does not associate with the mRNA 3' end processing machinery.

In the budding yeast *S. cerevisiae*, cellular depletion of functional Nab2 causes RNA hyperadenylation (151), which was suggested to be due to inefficient trimming of poly(A) tails from nascent transcripts by the nuclear exonuclease, Rrp6 (81). We therefore examined whether Nab2 is similarly involved in the regulation of poly(A) tail synthesis in fission yeast. Poly(A) tail distribution was analyzed by 3'-end labeling of total RNA prepared from wildtype and *nab2*Δ strains, followed by RNase digestion, leaving the poly(A) chains intact. Comparison between RNA prepared from wildtype and *nab2*Δ strains did not reveal a significant impact on bulk poly(A) tail distribution between the two samples (Figure 4.3A). We also examined the polyadenylation status of specific mRNAs by treatment with RNase H. RNase H treatment in the presence of a DNA oligonucleotide complementary to a region located in the 3' UTR of an mRNA will

release heterogeneous 3' fragments, as a consequence of different poly(A) tail lengths. The addition of oligo d(T) to the RNase H reaction causes this heterogeneous population of 3' fragments to collapse into discrete products, indicating the position of polyadenylation sites. As can be seen for the *ADH1* and *PYK1* mRNAs, poly(A) tail lengths and cleavage site decisions were similar between wildtype and *nab2*Δ cells (Figure 4.3B-3C, compare lanes 3-4 to 1-2). From these results, we conclude that mRNA polyadenylation occurs normally in *S. pombe* cells deleted for *nab2*, in contrast to what has been observed in *S. cerevisiae* and *Drosophila* .

Given the absence of a gross change in the polyadenylation status of the *nab2*Δ strain, we decided to identify Nab2-associated proteins to obtain further insight into the functional role of *S. pombe* Nab2. We exploited a strain in which a Nab2-Protein A fusion (Nab2-ProA) was expressed from its endogenous chromosomal locus using the *nab2* promoter. To control for specific interactions, we compared results obtained for Nab2-ProA to a control cytosolic protein Snd1-ProA. Following affinity purification optimized to preserve the integrity of cellular ribonucleoprotein (RNP) complexes (255), the eluted proteins were separated by SDS-PAGE (Figure 4.3D), and the resulting lanes were cut into eight equal-size pieces that were trypsin-digested and analyzed by LC-MS/MS using an LTQ Orbitrap. Table 4.1 lists proteins enriched in Nab2-ProA purification that were absent or barely detectable in the Snd1-ProA control purification.

The purification of Nab2-ProA resulted in the identification of 768 proteins. Interestingly, the majority of the known pre-mRNA 3' end processing factors were absent

from the Nab2 purification, consistent with the observation that mRNAs produced in *nab2*Δ cells are cleaved and polyadenylated properly (Figure 4.3A-3C). We next used computer algorithms (256) to distinguish functional protein classes within the top 10% (77 proteins) of the proteins that were identified in the Nab2 purification. The analysis identified a significant number of proteins involved in RNA splicing in the set of proteins copurified with Nab2 (Table 4.1). Accordingly, proteins associated with the U4/U6 x U5 tri-snRNP complex (p =1.6e-12), the U1 snRNP (p =5.5e-8), the U2 snRNP (p =1.5e-6), and the spliceosomal complex (p =2.4e-28) were recovered in the Nab2 purification. Overall, of the 77 proteins that ranked in the top 10% of the Nab2 purification, 31 (40%) have been previously shown or predicted to be involved in RNA splicing (Table 4.1). Interestingly, proteins involved in snoRNA binding and RNA decay were also enriched in the Nab2 purification (Table 4.1). In conclusion, our affinity purification approach suggests that Nab2 is associated, directly or via RNA, with factors involved in processing events that include RNA splicing, snoRNA metabolism, and RNA decay.

Genetic interactions between *nab2* and *pab2*.

The identification of proteins involved in RNA splicing, snoRNA binding, and RNA degradation in the Nab2 affinity purification revealed a striking parallel with functions attributed to the other fission yeast nuclear poly(A)-binding protein, Pab2, Pab2 functions in maturation of polyadenylated snoRNA precursors into mature snoRNAs (249, 257) as well as degradation of a specific set of unspliced pre-mRNAs in the nucleus

(84). To begin to characterize the functional relationship between Pab2 and Nab2, double mutant cells were generated. As can be seen in Figure 4.4A, growth of the *nab2*Δ *pab2*Δ double mutant strain was impaired at all temperatures tested as compared to either single mutant. The genetic interaction between *nab2* and *pab2* was also supported by RNA analyses: deletion of *nab2* from the *pab2*Δ strain exacerbated the previously described (254) hyperadenylation phenotype of the single *pab2*Δ mutant (Figure 4.4B, compare lanes 3-4). However, the increased level of hyperadenylated RNAs in the *nab2*Δ *pab2*Δ double mutant strain relative to the single *pab2*Δ mutant did not appear to affect mRNAs in general, as demonstrated by RNase H cleavage assays for the *ADH1* and *PYK1* transcripts, which showed similar poly(A) tail lengths between wildtype, *Δnab2*, *Δpab2*, and *nab2*Δ *pab2*Δ strains (Figure 4.4C-4D). This observation is consistent with results indicating that Pab2 is not a general factor required for mRNA polyadenylation (241) and suggests that the increased level of hyperadenylated RNAs in the double mutant may specifically affect transcripts targeted by Pab2-dependent regulation.

Opposing roles for Nab2 and Pab2 in gene regulation.

To test the hypothesis that Nab2 may target Pab2-dependent transcripts, we first examined the expression of two independent snoRNA genes. Consistent with our previous findings (249, 257), decreased levels of mature snoRNAs were observed in the *pab2*Δ mutant (Figure 4.5A, compare lane 3 to lane 1), a consequence of deficient maturation of polyadenylated snoRNA precursors into mature snoRNAs. Strikingly, a

reproducible increase in snoRNA levels was detected in *nab2*Δ cells (Figure 4.5A, compare lane 2 to lane 1). This converse effect in snoRNA expression between *nab2*Δ and *pab2*Δ mutants prompted us to analyze the expression of another Pab2-dependent gene, the ribosomal protein gene *rpl30-2*. Pab2 promotes a nuclear pre-mRNA degradation pathway that competes with RNA splicing to control the expression of selective genes, such as *rpl30-2* (84). Accordingly, in the absence of Pab2, both the mature mRNA and the unspliced pre-mRNA of *rpl30-2* are upregulated (Figure 4.5B, lane 3). In contrast, levels of *rpl30-2* mRNA were significantly reduced in the *nab2*Δ mutant (Figure 4.5B, lanes 1-2; Figure 4.5C), whereas the level of the *adh1* control mRNA was not affected in the absence of Nab2 (Figure 4.5B). We also found that the levels of unspliced *rpl30-2* pre-mRNA were increased in the *nab2*Δ *pab2*Δ double mutant relative to the single *pab2*Δ mutant (Figure 4.5B, compare lane 4 to lane 3; Figure 4.5C), which may reflect the increase in hyperadenylated RNA detected in the double mutant relative to *pab2*Δ cells (Figure 4.4B). To confirm that the decreased level of *rpl30-2* mRNA in the *nab2*Δ mutant was specifically due to the absence of Nab2, we tested whether the *nab2* cDNA could complement this phenotype. As shown in Figure 4.5D, expression of wildtype Nab2 in the *nab2*Δ mutant effectively restored the altered expression of the *rpl30-2* gene (compare lanes 2 and3). In contrast, a variant of Nab2 in which the first cysteine residue of the three zinc finger domains was substituted to alanine did not rescue the decreased levels of *rpl30-2* mRNA in the *nab2*Δ strain (Figure 4.5D, lanes 4). Altogether, these data support opposing roles for Nab2 and Pab2 in gene

regulation. Furthermore, given the critical role of the zinc finger domain of Nab2 in poly(A) binding (Figure 4.1E and (229)), our results suggest that *S. pombe* Nab2 controls *rpl30-2* expression via poly(A) binding.

Nab2 controls *rpl30-2* expression at the level of unspliced pre-mRNA.

To begin to understand how Nab2 and Pab2 play opposite roles in gene regulation, we used *rpl30-2* as a model gene to gain mechanistic insights into how Nab2 controls *rpl30-2* expression. Because *nab2*Δ cells show a 2-fold decrease in the steady-state level of *rpl30-2* mRNA, we first examined the effect of Nab2 deficiency on *rpl30-2* mRNA stability. The drug, 1,10-phenanthroline was used to inhibit transcription (258) in both wildtype and *nab2*Δ cells, and RNA decay was followed over time. As a control for transcription inhibition, the level of an unstable transcript, *pma1* (258), rapidly declined following treatment with 1,10-phenanthroline (Figure 4.6A-6B). As can be seen in Figures Figure 4.6A and 6B, *rpl30-2* showed similar mRNA stability between the wildtype and *nab2*Δ strains. As the bulk of mRNAs are present in the cytoplasm, mRNA stability assays primarily measure cytosolic decay. Accordingly, the similar stability of the *rpl30-2* mRNA between wildtype and *nab2*Δ cells, despite a 2-fold reduction in the steady-state level of the *rpl30-2* mRNA in the *nab2*Δ mutant, suggested a nuclear role for Nab2 not readily revealed by these assays which examine the stability primarily of mature, cytosolic mRNA. The proposed nuclear function of Nab2 is consistent with the steady-state localization of Nab2 with the nucleus (See Figure 4.2B). Given the lack of an

apparent effect on mRNA stability, we examined whether the decreased levels of *rpl30-2* mRNA observed in the *nab2*Δ mutant could result from reduced transcription. Chromatin immunoprecipitation (ChIP) assays were used to determine the density of RNA polymerase II (RNAPII) along the *rpl30-2* gene in wildtype and *nab2*Δ cells. ChIP experiments demonstrated similar levels of RNAPII along the *rpl30-2* gene in both strains indicating no difference in transcription in these mutants. This result suggests that the reduction in the steady-state level of *rpl30-2* transcript in *nab2*Δ cells occurs primarily due to regulation at the post-transcriptional level.

To address whether Nab2 directly regulates the expression of *rpl30-2*, RNA co-immunoprecipitation (RNA-IP) experiments were employed to examine whether *rpl30-2* transcripts copurify with Nab2. We affinity purified Nab2-ProA and compared the relative association with both spliced and unspliced *rpl30-2* transcripts by RT-PCR using a primer across the exon-exon junction for the spliced mRNA and an intron-specific primer for the unspliced pre-mRNA (Figure 4.6C). To ensure that the transcripts were posttranscriptional and had undergone polyadenylation, reverse transcriptase was primed with oligo d(T). Data were normalized to the *nda2* (tubulin) mRNA to control for experimental variation, and values were set to 1.0 for the control purification that was prepared from extracts of an untagged strain. As an additional control, we analyzed immunoprecipitates prepared using a non-RNA-binding protein (Rmt3-ProA), which recovered only low levels of *rpl30-2* transcripts relative to the Nab2-ProA fusion (Figure 4.6C). Importantly, we found that the unspliced *rpl30-2* pre-mRNA was ~4-fold more

highly associated with Nab2 than the spliced mRNA (Figure 4.6C) despite the fact that the unspliced pre-mRNA corresponds to only 5-10% of the total *rpl30-2* polyadenylated transcripts (84). These results indicate that a greater proportion of unspliced *rpl30-2* pre-mRNA is bound by Nab2 relative to the spliced mRNA, suggesting that Nab2 may control *rpl30-2* expression at the level of the unspliced transcript.

To test whether synthesis of the pre-mRNA was required for Nab2-dependent control of *rpl30-2* mRNA level, we used an intronless construct (RPL30-2Δi) that expresses the *rpl30-2* cDNA from native promoter and terminator sequences. As a control, we prepared a similar construct, but using the intron-containing version of *rpl30-2*. These two constructs were chromosomally-integrated as a single copy into an *rpl30-2Δ* strain. We then deleted *nab2* from *rpl30-2Δ* strains that expressed intronless and intron-containing versions of *rpl30-2*. As we observed for endogenous *rpl30-2*, expression of the *rpl30-2* intron-containing construct in the nab2Δ strain resulted in decreased levels of mRNA transcript relative to control (Figure 4.6D, lanes 1-2; Figure 4.6E). In contrast, mRNA levels were not affected in the nab2Δ strain when *rpl30-2* was expressed from the intronless construct (Figure 4.6D, lanes 3-4; Figure 4.6E). These results indicate that Nab2 controls *rpl30-2* expression at the level of the unspliced pre-mRNA.

We have previously described a cross-regulatory mechanism between the paralogous ribosomal protein genes *rpl30-1* and *rpl30-2*, in which Rpl30-1 negatively controls *rpl30-2* expression by interfering with RNA splicing, thereby sensitizing the unspliced *rpl30-2* pre-mRNA to nuclear decay via Pab2 and Rrp6 (84). Accordingly,

rpl30-2 pre-mRNA levels are reduced by 6-fold and spliced mRNA levels upregulated by ~8-fold in Δ*rpl30-1* cells, as *rpl30-2* splicing is no longer inhibited by Rpl30-1. To test whether the Nab2-dependent decrease in *rpl30-2* expression requires splicing interference by Rpl30-1, we compared the levels of *rpl30-2* mRNA between the single *rpl30-1Δ* strain and the double *rpl30-1Δ nab2*Δ mutant. As can be seen in Figure 4.6F, the single *rpl30-1Δ* mutant strain showed *rpl30-2* mRNA levels similar to cells deficient for both *nab2* and *rpl30-1* (compare lanes 3-4), suggesting that Nab2 acts downstream of Rpl30-1-dependent splicing inhibition. Altogether, the data presented in Figure 4.6 are consistent with a model whereby Nab2 promotes *rpl30-2* expression by targeting the unspliced pre-mRNA.

Nab2 impedes Pab2/Rrp6-dependent pre-mRNA decay.

The aforementioned results identify a function for Nab2 as a positive regulator of *rpl30-2* expression via a mechanism that targets the unspliced pre-mRNA. Given that pre-mRNA decay actively competes with splicing during *rpl30-2* expression (84), Nab2 could promote *rpl30-2* expression by interfering with Pab2/Rrp6-mediated pre-mRNA decay or by stimulating RNA splicing. We reasoned that if Nab2 impedes nuclear pre-mRNA decay, levels of *rpl30-2* pre-mRNA should be reduced in *nab2*Δ cells after splicing inhibition, whereas pre-mRNA levels should not change if Nab2 functions as a splicing activator. To distinguish between these possibilities, *nab2* was deleted in two independent strains containing temperature-sensitive mutations in genes (*prp1-4* and

prp2-1) that encode general splicing factors (259). Total RNA was then prepared from wildtype, nab2Δ, *prp1-4*, and *nab2*Δ *prp1-4* double mutant strains that were grown at the permissive temperature (25°C) or shifted at the non-permissive temperature of 37°C for 2h. Almost complete inhibition of pre-mRNA splicing was observed in the *prp1-4* strain following a shift to the non-permissive temperature, as demonstrated by the accumulation of *rpl30-2* and *tbp1* unspliced pre-mRNAs together with the concomitant loss of spliced mRNAs (Figure 4.7A, compare lane 7 to lane 3). Notably, *rpl30-2* pre-mRNA levels were reduced in the *nab2*Δ *prp1-4* double mutant relative to the single *prp1-4* mutant strain (Figure 4.7A, upper panel; compare lanes 7-8); yet, this reduction in pre-mRNA levels was not detected for a Nab2-insensitive control gene (Figure 4.7A, lower panel). Importantly, the Nab2-dependent reduction in *rpl30-2* pre-mRNA was also observed after the inhibition of RNA splicing using the *prp2-1* splicing mutant (Figure 4.7B, compare lanes 7-8). As *rpl30-2* transcription levels are not affected by the absence of Nab2, these results suggest that Nab2 promotes *rpl30*-2 expression upstream of splicing by interfering with pre-mRNA degradation.

The requirement for Nab2 to maintain proper levels of *rpl30-2* pre-mRNA after splicing inhibition suggested that Nab2 might compete with Pab2 to impede the decay of *rpl30-2* pre-mRNAs in the nucleus. If this is the case, excess Nab2 should lead to *rpl30-2* up-regulation. To test this idea, we expressed Nab2 from the inducible *nmt1*$^{+}$ promoter, which is induced in the absence of thiamine. In agreement with a direct role of Nab2 in the control of *rpl30-2* expression, excess Nab2 resulted in increased levels of *rpl30-2*

mRNA and pre-mRNA relative to cells transformed with a control vector (Figure 4.7C, compare lane 3 to lane 1), a phenotype that is similar to *pab2*Δ cells (lane 2). Interestingly, we also found that Nab2 can displace Pab2 from poly(A)-bound complexes *in vitro* (Figure 4.7D, lanes 5-8), whereas GST alone does not (lanes 9-12). In contrast, excess Pab2 did not displace previously formed Nab2:poly(A) complexes. Our data thus suggest that Nab2 and Pab2 promote opposing roles in *rpl30-2* expression by competing for the poly(A) tail of the unspliced *rpl30-2* pre-mRNA.

The exosome-associated exonuclease, Rrp6, is the principal degradation factor that promotes the turnover of unspliced *rpl30-2* pre-mRNA in the nucleus (84). Therefore, if Nab2 impedes Rrp6-mediated degradation of *rpl30-2* pre-mRNAs, the absence of Nab2 in the *rrp6Δ* strain is not expected to influence *rpl30-2* mRNA and pre-mRNA levels relative to the single *rrp6Δ* mutant. To test this prediction, we analyzed *rpl30-2* expression levels in wildtype, *nab2Δ*, *rrp6Δ*, and *nab2*Δ Δ*rrp6* double mutant strains. As shown in Figure 4.7E, cell deleted for both *nab2* and *rrp6* showed levels of *rpl30-2* mRNA and pre-mRNA similar to that of the single *rrp6Δ* mutant, consistent with a model in which Nab2 interferes with Rrp6-mediated degradation of *rpl30-2* pre-mRNAs in the nucleus.

To more directly test whether Nab2 can interfere with the 3'→5' exoribonuclease activity of Rrp6, we purified *S. pombe* Rrp6 from *E. coli* and reconstituted an *in vitro* degradation assay using recombinant Rrp6. Incubation of purified Rrp6 with a poly(A) RNA oligonucleotide ($r(A)_{25}$) labeled with Cy3 at the 5' end resulted in efficient RNA

decay (Figure 4.7F, lanes 2-5) relative to the $r(A)_{25}$ incubated in the absence of Rrp6 (lane 1). To confirm that this degradation activity was dependent on the exonucleolytic activity of Rrp6, we purified a version of Rrp6 in which an aspartate residue (D243) critical for metal ion coordination in the active site (260, 261) was substituted to alanine. When incubated with the $r(A)_{25}$ substrate RNA, the purified D243A version of *S. pombe* Rrp6 did not degrade poly(A) RNA (Figure 4.7F, lanes 6-9), indicating that catalytically active Rrp6 is required for poly(A) RNA decay. Importantly, both wildtype and D243A versions of Rrp6-Flag showed similar abundance after the *in vitro* reaction. We next tested whether Nab2 can interfere with Rrp6-mediated degradation *in vitro*. Wildtype and ZnF-defective versions of GST-Nab2 were incubated with poly(A) RNA before the addition of increasing amounts of wildtype Rrp6. Wildtype Nab2 clearly interfered with the degradation activity of Rrp6 (compare Figure 4.7G, lanes 2-5 to Figure 4.7F, lanes 2-5). In contrast, a ZnF-defective version of Nab2 (C184A) that did not bind poly(A) RNA (See Figure 4.2E) did not impair the exonucleolytic activity of Rrp6 (Figure 4.7G, lanes 6-9). These data indicate that poly(A)-bound Nab2 can suppress Rrp6-mediated degradation *in vitro*.

DISCUSSION

The addition of a poly(A) tail at the 3' end of an mRNA is a fundamental step in the course of the gene expression process in eukaryotic cells. Yet, because the product of polyadenylation corresponds to a widespread and repetitive sequence of adenosines, the

poly(A) tail is not generally considered to be involved in gene-specific regulation via *trans*-acting factors. Contrasting this view, we demonstrate here that the 3' poly(A) tail can function in gene regulation through the action of competing poly(A)-binding proteins (PABPs) in the nucleus.

Evolutionarily divergent roles for Nab2 orthologs.

Our work describes the identification of the fission yeast ortholog of *S. cerevisiae* Nab2 and human ZC3H14. This conclusion is supported by several observations: (i) the high level of sequence similarity between *S. pombe* Nab2 and its orthologs in the amino- and carboxy-terminal regions (Figure 4.1B,C); (ii) the domain organization of *S. pombe* Nab2, including an N-terminal PWI-like domain and C-terminal CCCH zinc finger motifs (Figure 4.1A); (iii) the ability of Nab2 to specifically and directly interact with poly(A) RNA *in vitro* (Figure 4.2C-2E); and (iv) the nuclear localization of fission yeast Nab2 (Figure 4.2B). Nevertheless, despite sequence and structural homologies, it appears that the function of Nab2 has diverged during the speciation of budding and fission yeasts from a common ancestor. First, in contrast to *S. cerevisiae*, Nab2 is not essential for viability in *S. pombe*. In addition, we did not observed global defects in poly(A) tail length control (Figure 4.3A) or poly(A) RNA export in Nab2-deficient *S. pombe* cells, contrasting to what has been reported for loss-of-function alleles of *S. cerevisiae NAB2* (151, 156). Although the reasons for the strikingly different phenotypes related to Nab2

deficiency between budding and fission yeasts are unclear, the presence of an additional nuclear PABP in *S. pombe* (Pab2) may be one possible explanation. Accordingly, Nab2 is the major nuclear PABP in *S. cerevisiae*, as the genome of *S. cerevisiae* does not encode a homolog of *S. pombe* Pab2/human PABPN1 (262). In contrast, Pab2 is the more abundant nuclear PABP in *S. pombe*, with approximately 5830 molecules of Pab2 and 2745 molecules of Nab2 reported per proliferating cell (263). For this reason, *S. pombe* should serve as a powerful model system to gain a detailed understanding of the functional interplay between nuclear PABPs. Accordingly, it will be interesting to define the function of ZC3H14, which shares the human nuclear transcriptome with PABPN1 in a manner analogous to *S. pombe* Nab2 and Pab2. Such studies should reveal whether ZC3H14 is more closely related to Nab2 of *S. cerevisiae* or *S. pombe*.

Nuclear PABPs and mRNA polyadenylation

Data obtained from biochemical studies and *in vitro* polyadenylation assays have defined roles for nuclear PABPs in the elongation process of poly(A) polymerase (PAP) and in poly(A) tail length control, suggesting fundamental roles for nuclear PABPs during mRNA polyadenylation in vivo (50, 185, 249). In *S. pombe*, however, the current data does not support a role for Pab2 as a general factor required for mRNA polyadenylation. Accordingly, the hyperadenylation phenotype of *pab2*Δ cells only affects a select group of transcripts that accumulate as hyperadenylated RNAs (136, 138,

139), whereas most mRNAs are properly expressed and polyadenylated in *pab2*Δ cells (249). Nevertheless, it was possible that another nuclear PABP, such as Nab2, could stimulate tethering of PAP to the 3′-end of nascent transcripts as well as PAP processivity in the absence of Pab2. We were therefore surprised to find that *S. pombe* cells deleted for either *pab2* or *nab2* were viable and produced mRNAs with poly(A) tail lengths similar to wildtype cells (Figure 4.4B-4D). Similarly, Nab2 is not required to stimulate the elongation process of poly(A) tail synthesis in budding yeast, but rather functions to proofread mRNP formation before nuclear export via polyadenylation-dependent RNA decay (81). Recent data also indicate that the large majority of protein-coding genes express normal levels of polyadenylated mRNA in PABPN1-deficient cells (248, 264). These observations question the need for nuclear PABPs to load onto nascent poly(A) tails to stimulate PAP activity during mRNA polyadenylation *in vivo*. Accordingly, it may be more efficient in the course of the gene expression process to directly load cytosolic PABPs (Pab1/PABPC1) onto the growing mRNA poly(A) tail before nuclear export, instead of a model in which an exchange reaction must occur between nuclear and cytosolic PABPs to allow efficient cap-dependent translation in the cytoplasm via interactions between the translation initiation complex and PABPC1. Consistent with loading of cytosolic PABPs onto nascent mRNA poly(A) tails in the nucleus, human PABPC1 has been shown to physically associate with unspliced pre-mRNAs (265) as well as to copurify with the mRNA 3’ end processing machinery (206). Functional evidence also support the critical role of Pab1 in the biogenesis and export of mRNAs in

S. cerevisiae (81, 142). The development of tools that can determine which PABP is most abundantly loaded onto the nascent poly(A) tail will be an important goal in the future, and should reveal critical insights into the mechanism underlying control of nuclear mRNA polyadenylation.

Antagonistic roles for nuclear PABPs in gene regulation

Our work shows that whereas the absence of Nab2 does not affect the expression of several housekeeping genes (*adh1, pyk1, pma1, nda2*), the expression of Pab2-dependent genes, such as snoRNAs and *rpl30-2*, is affected in *nab2*Δ cells. Specifically, the absence of Nab2 results in converse effects relative to *pab2*Δ cells: snoRNAs are up-regulated in *nab2*Δ cells, but down-regulated in the *pab2*Δ strain; *rpl30-2* is down-regulated in the *nab2*Δ strain, but up-regulated in *pab2*Δ cells. Using *rpl30-2* as a model gene, we provide evidence that Nab2 preferentially associates with the unspliced pre-mRNA relative to the mature mRNA. Consistent with this observation, we found that a significant number of splicing factors copurify with Nab2 and that the *rpl30-2* intron is required for Nab2-dependent regulation, suggesting that Nab2 acts at the levels of the unspliced pre-mRNA. Our data also suggest that Nab2 stabilizes *rpl30-2* pre-mRNAs, as reduced levels of unspliced *rpl30-2* transcripts were found in the absence of Nab2 after splicing inhibition. Based on these findings, we propose that Nab2 controls *rpl30-2* expression by competing with Pab2 for polyadenylated *rpl30-2* pre-mRNAs, thereby

interfering with Pab2/Rrp6-mediated pre-mRNA decay in the nucleus (Figure 4.8). Consistent with this model, increased dosage of Nab2 in *S. pombe* promotes *rpl30-2* expression by stabilizing the unspliced pre-mRNA, an outcome similar to Pab2 deficiency (Figure 4.7C). Our findings have therefore unveiled a gene regulation mechanism in which the 3' poly(A) tail acts as a platform for competing PABPs in the nucleus. Such a mechanism of gene regulation via antagonistic nuclear PABPs could be controlled by changing the relative Nab2:Pab2 stoichiometry and/or by altering their respective affinity to poly(A) RNA through post-translational modifications (150, 254, 266, 267).

Given the recently proposed role of *S. cerevisiae* Nab2 in a nuclear surveillance pathway that promotes removal of excess pre-mRNAs via Rrp6 degradation (81), it was surprising to find a role for *S. pombe* Nab2 as a positive regulator of *rpl30-2* expression by a mechanism that impedes nuclear pre-mRNA decay. Yet, it should be noted that phylogenetic studies indicate that *S. pombe* and *S. cerevisiae* are as different form one other as either is from animals (268). Such evolutionary distance between *S. pombe* and *S. cerevisiae* may explain the different use of nuclear PABPs in both species, as discussed earlier: Pab2 being the major nuclear PABP in *S. pombe*, whereas Pab2 is absent in *S. cerevisiae*. Therefore, although both fission and budding yeasts seem to have conserved a pathway in which pre-mRNA decay competes with RNA splicing to control gene expression, it appears that the large evolutionary distance between both species delegated

the RNA decay-promoting function of this pathway to different PABPs: Pab2 in *S. pombe* and Nab2 in *S. cerevisiae* (81, 84).

Our previous work revealed a cross-regulatory mechanism whereby Rpl30-1 negatively controls *rpl30-2* expression via splicing inhibition (84). Importantly, we show here that Nab2-dependent regulation of *rpl30-2* no longer takes place in the absence of Rpl30-1 (Figure 4.6F). This finding indicates that the ability of Nab2 to control *rpl30-2* expression at the level pre-mRNA turnover requires that Rpl30-1 interfere with *rpl30-2* splicing beforehand (Figure 4.8). As results indicate that inefficiently spliced transcripts accumulate near their site of transcription (269, 270), we propose that splicing inhibition by a *trans*-acting factor such as Rpl30-1 extends the nuclear lifetime of an unspliced pre-mRNA, allowing nuclear PABPs to compete for pre-mRNA association and regulation (Figure 4.8), and thereby allows for specific gene regulation by Pab2 and Nab2. Gene regulation at the level of nuclear pre-mRNA turnover may therefore provide a mean for rapid post-transcriptional control of gene expression in the many cases in which cells must respond quickly to changing environmental conditions (84).

In summary, we provide evidence that the functional interplay between nuclear poly(A)-binding proteins can induce post-transcriptional gene regulation. The opposing roles of Pab2 and Nab2 described in this study infer the need to strictly control the concentration of nuclear PABPs. In this view, it may be important to consider that diseases related to mutations in *PABPN1*, resulting in oculopharyngeal muscular dystrophy (170), and *ZC3H14*, which cause a form of intellectual disability (161), may be

linked to the disruption of this homeostasis.

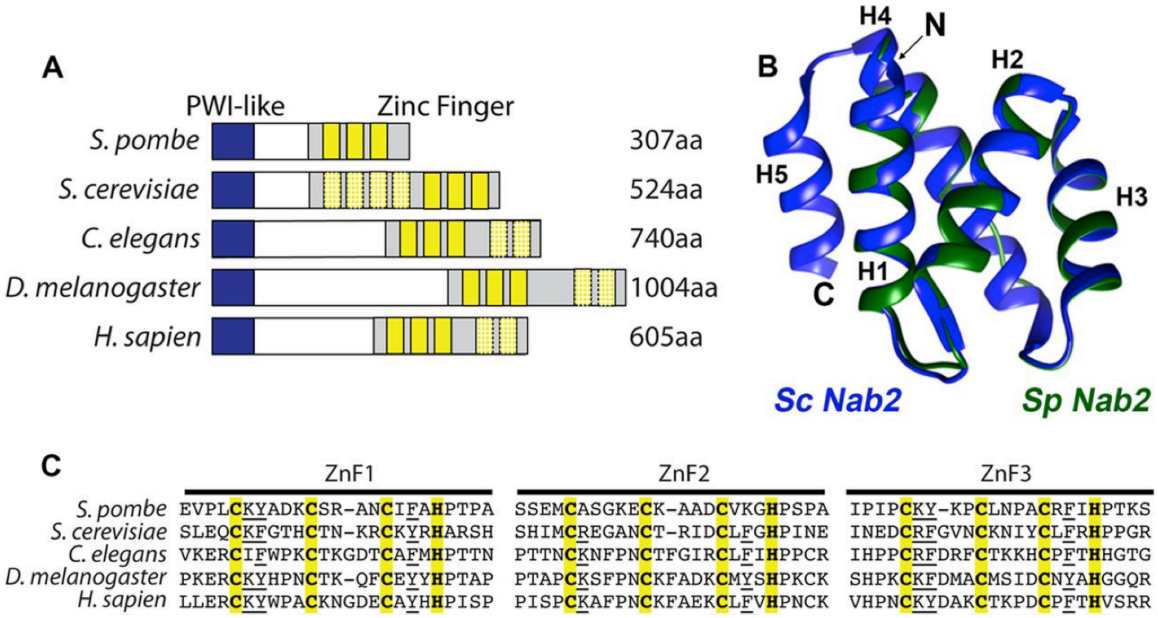

Figure 4.1. SPAC14C4.06c is a conserved CCCH zinc finger protein. (A) Domain alignment of *S. pombe* SPAC14C4.06c, *S. cerevisiae* Nab2, *C. elegans* Sut2, *D. melanogaster* dNab2, and *H. sapien* ZC3H14. The N-terminal domain contains a PWI-like motif (blue) and the C-terminal domain consists of a series of tandem zinc fingers (yellow). Zinc fingers most similar to *S. pombe* ZnF1-3 are shown in solid yellow boxes and are used in the alignment shown in (C). The hashed yellow boxes indicate additional zinc fingers present in other species. (B) Homology model of the N-terminal domain (amino acids 1-79) of *S. pombe* SPAC14C4.06c (green) overlaid with the N-terminal domain (amino acids 1-93) of *S. cerevisiae* Nab2 (blue). Homology modeling was carried out as described in Materials and Methods. Molecular images were generated using PyMol. (C) Alignment of the three C-terminal zinc finger motifs of *S. pombe* SPAC14C4.06c with zinc fingers of Nab2 orthologs: *S. cerevisiae* ZnF5-7; *C. elegans*, *Drosophila*, and human ZnF1-3. These zinc fingers share both spacing and conservation of key residues required for optimal RNA binding (indicated by the underline).

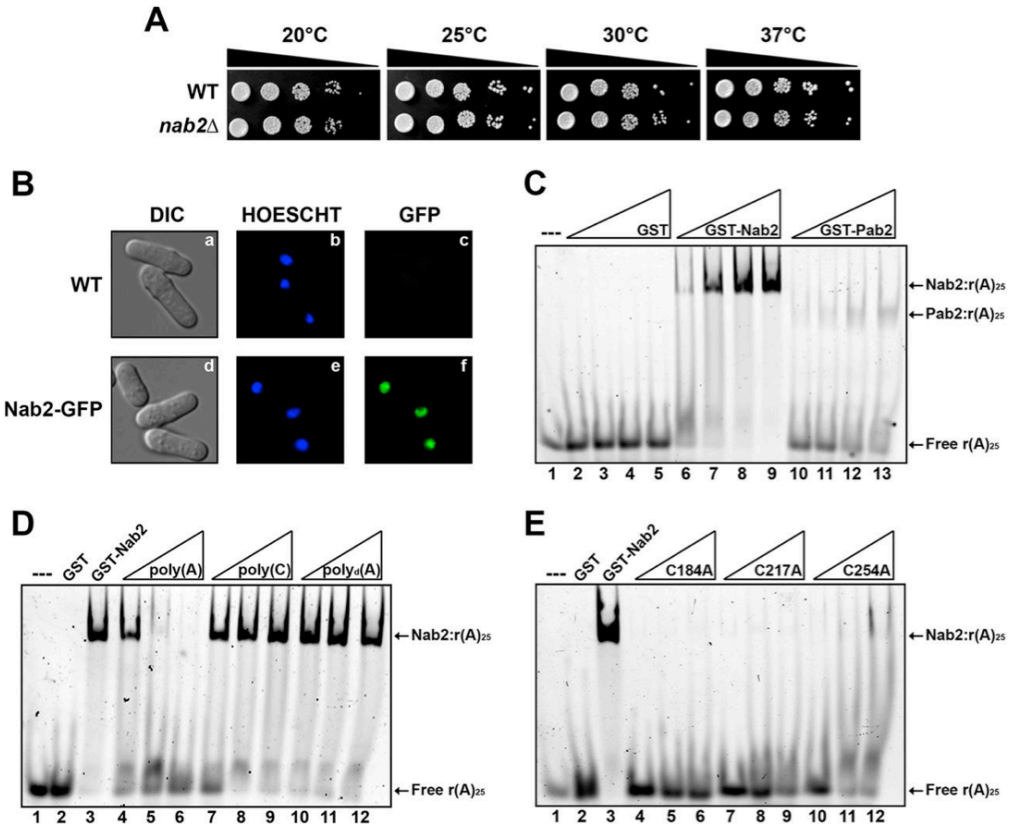

Figure 4.2. *S. pombe* Nab2 is a non-essential nuclear poly(A)-binding protein. (A) Tenfold serial dilution of wildtype (WT) and *nab2*Δ strains were spotted onto YES agar plates and grown at the indicated temperatures. (B) Visual analysis of control (a-c) and GFP-Nab2 (d-f) living cells. Direct fluorescence microscopy (GFP, panels c and f) was visualized in live cells and the corresponding differential interference contrast (DIC, panels a and d) images and Hoechst staining (panels b and e) are shown. (C) Equal amounts of GST (lanes 2-5), GST-Nab2 (lanes 6-9), and GST-Pab2 (lanes 10-13) were incubated with a Cy3-labeled poly(A) RNA ($r(A)_{25}$) oligonucleotide and RNA-protein complexes were analyzed on 5% nondenaturing polyacrylamide gels. The arrows point to the position of free $r(A)_{25}$ as well as Pab2:$r(A)_{25}$ and Nab2:$r(A)_{25}$ complexes. (D) Equal amounts of GST-Nab2 were incubated with Cy3-labeled $r(A)_{25}$ oligonucleotide in the presence of increasing concentrations of poly(A) (lanes 4-6), poly(C) (lanes 7-9), $poly_{deoxy}(A)$ (lanes 10-12) or without any competing nucleic acid (lane 3) (E) An equal amount of Cy3-labeled $r(A)_{25}$ oligonucleotide was incubated with GST (lane 2), wildtype GST-Nab2 (lane 3), and increasing concentrations of GST-Nab2 C184A (lanes 4-6), GST-Nab2 C217A (lanes 7-9), and GST-Nab2 C254A (lanes 10-12) and analyzed as describe in (C).

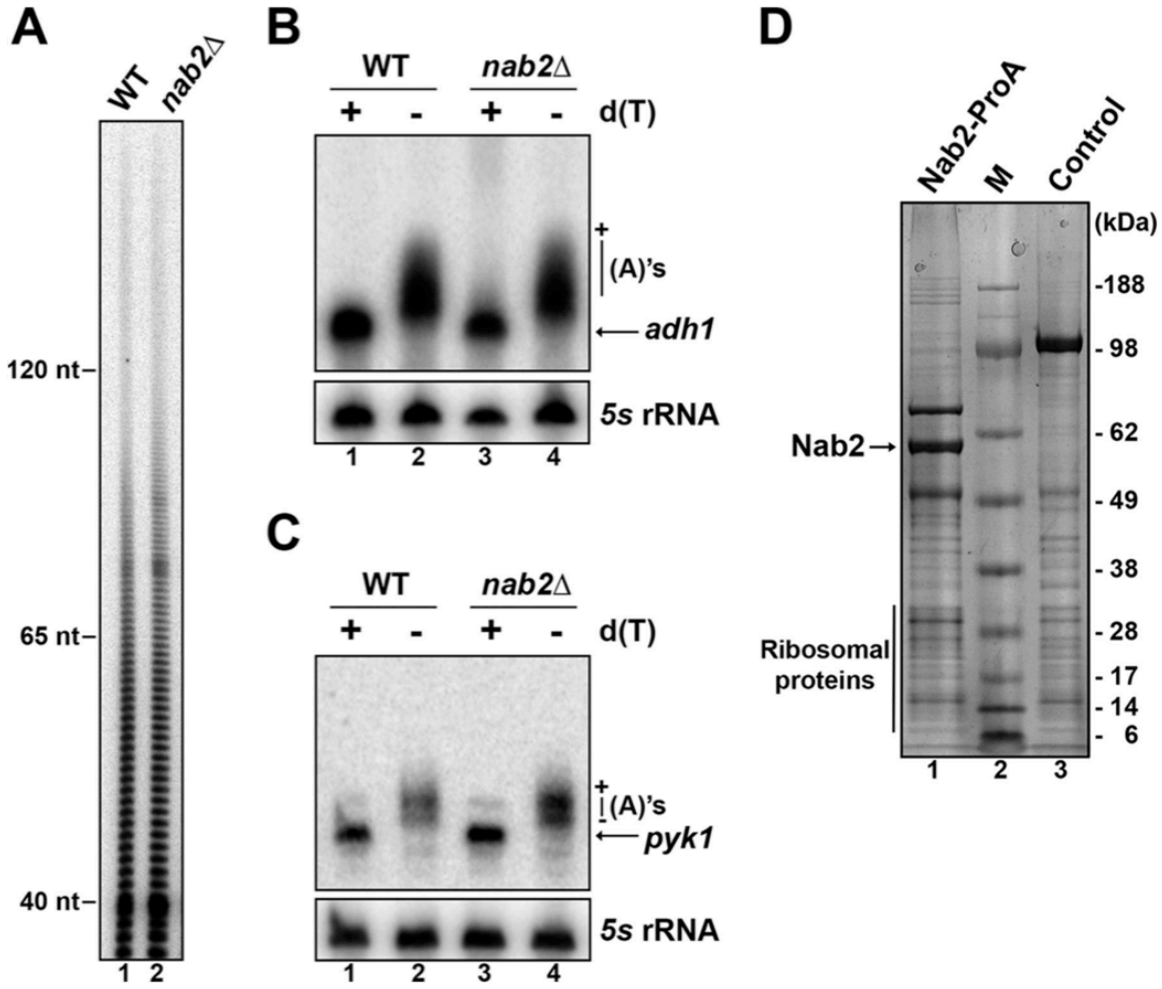

Figure 4.3. *S. pombe* Nab2 is not required for mRNA poly(A) tail length control. (A) Poly(A) tail length was analyzed by 3' end labeling of total RNA extracted from the indicated strains. Following RNase degradation of non-poly(A) sequences, the poly(A) tails were separated by electrophoresis through a 15% polyacrylamide-8 M urea gel. The positions of 3'-end labeled DNA fragments are indicated on the left. (B-C) Total RNA prepared from wildtype (lanes 1-2) and *nab2*Δ (lanes 3-4) cells was treated with RNase H in the presence of DNA oligonucleotides complementary to *adh1* (B) and *pyk1* (C) mRNAs. RNase H reactions were performed in the presence (+) or absence (-) of oligo d(T). The 5S rRNA was used as a loading control. (D) Commassie blue staining analysis of proteins copurified with Nab2-ProA (lane 1) and a control ProA fusion (lane 3) that were resolved using a Bis-Tris 4–12% gradient SDS–PAGE. Molecular weight markers (M; lane 2) are shown on the right in kilodaltons (kDa). The position of Nab2 is indicated on the left.

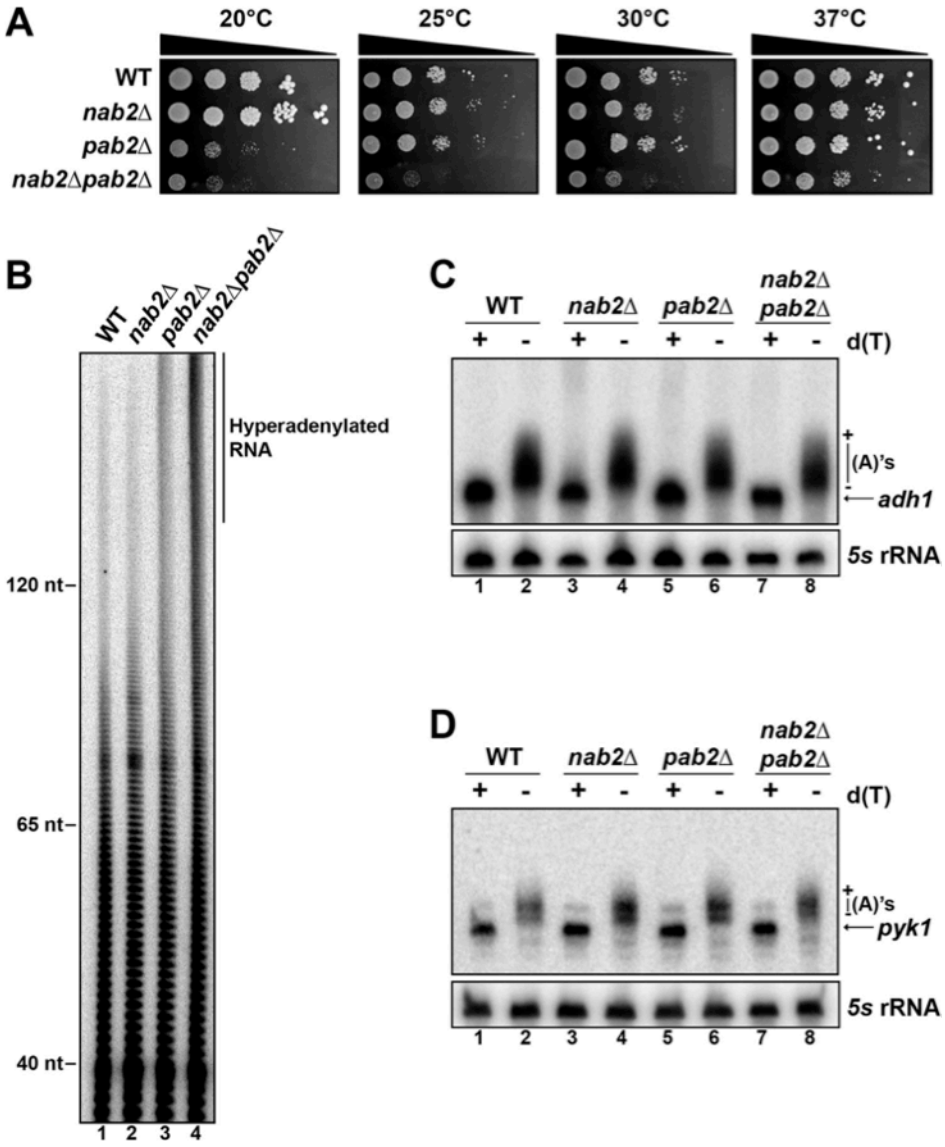

Figure 4.4. Genetic interaction between Nab2 and Pab2. (A) Tenfold serial dilutions of wildtype (WT), *nab2Δ*, *pab2Δ*, and *nab2*Δ *pab2*Δ strains. (B) Poly(A) tail length was analyzed by 3' end labeling of total RNA extracted from wildtype (lane 1-2), *nab2*Δ (lane 3-4), *pab2*Δ (lane 5-6), and *nab2*Δ *pab2*Δ (lane 7-8) cells as described in Figure 3A. (C-D) Total RNA prepared from wildtype (lanes 1-2), *nab2*Δ (lanes 3-4), *pab2*Δ (lanes 5-6), and *nab2*Δ *pab2*Δ (lanes 7-8) cells was treated with RNase H in the presence of DNA oligonucleotides complementary to *adh1* (C) and *pyk1* (D) mRNAs and analyzed as described in Figure 3B.

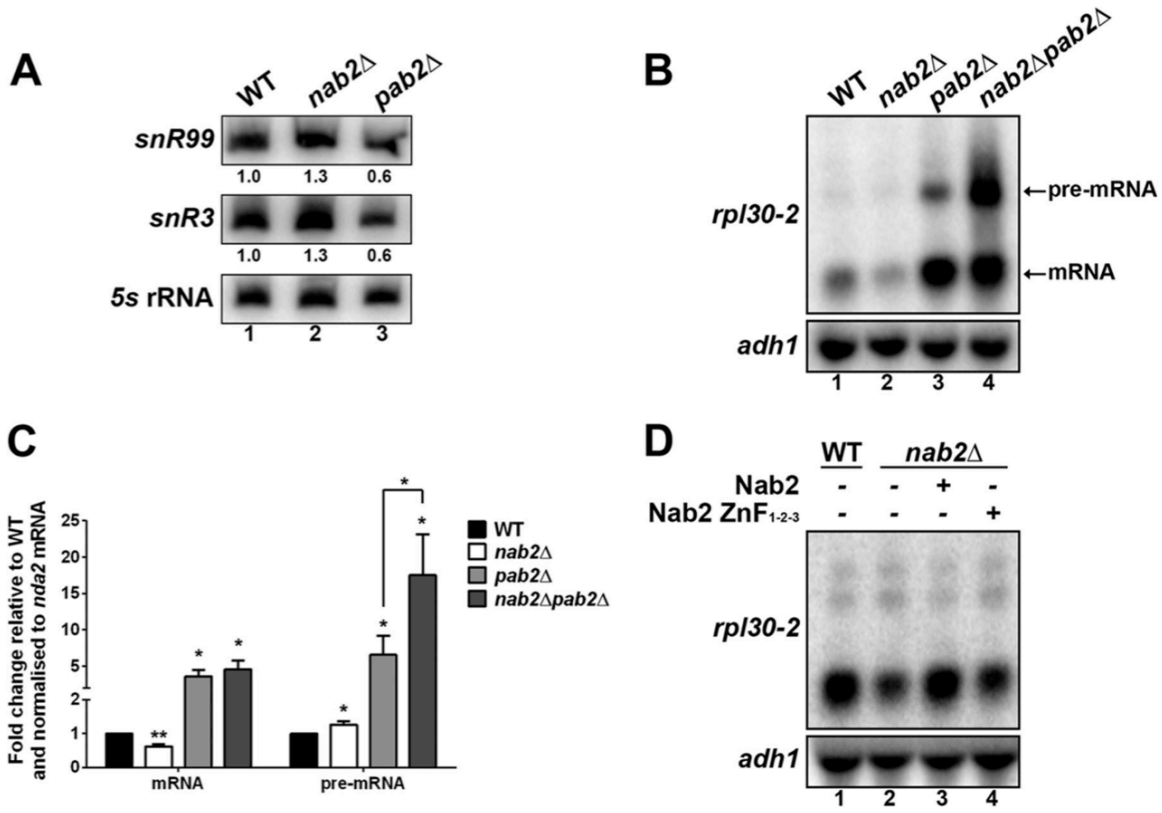

Figure 4.5. Antagonistic effects of *nab2* and *pab2* deletions. (A) Total RNA prepared from the indicated strains was subjected to northern blot analysis using probes complementary to the indicated snoRNAs. The 5S rRNA was used as a loading control. Normalized levels of each snoRNA relative to wildtype cells are indicated beneath each lane. (B) Northern blot analysis of RNA from the indicated strains. The blot was hybridized using a probe complementary to *rpl30-2* exon 1. The blot was also probed for the *adh1* mRNA. (C) Quantitative RT-PCR analysis of *rpl30-2* mRNA and unspliced pre-mRNA levels in the same strains as described in (B) using primer pairs in which one primer spans the exon-exon junction (mRNA) or is complementary to intronic sequences (pre-mRNA). The data and error bars represent the average and standard deviation from three independent experiments. (★★= *p*-value < 0.01; ★= *p*-value < 0.05; Student's t-test). (D) Northern blot analysis of *rpl30-2* using RNA from wildtype (lane 1) and *nab2*Δ (lanes 2-4) cells that were previously transformed with vectors expressing wildtype Nab2 (lane 3), a version of Nab2 with combinatorial cysteine to alanine substitutions ($ZnF_{1\text{-}2\text{-}3}$; lane 4), as well as an empty vector control (lane 2).

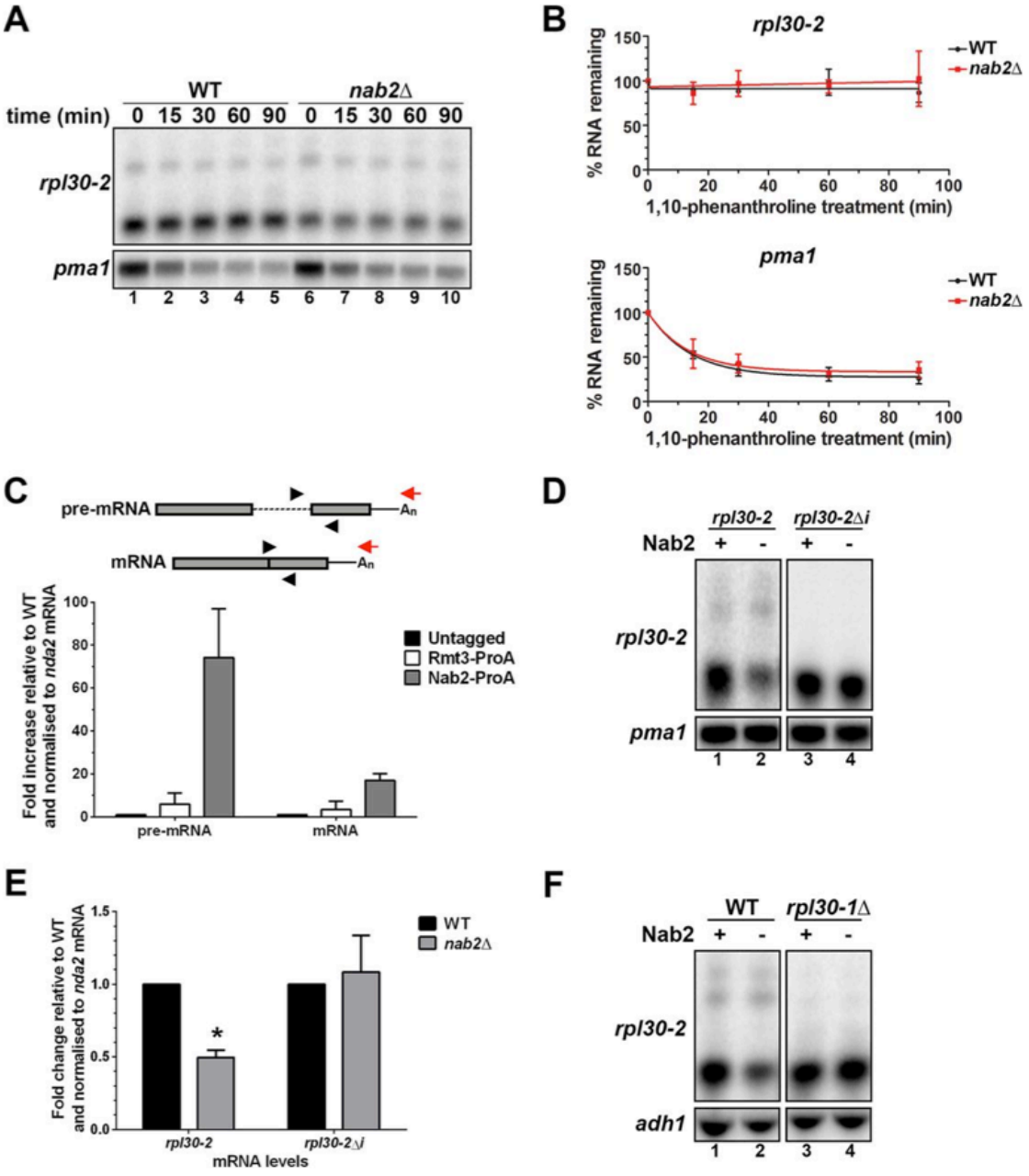
A
WT
nab2Δ
time (min)
0 15 30 60 90 0 15 30 60 90
rpl30-2
pma1
1 2 3 4 5 6 7 8 9 10
B
rpl30-2
% RNA remaining
WT
nab2Δ
1,10-phenanthroline treatment (min)
pma1
% RNA remaining
WT
nab2Δ
1,10-phenanthroline treatment (min)
C
pre-mRNA
An
mRNA
An
Fold increase relative to WT and normalised to nda2 mRNA
Untagged
Rmt3-ProA
Nab2-ProA
pre-mRNA
mRNA
D
rpl30-2
rpl30-2Δi
Nab2
+ - + -
rpl30-2
pma1
1 2 3 4
E
Fold change relative to WT and normalised to nda2 mRNA
WT
nab2Δ
*
rpl30-2
rpl30-2Δi
mRNA levels
F
WT
rpl30-1Δ
Nab2
+ - + -
rpl30-2
adh1
1 2 3 4

Figure 4.6. Nab2 promotes *rpl30-2* expression at the level of the unspliced pre-mRNA. (A) Total RNA prepared from wildtype (lanes 1-5) and *nab2*Δ (lanes 6-10) cells that were previously treated with 1,10-phenanthroline for the indicated times were analyzed by northern blot analysis for the *rpl30-2* and *pma1* mRNAs. (B) The percentage of RNA remaining for *rpl30-2* (upper panel) and *pma1* (lower panel) were determined by quantification of northern blot data and set to 100% at time zero. The data and error bars represent the average and standard deviation from three independent experiments. (C) Schematics of PCR primers (black arrowheads) used to measure unspliced (upper) and spliced (lower) *rpl30-2* RNA levels after oligo d(T)-mediated reverse transcription (red arrow). RNA immunoprecipitations (RIP) assays were performed using ProA-tagged versions of Nab2 and Rmt3, as well as using an untagged (WT) control strain. Pre-mRNA and mRNA associations (IP:Input ratio) were normalized to the *nda2* mRNA. Values were then set to 1.0 for the control purification using the untagged strain. The data and error bars represent the average and standard deviation from two biological replicates. (D) Northern blot analysis of RNA from wildtype (lanes 1 and 3) and *nab2*Δ (lanes 2 and 4) strains that express *rpl30-2* from intron-containing (lanes 1-2) and intronless (RPL30-2Δi; lanes 3-4) constructs. (E) Quantitative RT-PCR analysis of *rpl30-2* mRNA level in the same strains described in (D) using a primer pair in which one primer spans the exon-exon junction. (F) Northern analysis of RNA from wildtype (lanes 1), *nab2*Δ (lane 2), *rpl30-1Δ* (lanes 3), and *nab2*Δ *rpl30-1Δ* (lane 4) strains. The blot was probed for *rpl30-2* and *adh1* mRNAs.

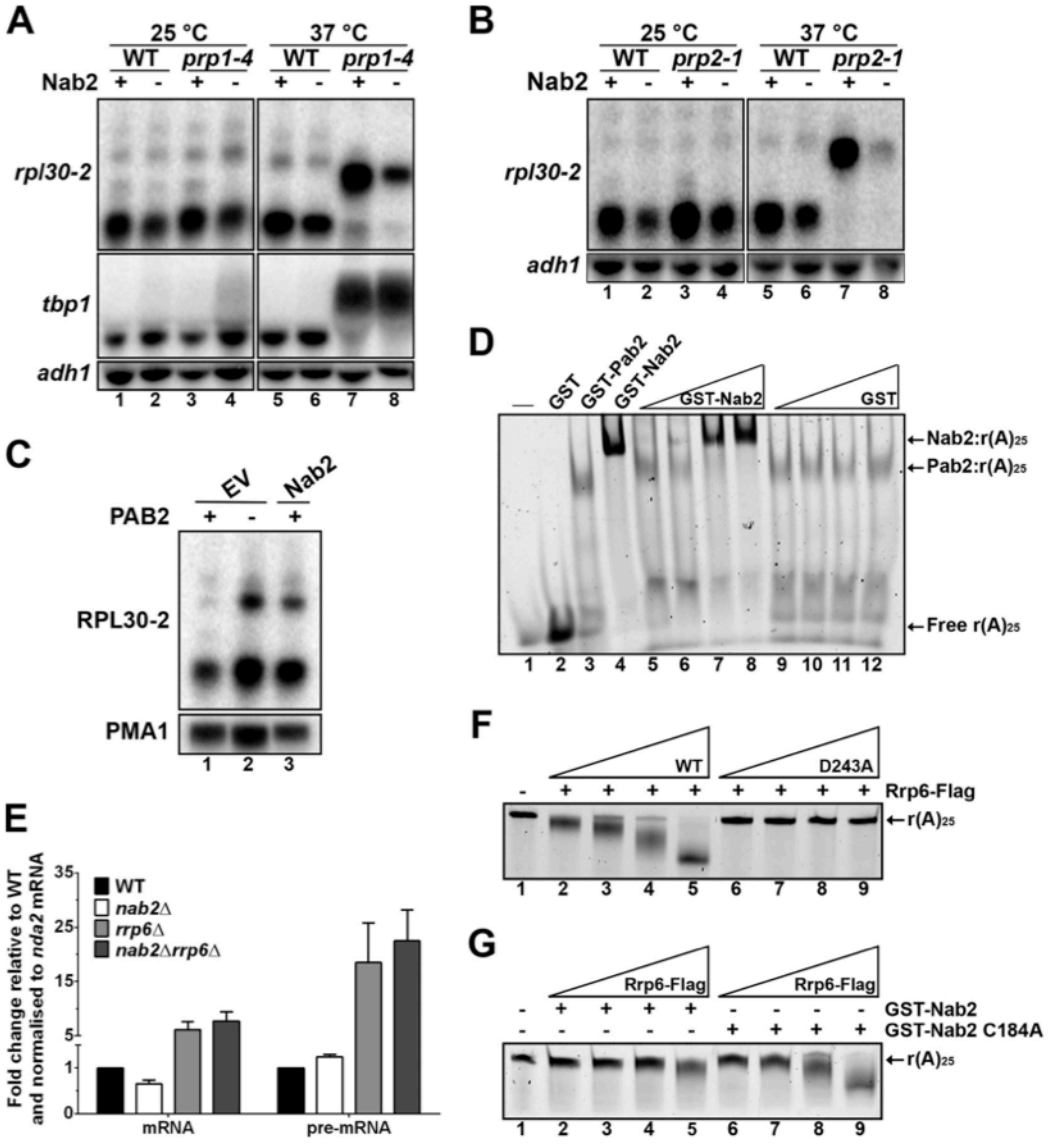
A
25 °C
37 °C
WT
prp1-4
WT
prp1-4
Nab2
+ - + - + - + -
rpl30-2
tbp1
adh1
1 2 3 4 5 6 7 8
B
25 °C
37 °C
WT
prp2-1
WT
prp2-1
Nab2
+ - + - + - + -
rpl30-2
adh1
1 2 3 4 5 6 7 8
C
EV
Nab2
PAB2
+ - +
RPL30-2
PMA1
1 2 3
D
—
GST
GST-Pab2
GST-Nab2
GST-Nab2
GST
←Nab2:r(A)25
←Pab2:r(A)25
←Free r(A)25
1 2 3 4 5 6 7 8 9 10 11 12
E
Fold change relative to WT and normalised to nda2 mRNA
35
25
15
5
1
0
WT
nab2Δ
rrp6Δ
nab2Δrrp6Δ
mRNA
pre-mRNA
F
WT
D243A
- + + + + + + + + Rrp6-Flag
←r(A)25
1 2 3 4 5 6 7 8 9
G
Rrp6-Flag
Rrp6-Flag
- + + + + - - - - GST-Nab2
- - - - - + + + + GST-Nab2 C184A
←r(A)25
1 2 3 4 5 6 7 8 9

Figure 4.7. Nab2 interferes with Pab2/Rrp6-mediated decay of unspliced *rpl30-2* pre-mRNA. (A) Total RNA prepared from wildtype (lanes 1 and 5), *nab2*Δ (lanes 2 and 6), *prp1-4* (lanes 3 and 7), and *nab2*Δ *prp1-4* (lanes 4 and 8) strains that were grown at permissive (lanes 1-4) and non-permissive (lanes 5-8) temperatures was subjected to northern blot analysis using probes complementary to *rpl30-2*, *tbp1*, and *adh1* transcripts. (B) Total RNA prepared from wildtype (lanes 1 and 5), *nab2*Δ (lanes 2 and 6), *prp2-1* (lanes 3 and 7), and *nab2*Δ *prp2-1* (lanes 4 and 8) strains that were grown at permissive (lanes 1-4) and non-permissive (lanes 5-8) temperatures was subjected to northern blot analysis using probes complementary to *rpl30-2* and *adh1* transcripts. (C) Total RNA prepared from wildtype (lanes 1 and 3) and *pab2*Δ (lane 2) cells that were previously transformed with an empty vector control (lanes 1-2) or a vector expressing Nab2 (lane 3) was subjected to northern analysis using probes specific to *rpl30-2* and *pma1* mRNAs. (D) Equal amounts of GST-Pab2 (lanes 3 and 5-12) were incubated with a Cy3-labeled poly(A) RNA ($r(A)_{25}$) oligonucleotide for 15 min before the addition of increasing amounts of GST-Nab2 (lanes 5-8) and GST (lanes 9-12) for an additional 15 min incubation. RNA-protein complexes were analyzed on 5% nondenaturing polyacrylamide gels. The arrows point to the position of free $r(A)_{25}$ as well as Pab2:$r(A)_{25}$ and Nab2:$r(A)_{25}$ complexes. (E) Quantification of northern blot data for *rpl30-2* spliced mRNA and unspliced pre-mRNA using wildtype, *nab2Δ*, *rrp6Δ*, and *nab2*Δ *rrp6Δ* strains. The data and error bars represent the average and standard deviation from at least three independent experiments. (F) Increasing amounts of wildtype (lanes 2-5) and D243A (lanes 6-9) versions of Rrp6 were incubated with Cy3-labeled poly(A) RNA ($r(A)_{25}$) oligonucleotide before analysis on a denaturing polyacrylamide gel. (G) Equal amounts of wildtype (lanes 2-5) and C184A (lanes 6-9) versions of GST-Nab2 were pre-incubated with Cy3-labeled poly(A) RNA ($r(A)_{25}$) oligonucleotide before the addition of increasing amounts of Rrp6 (lanes 2-9).

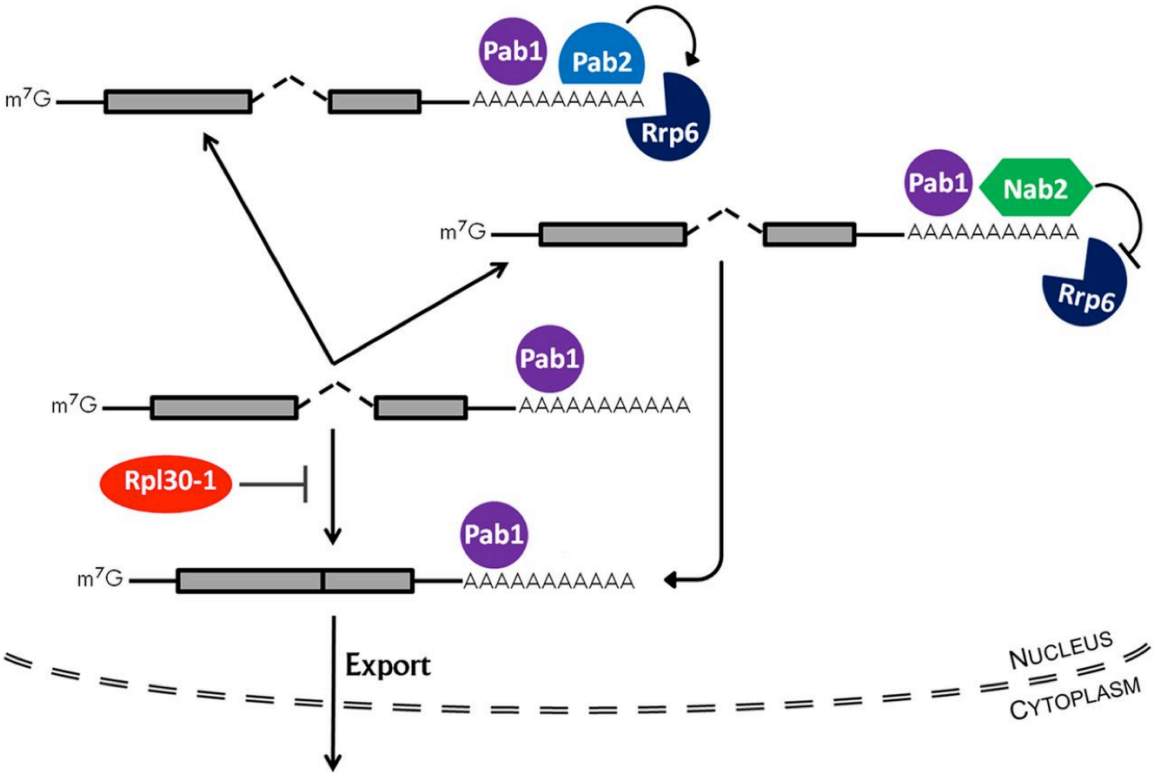

Figure 4.8. Model for opposing roles of Nab2 and Pab2 in nuclear pre-mRNA decay. Specific RNA-binding proteins, such as Rpl30-1, can interfere with RNA splicing, leading to the accumulation of unspliced pre-mRNA in the nucleus. Pab2-bound pre-mRNAs are targeted for complete degradation via Rrp6-mediated RNA decay, whereas unspliced pre-mRNAs bound by Nab2 are resistant to the degradation activity of Rrp6. Nab2-bound pre-mRNAs can ultimately complete RNA splicing to allow export of mature mRNAs. The equilibrium between RNA decay and processing is therefore influenced by the opposing roles of Pab2 and Nab2, thereby controlling gene expression.

Table 4.1: Proteins enriched in the Nab2-ProA purification

Table 1. Proteins enriched in the Nab2-ProA purification.

Protein name	Systematic name	MW (kDa)[a]	Intensity[b]	%[c]	#[d]
RNA Splicing					
Prp19	SPAC29A4.08c	54,2	92000000	54,1	23
Spp42	SPAC4F8.12c	274,6	68700000	56,8	120
Nop56	SPBC646.10c	55,4	33000000	62,4	23
Cwf10	SPBC215.12	11,2	32100000	59,4	55
Prp31	SPBC119.13c	57,7	30100000	8,7	3
Cwf11	SPBC646.02	148,4	27500000	53,6	56
Nop58	SPAC23G3.06	55,8	24500000	56,3	24
Cwf3	SPBC211.02c	92,6	22500000	65,1	53
Prp10	SPAC27F1.09c	135,2	21800000	52,6	48
Brr2	SPAC9.03c	248,8	21100000	43,1	77
Cwf4	SPBC31F10.11c	80,8	19000000	45,8	30
Nog1	SPBC651.01c	72,8	19000000	48,8	31
Prp12	SPAPJ698.03c	134,9	14600000	43,4	45
Prp17	SPBC6B1.10	63,1	14500000	43,9	24
Smd2	SPAC2C4.03c	13,1	13700000	55,7	6
Cdc5	SPAC644.12	86,8	12055000	53,6	37
Cwf22	SPBC13E7.01	102,7	9650000	40,4	35
Prp45	SPCC188.11	62,7	9010000	42,2	17
Spf38	SPBC1289.11	37,4	8910000	73,5	19
Smd1	SPAC27D7.07c	13,1	8340000	57,3	5
Prp43	SPBC16H5.10c	83,8	7860000	32,4	20
Smb1	SPAC26A3.08	15,5	7620000	59,2	8
Smd3	SPBC19C2.14	11,0	7410000	60,8	5
Prp5	SPBP22H7.07	52,4	7030000	59,2	20
Snu13	SPAC607.03	13,5	7010000	72,8	5
Lea1	SPBC1861.08c	27,2	6690000	77,0	14
Sap114	SPAC22A12.09c	54,4	6560000	37,6	13
Smf1	SPBC3E7.14	8,7	6040000	88,5	6
Sap145	SPAC22F8.10c	69,2	6020000	24,1	13
Usp105	SPBC4B4.09	71,3	5850000	39,1	27
Cwf15	SPBC337.06c	30,4	5610000	47,5	13
snoRNA processing					
Cbf5	SPAC29A4.04c	53,1	64500000	60,3	25
Fib1	SPBC2D10.10c	32,0	44500000	69,3	20
Rrp5	SPCC1183.07	187,5	31700000	50,8	75
Gar1	SPBC20F10.01	20,1	13900000	46,4	6
Nhp2	SPAC1782.10c	17,2	12100000	53,6	6
Nrap	SPBC776.08c	126,1	10577000	42,4	42
Nop2	SPBP8B7.20c	68,9	5620000	33,2	18
RNA decay					
Upf1	SPAC16C9.06c	104,5	63500000	74,4	64
SPAC17H9.02	SPAC17H9.02	118,5	14400000	45,5	41
Mmi1	SPCC736.12c	54,5	46600000	63,3	27
Mtr4	SPAC6F12.16c	126,2	6140000	37,2	35

[a], Molecular Weight; [b], relative abundance (peptide intensity); [c], sequence coverage; [d], number of unique peptides.

EXPERIMENTAL PROCEDURES

Strains and Media

Cells were grown at 30 °C in yeast extract medium with amino acid supplements (YES) or Edinburgh minimum medium (EMM) containing appropriate amino acids supplements. *prp1-4* and *prp2-1* mutants were grown at the permissive temperature of 25°C and shifted to the non-permissive temperature of 37°C for the indicated time. Conditional expression of Nab2 was achieved using the *nmt1* promoter, which is repressed in the presence of 15 μM thiamine. To allow Nab2 expression, cell were washed twice, and then grown without thiamine for 15h. Gene disruptions were done using either the PCR-mediated gene targeting method (271) or the two-step approach modified from this first method. All gene deletions were confirmed by colony PCR from genomic DNA and RT-PCR.

Structural homology modeling

Homology models of S. pombe Nab2 (SPAC14C4.06c) were constructed using Swiss-Model [version 8.05; (272)] starting with the known *S. cerevisiae* Nab2 crystal structure [PDB entry 2V75; (68)]. The model was energy minimized in CNS 1.2 to remove any steric strain introduced during modeling (273). This model was visualized and protein backbone torsion angles (phi and psi) were verified in Coot (274).

DNA Constructs

All of the DNA constructs used in this study are listed in Table S3. The GST-Nab2 expression construct was prepared by inserting the *S. pombe nab2* cDNA into pGEX-5X-3 using BamHI and XhoI restriction sites, creating pFB692. To express the wildtype version of Nab2 into the *nab2*Δ strain, the *S. pombe nab2* gene was amplified using genomic DNA with additional sequences corresponding to the promoter and the terminator of the *nab2* gene. This PCR product was cloned into pAde6 (275) using PstI and NotI restriction sites to create the plasmid, pFB815. Site-directed mutagenesis was performed using pFB815 to substitute the first cysteine of each CCCH zinc finger motifs for an alanine, generating plasmid pFB834. pAde6-derived constructs were linearized with BamHI and transformed in the *nab2*Δ strain for single integration at the *ade6* chromosomal locus. The expression of the various *S. pombe nab2* alleles and of *S. cerevisiae* Nab2 into *nab2*Δ cells was confirmed by RT-PCR. To express GFP-Nab2 under the control of *nmt1* promoter, the S. pombe *nab2* cDNA was cloned into pREP42 EGFP-N (276) using NdeI and BamHI sites to generate pFB720. All of the aforementioned plasmid constructs were confirmed by DNA sequencing.

Microscopy

Nab2-GFP was visualized by direct live microscopy as previously described (277). Briefly, cells were grown in EMM media, immobilised on concanavaline A pre-coated slides, and washed extensively with EMM media to discard unfixed cells. Nuclear DNA was stained using Hoechst 33342. GFP signals were visualized using a 62HE triple filters (Carl Zeiss Canada) on an Oberver.Z1 (Carl Zeiss Canada) equipped with a Cascade II

camera (Carl Zeiss Canada). Cellular auto-fluorescence background signals were removed using the axio vision rel. 4.7 software (Carl Zeiss Canada).

Recombinant Protein Expression, RNA Electrophoretic Mobility Shift Assays, and in vitro degradation assays.

GST, GST-Pab2, GST-Nab2, and GST-Nab2 with ZnF substitutions were expressed and purified as described previously (254) with the exception that 10 μM $ZnCl_2$ was systematically added throughout the purification to allow proper Nab2 folding. All proteins were stored at 4°C and binding assays were performed within 48h. Expression and purification of recombinant *S. pombe* Rrp6-Flag was described previously (249).

RNA gel-shift assays were performed by incubating control GST alone or GST fusion proteins in binding buffer (20 mM Tris-HCl pH 7.4, 50 mM NaCl, 2 μM $ZnCl_2$, 2% glycerol) in the presence of a Cy3-labeled 25-nt-long poly(A) RNA oligonucleotide (IDT) for 30 min at room temperature. Binding reactions were loaded onto a native 5% polyacrylamide gel (PAGE) in 0.3X TBE. Free Cy3-labeled poly(A) RNA and bound complexes were visualized using a Typhoon Trio instrument (GE Healthcare). For protein displacement experiments, GST-Pab2 and GST-Nab2 binding reactions were incubated for 15 min at room temperature, and then supplemented with GST-Nab2 or GST-Pab2, respectively, for an additional 15 min before PAGE analysis.

In vitro RNA degradation assays were performed with a constant amount of Cy3-labeled poly(A) RNA (20 nM) but with increasing amounts of Rrp6 enzyme in a solution containing 10 mM Tris-Cl, at pH 8.0, 50 mM KCl, 7.1 mM MgCl, and 75 μM MnCl. Degradation assays were allowed to proceed for 1 h at 25°C, after which they were quenched by addition of RNA loading buffer and separated by denaturing gel electrophoresis in 20% urea–acrylamide gels and visualized using a Typhoon Trio imager. To test the effect of Nab2 on Rrp6-mediated degradation, wildtype and C184A versions of GST-Nab2 were pre-incubated for 15 min with poly(A) RNA before the addition of increasing amounts of Rrp6.

Affinity Purification coupled to Mass Spectrometry Analysis

Nab2-ProA was affinity purified using a previously described method (278). Briefly, cells were harvested at mid-log phase and frozen in liquid nitrogen. Cell pellets were washed once with water and once in re-suspension buffer (1.2% polyvinylpyrrolidone, 20 mM Hepes pH 7.4, 1 mM DTT, and protein inhibitors) before lysis by cryogenic grinding. Extraction buffer (100 mM Hepes pH 7.4, 150 mM NaCl, 0.5% Triton, 1 mM DTT, 1,5 mM $MgCl_2$, 20 ng pepstatin, 900 ng PMSF, 0.1 % ethanol) was then added to the grinded cells and homogenized using a polytron. Cell lysates were centrifuged for 10 min at 3500 rpm (4°C) and incubated with pre-washed antibody-conjugated magnetic beads for 30 min (4°C). The beads were washed three times with extraction buffer and five times with wash buffer (0.1 M NH_4OAc, 0.1 mM $MgCl_2$). Proteins were eluted twice in elution buffer (0.5 M NH_4OAc, 0.5 mM EDTA) for 20 min

at room temperature and vacuum-dried. Proteins samples were resuspended in loading buffer before being reduced in 10 mM DTT and alkylated in 50 mM iodoacetamide prior to SDS-PAGE (4–12% Bis-Tris Novex mini-gel, Invitrogen) separation. Following visualization by colloidal coomassie staining, entire gel lanes were excised and cut into eight equal-size pieces that were subjected to in-gel digestion using trypsin. Tryptic peptides were separated using an Ultimate U3000 (Dionex Corporation) nanoflow liquid chromatography (LC) system coupled to a LTQ OrbiTrap Velos mass spectrometer. The resulting MS/MS spectra were search against the PomBase protein dataset using MASCOT for peptide identifications.

RNA Analyses

Total RNA was extracted using the hot-acid phenol method. For northern blots analyses, total RNA was resolved on agarose-formaldehyde or polyacrylamide-urea gels, transferred onto nylon membranes, and probed using ^{32}P-labeled gene-specific probes. Bulk poly(A) tail length analysis was done as described (254). RNase H cleavage assays (249) and real-time RT-PCR (139) analyses were performed as previously described. To measure *rpl30-2* mRNA stability, transcription was blocked with 300 μg/ml 1,10-phenanthroline as described (258), followed by RNA extraction from cells harvested at the indicated time points.

Chromatin immunoprecipitation (ChIP) assays

ChIP assays were carried out as previously described (257).

Chapter 5: Characterization of the RNA Binding Protein, Mmi1: Regulation of Meiotic Transcripts

INTRODUCTION

Whole gene expression programs must be modulated and coordinated to ensure proper cellular responses and to allow for cellular transitions. Many of these global changes are mediated by RNA binding proteins (132). During the cell cycle switch from mitosis to meiosis, a striking change in gene expression occurs. Many of the genes required for the progression of meiosis are upregulated by transcription factors; however, emerging evidence has also revealed a key role for post-transcriptional regulation of this gene expression program (135). Accordingly, a number of RNA binding proteins that play roles in post-transcriptional regulation during vegetative growth also function in the regulation of meiotic transcripts (135).

Meiosis is a fundamental differentiation process necessary for sexual reproduction in eukaryotes and has been best studied in the yeast model system. During meiosis in yeast, two cells of opposite mating types fuse to form a diploid cell (133, 279). This diploid cell containing paired homologous chromosomes undergoes DNA replication, followed by two rounds of cell division to produce four haploid cells (133). While the process of cell division is similar between meiosis and mitosis, there are key differences between the two processes. Notably, meiosis and mitosis are mutually exclusive, whereby genes required for meiosis are only expressed in meiosis (135). Regulating the expression of meiotic genes during mitosis is critical to avoid untimely activation of meiosis. Currently, the molecular mechanisms employed to suppress expression of meiotic genes during mitosis is poorly understood.

Meiotic differentiation has been most extensively studied in the fission yeast, *Schizosaccharomyces pombe* (134). During meiosis in fission yeast, the expression of hundreds of meiotic genes is altered both at the transcriptional and post-transcriptional mechanisms (134, 280). Importantly, recent studies reveal that specific post-transcriptional processes, including pre-mRNA splicing, 3'-end processing, and mRNA decay, are critical for regulating meiotic gene expression (136-139). Central to post-transcriptional meiotic gene expression is the Tyrosine-Threonine-Histidine (YTH)-family RNA binding protein, Mmi1 (138). Mmi1 plays a crucial role in selectively targeting meiosis-specific transcripts in mitotic cells for destruction (135, 137). Mmi1 contains a YTH RNA binding domain that recognizes a region termed the determinant of selective removal (DSR), which is enriched with repeats of hexanucleotide motifs (138). Mmi1 can bind specifically to meiotic transcripts and control their fate by regulating pre-mRNA splicing, modifying the poly(A) tail, and mediating decay (136, 138, 139). For example, in vegetatively growing cells mutant for *MMI1*, meiotic transcripts remain unspliced and hyperadenylated (136, 138). In addition, these intron-containing and hyperadenylated meiotic transcripts are targeted for decay by the exosome component, Rrp6 (136, 139). Thus, misregulation of Mmi1 results in untimely expression of meiotic transcripts that ultimately results in cell death (137). How Mmi1 stimulates polyadenylation to recruit mRNA decay machinery is poorly understood.

One class of RNA binding proteins that have the potential to regulate meiotic transcripts are poly(A) RNA binding proteins (Pabs). For example, the *S. pombe* Pab2

poly(A) RNA binding protein regulates meiotic transcripts (139). Pab2, Mmi1, and the nuclear exosome complex cooperate to rapidly eliminate several meiotic transcripts during mitosis (139). Importantly, Pab2 promotes decay of meiotic transcripts using a polyadenylation-mediated mechanism (139). However, these studies revealed a complex mechanism for meiotic RNA degradation and suggest a model where there are additional RNA binding proteins that coordinate meiotic gene expression. One prediction from this model is that additional Pabs may cooperate with Mmi1 to promote specific degradation of meiotic mRNAs during vegetative growth.

The genetic interaction between *nab2* and *pab2* described in Chapter 4 (85) suggests that nuclear Pabs coordinate functions to regulate gene expression. In order to understand how the two nuclear Pabs, Nab2 and Pab2, regulate meiotic transcripts via Mmi1, we focused our efforts on characterizing the Mmi1 protein in *S. cerevisiae* which has never been defined. One reason for characterizing the Mmi1 protein in budding yeast is that there is no apparent *S. cerevisiae* Pab2 orthologue, suggesting that Nab2 may be the sole nuclear Pab that cooperates with Mmi1 to eliminate meiotic transcripts during vegetative growth. Furthermore, a link between Nab2 and Mmi1 is supported by the mass spectrometry results presented in Chapter 4 (see Table 4.1) (85). How different Pabs coexist in the eukaryotic nucleus and whether there is functional interplay between nuclear Pabs, such as between Nab2 and Pab2, during meiosis remains elusive.

Here, we characterize the *S. cerevisiae* Mmi1 protein to gain a better understanding of the interplay between RNA binding proteins and their effect on specific

transcripts important for meiosis in budding yeast. We find that the *MMI1* gene is not essential in *S. cerevisiae*; however, deletion of *MMI1* results in accumulation of meiotic transcripts during vegetative growth and sporulation defects. This chapter identifies Mmi1 as a novel RNA binding protein in budding yeast and explores the impact on meiotic gene expression.

RESULTS

Characterization of the *S. cerevisiae* RNA binding protein, Mmi1

To assess the possible interplay between Nab2 and Mmi1 in budding yeast, we sought to characterize the *S. cerevisiae* Mmi1 protein. We performed BLAST analysis to identify putative orthologues of Mmi1 in *S. cerevisiae*, seeking proteins containing a conserved YTH domain. Our sequence analysis identified the *S. cerevisiae* protein, YDR374C, as the *S. cerevisiae* protein with a domain structure most similar to *S. pombe* Mmi1 (Figure 5.1A). In addition, we indentified the *H. sapiens* protein, YTH521, as the *H. sapiens* protein with a domain structure most similar to *S. pombe* Mmi1 (Figure 5.1A). Comparison of the overall sequence similarity of *S. cerevisiae* YDR374C to *S. pombe* Mmi1 and *H. sapiens* YTH521 revealed a high level of similarity in the YTH domain. Interestingly, we found that there was more sequence identity between the *S. cerevisiae* and *H. sapiens* (29%) YTH domains compared to *S. cerevisiae* and *S. pombe* (24%) YTH domains (Figure 5.1B). On the basis of sequence similarities, we named the previously uncharacterized *S. cerevisiae* open reading frame, YDR374C, as Mmi1.

The similarities between the domain structures of S. *pombe, S. cerevisiae,* and *H. sapiens* prompted us to further characterize *S. cerevisiae* Mmi1. *S. pombe* Mmi1 is an essential protein (137). To assess whether *S. cerevisiae* Mmi1 is required for cell growth, we used a PCR-mediated method to delete the *MMI1* locus. As shown in Figure 5.2A, we obtained recombinant colonies where the *MMI1* gene was deleted and deletion was confirmed by PCR. Examination of cell growth revealed that deletion of *MMI1* results in a slow growth phenotype at all temperatures, particularly at 37°C (Figure 5.2A). These data indicate that *S. cerevisiae* Mmi1 is not essential, but is required for proper cell growth.

The *S. pombe* RNA-binding protein Mmi1 functions in the post-transcriptional destruction of specific meiotic mRNAs during fission yeast vegetative growth (137). To examine whether *S. cerevisiae* Mmi1 also contributes to the destruction of meiotic transcripts, we tested for the expression of meiotic transcripts during vegetative growth in the *S. cerevisiae* Δ*mmi1* mutant. To test for the presence of meiotic RNAs in wildtype and Δ*mmi1* mutant cells during vegetative growth, cells were grown to mid-log phase at 30˚C and RT-PCR was performed. We amplified the meiotic transcripts, *MEI4*, which is upregulated in *S. pombe mmi1* mutant cells and is conserved in budding yeast (133, 135). As observed in *S. pombe mmi1* temperature sensitive mutants, deletion of *MMI1* in *S. cerevisiae* results in the accumulation of the *MEI4* transcripts during vegetative growth as compared to wildtype cells grown under the same conditions (Figure 5.2B). These data

indicate that the *S. cerevisiae* Mmi1 regulates the expression of at least one representative meiotic transcript during mitosis.

One consequence of accumulation of meiotic transcripts during mitosis is meiotic arrest. Meiotic arrest in yeast cells results in a sporulation defect (133, 281). To test whether *S. cerevisiae* Δ*mmi1* cells show a sporulation defect, diploid cells were grown in media lacking nitrogen to induce sporulation. Wildtype cells produced many sporulated tetrads whereas Δ*mmi1* cells resulted in few sporulated tetrads (Figure 5.2C). As a control, a transcription activator of early meiotic genes that is required for meiosis (282), Δ*ime1,* is shown. As expected, cells deleted for *IME1* have poor sporulation efficiency (Figure 5.2C). Taken together, these data indicate that the deletion of *S. cerevisiae MMI1* causes meiotic defects that mirror the phenotypes observed in *S. pombe mmi1* mutant cells.

DISCUSSION

This study presents the first characterization of the *S. cerevisiae MMI1* (*YDR374C*) gene which encodes a YTH-containing protein with homology to the *S. pombe* mRNA processing factor Mmi1. Mmi1 is not an essential protein in *S. cerevisiae*; however, deletion of *MMI1* results in a temperature sensitive growth phenotype, indicating that *S. cerevisiae* Mmi1 is critical for proper cell growth. We show that deletion of *MMI1* results in accumulation of meiotic transcripts and causes sporulation defects. These results suggest that *S. cerevisiae* Mmi1, like *S. pombe* Mmi1, is important

for regulating the expression of meiotic transcripts during vegetative growth in budding yeast.

Further studies will examine the functional interactions mediated by Mmi1 and select RNA processing machinery. In *S. pombe*, Mmi1 interacts with the 3'-end processing components, Rna15 and Pap1, and the nuclear exosome, Rrp6 (136). Interestingly, RIP-Chip analysis in budding yeast indicates the recruitment of exosome components to meiotic intron-containing genes (129), suggesting that the role of the exosome in the negative regulation of meiotic gene expression is conserved between fission and budding yeasts. However, the adaptor proteins utilized to recruit the exosome differ between the two yeasts. As illustrated in Chapter 4, there are key differences between *S. pombe* and *S. cerevisiae* in control of 3'-end processing and decay. Importantly, Nab2 does not appear to play a major role in 3'-end processing in *S. pombe*. Given that pre-mRNA hyperadenylation is an important characteristic of aberrantly expressed meiotic transcripts, Nab2 may play a role in this hyperadenylation in budding yeast.

Further studies will be required to assess the functional interactions mediated by the YTH domain of Mmi1 in *S. cerevisiae*. A RIP-Chip or RIP-seq study will be critical to identify Mmi1-regulated meiotic genes. Subsequent bioinformatic analysis can be used to search for meiotic transcripts containing the DSR target region, which is necessary for Mmi1-mediated recognition of RNA (135). Furthermore, RNA analysis can reveal if meiotic transcripts expressed during vegetative growth contain introns and are

hyperadenylated in Δ*mmi1* mutant cells. In addition, overlap between transcripts targeted by Mmi1 and transcripts targeted by other RNA binding proteins, including Nab2, can shed light onto how these transcripts are functionally regulated. Taken together, the characterization of Mmi1 in *S. cerevisiae* lays the groundwork for further studies to understand how specific meiotic transcripts are regulated in budding yeast.

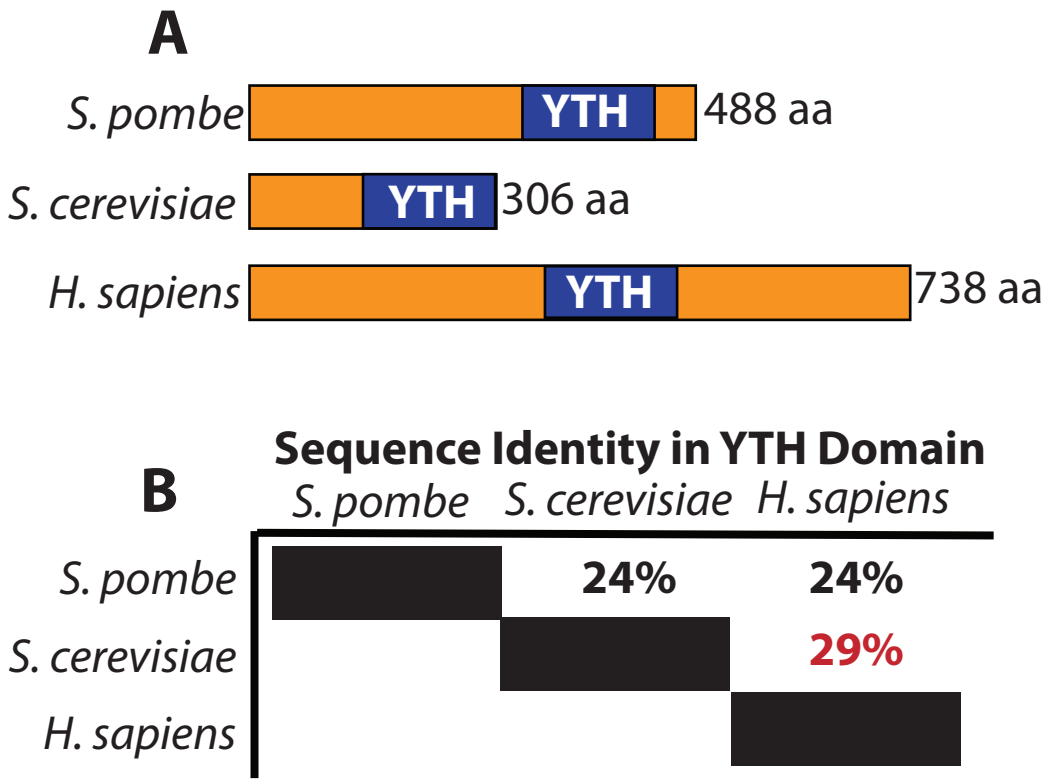

Figure 5.1. Mmi1 is an evolutionarily conserved RNA binding protein. (A) The Mmi1 protein family contains a conserved RNA binding domain, YTH, in *S. pombe* Mmi1, *S. cerevisiae* YDR374C, and *H. sapiens* YTH521. (B) The sequence identity in the YTH domain between *S. cerevisiae* and *S. pombe* is 29% compared to *S. cerevisiae* and *S. pombe* that is 24%.

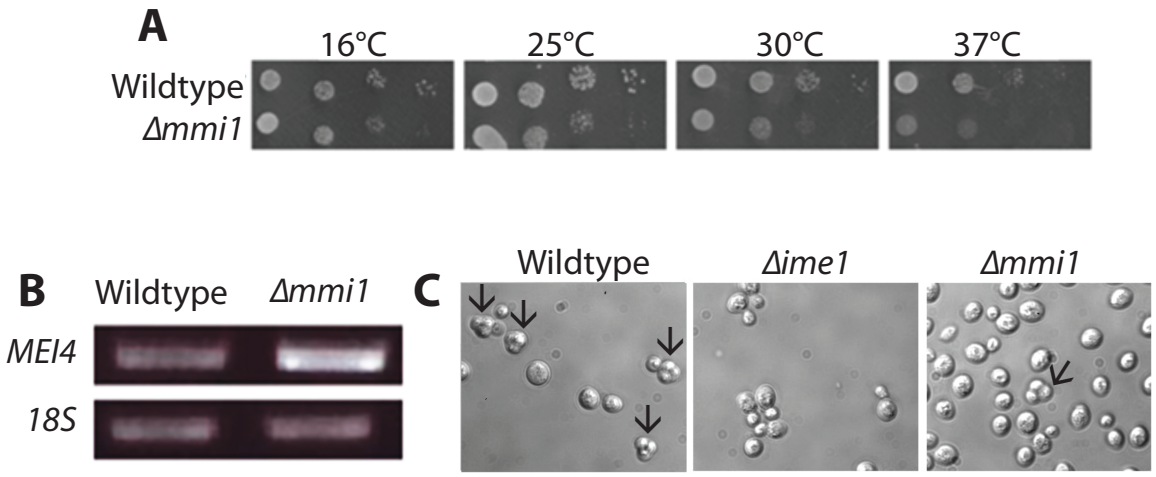

Figure 5.2. Deletion of *MMI1* results in slow growth and meiotic defects. (A) Deletion of *MMI1* was created using PCR mediated knockout. Wildtype and *Δmmi1* cells were grown, serially diluted, and spotted onto YEPD plates at 16°C, 25°C, 30°C, and 37°C for growth analysis. (B) Wildtype and *Δmmi1* haploid cells were grown during vegetative growth at 30°C, RNA was isolated, and cDNA generated to perform PCR on the meiotic *MEI4* transcript and loading control, 18S RNA. (C) Wildtype, Δ*mmi1* and a control meiosis mutant, Δ*ime1,* diploid cells were grown in sporulation media to induce sporulation. DIC, differential interference contrast microscropy pictures were taken to differentiate between sporulated and non-sporulated cells. Arrows indicate sporulated cells.

MATERIALS AND METHODS

Phylogenetic analysis

BLAST searches were performed to identify amino acid sequences similar to the *S. pombe* Mmi1 protein across eukaryotic species. The putative homologous proteins indentified from the BLAST search were aligned with the *S. pombe* sequence of Mmi1 using ClustalW. The sequence identity for the YTH domain in the Mmi1 protein was determined using ClustalW.

PCR-generated knockout

A PCR was performed with primers containing sequence homology to *S. cerevisiae* YDR374C, *MMI1*, and TEF promoter and terminator sequences. The HYGRO cassette in pAC2703 was utilized. The PCR product was purified and transformed into WT S288C strain ACY233 (283) and plated onto YEPD plates. The transformants were replicated plate to hygromycin and select colonies were regrown on hygromycin plates. Positive colonies were checked by PCR and put into the yeast collection as ACY2303.

RT-PCR

To prepare total RNA, 10 ml cultures were grown in appropriate media to an A_{600}=0.4-0.6 at 30°C. Total RNA was isolated using the Trizol method. Two scoops of glass beads were added to cell pellets, and bead beat for two minutes. For each sample, 100 μl of 1-bromo-3-chloropropane was added, vortexed for 15 seconds, and incubated at

room temperature for 2 minutes. Samples were centrifuged for 8 minutes at 16,300 X *g* at 4°C and the upper layer was transferred to a fresh tube. RNA was precipitated with 500 µl of isopropanol, vortexed, and centrifuged for 8 minutes at 16,300 X *g* at 4°C. The supernatant was decanted and the RNA pellet was washed with 75% ethanol. Samples were centrifuged for 5 minutes at 16,300 X *g* at 4°C, the supernatant was decanted, and the pellet was air dried. The RNA pellet was resuspended in 30 µl of 10 mM Tris-HCl pH7.5. To measure mRNA levels, 1 µg of total RNA was transcribed to cDNA using QuantiTect Reverse Transcription Kit (Qiagen) according to the manufacturer protocol. Relative mRNA levels were detected by RT-PCR using *Taq* DNA polymerase (Qiagen).

Microscopy

Cells were grown overnight in potassium acetate presporulation media (PSP2) supplemented with 25% of the recommended concentration of amino acids (281). Cells were spun down, washed with water, and resuspended in sporulation media (SPM). The cells were incubated at 25°C for 3 days to induce sporulation. Cells were visualized using differential contract microscopy on an Olympus BX60 epifluorescence microscope equipped with a Photometrics Quantix digital camera.

Chapter 6: Discussion

Here I describe how RNA binding proteins target and impact specific transcripts at the post-transcriptional level. I characterize the Nab2 class of Cys3His (CCCH) tandem zinc finger (ZnF) polyadenosine RNA binding proteins. I show that Nab2 ZnF5-7 forms a novel single coherent structural unit that binds eight adenosines and our results predict critical amino acid residues for polyadenosine binding (Chapter 2). Furthermore, mutations in Nab2 ZnFs result in extended poly(A) tail length *in vivo* that correlate with genetic interactions between *NAB2* and genes encoding machinery critical for the generation of export-competent mRNPs (Chapter 2). I go on to explore how export-competent mRNPs form by defining a novel role for Nab2 in splicing, implicating Nab2 in early mRNA biogenesis (Chapter 3). Biochemical and genetic data indicate that Nab2 restricts accumulation of unspliced pre-mRNA and bulk poly(A) tail length by interfacing with the nuclear exosome (Chapter 3). In addition, I identify a role for the splicing factor, Mud2, in the control of poly(A) tail length (Chapter 3). I demonstrate that the 3'-end poly(A) tail acts as a binding platform for competing Pabs, suggesting that the interplay between nuclear poly(A) RNA binding proteins is critical for the regulation of gene expression (Chapter 4). To begin to understand the full collection of RNA binding proteins in the nucleus that contact the poly(A) tail to influence mRNA processing, I characterize the RNA binding protein, Mmi1, in budding yeast (Chapter 5). These studies reveal a critical role for RNA binding proteins at multiple steps of mRNA biogenesis and allow for future studies on the molecular mechanisms underlying gene expression.

The work detailed in this dissertation has addressed three outstanding questions in the RNA processing field: 1) How are polyadenylated transcripts recognized by RNA binding proteins; 2) How are post-transcriptional RNA processing events coupled by RNA binding proteins; 3) What are the implications of altered pre-mRNA processing? Using the RNA binding protein, Nab2, as a model, we investigated the molecular mechanisms for recognition of polyadenosine RNA and the role of Nab2 in coupling splicing, 3'-end processing, and RNA surveillance. We extended our analysis to the Mmi1 protein to begin to probe for how specific transcripts or specific classes of transcripts are targeted by RNA binding proteins.

A model for Nab2 at the crux of mRNP assembly

Our findings that Nab2 interacts with a variety of RNA binding proteins at different stages of RNA processing to promote proper mRNA processing, illustrates the overall significance of Nab2 in mRNP assembly. These observations lead to a model where the nuclear history of the mRNA, particularly at the stage of RNP assembly, affects the export competence of mRNA transcripts. The studies presented here lead to an expanded model of RNP assembly by exploring the potential roles of Nab2 in multiple roles of RNA processing (Figure 6.1). Indeed, our studies provide evidence supporting a role for Nab2 in the assembly of export-competent mRNPs through interactions with the export adaptor protein, Yra1, and the export receptor, Mex67 (Chapter 2). Nab2 may poise the mRNA for efficient export by actively helping to ensure that the mRNP is

assembled. Alternatively, Nab2 may sequester aberrant mRNP complexes and thus keep mRNPs from interacting with the export machinery. This model is supported by the genetic interaction between *NAB2* and genes encoding the nuclear retention machinery (Chapter 3). By delaying export, Nab2 may serve as a surveillance factor to either facilitate proper pre-mRNA processing or aid in targeting the transcript for decay. A third possibility is that Nab2 senses the nuclear processing history of the transcript based on the proteins bound to the RNA prior to generation of export-competent mRNPs (Chapter 3 and 4). This model is supported by the role of Nab2 in splicing, whereby Nab2 contacts multiple components of the spliceosome. Any deficiency in upstream RNA processing steps leads to reduced recruitment of Nab2 and likely additional export machinery, providing a checkpoint for mRNA processing and mRNP assembly. Whether extended poly(A) tails result in poorly assembled mRNP complexes or whether the generation of these aberrant mRNP complexes results in hyperadenylation is not known. Uncoupling export from polyadenylation will be required to answer this question and ultimately reveal precisely how Nab2 functions.

Molecular recognition of polyadenosine RNA

Until our recent studies (146, 156), the only known RNA binding proteins that contacted polyadenosine RNA were those that contained at least one RRM (284). In Chapter 2, we show the structure of the CCCH-containing zinc finger RNA binding protein, Nab2, and provide insight into how this class of Pabs specifically recognize

polyadenosine RNA. We use the Nab2 protein, which contains seven zinc fingers, and describe the solution structure of fingers 5-7, which are necessary and sufficient for high-affinity polyadenosine RNA binding (156). The solution structure of Nab2 ZnF5-7 forms a single coherent structure with numerous interactions between individual ZnFs. We also identify key residues, including the positive and aromatic residues, in zinc fingers 5-7 involved in polyadenosine RNA binding. However these structures were not solved in the presence of a stretch of 8 adenosine, so it was not possible to precisely establish how these key residues are bound to Nab2 ZnF or to define how the Nab2 zinc fingers are able to distinguish adenosine from other nucleotides. Recent structural data from the Stewart laboratory revealed the crystal structure of Nab2 bound to polyadenosine RNA (285). Consistent with the solution structure of Nab2, the crystal structure of Nab2 shows that the positively charged residues and aromatic residues mediate polyadenosine RNA binding. Although eight adenosines are required to bridge ZnF5-7, the crystal structure indicates that only five of these adenosine bases are bound by the zinc fingers. These results indicate that Nab2 can recognize A-rich motifs in the transcript, whereby key adenosines can be separated by spacer nucleotides in which the base is not crucial. Taken together, these results have important implications for how transcript specificity is achieved by poly(A) RNA binding proteins.

Although the polyadenosine RNA binding protein, Nab2, should bind all mRNA transcripts containing polyadenosine tails (176), results presented in Chapter 3 show that Nab2 only affects splicing of a subset of intron-containing transcripts. This finding is not

unprecedented as some mutants of genes that encode the core spliceosome also show differential effects on specific transcripts (218). Neither cis-regulatory elements within introns nor the catalytic activity of the core spliceosome provides a simple explanation for why specific transcripts accumulate introns (218). Instead, the complete mRNP complex that associates with a given transcript likely influences the pre-mRNA splicing fate. We propose that Nab2 associates with the splicing mRNP complex to regulate a subset of transcripts by contacting the RNA and associating with specific splicing factors.

Consistent with Nab2 interactions beyond the poly(A) tail, transcriptome-wide analysis of RNP composition (130) and ChIP studies (93) indicate that Nab2 is bound throughout the body of the RNA in addition to the 3'end of the transcript. Nab2 has the potential to bind to other sequences within RNAs perhaps via the zinc fingers or via the RGG domain. Furthermore, the recent crystal structure of the Nab2 ZnF5-7 shows that Nab2 recognizes specific adenosine residues within a sequence, but those adenosines may be interspersed with other nucleotides (285). These data suggest a model where Nab2 could bind regions other than the poly(A) tail, such as intronic sequences, and in turn regulate RNA splicing of a subset of transcripts. To test this possibility, a PAR-CLIP experimental approach could identify potential Nab2 binding sites in mRNA transcripts. Alternatively, the transcript specificity effects observed in *nab2* mutant cells could result from the loss of Nab2 interaction with other spliceosomal components that confer specificity. While we cannot currently rule out either model, our data suggest that the association between Nab2 and a subset of splicing factors may contribute to transcript

specificity. This model is supported by the genetic interaction observed between *NAB2* and genes encoding splicing factors in Chapter 3 and by the mass spectrometry data presented in Chapter 4. Importantly, these studies suggest a previously unappreciated role for Nab2 in the regulation of intron-containing pre-mRNA transcripts.

While we found that a subset of intron-containing pre-mRNA transcripts are prone to Nab2-dependent regulation, there are likely other classes of transcripts that Nab2 contacts. One class of transcripts that has the potential to be regulated by Nab2 are meiotic transcripts. Meiotic transcripts expressed during mitosis are targeted for decay through a splicing and polyadenylation dependent mechanism, best characterized in fission yeast (136-139). We reasoned that the role of Nab2 in splicing, polyadenylation, and decay, positions Nab2 to target unspliced and hyperadenylated meiotic transcripts for the exosome in budding yeast. In addition, preliminary evidence indicates that *nab2* mutants result in poor sporulatation, suggesting a potential defect in meiosis (Soucek and Corbett, unpublished data). In order for Nab2 to assist in meiotic gene expression, Nab2 would likely collaborate with the RNA binding protein, Mmi1. However, an *S. cerevisiae* Mmi1 had never been identified prior to this dissertation. Therefore, we identified and characterized the putative Mmi1 in the budding yeast model system and show Mmi1 is required for efficient meiosis and decay of meiotic-specific transcripts (Chapter 5). To begin to explore the relationship between Nab2 and Mmi1, further studies must be performed. RNA-seq analysis would provide information about all the meiotic transcripts affected in Δ*mmi1* mutants and allow us to compare data already

generated for *nab2* mutants to an *mmi1* mutant. If there is overlap in common meiotic targets, this would provide strong evidence that Nab2 and Mmi1 work together to regulate meiotic gene expression. Additional studies could be performed to confirm a genetic or physical interaction between Nab2 and Mmi1. If Nab2 and Mmi1 associate with each other to regulate meiotic transcripts, further studies would uncover new mechanisms of meiotic gene relation in budding yeast. In addition, these studies would provide further evidence that Nab2 associates with a myriad of RNA binding proteins to regulate gene expression within key biological processes.

Coupling splicing, 3'-end processing, export, and RNA surveillance

To understand in detail how mRNPs are built, it is important to decipher the complicated web of interactions down to individual molecular interactions. In Chapter 2, we demonstrate that mutations in *nab2* impair polyadenosine RNA binding. Strikingly, Nab2 reduced affinity for polyadenosine RNA *in vitro* does not directly correlate with poly(A) tail length *in vivo*. This is the first evidence that Nab2 control of poly(A) tail length may be attributed to its association with other proteins rather than affinity for the polyadenosine RNA. More specifically, these data suggest that Nab2 is intimately involved in the generation of export-competent mRNPs by associating with the mRNP assembly export factors, Yra1 and Dbp5. Our analysis of key residues within Nab2 zinc fingers reveal that *nab2* mutant cells which show the strongest genetic interaction with alleles of *YRA1* and *DBP5* have extended poly(A) tails (229). This finding suggests a role

for Nab2 in the generation of export-competent mRNPs and raises several important questions: Does the zinc finger domain of Nab2 participate directly in Yra1 interactions and recruiting the RNA export receptor, Mex67? Do the inter-domain interactions between ZnF domains in Nab2 provide a mechanism for packaging polyadenosine RNA around an RNP complex consisting of multiple Nab2 molecules? If the last three zinc fingers of Nab2 are sufficient for polyadenosine binding and mRNP assembly, then what is the role of other protein domains in Nab2?

To determine if Nab2 zinc fingers mediate an interaction with Yra1, protein binding experiments using recombinantly expressed Nab2 and Yra1 should be performed to detect an interaction between Nab2 and Yra1. Indeed, previous studies have reported an interaction between Nab2 and Mex67, in which the presence of Yra1 enhances the interaction (67). Studies to examine whether Nab2 ZnF mutants that show severely impaired binding to RNA can still maintain interactions with these export factors can provide insight into key protein-protein interactions that may exist in an mRNP.

To begin to understand the importance of inter-domain interactions of Nab2 zinc fingers, engineering mutants that disrupt structural coherence will be crucial. Studies presented in Chapter 2 show that *nab2-C437S* disrupts zinc finger structure. However, *nab2-C437S* also exhibits poor polyadenosine RNA binding, extended poly(A) tails, and genetic interactions with alleles of *YRA1* and *DBP5*. Therefore, uncoupling the rigid structure of Nab2 ZnF5-7 from its role in RNP packaging may prove to be difficult. However, an examination of the ZnF5-7 structure reveals a number of ZnF inter-domain

residues that could serve as candidates for structure-function analysis, including the conserved I454 amino acid, which makes multiple contacts between all three zinc fingers. One prediction for mutating the inter-domain residues is that Nab2 could still bind polyadenosine RNA with high affinity, but these mutants would exhibit extended poly(A) tails and genetic interactions with alleles of *YRA1* and *DBP5*. This would provide evidence that Nab2 binding to polyadenosine RNA can be uncoupled from its role in assembly of mRNPs.

To understand how Nab2 generates export-competent mRNPs, the last three zinc fingers must be considered in the context of the whole protein. The last three zinc fingers are necessary and sufficient for high affinity polyadenosine RNA binding (146); yet, Nab2 lacking the last three zinc fingers displays weak binding to polyadenosine RNA (156). In addition, Nab2 orthologues, ZC3H14 and dNab2, contain five zinc fingers, indicating that there may be a function for additional zinc fingers that are not required for high affinity polyadenosine RNA binding. These additional zinc fingers may mediate protein-protein or protein-RNA interactions. Alternatively, other Nab2 domains, including the RGG domain and QQQP-rich domain, may mediate weak RNA binding or RNP packaging. The arginine-glycine-glycine (RGG) repeat is a motif characterized as a nucleic acid interaction motif in other proteins (286). Interestingly, recent data implicates glutamine (Q)-rich domains in self-assembly (287, 288). One prediction is that Nab2 uses its QQQP-rich domain to self-assemble on stretches of polyadenosine RNA, providing a mechanism for packaging polyadenosine RNA around a multimetric core of

Nab2 molecules. One experimental approach would be to test mutants of *nab2* lacking the first four zinc fingers, an RGG domain, or a QQQP-rich domain for bulk poly(A) tail length defects and genetic interactions with alleles of *YRA1* and *DBP5*. Preliminary data indicates that *nab2* mutants lacking an RGG or QQQP domain have extended poly(A) tails that are even more severe than in *nab2* C-terminal mutant cells (Soucek and Corbett, unpublished data). These studies could provide further insight into the mechanisms that Nab2 uses package export-competent mRNPs.

We also identified a role for Nab2 and Mud2 in the splicing and 3'-end processing, providing further evidence for coupling mRNA processing events through RNA binding proteins. A genetic interaction was identified between mutant alleles of *nab2* and the splicing factor encoding *MUD2* with *in vivo* consequences of altered pre-mRNA splicing and poly(A) tail length control. These data indicate that Nab2 functions earlier in mRNA biogenesis than previously described and that the splicing factor, Mud2, plays an additional role in the control of poly(A) tail length. Additional experiments will be needed to investigate if Mud2 contacts the 3'-end processing machinery to influence poly(A) tail length. One experimental approach would be to test a deletion of *MUD2* with alleles of the cleavage machinery, *RNA15*, and the poly(A) polymerase polyadenylation factor, *PAP1*. Previous studies in human cells revealed a role for the putative Mud2 orthologue, U2AF65, in stimulating poly(A) polymerase *in vitro* (101). Therefore, the prediction from these human studies is that the link between Mud2 and Pap1 is conserved in budding yeast. Taken together, these data support a role for RNA binding proteins in

multiple mRNA processing events.

Based on results presented in Chapter 3, we suggest that Nab2 is present during the crucial mRNP remodeling event from prespliceosome to catalytically active spliceosome via the commitment complex. Although Mud2 enhances the association of Msl5 with the branchpoint (23, 124, 125, 209), Mud2 is not required for branchpoint recognition and the absence of Mud2 bypasses the requirement for the otherwise essential spliceosomal ATPase, Sub2 (26). These data suggest that Mud2 facilitates proper assembly of mRNP complexes and that Sub2 is well poised to remodel RNA binding proteins during prespliceosome formation. Importantly, Nab2 also interacts with Sub2 (176, 289). One prediction from these results is that when Mud2 is absent and Nab2 interaction with the RNA is impaired, mRNP remodeling is severely impaired, resulting in misprocessing of mRNA. Further experiments could test this prediction by testing for genetic interactions between alleles of *NAB2* and *SUB2*. A genetic interaction between *NAB2* and *SUB2* may suggest that the presence of Nab2 is crucial for proper mRNP remodeling through Sub2. Proper mRNP remodeling is highlighted by the recruitment of Yra1 by Sub2 during RNA processing and by removal of Yra1 prior to mRNA export via Mex67 (74, 118). Given the rapid remodeling of Sub2 and Yra1 during different steps of RNA processing and mRNP assembly, Nab2 my serve as the continuous link between assembly of splicing-competent mRNPs to export-competent mRNPs. Furthermore, Nab2 could be present from the onset of transcription (93) to translation of mRNA (Pak and Corbett, unpublished data) to monitor mRNP assembly. Taken together, these findings are

consistent with a role for Nab2 in mRNP assembly during splicing as well as during 3'-end processing and export.

Additional genetic interactions between *NAB2* and factors encoding splicing machinery involved in retention point to a role for Nab2 in bridging mRNA splicing and downstream mRNA biogenesis steps such as export. This model is supported by the previous observation that the poly(A) RNA export-deficient *nab2* mutant allele*, nab2-*Δ*N*, is suppressed by mutant alleles of the retention and export complex proteins, Pml39 and Mlp1 (68, 127). Taken together, these data suggest that relaxing the requirements for quality of export material under conditions where RNA export is decreased, such as in nab2-Δ*N* mutant cells, allows for an increased flow of RNA into cytoplasm even when some of the exported RNAs are less than perfect and might normally be retained in the nucleus. These observations would suggest that, at least under some conditions, release of aberrant mRNAs to the cytoplasm is less detrimental than overly stringent quality control and retention of mRNAs within the nucleus. One possibility is that the cytoplasmic decay machinery may target these aberrant mRNA transcripts. This hypothesis could be tested by investigating whether components of the cytoplasmic decay machinery interact with Nab2. Indeed, preliminary studies from our laboratory show that mutation in *NAB2* genetically interacts with alleles of cytoplasmic nonsense-mediated decay (NMD) machinery (Green and Corbett, unpublished data). Alternatively, leakage of pre-mRNA transcripts could be assessed using a reporter that only expresses a protein when it retains an intron in the mRNA reporter transcript. Our study extends these

previous observations by providing a cohesive, integrated role for Nab2 in splicing and export to ensure correct mRNA processing.

Finally, we observed a striking interaction between Nab2 and the nuclear exosome component, Rrp6. The data presented in Chapter 3 and 4 suggest a model where Nab2 coordinates with Rrp6 to regulate the expression of aberrant mRNAs. One interesting question from these studies is whether Nab2 recruits or impedes nuclear decay. Recent *in vitro* studies have proposed a role for Nab2 in the nuclear surveillance pathway by promoting removal of pre-mRNAs via Rrp6 (81). This model was built based on the finding that the absence of Rrp6 allows or enhances Nab2 binding to pre-mRNA and that Nab2 can be competed off mRNPs when challenged with extracts containing Rrp6 (81). Studies from Chapter 3 are consistent with a model in budding yeast where the catalytic activity of Rrp6 is necessary for eliminating pre-mRNAs with extended poly(A) tails. Interestingly, Chapter 4 provides evidence for fission yeast Nab2 as a positive regulator of pre-mRNA expression, whereby Nab2 prevents decay of an aberrant *rpl30-2* transcript. There are two possibilities for the discrepancy: 1) the evolutionary difference between *S. cerevisiae* and *S. pombe* results in different uses of nuclear Pabs; or 2) *S. pombe* Nab2 regulates other pre-mRNA transcripts differently from *rpl30-2*. A complete investigation of how *S. pombe* Nab2 influences other pre-mRNA transcripts will be required to distinguish between these two possibilities. A planned RNA-seq identifying transcripts affected in Δ*nab2* will provide insight into the amount of overlap between the two nuclear Pabs in *S. pombe*. Ultimately, Nab2 could recruit Rrp6 to either trim

polyadenosine tails and ensure a proper mature transcript or target the transcript for decay. Both courses of action would result in a population of transcripts with wildtype length of poly(A) tails, thereby eliminating a hyperadenylation phenotype. An underlying question is our lack of understanding of how the exosome, here in the form of Rrp6, plays a dual role in precise processing of some RNA targets with complete destruction of other targets (76).

The implications of coupling RNA processing events: control of poly(A) tail length

Steps in mRNA processing upstream of 3'-end processing, such as transcription or splicing, and events downstream, such as nuclear export, impact the quality of the 3′-end of an mRNA transcript (Chapter 2 and 3). In addition, changes in mRNA poly(A) tail length likely act as a signal to the RNA quality control machinery, where Nab2 and other RNA binding proteins can assist in the recognition of a faulty transcript. RNA binding proteins can help communicate this information to nuclear pore components to block the export of the transcript or trigger ribonucleases to degrade the transcript. While one of the consequences of coupling RNA processing events includes altered poly(A) tail length, the precise molecular mechanisms underlying poly(A) tail length control must be studied in the future. One limitation of the studies presented here is that it is unclear whether RNA binding proteins, including Nab2, Pab2, and Mud2, play direct roles in splicing or 3'-end processing. To understand how poly(A) tail length is controlled, one experimental

approach is to uncouple poly(A) tail length control from post-transcriptional gene regulation.

To separate events of 3'-end processing from other post-transcriptional events, a hammerhead ribozyme and a DNA-encoded poly(A) sequence can be used to generate 3' ends with poly(A) tails without using the cellular machinery required for mRNA 3'-end processing. The hammerhead ribozyme catalyses the site-specific hydrolysis of a phosphodiester, leaving the encoded poly(A) tail at the end of the transcript, but terminating with a 2', 3' cyclic phosphate instead of a 3' OH (43). By pairing an intron-containing transcript with a hammerhead ribozyme, we could distinguish whether Nab2 requires a poly(A) tail to mediate pre-mRNA splicing. In addition, we could uncouple the loading of nascent 3'-end processing machinery from mRNA export, thereby gaining insight into whether Nab2 controls poly(A) tail length through the canonical 3'-end processing machinery. Our results also implicate the splicing factor, Mud2, in the control of poly(A) tail length. Similar experiments could be performed for Mud2 to determine if shorter poly(A) tails in Δ*mud2* mutants is linked to the function of Mud2 in splicing.

How could Nab2 restrict the poly(A) tail length to an average length of 60-80 adenosines in *S. cerevisiae*? An important challenge in the future will be to determine if Nab2 directly modulates the poly(A) tail by inhibiting poly(A) polymerase, stimulating ribonucleases, or both. Genetic experiments indicate that Nab2 interacts with the 3′-end processing machinery, but physical interactions with these 3′-end processing factors must be tested to determine which cleavage and polyadenylation components directly contact

Nab2. Upon identifying these physical interactors, biochemical and structural analysis of Nab2 interactions with polyadenylation factors could help to determine how and where Nab2 interfaces with the polyadenylation machinery. Unbiased identification of all the proteins that physically interact with Nab2 by co-precipitation and mass spectroscopy is also required. Such an approach needs to dissect protein-protein interactions from those mediated by RNA. Knowledge of these Nab2 physical interactors would shed light on how Nab2 influences the poly(A) tail length of transcripts. At present, most co-precipitation of 3′-end processing components from mammalian cell lysates and identification of the protein interactors by mass spectrometry have not identified ZC3H14. Only one proteomic study identified ZC3H14 in a complex with the splicing and 3'-end processing factor, Srm160 (290). However, Pabs such as ZC3H14 may only interact transiently with the 3′-end processing machinery, making it difficult to identify the ZC3H14 interactors without further optimization of binding conditions. Future biochemical experiments using recombinant Nab2 in yeast lysates from polyadenylation factor mutant strains or *in vitro* reconstituted assays with purified polyadenylation components would provide insight into the role of Nab2 in limiting or trimming poly(A) tails. Importantly, analysis of the function of Nab2 in polyadenylation control must be performed in the presence of additional RNA binding proteins in order to decipher the complete mechanism of poly(A) tail control and the dynamic interplay between different RNA binding proteins.

Future directions: implications for ZC3H14 human disease

We have exploited the budding yeast model system as a discovery tool to pursue the mechanisms by which zinc finger Pabs regulate gene expression. The budding yeast model provides a glimpse into the molecular mechanisms that ZC3H14 could use to regulate RNA transcripts. Importantly, the work presented here lays the groundwork for future studies in ZC3H14 and will be critical to understanding the molecular mechanisms underlying brain dysfunction in patients with intellectual disability.

Our current understanding of the nuclear roles of Nab2 is based on studies performed in *S. cerevisiae*, *D. melanogaster*, and cultured mammalian cells. Prior to this dissertation, studies in budding yeast implicated Nab2 in poly(A) tail length control and export. Studies in *D. melanogaster* show that dNab2 is important for proper poly(A) tail length of bulk poly(A) RNA and indicate that dNab2 is required for normal neuronal function in flies (161). Furthermore, depletion of ZC3H14 in a neuronal cell line leads to extended poly(A) tails (291). The analysis of dNab2 and ZC3H14 supports a role for dNab2/ZC3H14 in poly(A) tail length control, while a role for poly(A) RNA export has only been described for budding yeast.

We provide a deeper analysis of the molecular mechanisms that underlie gene expression by exploring alternative roles for Nab2 in mRNA biogenesis. By characterizing a role of Nab2 in splicing and decay, we offer insight into mechanisms that could not only influence poly(A) tail length, but also the processing of a variety of

transcripts. This work provides a framework to test if dNab2/ZC3H14 affects splicing of intron-containing transcripts. We also introduce novel links between Nab2 and poly(A) RNA binding proteins that have the potential to influence mRNA processing and poly(A) tail length. While *S. pombe* Δ*nab2* mutants do not show defects in poly(A) tail length, Δ*nab2* Δ*pab2* mutant cells result in bulk hyperadenylated tails (85). Importantly, studies in flies show that dNab2 (Nab2) functions antagonistically to Pabp2 (Pab2) to limit the length of poly(A) tails (161). These results suggest that Nab2/dNab2 interacts with other Pabs to influence poly(A) tail length. Critically, the interaction in Pabp2 and dNab2 in flies may also depend on splicing specific transcripts as demonstrated in fission yeast for Nab2 and Pab2. Our structural studies on the Nab2 zinc fingers provided the first evidence that reduced affinity for polyadenosine RNA does not necessarily correlate with extended poly(A) tails (229). This result was significant in understanding how Nab2 interfaces with RNA and other RNA binding proteins to influence mRNA fate, particularly at the post-transcriptional level. It is essential to understand if dNab2/ZC3H14 also plays a role in splicing, assembling mRNPs, and surveillance to identify the reason for poly(A) tail length defects in Nab2 mutants. To begin to understand the role of dNab2/ZC3H14 in RNA processing, we can begin to probe for physical interactions between dNab2/ZC3H14 and machinery critical for the generation of mature mRNA through mass spectrometry. The range of RNA binding proteins and the modularity of RNA binding elements in transcripts permits mRNA biogenesis to be fine-tuned in a tissue specific manner.

Understanding the transcripts or classes of transcripts regulated by ZC3H14 is a major source of study. Presumably, patients with intellectual disability exhibit brain dysfunction because neuronal transcripts are misregulated by ZC3H14. Using the budding yeast model system, we showed that a subset of transcripts are regulated by Nab2 in Chapter 2. Critically, we find that intron-containing transcripts are affected in *nab2* mutant cells, proving the first evidence that Nab2 can regulate a specific class of transcripts. These results have important implications in higher eukaryotes and offers insight into how a ubiquitously expressed protein like ZC3H14 can specifically affect neuronal transcripts. RNA processing in neurons is highly regulated temporally and spatially (292) and one hypothesis is that neurons are extremely reliant on the function of ZC3H14. Mediating splicing and polyadenylation through ZC3H14 provides multiple layers of gene control that have the potential to impact a variety of different transcripts. An RNA-immunoprecipitation/RNA-sequencing experiment will be required to identify transcripts that physically associate with ZC3H14.

To determine if splicing is affected in higher eukaryotes, qRT-PCR could be performed to detect unspliced intron-containing transcripts. Indeed, preliminary evidence from our lab indicates that upon depletion of ZC3H14 in mammalian cells, splicing is misregulated (Leung and Corbett, unpublished data). Alternatively, RNA-seq can be utilized to obtain a global view of intron-containing transcripts affected in flies and human cells. An interesting experiment to extend these splicing studies to poly(A) tail length is to perform polyadenylation state microarray (PASTA). This technique involves

purification of mRNA based on poly(A) tail length using thermal elution from poly(U) sepharose (293). The fractions collected at different temperatures can be analyzed using microarray or RNA-seq (293). It would be interesting to see which mRNAs result in longer tails upon Nab2/dNab2/ZC3H14 depletion and whether those transcripts with altered tail length are also improperly spliced. This experiment could give us significant insight into how splicing and 3'-end processing are coordinately regulated for a single mRNA transcript. Alternatively, newly developed methods to globally sequence poly(A) tail length, TAIL-seq (294) or PAL-seq (295), can provide information about the status of 3'-ends regulated by Nab2 and its orthologues.

Investigating the molecular mechanisms of meiosis is also important for understanding gene control in higher eukaryotes. In the human body, the gonads are key areas that undergo meiosis to produce gametes. A number of proteins regulate meiosis and one potential RNA binding protein candidate for regulating meiosis is ZC3H14. This hypothesis is supported by the fact that ZC3H14 is highly expressed in both the brain and testes (160). While there is clear rationale to studying ZC3H14 in the context of neurons, there may also be a function for ZC3H14 in the gonad that has not yet been explored.

By deciphering the details of RNA processing and mRNP assembly in higher eukaryotes, we will gain novel insights into how RNA binding proteins like the ubiquitously expressed ZC3H14 give rise to neuronal-specific defects that underlie intellectual disability.

Final conclusions

These studies highlight the intricately connected web of RNA processing events in the nucleus. Each step of RNA maturation is controlled by a different set of RNA binding proteins; however, there is extensive contact between these RNA binding proteins at each stage of RNA processing. This coupled nature of mRNA biogenesis ensures that mRNA is properly processed, whereby each step is surveyed for correct formation of mRNA. Interestingly, a new model has emerged implicating the collection of RNA binding proteins bound to an mRNA transcript as a way to survey correct RNA processing. The mRNP thus serves as an important regulator of gene expression. Our studies have identified Nab2 as an important component of the mRNP, where Nab2 is critical for integrating the function of multiple mRNA processing events to ensure properly processed mRNA.

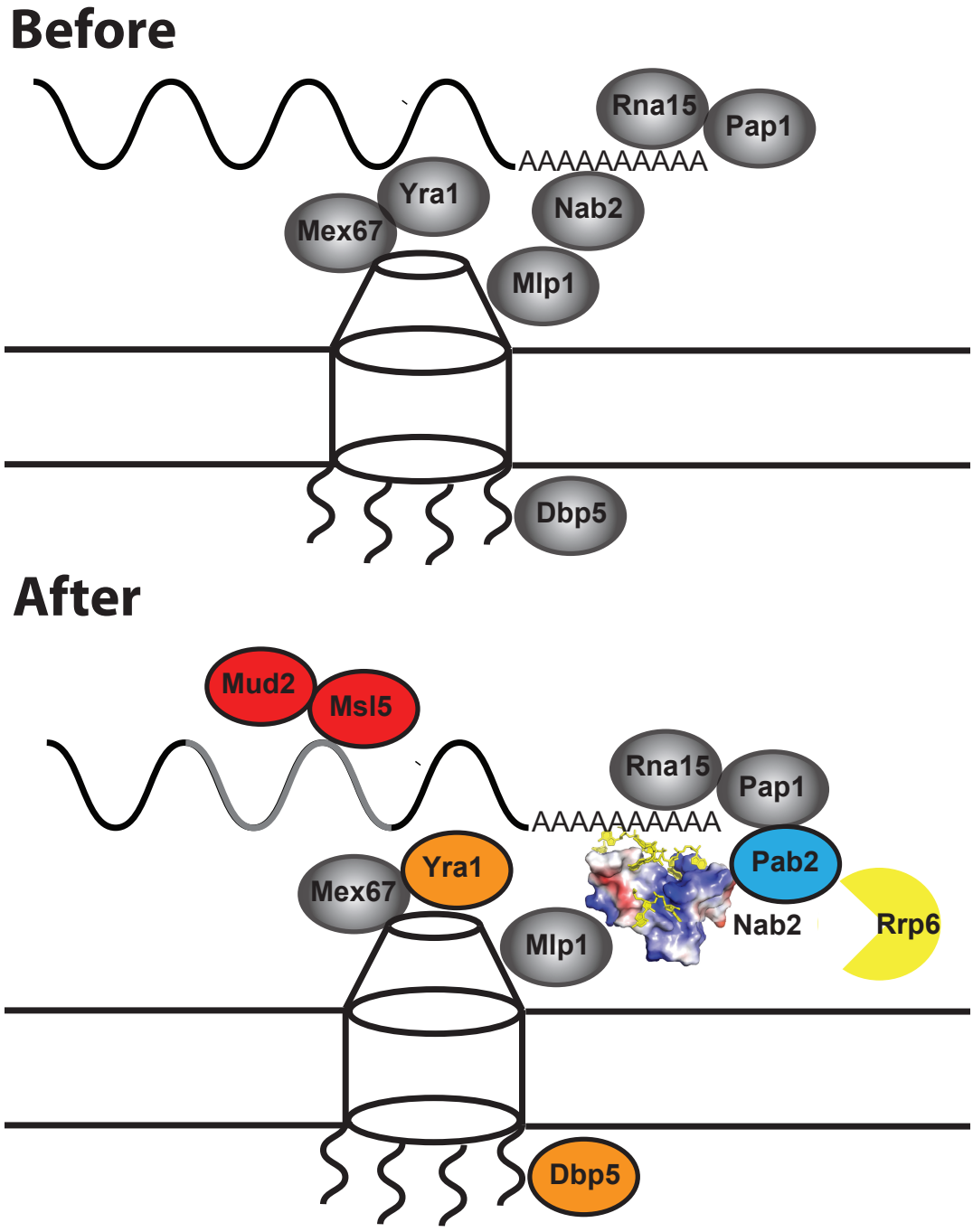
Before
Rna15
Pap1
AAAAAAAAAA
Yra1
Nab2
Mex67
Mlp1
Dbp5
After
Mud2
Msl5
Rna15
Pap1
AAAAAAAAAA
Pab2
Yra1
Mex67
Nab2
Rrp6
Mlp1
Dbp5

Figure 6.1: A model for export of mRNP complexes facilitated by Nab2. Previous studies showed that Nab2 binds polyadenosine RNA and genetically interacts with genes encoding the 3'-end processing components, *RNA15* and *PAP1* along with the export factors, *MEX67*, *YRA1*, *MLP1*, and *DBP5.* Prior to this dissertation, there were three outstanding questions: 1) how does Nab2 specifically contact polyadenosine RNA; 2) what RNA processing are mediated by Nab2; and 3) what are the consequences of altered pre-mRNA processing? During the course of this dissertation I determined that Nab2 binds to polyadenosine RNA with high affinity and associates with the spliceosome, export machinery, and RNA decay factors. I determined the solution structure of Nab2 and identified key residues critical for polyadenosine RNA binding. I found that Nab associates with the mRNA export factors, Yra1 and Dbp5. In addition, I determined that Nab2 associates with spliceosome factors to regulate pre-mRNA processing. Finally, I provided evidence that Nab2 and Pab2 both interact with the poly(A) tail to regulate pre-mRNA splicing and target aberrant transcripts for the nuclear exosome.

REFERENCES

1. **Moore MJ, Proudfoot NJ.** 2009. Pre-mRNA processing reaches back to transcription and ahead to translation. Cell **136:**688-700.
2. **Proudfoot NJ, Furger A, Dye MJ.** 2002. Integrating mRNA processing with transcription. Cell **108:**501-512.
3. **Schmidt K, Butler JS.** 2013. Nuclear RNA surveillance: role of TRAMP in controlling exosome specificity. Wiley Interdisciplinary Reviews: RNA **4:**217-231.
4. **Doma MK, Parker R.** 2007. RNA quality control in eukaryotes. Cell **131:**660-668.
5. **Lebreton A, Seraphin B.** 2008. Exosome-mediated quality control: substrate recruitment and molecular activity. Biochimicaet Biophysica Acta **1779:**558-565.
6. **Rodriguez-Navarro S, Hurt E.** 2011. Linking gene regulation to mRNA production and export. Current Opinion in Cell Biology **23:**302-309.
7. **Stewart M.** 2007. Ratcheting mRNA out of the nucleus. Molecular Cell **25:**327-330.
8. **Kelly SM, Corbett AH.** 2009. Messenger RNA export from the nucleus: a series of molecular wardrobe changes. Traffic **10:**1199-1208.
9. **Gu M, Lima CD.** 2005. Processing the message: structural insights into capping and decapping mRNA. Current Opinion in Structural Biology **15:**99-106.
10. **Wen Y, Shatkin AJ.** 2000. Cap methyltransferase selective binding and methylation of GpppG-RNA are stimulated by importin-alpha. Genes & Development **14:**2944-2949.
11. **Decker CJ, Parker R.** 1993. A turnover pathway for both stable and unstable mRNAs in yeast: evidence for a requirement for deadenylation. Genes & Development **7:**1632-1643.
12. **Couttet P, Fromont-Racine M, Steel D, Pictet R, Grange T.** 1997. Messenger RNA deadenylylation precedes decapping in mammalian cells. Proceedings of the National Academy of Sciences of the United States of America **94:**5628-5633.
13. **Izaurralde E, Lewis J, McGuigan C, Jankowska M, Darzynkiewicz E, Mattaj IW.** 1994. A nuclear cap binding protein complex involved in pre-mRNA splicing. Cell **78:**657-668.
14. **Lewis JD, Gorlich D, Mattaj IW.** 1996. A yeast cap binding protein complex (yCBC) acts at an early step in pre-mRNA splicing. Nucleic Acids Research **24:**3332-3336.
15. **Flaherty SM, Fortes P, Izaurralde E, Mattaj IW, Gilmartin GM.** 1997. Participation of the nuclear cap binding complex in pre-mRNA 3' processing. Proceedings of the National Academy of Sciences of the United States of America **94:**11893-11898.

16. **Fortes P, Inada T, Preiss T, Hentze MW, Mattaj IW, Sachs AB.** 2000. The yeast nuclear cap binding complex can interact with translation factor eIF4G and mediate translation initiation. Molecular Cell **6:**191-196.
17. **Staley JP, Guthrie C.** 1998. Mechanical devices of the spliceosome: motors, clocks, springs, and things. Cell **92:**315-326.
18. **Wahl MC, Will CL, Luhrmann R.** 2009. The spliceosome: design principles of a dynamic RNP machine. Cell **136:**701-718.
19. **Will CL, Luhrmann R.** 2011. Spliceosome structure and function. Cold Spring Harbor Perspectives in Biology **3:** a003707
20. **Rappsilber J, Ryder U, Lamond AI, Mann M.** 2002. Large-scale proteomic analysis of the human spliceosome. Genome Research **12:**1231-1245.
21. **Zhou Z, Licklider LJ, Gygi SP, Reed R.** 2002. Comprehensive proteomic analysis of the human spliceosome. Nature **419:**182-185.
22. **Rosbash M, Seraphin B.** 1991. Who's on first? The U1 snRNP-5' splice site interaction and splicing. Trends in Biochemical Science **16:**187-190.
23. **Abovich N, Rosbash M.** 1997. Cross-intron bridging interactions in the yeast commitment complex are conserved in mammals. Cell **89:**403-412.
24. **Berglund JA, Abovich N, Rosbash M.** 1998. A cooperative interaction between U2AF65 and mBBP/SF1 facilitates branchpoint region recognition. Genes & Development **12:**858-867.
25. **Berglund JA, Chua K, Abovich N, Reed R, Rosbash M.** 1997. The splicing factor BBP interacts specifically with the pre-mRNA branchpoint sequence UACUAAC. Cell **89:**781-787.
26. **Kistler AL, Guthrie C.** 2001. Deletion of MUD2, the yeast homolog of U2AF65, can bypass the requirement for sub2, an essential spliceosomal ATPase. Genes & Development **15:**42-49.
27. **Chen JY, Stands L, Staley JP, Jackups RR, Jr., Latus LJ, Chang TH.** 2001. Specific alterations of U1-C protein or U1 small nuclear RNA can eliminate the requirement of Prp28p, an essential DEAD box splicing factor. Molecular Cell **7:**227-232.
28. **Staley JP, Guthrie C.** 1999. An RNA switch at the 5' splice site requires ATP and the DEAD box protein Prp28p. Molecular Cell **3:**55-64.
29. **Ares M, Jr., Weiser B.** 1995. Rearrangement of snRNA structure during assembly and function of the spliceosome. Progress in Nucleic Acid Research and Molecular Biology **50:**131-159.
30. **Raghunathan PL, Guthrie C.** 1998. RNA unwinding in U4/U6 snRNPs requires ATP hydrolysis and the DEIH-box splicing factor Brr2. Current biology : CB **8:**847-855.
31. **Kim SH, Lin RJ.** 1996. Spliceosome activation by PRP2 ATPase prior to the first transesterification reaction of pre-mRNA splicing. Molecular and Cellular Biology **16:**6810-6819.

32. **Schwer B, Guthrie C.** 1992. A conformational rearrangement in the spliceosome is dependent on PRP16 and ATP hydrolysis. EMBO J **11:**5033-5039.
33. **Company M, Arenas J, Abelson J.** 1991. Requirement of the RNA helicase-like protein PRP22 for release of messenger RNA from spliceosomes. Nature **349:**487-493.
34. **Martin A, Schneider S, Schwer B.** 2002. Prp43 is an essential RNA-dependent ATPase required for release of lariat-intron from the spliceosome. Journal of Biological Chemistry **277:**17743-17750.
35. **Arenas JE, Abelson JN.** 1997. Prp43: An RNA helicase-like factor involved in spliceosome disassembly. Proceedings of the National Academy of Sciences of the United States of America **94:**11798-11802.
36. **Small EC, Leggett SR, Winans AA, Staley JP.** 2006. The EF-G-like GTPase Snu114p regulates spliceosome dynamics mediated by Brr2p, a DExD/H box ATPase. Molecular Cell **23:**389-399.
37. **Black DL.** 2003. Mechanisms of alternative pre-messenger RNA splicing. Annual Review of Biochemistry **72:**291-336.
38. **Nilsen TW, Graveley BR.** 2010. Expansion of the eukaryotic proteome by alternative splicing. Nature **463:**457-463.
39. **Goldstrohm AC, Greenleaf AL, Garcia-Blanco MA.** 2001. Co-transcriptional splicing of pre-messenger RNAs: considerations for the mechanism of alternative splicing. Gene **277:**31-47.
40. **Clark T, Sugnet C, Ares M.** 2002. Genomewide analysis of mRNA processing in yeast using splicing-specific microarrays. Science **296**: 907-910.
41. **Tian B, Graber JH.** 2012. Signals for pre-mRNA cleavage and polyadenylation. Wiley interdisciplinary reviews: RNA **3:**385-396.
42. **Ford LP, Bagga PS, Wilusz J.** 1997. The poly(A) tail inhibits the assembly of a 3'-to-5' exonuclease in an in vitro RNA stability system. Molecular and Cellular Biology **17:**398-406.
43. **Dower K, Kuperwasser N, Merrikh H, Rosbash M.** 2004. A synthetic A tail rescues yeast nuclear accumulation of a ribozyme-terminated transcript. RNA **10:**1888-1899.
44. **Preiss T, Muckenthaler M, Hentze MW.** 1998. Poly(A)-tail-promoted translation in yeast: implications for translational control. RNA **4:**1321-1331.
45. **Tian B, Graber JH.** 2011. Signals for pre-mRNA cleavage and polyadenylation. Wiley interdisciplinary reviews: RNA **3:**385-96.
46. **Gordon JM, Shikov S, Kuehner JN, Liriano M, Lee E, Stafford W, Poulsen MB, Harrison C, Moore C, Bohm A.** 2011. Reconstitution of CF IA from Overexpressed Subunits Reveals Stoichiometry and Provides Insights into Molecular Topology. Biochemistry **50:**10203-10214.
47. **Moreno-Morcillo M, Minvielle-Sebastia L, Fribourg S, Mackereth CD.** 2011. Locked tether formation by cooperative folding of Rna14p monkeytail and Rna15p hinge domains in the yeast CF IA complex. Structure **19:**534-545.

48. **Leeper TC, Qu X, Lu C, Moore C, Varani G.** 2010. Novel protein-protein contacts facilitate mRNA 3'-processing signal recognition by Rna15 and Hrp1. Journal of Molecular Biology **401:**334-349.
49. **Kessler MM, Henry MF, Shen E, Zhao J, Gross S, Silver PA, Moore CL.** 1997. Hrp1, a sequence-specific RNA-binding protein that shuttles between the nucleus and the cytoplasm, is required for mRNA 3'-end formation in yeast. Genes & Development **11:**2545-2556.
50. **Eckmann CR, Rammelt C, Wahle E.** 2011. Control of poly(A) tail length. Wiley interdisciplinary reviews. RNA **2:**348-361.
51. **Wahle E.** 1991. A novel poly(A)-binding protein acts as a specificity factor in the second phase of messenger RNA polyadenylation. Cell **66:**759-768.
52. **Wahle E, Lustig A, Jeno P, Maurer P.** 1993. Mammalian poly(A)-binding protein II. Physical properties and binding to polynucleotides. Journal of Biological Chemistry **268:**2937-2945.
53. **Bienroth S, Keller W, Wahle E.** 1993. Assembly of a processive messenger RNA polyadenylation complex. EMBO J **12:**585-594.
54. **Sagawa F, Ibrahim H, Morrison AL, Wilusz CJ, Wilusz J.** 2011. Nucleophosmin deposition during mRNA 3' end processing influences poly(A) tail length. EMBO J **30:**3994-4005.
55. **Preker PJ, Lingner J, Minvielle-Sebastia L, Keller W.** 1995. The FIP1 gene encodes a component of a yeast pre-mRNA polyadenylation factor that directly interacts with poly(A) polymerase. Cell **81:**379-389.
56. **Helmling S, Zhelkovsky A, Moore CL.** 2001. Fip1 regulates the activity of Poly(A) polymerase through multiple interactions. Molecular and Cellular Biology **21:**2026-2037.
57. **Kaufmann I, Martin G, Friedlein A, Langen H, Keller W.** 2004. Human Fip1 is a subunit of CPSF that binds to U-rich RNA elements and stimulates poly(A) polymerase. EMBO J **23:**616-626.
58. **Di Giammartino DC, Nishida K, Manley JL.** 2011. Mechanisms and consequences of alternative polyadenylation. Molecular Cell **43:**853-866.
59. **Fabian MR, Sonenberg N, Filipowicz W.** 2010. Regulation of mRNA translation and stability by microRNAs. Annual Reviews of Biochemistry **79:**351-379.
60. **Barreau C, Paillard L, Osborne HB.** 2005. AU-rich elements and associated factors: are there unifying principles? Nucleic Acids Research **33:**7138-7150.
61. **Ozsolak F, Kapranov P, Foissac S, Kim SW, Fishilevich E, Monaghan AP, John B, Milos PM.** 2010. Comprehensive polyadenylation site maps in yeast and human reveal pervasive alternative polyadenylation. Cell **143:**1018-1029.
62. **Mayer SA, Dieckmann CL.** 1991. Yeast CBP1 mRNA 3' end formation is regulated during the induction of mitochondrial function. Molecular and Cellular Biology **11:**813-821.

63. **Hoopes BC, Bowers GD, DiVisconte MJ.** 2000. The two Saccharomyces cerevisiae SUA7 (TFIIB) transcripts differ at the 3'-end and respond differently to stress. Nucleic Acids Research **28:**4435-4443.
64. **Mandart E, Parker R.** 1995. Effects of mutations in the Saccharomyces cerevisiae RNA14, RNA15, and PAP1 genes on polyadenylation in vivo. Molecular and Cellular Biology **15:**6979-6986.
65. **Zenklusen D, Vinciguerra P, Wyss JC, Stutz F.** 2002. Stable mRNP formation and export require cotranscriptional recruitment of the mRNA export factors Yra1p and Sub2p by Hpr1p. Molecular and Cellular Biology **22:**8241-8253.
66. **Strasser K, Masuda S, Mason P, Pfannstiel J, Oppizzi M, Rodriguez-Navarro S, Rondon AG, Aguilera A, Struhl K, Reed R, Hurt E.** 2002. TREX is a conserved complex coupling transcription with messenger RNA export. Nature **417:**304-308.
67. **Iglesias N, Tutucci E, Gwizdek C, Vinciguerra P, Von Dach E, Corbett AH, Dargemont C, Stutz F.** 2010. Ubiquitin-mediated mRNP dynamics and surveillance prior to budding yeast mRNA export. Genes & Devevelopment **24:**1927-1938.
68. **Grant RP, Marshall NJ, Yang JC, Fasken MB, Kelly SM, Harreman MT, Neuhaus D, Corbett AH, Stewart M.** 2008. Structure of the N-terminal Mlp1-binding domain of the Saccharomyces cerevisiae mRNA-binding protein, Nab2. Journal of Molecular Biology **376:**1048-1059.
69. **Green DM, Johnson CP, Hagan H, Corbett AH.** 2003. The C-terminal domain of myosin-like protein 1 (Mlp1p) is a docking site for heterogeneous nuclear ribonucleoproteins that are required for mRNA export. Proceedings of the National Academy of Sciences of the United States of America **100:**1010-1015.
70. **Fasken MB, Stewart M, Corbett AH.** 2008. Functional significance of the interaction between the mRNA-binding protein, Nab2, and the nuclear pore-associated protein, Mlp1, in mRNA export. Journal of Biological Chemistry **283:**27130-27143.
71. **Suntharalingam M, Alcazar-Roman AR, Wente SR.** 2004. Nuclear export of the yeast mRNA-binding protein Nab2 is linked to a direct interaction with Gfd1 and to Gle1 function. Journal of Biological Chemistry **279:**35384-35391.
72. **Zheng C, Fasken MB, Marshall NJ, Brockmann C, Rubinson ME, Wente SR, Corbett AH, Stewart M.** 2010. Structural basis for the function of the Saccharomyces cerevisiae Gfd1 protein in mRNA nuclear export. Journal of Biological Chemistry **285:**20704-20715.
73. **Tran EJ, Zhou Y, Corbett AH, Wente SR.** 2007. The DEAD-box protein Dbp5 controls mRNA export by triggering specific RNA:protein remodeling events. Molecular Cell **28:**850-859.
74. **Lund MK, Guthrie C.** 2005. The DEAD-box protein Dbp5p is required to dissociate Mex67p from exported mRNPs at the nuclear rim. Molecular Cell **20:**645-651.

75. **Fasken MB, Corbett AH.** 2005. Process or perish: quality control in mRNA biogenesis. Nature Structural and Molecular Biology **12:**482-488.
76. **Chlebowski A, Lubas M, Jensen TH, Dziembowski A.** 2013. RNA decay machines: the exosome. Biochimica et Biophysica Acta **1829:**552-560.
77. **Allmang C, Kufel J, Chanfreau G, Mitchell P, Petfalski E, Tollervey D.** 1999. Functions of the exosome in rRNA, snoRNA and snRNA synthesis. EMBO J **18:**5399-5410.
78. **Allmang C, Mitchell P, Petfalski E, Tollervey D.** 2000. Degradation of ribosomal RNA precursors by the exosome. Nucleic Acids Research **28:**1684-1691.
79. **Lykke-Andersen S, Tomecki R, Jensen TH, Dziembowski A.** 2011. The eukaryotic RNA exosome: same scaffold but variable catalytic subunits. RNA Biology **8:**61-66.
80. **Milligan L, Torchet C, Allmang C, Shipman T, Tollervey D.** 2005. A nuclear surveillance pathway for mRNAs with defective polyadenylation. Molecular and Cellular Biology **25:**9996-10004.
81. **Schmid M, Poulsen MB, Olszewski P, Pelechano V, Saguez C, Gupta I, Steinmetz LM, Moore C, Jensen TH.** 2012. Rrp6p controls mRNA poly(A) tail length and its decoration with poly(A) binding proteins. Molecular Cell **47:**267-280.
82. **Hilleren P, McCarthy T, Rosbash M, Parker R, Jensen TH.** 2001. Quality control of mRNA 3'-end processing is linked to the nuclear exosome. Nature **413:**538-542.
83. **Bousquet-Antonelli C, Presutti C, Tollervey D.** 2000. Identification of a regulated pathway for nuclear pre-mRNA turnover. Cell **102:**765-775.
84. **Lemieux C, Marguerat S, Lafontaine J, Barbezier N, Bahler J, Bachand F.** 2011. A Pre-mRNA degradation pathway that selectively targets intron-containing genes requires the nuclear poly(A)-binding protein. Molecular Cell **44:**108-119.
85. **St-Sauveur VG, Soucek S, Corbett AH, Bachand F.** 2013. Poly(A) tail-mediated gene regulation by opposing roles of Nab2 and Pab2 nuclear poly(A)-binding proteins in pre-mRNA decay. Molecular and Cellular Biology **33:**4718-31.
86. **Jensen TH, Dower K, Libri D, Rosbash M.** 2003. Early formation of mRNP: license for export or quality control? Molecular Cell **11:**1129-1138.
87. **Vinciguerra P, Stutz F.** 2004. mRNA export: an assembly line from genes to nuclear pores. Current Opinion in Cell Biology **16:**285-292.
88. **LaCava J, Houseley J, Saveanu C, Petfalski E, Thompson E, Jacquier A, Tollervey D.** 2005. RNA degradation by the exosome is promoted by a nuclear polyadenylation complex. Cell **121:**713-724.

89. **Zhang S, Welch EM, Hogan K, Brown AH, Peltz SW, Jacobson A.** 1997. Polysome-associated mRNAs are substrates for the nonsense-mediated mRNA decay pathway in Saccharomyces cerevisiae. RNA **3:**234-244.
90. **Vasudevan S, Peltz SW, Wilusz CJ.** 2002. Non-stop decay--a new mRNA surveillance pathway. BioEssays : news and reviews in molecular, cellular and developmental biology **24:**785-788.
91. **Harigaya Y, Parker R.** 2010. No-go decay: a quality control mechanism for RNA in translation. Wiley Interdisciplinary Reviews: RNA **1:**132-141.
92. **Dreyfuss G, Kim VN, Kataoka N.** 2002. Messenger-RNA-binding proteins and the messages they carry. Nature Reviews Molecular Cellular Biology **3:**195-205.
93. **Gonzalez-Aguilera C, Tous C, Babiano R, de la Cruz J, Luna R, Aguilera A.** 2011. Nab2 functions in the metabolism of RNA driven by polymerases II and III. Molecular Biology of the Cell **22:**2729-2740.
94. **Stewart M.** 2010. Nuclear export of mRNA. Trends Biochem Sci **35:**609-617.
95. **Hirose Y, Tacke R, Manley JL.** 1999. Phosphorylated RNA polymerase II stimulates pre-mRNA splicing. Genes & Development **13:**1234-1239.
96. **McCracken S, Fong N, Yankulov K, Ballantyne S, Pan G, Greenblatt J, Patterson SD, Wickens M, Bentley DL.** 1997. The C-terminal domain of RNA polymerase II couples mRNA processing to transcription. Nature **385:**357-361.
97. **Fong N, Bentley DL.** 2001. Capping, splicing, and 3' processing are independently stimulated by RNA polymerase II: different functions for different segments of the CTD. Genes & Development **15:**1783-1795.
98. **Alexander RD, Innocente SA, Barrass JD, Beggs JD.** 2010. Splicing-dependent RNA polymerase pausing in yeast. Molecular Cell **40:**582-593.
99. **Niwa M, Berget SM.** 1991. Mutation of the AAUAAA polyadenylation signal depresses in vitro splicing of proximal but not distal introns. Genes & Development **5:**2086-2095.
100. **Bauren G, Belikov S, Wieslander L.** 1998. Transcriptional termination in the Balbiani ring 1 gene is closely coupled to 3'-end formation and excision of the 3'-terminal intron. Genes & Development **12:**2759-2769.
101. **Vagner S, Vagner C, Mattaj IW.** 2000. The carboxyl terminus of vertebrate poly(A) polymerase interacts with U2AF 65 to couple 3'-end processing and splicing. Genes & Development **14:**403-413.
102. **Niwa M, Rose SD, Berget SM.** 1990. In vitro polyadenylation is stimulated by the presence of an upstream intron. Genes & Development **4:**1552-1559.
103. **Dye MJ, Proudfoot NJ.** 1999. Terminal exon definition occurs cotranscriptionally and promotes termination of RNA polymerase II. Molecular Cell **3:**371-378.
104. **Ahn SH, Kim M, Buratowski S.** 2004. Phosphorylation of serine 2 within the RNA polymerase II C-terminal domain couples transcription and 3' end processing. Molecular Cell **13:**67-76.

105. **Kim M, Ahn SH, Krogan NJ, Greenblatt JF, Buratowski S.** 2004. Transitions in RNA polymerase II elongation complexes at the 3' ends of genes. EMBO J **23:**354-364.
106. **Barilla D, Lee BA, Proudfoot NJ.** 2001. Cleavage/polyadenylation factor IA associates with the carboxyl-terminal domain of RNA polymerase II in Saccharomyces cerevisiae. Proceedings of the National Academy of Sciences of the United States of America **98:**445-450.
107. **Sadowski M, Dichtl B, Hubner W, Keller W.** 2003. Independent functions of yeast Pcf11p in pre-mRNA 3' end processing and in transcription termination. EMBO J **22:**2167-2177.
108. **Brodsky AS, Silver PA.** 2000. Pre-mRNA processing factors are required for nuclear export. RNA **6:**1737-1749.
109. **Hammell CM, Gross S, Zenklusen D, Heath CV, Stutz F, Moore C, Cole CN.** 2002. Coupling of termination, 3' processing, and mRNA export. Molecular Cell Biol **22:**6441-6457.
110. **Strasser K, Hurt E.** 1999. Nuclear RNA export in yeast. FEBS letters **452:**77-81.
111. **Abruzzi KC, Lacadie S, Rosbash M.** 2004. Biochemical analysis of TREX complex recruitment to intronless and intron-containing yeast genes. EMBO J **23:**2620-2631.
112. **Chavez S, Beilharz T, Rondon AG, Erdjument-Bromage H, Tempst P, Svejstrup JQ, Lithgow T, Aguilera A.** 2000. A protein complex containing Tho2, Hpr1, Mft1 and a novel protein, Thp2, connects transcription elongation with mitotic recombination in Saccharomyces cerevisiae. EMBO J **19:**5824-5834.
113. **Libri D, Graziani N, Saguez C, Boulay J.** 2001. Multiple roles for the yeast SUB2/yUAP56 gene in splicing. Genes & Development **15:**36-41.
114. **Strasser K, Hurt E.** 2001. Splicing factor Sub2p is required for nuclear mRNA export through its interaction with Yra1p. Nature **413:**648-652.
115. **Jensen TH, Boulay J, Rosbash M, Libri D.** 2001. The DECD box putative ATPase Sub2p is an early mRNA export factor. Current Biology : CB **11:**1711-1715.
116. **Johnson SA, Kim H, Erickson B, Bentley DL.** 2011. The export factor Yra1 modulates mRNA 3' end processing. Nature Structural and Molecular Biology **18:**1164-1171.
117. **Zenklusen D, Vinciguerra P, Strahm Y, Stutz F.** 2001. The yeast hnRNP-Like proteins Yra1p and Yra2p participate in mRNA export through interaction with Mex67p. Molecular and Cellular Biology **21:**4219-4232.
118. **Strasser K, Hurt E.** 2000. Yra1p, a conserved nuclear RNA-binding protein, interacts directly with Mex67p and is required for mRNA export. EMBO J **19:**410-420.
119. **Ma WK, Cloutier SC, Tran EJ.** 2013. The DEAD-box protein Dbp2 functions with the RNA-binding protein Yra1 to promote mRNP assembly. Journal of Molecular Biology **425:**3824-3838.

120. **Libri D, Dower K, Boulay J, Thomsen R, Rosbash M, Jensen TH.** 2002. Interactions between mRNA export commitment, 3'-end quality control, and nuclear degradation. Molecular and Cellular Biology **22:**8254-8266.
121. **Dower K, Rosbash M.** 2002. T7 RNA polymerase-directed transcripts are processed in yeast and link 3' end formation to mRNA nuclear export. RNA **8:**686-697.
122. **Assenholt J, Mouaikel J, Andersen KR, Brodersen DE, Libri D, Jensen TH.** 2008. Exonucleolysis is required for nuclear mRNA quality control in yeast THO mutants. RNA **14:**2305-2313.
123. **Saguez C, Schmid M, Olesen JR, Ghazy MA, Qu X, Poulsen MB, Nasser T, Moore C, Jensen TH.** 2008. Nuclear mRNA surveillance in THO/sub2 mutants is triggered by inefficient polyadenylation. Molecular Cell **31:**91-103.
124. **Legrain P, Seraphin B, Rosbash M.** 1988. Early commitment of yeast pre-mRNA to the spliceosome pathway. Molecular and Cellular Biology **8:**3755-3760.
125. **Rutz B, Seraphin B.** 1999. Transient interaction of BBP/ScSF1 and Mud2 with the splicing machinery affects the kinetics of spliceosome assembly. RNA **5:**819-831.
126. **Galy V, Gadal O, Fromont-Racine M, Romano A, Jacquier A, Nehrbass U.** 2004. Nuclear retention of unspliced mRNAs in yeast is mediated by perinuclear Mlp1. Cell **116:**63-73.
127. **Palancade B, Zuccolo M, Loeillet S, Nicolas A, Doye V.** 2005. Pml39, a novel protein of the nuclear periphery required for nuclear retention of improper messenger ribonucleoparticles. Molecular Biology of the Cell **16:**5258-5268.
128. **Anko ML, Neugebauer KM.** 2012. RNA-protein interactions in vivo: global gets specific. Trends in Biochemical Science **37:**255-262.
129. **Moore MJ, Schwartzfarb EM, Silver PA, Yu MC.** 2006. Differential recruitment of the splicing machinery during transcription predicts genome-wide patterns of mRNA splicing. Molecular Cell **24:**903-915.
130. **Tuck AC, Tollervey D.** 2013. A Transcriptome-wide Atlas of RNP Composition Reveals Diverse Classes of mRNAs and lncRNAs. Cell **154:**996-1009.
131. **Moore MJ.** 2005. From birth to death: the complex lives of eukaryotic mRNAs. Science **309:**1514-1518.
132. **Glisovic T, Bachorik JL, Yong J, Dreyfuss G.** 2008. RNA-binding proteins and post-transcriptional gene regulation. FEBS letters **582:**1977-1986.
133. **Roeder GS.** 1995. Sex and the single cell: meiosis in yeast. Proceedings of the National Academy of Sciences of the United States of America **92:**10450-10456.
134. **Mata J, Lyne R, Burns G, Bahler J.** 2002. The transcriptional program of meiosis and sporulation in fission yeast. Nature Genetics **32:**143-147.
135. **Harigaya Y, Yamamoto M.** 2007. Molecular mechanisms underlying the mitosis-meiosis decision. Chromosome research : an international journal on the

molecular, supramolecular and evolutionary aspects of chromosome biology **15:**523-537.

136. **Chen HM, Futcher B, Leatherwood J.** 2011. The fission yeast RNA binding protein Mmi1 regulates meiotic genes by controlling intron specific splicing and polyadenylation coupled RNA turnover. PloS one **6:**e26804.
137. **Harigaya Y, Tanaka H, Yamanaka S, Tanaka K, Watanabe Y, Tsutsumi C, Chikashige Y, Hiraoka Y, Yamashita A, Yamamoto M.** 2006. Selective elimination of messenger RNA prevents an incidence of untimely meiosis. Nature **442:**45-50.
138. **Yamanaka S, Yamashita A, Harigaya Y, Iwata R, Yamamoto M.** 2010. Importance of polyadenylation in the selective elimination of meiotic mRNAs in growing S. pombe cells. EMBO J **29:**2173-2181.
139. **St-Andre O, Lemieux C, Perreault A, Lackner DH, Bahler J, Bachand F.** 2010. Negative regulation of meiotic gene expression by the nuclear poly(a)-binding protein in fission yeast. Journal of Biological Chemistry **285:**27859-27868.
140. **Mangus DA, Evans MC, Jacobson A.** 2003. Poly(A)-binding proteins: multifunctional scaffolds for the post-transcriptional control of gene expression. Genome Biology **4:**223.
141. **Apponi LH, Kelly SM, Harreman MT, Lehner AN, Corbett AH, Valentini SR.** 2007. An interaction between two RNA binding proteins, Nab2 and Pub1, links mRNA processing/export and mRNA stability. Molecular and Cellular Biology **27:**6569-6579.
142. **Dunn EF, Hammell CM, Hodge CA, Cole CN.** 2005. Yeast poly(A)-binding protein, Pab1, and PAN, a poly(A) nuclease complex recruited by Pab1, connect mRNA biogenesis to export. Genes & Development **19:**90-103.
143. **Brune C, Munchel SE, Fischer N, Podtelejnikov AV, Weis K.** 2005. Yeast poly(A)-binding protein Pab1 shuttles between the nucleus and the cytoplasm and functions in mRNA export. RNA **11:**517-531.
144. **Kuhn U, Wahle E.** 2004. Structure and function of poly(A) binding proteins. Biochimia and Biophysica Acta **1678:**67-84.
145. **Maris C, Dominguez C, Allain FH.** 2005. The RNA recognition motif, a plastic RNA-binding platform to regulate post-transcriptional gene expression. The FEBS journal **272:**2118-2131.
146. **Kelly SM, Pabit SA, Kitchen CM, Guo P, Marfatia KA, Murphy TJ, Corbett AH, Berland KM.** 2007. Recognition of polyadenosine RNA by zinc finger proteins. Proceedings of the National Academy of Sciences of the United States of America **104:**12306-12311.
147. **Kelly S, Pak C, Garshasbi M, Kuss A, Corbett AH, Moberg K.** 2012. New kid on the ID block: neural functions of the Nab2/ZC3H14 class of Cys(3)His tandem zinc-finger polyadenosine RNA binding proteins. RNA biology **9:**555-562.

148. **Wilson SM, Datar KV, Paddy MR, Swedlow JR, Swanson MS.** 1994. Characterization of nuclear polyadenylated RNA-binding proteins in Saccharomyces cerevisiae. The Journal of Cell Biology **127:**1173-1184.
149. **Anderson JT, Wilson SM, Datar KV, Swanson MS.** 1993. NAB2: a yeast nuclear polyadenylated RNA-binding protein essential for cell viability. Molecular and Cellular Biology **13:**2730-2741.
150. **Green DM, Marfatia KA, Crafton EB, Zhang X, Cheng X, Corbett AH.** 2002. Nab2p is required for poly(A) RNA export in Saccharomyces cerevisiae and is regulated by arginine methylation via Hmt1p. Journal of Biological Chemistry **277:**7752-7760.
151. **Hector RE, Nykamp KR, Dheur S, Anderson JT, Non PJ, Urbinati CR, Wilson SM, Minvielle-Sebastia L, Swanson MS.** 2002. Dual requirement for yeast hnRNP Nab2p in mRNA poly(A) tail length control and nuclear export. EMBO J **21:**1800-1810.
152. **Marfatia KA, Crafton EB, Green DM, Corbett AH.** 2003. Domain analysis of the Saccharomyces cerevisiae heterogeneous nuclear ribonucleoprotein, Nab2p. Dissecting the requirements for Nab2p-facilitated poly(A) RNA export. Journal of Biological Chemistry **278:**6731-6740.
153. **Aitchison JD, Blobel G, Rout MP.** 1996. Kap104p: a karyopherin involved in the nuclear transport of messenger RNA binding proteins. Science **274:**624-627.
154. **Lee DC, Aitchison JD.** 1999. Kap104p-mediated nuclear import. Nuclear localization signals in mRNA- binding proteins and the role of Ran and Rna. Journal of Biological Chemistry **274:**29031-29037.
155. **Truant R, Fridell RA, Benson RE, Bogerd H, Cullen BR.** 1998. Identification and functional characterization of a novel nuclear localization signal present in the yeast Nab2 poly(A)+ RNA binding protein. Molecular and Cellular Biolog **18:**1449-1458.
156. **Kelly SM, Leung SW, Apponi LH, Bramley AM, Tran EJ, Chekanova JA, Wente SR, Corbett AH.** 2010. Recognition of polyadenosine RNA by the zinc finger domain of nuclear poly(A) RNA-binding protein 2 (Nab2) is required for correct mRNA 3'-end formation. Journal of Biological Chemistry **285:**26022-26032.
157. **Strambio-de-Castillia C, Blobel G, Rout MP.** 1999. Proteins connecting the nuclear pore complex with the nuclear interior. The Journal of Cell Biology **144:**839-855.
158. **Kolling R, Nguyen T, Chen EY, Botstein D.** 1993. A new yeast gene with a myosin-like heptad repeat structure. Molecular Genetics and Genomics **237:**359-369.
159. **Hodge CA, Colot HV, Stafford P, Cole CN.** 1999. Rat8p/Dbp5p is a shuttling transport factor that interacts with Rat7p/Nup159p and Gle1p and suppresses the mRNA export defect of xpo1-1 cells. EMBO J **18:**5778-5788.

160. **Leung S, Apponi L, Cornejo O, Kitchen C, Valentini S, Pavlath G, Dunham C, Corbett A.** 2009. Splice variants of the human ZC3H14 gene generate multiple isoforms of a zinc finger polyadenosine RNA binding protein. Gene **439:** 71-8.

161. **Pak C, Garshasbi M, Kahrizi K, Gross C, Apponi LH, Noto JJ, Kelly SM, Leung SW, Tzschach A, Behjati F, Abedini SS, Mohseni M, Jensen LR, Hu H, Huang B, Stahley SN, Liu G, Williams KR, Burdick S, Feng Y, Sanyal S, Bassell GJ, Ropers HH, Najmabadi H, Corbett AH, Moberg KH, Kuss AW.** 2011. Mutation of the conserved polyadenosine RNA binding protein, ZC3H14/dNab2, impairs neural function in Drosophila and humans. Proceedings of the National Academy of Sciences of the United States of America **108:**12390-12395.

162. **Wilmes GM, Bergkessel M, Bandyopadhyay S, Shales M, Braberg H, Cagney G, Collins SR, Whitworth GB, Kress TL, Weissman JS, Ideker T, Guthrie C, Krogan NJ.** 2008. A genetic interaction map of RNA-processing factors reveals links between Sem1/Dss1-containing complexes and mRNA export and splicing. Molecular Cell **32:**735-746.

163. **Kerr SC, Azzouz N, Fuchs SM, Collart MA, Strahl BD, Corbett AH, Laribee RN.** 2011. The Ccr4-Not complex interacts with the mRNA export machinery. PloS One **6:**e18302.

164. **Yu H, Braun P, Yildirim MA, Lemmens I, Venkatesan K, Sahalie J, Hirozane-Kishikawa T, Gebreab F, Li N, Simonis N, Hao T, Rual JF, Dricot A, Vazquez A, Murray RR, Simon C, Tardivo L, Tam S, Svrzikapa N, Fan C, de Smet AS, Motyl A, Hudson ME, Park J, Xin X, Cusick ME, Moore T, Boone C, Snyder M, Roth FP, Barabasi AL, Tavernier J, Hill DE, Vidal M.** 2008. High-quality binary protein interaction map of the yeast interactome network. Science **322:**104-110.

165. **Dheur S, Nykamp KR, Viphakone N, Swanson MS, Minvielle-Sebastia L.** 2005. Yeast mRNA Poly(A) tail length control can be reconstituted in vitro in the absence of Pab1p-dependent Poly(A) nuclease activity. Journal of Biological Chemistry **280:**24532-24538.

166. **Lukong KE, Chang KW, Khandjian EW, Richard S.** 2008. RNA-binding proteins in human genetic disease. Trends in Genetics **24:**416-425.

167. **Hino H, Araki K, Uyama E, Takeya M, Araki M, Yoshinobu K, Miike K, Kawazoe Y, Maeda Y, Uchino M, Yamamura K.** 2004. Myopathy phenotype in transgenic mice expressing mutated PABPN1 as a model of oculopharyngeal muscular dystrophy. Human Molecular Genetics **13:**181-190.

168. **Danckwardt S, Hentze MW, Kulozik AE.** 2008. 3' end mRNA processing: molecular mechanisms and implications for health and disease. EMBO J **27:**482-498.

169. **Banerjee A, Apponi LH, Pavlath GK, Corbett AH.** 2013. PABPN1: molecular function and muscle disease. The FEBS journal **280:**4230-4250.

170. **Brais B, Bouchard JP, Xie YG, Rochefort DL, Chretien N, Tome FM, Lafreniere RG, Rommens JM, Uyama E, Nohira O, Blumen S, Korczyn AD, Heutink P, Mathieu J, Duranceau A, Codere F, Fardeau M, Rouleau GA.** 1998. Short GCG expansions in the PABP2 gene cause oculopharyngeal muscular dystrophy. Nature Genetics **18:**164-167.
171. **Soucek S, Corbett AH, Fasken MB.** 2012. The long and the short of it: the role of the zinc finger polyadenosine RNA binding protein, Nab2, in control of poly(A) tail length. Biochimia Biophysica Acta **1819:**546-554.
172. **Carmody SR, Wente SR.** 2009. mRNA nuclear export at a glance. Journal of Cell Science **122:**1933-1937.
173. **Grunwald D, Singer RH, Rout M.** 2011. Nuclear export dynamics of RNA-protein complexes. Nature **475:**333-341.
174. **Kohler A, Hurt E.** 2007. Exporting RNA from the nucleus to the cytoplasm. Nat Rev Molecular and Cellular Biology **8:**761-773.
175. **Iglesias N, Stutz F.** 2008. Regulation of mRNP dynamics along the export pathway. FEBS letters **582:**1987-1996.
176. **Batisse J, Batisse C, Budd A, Boettcher B, Hurt E.** 2009. Purification of Nuclear poly(A)-binding protein Nab2 reveals association with the yeast transcriptome and a messenger ribonucleoprotein (mRNP) core structure. Journal of Biological Chemistry**:**1-12.
177. **Alcazar-Roman AR, Tran EJ, Guo S, Wente SR.** 2006. Inositol hexakisphosphate and Gle1 activate the DEAD-box protein Dbp5 for nuclear mRNA export. Nature Cell Biology **8:**711-716.
178. **Weirich CS, Erzberger JP, Flick JS, Berger JM, Thorner J, Weis K.** 2006. Activation of the DExD/H-box protein Dbp5 by the nuclear-pore protein Gle1 and its coactivator InsP6 is required for mRNA export. Nature Cell Biology **8:**668-676.
179. **Cole CN, Scarcelli JJ.** 2006. Transport of messenger RNA from the nucleus to the cytoplasm. Current Opinion in Cell Biology **18:**299-306.
180. **Snay-Hodge CA, Colot HV, Goldstein AL, Cole CN.** 1998. Dbp5p/Rat8p is a yeast nuclear pore-associated DEAD-box protein essential for RNA export. EMBO J **17:**2663-2676.
181. **Strahm Y, Fahrenkrog B, Zenklusen D, Rychner E, Kantor J, Rosbach M, Stutz F.** 1999. The RNA export factor Gle1p is located on the cytoplasmic fibrils of the NPC and physically interacts with the FG-nucleoporin Rip1p, the DEAD-box protein Rat8p/Dbp5p and a new protein Ymr 255p. EMBO J **18:**5761-5777.
182. **Berg JM.** 1988. Proposed structure for the zinc-binding domains from transcription factor IIIA and related proteins. Proceedings of the National Academy of Sciences of the United States of America **85:**99-102.
183. **Hudson BP, Martinez-Yamout MA, Dyson HJ, Wright PE.** 2004. Recognition of the mRNA AU-rich element by the zinc finger domain of TIS11d. Nature Structural and Molecular Biology **11:**257-264.

184. **He F, Dang W, Abe C, Tsuda K, Inoue M, Watanabe S, Kobayashi N, Kigawa T, Matsuda T, Yabuki T, Aoki M, Seki E, Harada T, Tomabechi Y, Terada T, Shirouzu M, Tanaka A, Guntert P, Muto Y, Yokoyama S.** 2009. Solution structure of the RNA binding domain in the human muscleblind-like protein 2. Protein science : a publication of the Protein Society **18:**80-91.
185. **Viphakone N, Voisinet-Hakil F, Minvielle-Sebastia L.** 2008. Molecular dissection of mRNA poly(A) tail length control in yeast. Nucleic Acids Research **36:**2418-2433.
186. **Vinciguerra P, Iglesias N, Camblong J, Zenklusen D, Stutz F.** 2005. Perinuclear Mlp proteins downregulate gene expression in response to a defect in mRNA export. EMBO J **24:**813-823.
187. **Johnson SA, Cubberley G, Bentley DL.** 2009. Cotranscriptional recruitment of the mRNA export factor Yra1 by direct interaction with the 3' end processing factor Pcf11. Molecular Cell **33:**215-226.
188. **Qu X, Lykke-Andersen S, Nasser T, Saguez C, Bertrand E, Jensen TH, Moore C.** 2009. Assembly of an export-competent mRNP is needed for efficient release of the 3'-end processing complex after polyadenylation. Molecular and Cellular Biology **29:**5327-5338.
189. **Rougemaille M, Dieppois G, Kisseleva-Romanova E, Gudipati RK, Lemoine S, Blugeon C, Boulay J, Jensen TH, Stutz F, Devaux F, Libri D.** 2008. THO/Sub2p functions to coordinate 3'-end processing with gene-nuclear pore association. Cell **135:**308-321.
190. **Baker KE, Parker R.** 2004. Nonsense-mediated mRNA decay: terminating erroneous gene expression. Current Opinion in Cell Biology **16:**293-299.
191. **Scarcelli JJ, Viggiano S, Hodge CA, Heath CV, Amberg DC, Cole CN.** 2008. Synthetic genetic array analysis in Saccharomyces cerevisiae provides evidence for an interaction between RAT8/DBP5 and genes encoding P-body components. Genetics **179:**1945-1955.
192. **Legge GB, Martinez-Yamout MA, Hambly DM, Trinh T, Lee BM, Dyson HJ, Wright PE.** 2004. ZZ domain of CBP: an unusual zinc finger fold in a protein interaction module. Journal of Molecular Biology **343:**1081-1093.
193. **Boeke JD, Truehart J, Natsoulis G, Fink G.** 1987. 5-Fluoroorotic acid as a selective agent in yeast molecular genetics. Methods in Enzymology. **154:**164-175.
194. **Minvielle-Sebastia L, Winsor B, Bonneaud N, Lacroute F.** 1991. Mutations in the yeast RNA14 and RNA15 genes result in an abnormal mRNA decay rate; sequence analysis reveals an RNA-binding domain in the RNA15 protein. Molecular and Cellular Bioliogy **11:**3075-3087.
195. **Chekanova JA, Belostotsky DA.** 2003. Evidence that poly(A) binding protein has an evolutionarily conserved function in facilitating mRNA biogenesis and export. RNA **9:**1476-1490.

196. **Wong DH, Corbett AH, Kent HM, Stewart M, Silver PA.** 1997. Interaction between the small GTPase Ran/Gsp1p and Ntf2p is required for nuclear transport. Molecular and Cellular Biology **17:**3755-3767.
197. **Goguel V, Rosbash M.** 1993. Splice site choice and splicing efficiency are positively influenced by pre-mRNA intramolecular base pairing in yeast. Cell **72:**893-901.
198. **Stevens SW, Ryan DE, Ge HY, Moore RE, Young MK, Lee TD, Abelson J.** 2002. Composition and functional characterization of the yeast spliceosomal penta-snRNP. Molecular Cell **9:**31-44.
199. **Fabrizio P, Dannenberg J, Dube P, Kastner B, Stark H, Urlaub H, Luhrmann R.** 2009. The evolutionarily conserved core design of the catalytic activation step of the yeast spliceosome. Molecular Cell **36:**593-608.
200. **Warkocki Z, Odenwalder P, Schmitzova J, Platzmann F, Stark H, Urlaub H, Ficner R, Fabrizio P, Luhrmann R.** 2009. Reconstitution of both steps of Saccharomyces cerevisiae splicing with purified spliceosomal components. Nature Structural and Molecular Biology **16:**1237-1243.
201. **Agafonov DE, Deckert J, Wolf E, Odenwalder P, Bessonov S, Will CL, Urlaub H, Luhrmann R.** 2011. Semiquantitative proteomic analysis of the human spliceosome via a novel two-dimensional gel electrophoresis method. Molecular and Cellular Biology **31:**2667-2682.
202. **Fourmann JB, Schmitzova J, Christian H, Urlaub H, Ficner R, Boon KL, Fabrizio P, Luhrmann R.** 2013. Dissection of the factor requirements for spliceosome disassembly and the elucidation of its dissociation products using a purified splicing system. Genes & Development **27:**413-428.
203. **Proudfoot NJ.** 2011. Ending the message: poly(A) signals then and now. Genes & Development **25:**1770-1782.
204. **Mandel CR, Bai Y, Tong L.** 2008. Protein factors in pre-mRNA 3'-end processing. Cellular and Molecular Life Sciences **65:**1099-1122.
205. **Chan S, Choi EA, Shi Y.** 2011. Pre-mRNA 3'-end processing complex assembly and function. Wiley Interdisciplinary Reviews: RNA **2:**321-335.
206. **Shi Y, Di Giammartino DC, Taylor D, Sarkeshik A, Rice WJ, Yates JR, 3rd, Frank J, Manley JL.** 2009. Molecular architecture of the human pre-mRNA 3' processing complex. Molecular Cell **33:**365-376.
207. **Millevoi S, Loulergue C, Dettwiler S, Karaa SZ, Keller W, Antoniou M, Vagner S.** 2006. An interaction between U2AF 65 and CF I(m) links the splicing and 3' end processing machineries. EMBO J **25:**4854-4864.
208. **Kyburz A, Friedlein A, Langen H, Keller W.** 2006. Direct interactions between subunits of CPSF and the U2 snRNP contribute to the coupling of pre-mRNA 3' end processing and splicing. Molecular Cell **23:**195-205.
209. **Rymond BC.** 2010. The branchpoint binding protein: in and out of the spliceosome cycle. Advances in Experimental Medicine and Biology **693:**123-141.

210. **Hilleren PJ, Parker R.** 2003. Cytoplasmic degradation of splice-defective pre-mRNAs and intermediates. Molecular Cell **12:**1453-1465.
211. **Semlow DR, Staley JP.** 2012. Staying on message: ensuring fidelity in pre-mRNA splicing. Trends in Biochemical Science **37:**263-273.
212. **Mitchell P, Petfalski E, Shevchenko A, Mann M, Tollervey D.** 1997. The exosome: a conserved eukaryotic RNA processing complex containing multiple 3'-->5' exoribonucleases. Cell **91:**457-466.
213. **Garneau NL, Wilusz J, Wilusz CJ.** 2007. The highways and byways of mRNA decay. Nat Rev Molecular and Cellular Biology **8:**113-126.
214. **Abovich N, Liao XC, Rosbash M.** 1994. The yeast MUD2 protein: an interaction with PRP11 defines a bridge between commitment complexes and U2 snRNP addition. Genes & Development **8:**843-854.
215. **Leung S, Apponi L, Cornejo O, Kitchen C, Valentini S, Pavlath G, Dunham C, Corbett A.** 2009. Splice variants of the human ZC3H14 gene generate multiple isoforms of a zinc finger polyadenosine RNA binding protein. Gene **439:**71-78.
216. **St-Sauveur VG, Soucek S, Corbett AH, Bachand F.** 2013. Poly(A) tail-mediated gene regulation by opposing roles of Nab2 and Pab2 nuclear poly(A)-binding proteins in pre-mRNA decay. Molecular and Cellular Biology **33:**4718-4731.
217. **King DS, Beggs JD.** 1990. Interactions of PRP2 protein with pre-mRNA splicing complexes in Saccharomyces cerevisiae. Nucleic Acids Research **18:**6559-6564.
218. **Pleiss JA, Whitworth GB, Bergkessel M, Guthrie C.** 2007. Transcript specificity in yeast pre-mRNA splicing revealed by mutations in core spliceosomal components. PLoS Biology **5:**e90.
219. **Pleiss JA, Whitworth GB, Bergkessel M, Guthrie C.** 2007. Rapid, transcript-specific changes in splicing in response to environmental stress. Molecular Cell **27:**928-937.
220. **Umen JG, Guthrie C.** 1995. Prp16p, Slu7p, and Prp8p interact with the 3' splice site in two distinct stages during the second catalytic step of pre-mRNA splicing. RNA **1:**584-597.
221. **Wang Q, Zhang L, Lynn B, Rymond BC.** 2008. A BBP-Mud2p heterodimer mediates branchpoint recognition and influences splicing substrate abundance in budding yeast. Nucleic Acids Research **36:**2787-2798.
222. **Dziembowski A, Ventura AP, Rutz B, Caspary F, Faux C, Halgand F, Laprevote O, Seraphin B.** 2004. Proteomic analysis identifies a new complex required for nuclear pre-mRNA retention and splicing. EMBO J **23:**4847-4856.
223. **Yan D, Perriman R, Igel H, Howe KJ, Neville M, Ares M, Jr.** 1998. CUS2, a yeast homolog of human Tat-SF1, rescues function of misfolded U2 through an unusual RNA recognition motif. Molecular and Cellular Biology **18:**5000-5009.

224. **Valcarcel J, Gaur RK, Singh R, Green MR.** 1996. Interaction of U2AF65 RS region with pre-mRNA branch point and promotion of base pairing with U2 snRNA [corrected]. Science **273:**1706-1709.
225. **Sickmier EA, Frato KE, Shen H, Paranawithana SR, Green MR, Kielkopf CL.** 2006. Structural basis for polypyrimidine tract recognition by the essential pre-mRNA splicing factor U2AF65. Molecular Cell **23:**49-59.
226. **Selenko P, Gregorovic G, Sprangers R, Stier G, Rhani Z, Kramer A, Sattler M.** 2003. Structural basis for the molecular recognition between human splicing factors U2AF65 and SF1/mBBP. Molecular Cell **11:**965-976.
227. **Chang J, Schwer B, Shuman S.** 2012. Structure-function analysis and genetic interactions of the yeast branchpoint binding protein Msl5. Nucleic Acids Research **40:**4539-4552.
228. **Rain JC, Legrain P.** 1997. In vivo commitment to splicing in yeast involves the nucleotide upstream from the branch site conserved sequence and the Mud2 protein. EMBO J **16:**1759-1771.
229. **Brockmann C, Soucek S, Kuhlmann SI, Mills-Lujan K, Kelly SM, Yang JC, Iglesias N, Stutz F, Corbett AH, Neuhaus D, Stewart M.** 2012. Structural basis for polyadenosine-RNA binding by Nab2 Zn fingers and its function in mRNA nuclear export. Structure **20:**1007-1018.
230. **Burkard KT, Butler JS.** 2000. A nuclear 3'-5' exonuclease involved in mRNA degradation interacts with Poly(A) polymerase and the hnRNA protein Npl3p. Molecular and Cellular Biology **20:**604-616.
231. **Gudipati RK, Xu Z, Lebreton A, Seraphin B, Steinmetz LM, Jacquier A, Libri D.** 2012. Extensive degradation of RNA precursors by the exosome in wild-type cells. Molecular Cell **48:**409-421.
232. **Sachs AB, Bond MW, Kornberg RD.** 1986. A single gene from yeast for both nuclear and cytoplasmic polyadenylate-binding proteins: domain structure and expression. Cell **45:**827-835.
233. **M.Ausubel F, Brent R, Kingston RE, Moore DD, Seidman JG, Smith JA, Struhl K.** 2001. Current protocols in molecular biology. John Wiley & Sons, New York, NY.
234. **Wach A, Brachat A, Pohlmann R, Philippsen P.** 1994. New heterologous modules for classical or PCR-based gene disruptions in Saccharomyces cerevisiae. Yeast **10:**1793-1808.
235. **Chang J, Schwer B, Shuman S.** 2010. Mutational analyses of trimethylguanosine synthase (Tgs1) and Mud2: proteins implicated in pre-mRNA splicing. RNA **16:**1018-1031.
236. **Sikorski RS, Hieter P.** 1989. A system of shuttle vectors and yeast host strains designed for efficient manipulation of DNA in Saccharomyces cerevisiae. Genetics **122:**19-27.

237. **Chomczynski P.** 1993. A reagent for the single-step simultaneous isolation of RNA, DNA and proteins from cell and tissue samples. Biotechniques **15:**532-534, 536-537.
238. **Livak KJ, Schmittgen TD.** 2001. Analysis of relative gene expression data using real-time quantitative PCR and the 2(-Delta Delta C(T)) Method. Methods **25:**402-408.
239. **de Hoon MJ, Imoto S, Nolan J, Miyano S.** 2004. Open source clustering software. Bioinformatics **20:**1453-1454.
240. **Boeke JD, Trueheart J, Natsoulis G, Fink GR.** 1987. 5-Fluoroorotic acid as a selective agent in yeast molecular genetics. Methods in Enzymology **154:**164-175.
241. **Lemay JF, Lemieux C, St-Andre O, Bachand F.** 2010. Crossing the borders: poly(A)-binding proteins working on both sides of the fence. RNA Biology **7:**291-295.
242. **Vanacova S, Wolf J, Martin G, Blank D, Dettwiler S, Friedlein A, Langen H, Keith G, Keller W.** 2005. A new yeast poly(A) polymerase complex involved in RNA quality control. PLoS Biology **3:**e189.
243. **Wyers F, Rougemaille M, Badis G, Rousselle JC, Dufour ME, Boulay J, Regnault B, Devaux F, Namane A, Seraphin B, Libri D, Jacquier A.** 2005. Cryptic pol II transcripts are degraded by a nuclear quality control pathway involving a new poly(A) polymerase. Cell **121:**725-737.
244. **Kuhn U, Gundel M, Knoth A, Kerwitz Y, Rudel S, Wahle E.** 2009. Poly(A) tail length is controlled by the nuclear poly(A)-binding protein regulating the interaction between poly(A) polymerase and the cleavage and polyadenylation specificity factor. Journal of Biological Chemistry **284:**22803-22814.
245. **Apponi LH, Leung SW, Williams KR, Valentini SR, Corbett AH, Pavlath GK.** 2010. Loss of nuclear poly(A)-binding protein 1 causes defects in myogenesis and mRNA biogenesis. Human Molecular Genetics **19:**1058-1065.
246. **de Klerk E, Venema A, Anvar SY, Goeman JJ, Hu O, Trollet C, Dickson G, den Dunnen JT, van der Maarel SM, Raz V, t Hoen PA.** 2012. Poly(A) binding protein nuclear 1 levels affect alternative polyadenylation. Nucleic Acids Research **40:**9089-9101.
247. **Jenal M, Elkon R, Loayza-Puch F, van Haaften G, Kuhn U, Menzies FM, Oude Vrielink JA, Bos AJ, Drost J, Rooijers K, Rubinsztein DC, Agami R.** 2012. The poly(A)-binding protein nuclear 1 suppresses alternative cleavage and polyadenylation sites. Cell **149:**538-553.
248. **Beaulieu YB, Kleinman CL, Landry-Voyer AM, Majewski J, Bachand F.** 2012. Polyadenylation-dependent control of long noncoding RNA expression by the poly(A)-binding protein nuclear 1. PLoS Genetics **8:**e1003078.
249. **Lemay JF, D'Amours A, Lemieux C, Lackner DH, St-Sauveur VG, Bahler J, Bachand F.** 2010. The nuclear poly(A)-binding protein interacts with the

exosome to promote synthesis of noncoding small nucleolar RNAs. Molecular Cell **37:**34-45.

250. **Januszyk K, Lima CD.** 2010. Structural components and architectures of RNA exosomes. Advances in Experimental Medicine and Biology **702:**9-28.
251. **Schmid M, Jensen TH.** 2008. The exosome: a multipurpose RNA-decay machine. Trends in Biochemical Science **33:**501-510.
252. **Green DM, Marfatia KA, Crafton EB, Zhang X, Cheng X, Corbett AH.** 2002. Nab2p Is Required for Poly(A) RNA Export in Saccharomyces cerevisiae and Is Regulated by Arginine Methylation via Hmt1p. Journal of Biological Chemistry **277:**7752-7760.
253. **Guthrie CR, Schellenberg GD, Kraemer BC.** 2009. SUT-2 potentiates tau-induced neurotoxicity in Caenorhabditis elegans. Human Molecular Genetics **18:**1825-1838.
254. **Perreault A, Lemieux C, Bachand F.** 2007. Regulation of the Nuclear Poly(A)-binding Protein by Arginine Methylation in Fission Yeast. Journal of Biological Chemistry **282:**7552-7562.
255. **Oeffinger M.** 2012. Two steps forward--one step back: advances in affinity purification mass spectrometry of macromolecular complexes. Proteomics **12:**1591-1608.
256. **Berriz GF, King OD, Bryant B, Sander C, Roth FP.** 2003. Characterizing gene sets with FuncAssociate. Bioinformatics **19:**2502-2504.
257. **Larochelle M, Lemay JF, Bachand F.** 2012. The THO complex cooperates with the nuclear RNA surveillance machinery to control small nucleolar RNA expression. Nucleic Acids Research **40:**10240-10253.
258. **Lackner DH, Beilharz TH, Marguerat S, Mata J, Watt S, Schubert F, Preiss T, Bahler J.** 2007. A network of multiple regulatory layers shapes gene expression in fission yeast. Molecular Cell **26:**145-155.
259. **Habara Y, Urushiyama S, Shibuya T, Ohshima Y, Tani T.** 2001. Mutation in the prp12+ gene encoding a homolog of SAP130/SF3b130 causes differential inhibition of pre-mRNA splicing and arrest of cell-cycle progression in Schizosaccharomyces pombe. RNA **7:**671-681.
260. **Midtgaard SF, Assenholt J, Jonstrup AT, Van LB, Jensen TH, Brodersen DE.** 2006. Structure of the nuclear exosome component Rrp6p reveals an interplay between the active site and the HRDC domain. Proceedings of the National Academy of Sciences of the United States of America **103:**11898-11903.
261. **Phillips S, Butler JS.** 2003. Contribution of domain structure to the RNA 3' end processing and degradation functions of the nuclear exosome subunit Rrp6p. RNA **9:**1098-1107.
262. **Winstall E, Sadowski M, Kuhn U, Wahle E, Sachs AB.** 2000. The Saccharomyces cerevisiae RNA-binding protein Rbp29 functions in cytoplasmic mRNA metabolism. Journal of Biological Chemistry **275:**21817-21826.

263. **Marguerat S, Schmidt A, Codlin S, Chen W, Aebersold R, Bahler J.** 2012. Quantitative analysis of fission yeast transcriptomes and proteomes in proliferating and quiescent cells. Cell **151:**671-683.
264. **Bhattacharjee RB, Bag J.** 2012. Depletion of nuclear poly(A) binding protein PABPN1 produces a compensatory response by cytoplasmic PABP4 and PABP5 in cultured human cells. PloS One **7:**e53036.
265. **Hosoda N, Lejeune F, Maquat LE.** 2006. Evidence that poly(A) binding protein C1 binds nuclear pre-mRNA poly(A) tails. Molecular Cell Biol **26:**3085-3097.
266. **Le H, Browning KS, Gallie DR.** 2000. The phosphorylation state of poly(A)-binding protein specifies its binding to poly(A) RNA and its interaction with eukaryotic initiation factor (eIF) 4F, eIFiso4F, and eIF4B. Journal of Biological Chemistry **275:**17452-17462.
267. **Lee J, Bedford MT.** 2002. PABP1 identified as an arginine methyltransferase substrate using high-density protein arrays. EMBO Reports **3:**268-273.
268. **Sipiczki M.** 2000. Where does fission yeast sit on the tree of life? Genome Biology **1:**REVIEWS1011.
269. **de Almeida SF, Garcia-Sacristan A, Custodio N, Carmo-Fonseca M.** 2010. A link between nuclear RNA surveillance, the human exosome and RNA polymerase II transcriptional termination. Nucleic Acids Research **22:** 8015-26.
270. **Eberle AB, Hessle V, Helbig R, Dantoft W, Gimber N, Visa N.** 2010. Splice-site mutations cause Rrp6-mediated nuclear retention of the unspliced RNAs and transcriptional down-regulation of the splicing-defective genes. PloS One **5:**e11540.
271. **Bahler J, Wu JQ, Longtine MS, Shah NG, McKenzie A, 3rd, Steever AB, Wach A, Philippsen P, Pringle JR.** 1998. Heterologous modules for efficient and versatile PCR-based gene targeting in Schizosaccharomyces pombe. Yeast **14:**943-951.
272. **Arnold K, Bordoli L, Kopp J, Schwede T.** 2006. The SWISS-MODEL workspace: a web-based environment for protein structure homology modelling. Bioinformatics **22:**195-201.
273. **Brunger AT.** 2007. Version 1.2 of the Crystallography and NMR system. Nature Protocols **2:**2728-2733.
274. **Emsley P, Cowtan K.** 2004. Coot: model-building tools for molecular graphics. Acta crystallographica. Section D, Biological Crystallography **60:**2126-2132.
275. **Beaudoin J, Labbe S.** 2006. Copper induces cytoplasmic retention of fission yeast transcription factor cuf1. Eukaryotic Cell **5:**277-292.
276. **Craven RA, Griffiths DJ, Sheldrick KS, Randall RE, Hagan IM, Carr AM.** 1998. Vectors for the expression of tagged proteins in Schizosaccharomyces pombe. Gene **221:**59-68.
277. **Mallet PL, Bachand F.** 2013. A proline-tyrosine nuclear localization signal (PY-NLS) is required for the nuclear import of fission yeast PAB2, but not of human PABPN1. Traffic **14:**282-294.

278. **Oeffinger M, Fatica A, Rout MP, Tollervey D.** 2007. Yeast Rrp14p is required for ribosomal subunit synthesis and for correct positioning of the mitotic spindle during mitosis. Nucleic Acids Research **35:**1354-1366.
279. **Malavasic MJ, Elder RT.** 1990. Complementary transcripts from two genes necessary for normal meiosis in the yeast Saccharomyces cerevisiae. Molecular and Cellular Biology **10:**2809-2819.
280. **Mata J, Bahler J.** 2006. Global roles of Ste11p, cell type, and pheromone in the control of gene expression during early sexual differentiation in fission yeast. Proceedings of the National Academy of Sciences of the United States of America **103:**15517-15522.
281. **Roth R, Halvorson HO.** 1969. Sporulation of yeast harvested during logarithmic growth. Journal of Bacteriology **98:**831-832.
282. **Kassir Y, Granot D, Simchen G.** 1988. IME1, a positive regulator gene of meiosis in S. cerevisiae. Cell **52:**853-862.
283. **Mortimer RK, Johnston JR.** 1986. Genealogy of principal strains of the yeast genetic stock center. Genetics **113:**35-43.
284. **Messias AC, Sattler M.** 2004. Structural basis of single-stranded RNA recognition. Accounts of Chemical Research **37:**279-287.
285. **Kuhlmann SI, Valkov E, Stewart M.** 2013. Structural basis for the molecular recognition of polyadenosine RNA by Nab2 Zn fingers. Nucleic Acids Research **42:** 672-80.
286. **Zanotti KJ, Lackey PE, Evans GL, Mihailescu MR.** 2006. Thermodynamics of the fragile X mental retardation protein RGG box interactions with G quartet forming RNA. Biochemistry **45:**8319-8330.
287. **Whitson SR, LeStourgeon WM, Krezel AM.** 2005. Solution structure of the symmetric coiled coil tetramer formed by the oligomerization domain of hnRNP C: implications for biological function. Journal of Molecular Biology **350:**319-337.
288. **Loya TJ, O'Rourke TW, Reines D.** 2013. Yeast Nab3 protein contains a self-assembly domain found in human heterogeneous nuclear ribonucleoprotein-C (hnRNP-C) that is necessary for transcription termination. Journal of Biological Chemistry **288:**2111-2117.
289. **Gonzalez-Aguilera C, Tous C, Gomez-Gonzalez B, Huertas P, Luna R, Aguilera A.** 2008. The THP1-SAC3-SUS1-CDC31 complex works in transcription elongation-mRNA export preventing RNA-mediated genome instability. Molecular Biology of the Cell **19:**4310-4318.
290. **McCracken S, Longman D, Marcon E, Moens P, Downey M, Nickerson JA, Jessberger R, Wilde A, Caceres JF, Emili A, Blencowe BJ.** 2005. Proteomic analysis of SRm160-containing complexes reveals a conserved association with cohesin. Journal of Biological Chemistry **280:**42227-42236.

291. **Kelly SM, Leung SW, Pak C, Banerjee A, Moberg KH, Corbett AH.** 2014. A conserved role for the zinc finger polyadenosine RNA binding protein, ZC3H14, in control of poly(A) tail length. RNA **20:**681-8.
292. **Goldie BJ, Cairns MJ.** 2012. Post-transcriptional trafficking and regulation of neuronal gene expression. Molecular Neurobiology **45:**99-108.
293. **Beilharz TH, Preiss T.** 2011. Polyadenylation state microarray (PASTA) analysis. Methods in Molecular Biology **759:**133-148.
294. **Chang H, Lim J, Ha M, Kim VN.** 2014. TAIL-seq: Genome-wide Determination of Poly(A) Tail Length and 3' End Modifications. Molecular Cell **53:**1044-1052.
295. **Subtelny AO, Eichhorn SW, Chen GR, Sive H, Bartel DP.** 2014. Poly(A)-tail profiling reveals an embryonic switch in translational control. Nature **508:** 66-71.